MODELING THE NON-TRANSFERRED ARC PLASMA TORCH AND PLUME FOR PLASMA PROCESSING

by

RICHARD WESTHOFF

B.A. Mathematics, Carroll College, Helena, Montana
(1985)

B.S. Mechanical Engineering, Arizona State University
(1985)

S.M. Materials Engineering
Massachusetts Institute Institute of Technology
(1989)

Submitted to the Department of
Materials Science and Engineering
in partial fulfillment of the requirements for the Degree of

DOCTOR OF SCIENCE IN
MATERIALS ENGINEERING

at the

MASSACHUSETTS INSTITUTE OF TECHNOLOGY

May 1992

© Massachusetts Institute of Technology, 1992

Signature of Author_____
Department of Materials Science and Engineering
May 1, 1992

Certified by_____
Prof. Julian Szekely
Thesis Supervisor

Accepted by_____
Linn W. Hobbs,
Professor of Materials Science
Chairman, Departmental Committee on Graduate Students

ARCHIVES
MASSACHUSETTS INSTITUTE
OF TECHNOLOGY

JUL 30 1992

LIBRARIES

MODELING THE NON-TRANSFERRED ARC PLASMA TORCH AND PLUME FOR PLASMA PROCESSING

Richard Westhoff

Submitted to the Department of Materials Science and Engineering in partial fulfillment of the requirements for the degree of Doctor of Science in Materials Engineering

ABSTRACT

Plasma torches are used in processing of materials for spraying, melting, heat treatment or plasma synthesis. Mathematical modeling of the phenomena which occur in plasma processing is presented for different plasma torches. Emphasis is placed on modeling the plasma jet exiting the torch, the transport processes inside the torch, and the behavior of small particles injected into the plasma.

The literature is reviewed and a mathematical model is presented for the plasma jets exiting plasma torches. Calculations are presented for laminar and turbulent cases and single and two gas systems. In general the agreement with experimental measurements is reasonable, though in turbulent systems the modeling may be hindered by the use of a fully turbulent model for jets which are in the transitional range. The work also indicates the importance of knowing the temperature and velocity profiles at the torch exit accurately.

The literature on the modeling of plasma torches is reviewed. A simplified model of the transport phenomena inside a plasma torch is presented and applied to laminar and turbulent systems. The simplified model provides useful insight, but is limited by the neglect of electromagnetic forces on the system.

A mathematical model is presented which describes the electromagnetic, heat flow and fluid flow phenomena within a non-transferred arc plasma torch and in the resultant plume. The development of the model is based on the conservation of mass, momentum, thermal energy, species and the continuity of the current. An important, novel feature of the model is that it can predict both the pattern of heat generation within the torch and the electromagnetic forces, thus providing a fundamental basis for predicting plume behavior. Calculations are presented for a pure argon system as well as an argon-nitrogen system, both operating in a laminar mode, and the theoretical predictions appear to be in quite good agreement with experimental measurements. An important finding of the work is that the electromagnetic forces markedly modify the velocity profiles of the plasma gas exiting the torch. In addition, swirl is shown to have a significant affect on the behavior of the arc and thus affects the resulting plume.

Finally, a case study on the spraying of fine ceramic powders in a plasma torch is presented, which is based on the simplified model of the plasma torch. The plasma effects, namely variable properties, non-continuum effects, and vaporization are investigated. A comparison is made with experimentally determined particle temperatures and velocities in a plasma plume and the agreement is quite good.

Thesis Supervisor: Julian Szekely, Professor of Materials Engineering

Table of Contents

Title Page 1
Abstract 2
Table of Contents 3
List of Tables 4
List of Figures 6
Acknowledgements 16

I. Introduction 17
- A. Plasma and Arc Phenomena 17
- B. Plasma Torches 19
- C. Applications in Materials Processing 19
- D. Significance of the Work 21
- E. Thesis Organization 22
- F. References 22

II. Modeling of the Plasma Plume 30
- A. Literature Survey 30
- B. Laminar Plume - Argon in Nitrogen 34
- C. Turbulent Plume - Argon in Air 40
- D. Turbulent Plume - Argon in Argon 47
- E. References 51

III. Modeling the Plasma Torch - A Simplified Approach 79
- A. Literature Review of Plasma Torch Models 79
- B. Application of the Simplified Model of the Plasma Torch to a Laminar, Argon-Argon System 83
- C. Application of the Simplified Model to Turbulent Systems 95

IV. A Model of the Plasma Torch Including Electromagnetic Phenomena..... 129
- A. Application to a Laminar, Argon in Argon System 129
- B. Application to a Laminar Argon in Nitrogen System 145
- C. Turbulent Argon-Argon System - Metco Torch 152
- D. Turbulent Argon-Air System - Miller Torch 161
- E. Dimensional Analysis 166
- F. References 170

V. Modeling of Plasma Spraying 249
- A. Particles in the Simplified Torch-Plume Model 249

VI. Conclusion 282
- A. Discussion 282
- B. Suggested Future Work 286

AI. Appendix I. Plasma Properties 289
AII. Appendix II. Current - Voltage Correlation Program 297
Biographical Note..... 306

LIST OF TABLES

II.B.I. Operating conditions used in the BES experiment at INEL.

II.B.II. Summary of the uncertainties in the BES experiments.

II.B.III. Boundary conditions used in the model with reference to Figure II.B.3.

II.C.I. Averaged torch conditions for the Metco torch experiments of Brossa and Pfender [32]

II.C.II. Constants used in the K–ε turbulence model

II.C.III. Boundary conditions used in the model (turbulent case) with reference to Figure II.C.1.

II.D.I. Averaged torch conditions for the Metco torch experiments of Capetti and Pfender [37]

II.D.II. Summary of the analysis of the overall heat and mass balances performed on the Metco torch.

II.D.III. Parameters used in the model to represent the Metco torch (argon in argon).

Chapter III

III.B.I. Boundary conditions used in the simplified plasma torch model (laminar case)

III.B.II. Effect of swirl number on cold flow in a plasma torch

III.B.III. Effect of Swirl Number on Hot Flow in INEL Plasma torch

III.B.IV. Operating Conditions for Studying the Effect of Arc Dimensions on Transport Phenomena in the Plasma Torch

III.B.V. Simulation of a System Studied Experimentally at INEL

III.C.I. Constants used in the K–ε turbulence model

III.C.II. Boundary Conditions for the Turbulent Case

Chapter IV

IV.A.I. Operating conditions for plasma torch experiments at INEL.

IV.A.II. Boundary conditions for the solution of the governing equations of a non-transferred arc plasma torch.

IV.A.III. Effect of electromagnetic forces on fluid flow in the plasma torch used at INEL, cases B23 and B31 (calculations done without swirl).

IV.A.IV. Operating conditions and results of the study concerning the effect of swirl number on the arc behavior in the plasma torch.

IV.A.V. Experimental and calculated current-voltage characteristics of the INEL plasma torch.

IV.A.VI. Operating conditions used for studying the effect of the cathode spot current density, j_c on transport phenomena in the plasma torch (all values calculated using a constant swirl number of 5.0).

IV.C.I. Boundary Conditions used in the model (turbulent case) with reference to Figure IV.C.2.

IV.C.II. Averaged conditions for the Metco torch experiments of Capetti and Pfender[37].

IV.C.III. Summary of calculated results for the Metco torch.

IV.D.I. Averaged conditions for the Miller torch experiments at INEL.

IV.D.II. Summary of calculated results for the Miller torch.

IV.E.I. Dimensionless numbers of interest in plasma torch systems.

IV.E.II. Characteristic dimensionless numbers for the BES experiments at INEL.

IV.E.III. Characteristic dimensionless numbers for the experiments on the Metco torch at the University of Minnesota.

IV.E.IV. Characteristic dimensionless numbers for the experiments on the Miller torch at INEL (pure argon cases).

IV.E.V. Characteristic dimensionless numbers for the experiments on the Miller torch at INEL (argon - helium cases).

Chapter V

V.A.I. Input data (Alumina particles in a Ar/He plasma)

LIST OF FIGURES

Chapter I

I.A.1. Equilibrium composition of an LTE argon plasma versus temperature.

I.A.2. Relative magnitudes of plasma parameters for thermal and non-equilibrium plasma processing of materials.(1)

I.A.3. Behavior of the electron temperature (T_e) and the heavy particle temperature (T_h) in an arc plasma.(1)

I.A.4. Steady-state voltage -current characteristic of a discharge at about 100 N/m^2, showing order of magnitude values.(2)

I.A.5. Schematic sketch of an arc illustrating several key phenomena.

I.B.1. Cut away view of a Metco 7mb plasma torch (courtesy Metco Corp., Westbury, NY)

I.B.2. Cutaway view of a Miller SG-100 torch (courtesy Miller Thermal, Inc. Tustin, CA)

I.B.3. Illustration of plasma torch modes of operation: (a) non-transferred mode, (b) transferred mode.(1)

Chapter II

II.A.1. Sketch of the phenomena associated with a plasma plume issuing from a plasma torch.

II.A.2. Schematic illustration of transitional flow in a plasma jet (19).

II.B.1. Cut-away view of the non-transferred arc plasma torch used in the BES experiments (17-18).

II.B.2. Atmosphere control chamber used in the BES experiments (14-15).

II.B.3. Integration domain used in the BES calculations (14-15).

II.B.4. Comparison of calculated and experimental data for run BES25. (a) Radial temperature profiles at several axial positions, and (b) Temperature profile and calculated argon concentration profile on the axis.

II.B.5. Comparison of calculated and experimental data for run BES26. (a) Radial temperature profiles at several axial positions, and (b) Temperature profile and calculated argon concentration profile on the axis.

II.B.6. Comparison of calculated and experimental data for run BES29. (a) Radial temperature profiles at several axial positions, and (b) Temperature profile and calculated argon concentration profile on the axis.

II.B.7. Comparison of calculated and experimental data for run BES30. (a) Radial temperature profiles at several axial positions, and (b) Temperature profile and calculated argon concentration profile on the axis.

II.B.8. Comparison of calculated and experimental data for run BES34. (a) Radial temperature profiles at several axial positions, and (b) Temperature profile and calculated argon concentration profile on the axis.

II.B.9. Comparison of the temperature dependence of the heat capacity of argon and nitrogen plasma.

II.C.1. Calculation domain used in modeling the results of Brossa and Pfender [32].

II.C.2. Temperature profiles on the axis of the plume - 450 amp cases.

II.C.3. Temperature profiles on the axis of the plume - 600 amp cases.

II.C.4. Argon concentration profiles on the axis of the plume - 450 amp cases.

II.C.5. Argon concentration profiles on the axis of the plume - 600 amp cases.

II.C.6. Comparison of calculated and measured temperature contours in the plume - Case #12.

II.C.7. Comparison of calculated and measured temperature contours in the plume - Case #8.

II.C.8. Comparison of calculated and measured argon mole fraction contours in the plume - Case #12.

II.C.9. Comparison of calculated and measured argon mole fraction contours in the plume - Case #8.

II.C.10. Comparison of calculated and measured radial temperature profiles in the plume at several axial positions - Case #8.

II.C.11. Temperature profiles on the plume axis illustrating the insensitivity of the experimental vs. calculated discrepancies to the torch exit temperature profile.

II.C.12. Normalized jet diameter (radial position at which U=100 m/s) versus the torch flow rate and current - comparison of calculated and experimental data.

II.D.1. Mass flow and power from the torch exit versus the maximum velocity, for three different maximum temperatures ($n_u = n_t = 2.8$).

II.D.2. Mass flow and power from the torch exit versus the exponent of velocity for three different temperature exponents (U_{max} = 700 m/s, T_{max} = 12,000k).

II.D.3. Mass flow and power from the torch exit versus the exponent of temperature for three different velocity exponents (U_{max} = 700 m/s, T_{max} = 12,000k).

II.D.4. Comparison of the measured and calculated (a) temperature and (b) velocity contours (450 amp, 35.4 lit/min).

II.D.5. Comparison of the measured and calculated (a) temperature and (b) velocity contours (600 amp, 35.4 lit/min).

II.D.6. Comparison of the experimental and theoretical (a) temperature and (b) velocity profiles on the plume axis (450 amp cases).

II.D.7. Comparison of the experimental and theoretical (a) temperature and (b) velocity profiles on the plume axis (600 amp cases).

Chapter III

III.A.1. Schematic illustration of the key phenomena in a plasma torch.

III.A.2. Schematic sketch of a wall stabilized constricted arc after Schaeffer.(9)

III.A.3. Normalized plasma enthalpy for the calculations of Watson and Pegot.(8)

III.A.4. Temperature distribution in a non-transferred arc reactor by Mazza and Pfender.(11)

III.A.5. Temperature contours in a confined arc plasma with injected cold gas from Chen et al.(12) Dashed line indicates the penetration of the injected flow.

III.A.6. Velocity vectors and configuration in a plasma thruster from Park and Choi.(17)

III.B.1. Schematic of a plasma torch.

III.B.2. Calculation domain used in the simplified modeling approach.

III.B.3. Effect of swirl on axial velocity decay for an unheated torch.

III.B.4. Effect of swirl on axial temperature decay for a heated torch.

III.B.5. Effect of arc radius on the (a) axial temperature profile and (b) radial temperature profiles for 6.1 mm Long Arcs.

III.B.6. Effect of arc radius on the (a) axial temperature profile and (b) radial temperature profiles for 13.7 mm Long Arcs.

III.B.7. Effect of arc radius on the (a) axial temperature profile and (b) radial temperature profiles for 24.5 mm Long Arcs.

III.B.8. Effect of arc length on the (a) axial temperature profile and (b) radial temperature profiles for 2.9 mm Radius Arcs.

III.B.9. Temperature contours for case B28.

III.B.10. The radial temperature profiles (a) at five axial positions and (b) the axial temperature profile – B23.

III.B.11. The radial temperature profiles (a) at five axial positions and (b) the axial temperature profile – B28.

III.B.12. The radial temperature profiles (a) at five axial positions and (b) the axial temperature profile – B32.

III.C.1. Cutaway view of the plasma torch in the experimental study of Lewis and Gauvin.(38)

III.C.2. (a) Axial temperature profile calculated using the inside torch and plume models compared to measurements by Brossa and Pfender, 600 amp case.(37)
(b) Axial concentration profile calculated using the inside torch and plume models compared to measurements by Brossa and Pfender, 600 amp case.(37)

III.C.3. Plasma velocity on the torch axis calculated by the inside torch model and the plume model, 600 amp case.(37)

III.C.4. Plasma temperature calculated with the inside torch model and the plume model compared to measurements by Brossa and Pfender, 450 amp case.(37)

III.C.5. Plasma velocity on the torch axis calculated by the inside torch model and the plume model, 450 amp case.(37)

III.C.6. Comparison of the radial profiles of (a) temperature and (b) velocity at a position 6 mm inside the torch nozzle for the plume and the simplified torch models.

III.C.7. Comparison of experimental and calculated axial temperature profile for the U-51 Thermal Dynamics torch studied by Lewis and Gauvin, operating at 650 amps.(38)

III.C.8. Comparison of experimental and calculated axial profile of argon concentration for the U-51 Thermal Dynamics torch studied by Lewis and Gauvin, operating at 650 amps.(38)

III.C.9. Comparison of experimental and calculated axial velocity profile for the U-51 Thermal Dynamics torch studied by Lewis and Gauvin, operating at 650 amps.(38)

Chapter IV

IV.A.1. Schematic of an axi-symmetric arc in a non-transferred plasma torch.

IV.A.2. Schematic of the non-transferred arc plasma torch used at INEL.

IV.A.3. Computational domain used in this study.

IV.A.4. Isotherms (a) current density vectors (b) and mass flow (ru product) vectors (c) in the non-transferred plasma torch, (case B23, 250 A, 0.59 scmh of argon, Sw=5.0). Minimum isotherm is 2000K, interval is 2000K, maximum is 16000K.

IV.A.5. Effect of electromagnetic forces on the radial profiles of temperature (a) and velocity (b) at the torch exit, (case B23, 250 A, 0.59 scmh argon, Sw=0.0).

IV.A.6. Effect of electromagnetic forces on the radial profiles of temperature (a) and velocity (b) at the torch exit, (case B31, 750 A, 0.59 scmh argon, Sw=0.0).

IV.A.7. Isotherms (a) current density vectors (b) and mass flow (ru product) vectors (c) in the non-transferred plasma torch, (case B23, 250 A, 0.59 scmh of argon, no swirl). Minimum isotherm is 2000K, interval is 2000K, maximum is 18000K.

IV.A.8. Effect of swirl on the axial profile (a) and on the radial profile at the torch exit (b). (case B23, 250 A, 0.59 scmh argon).

IV.A.9. Effect of swirl on the radial current density at the anode. (case B23, 250 A, 0.59 scmh argon).

IV.A.10. Calculated and experimental current-voltage characteristics of the plasma torch, calculated (solid symbols) and measured (open symbols).

IV.A.11. Effect of current and flow rate on the calculated radial current density at the anode - Runs B23,B24,B27,B28,B31,B32.

IV.A.12. Dependence of the calculated current-voltage characteristics of the torch on the cathode spot current density.

IV.A.13. Axial (a) and radial (b) profiles of temperature for case B23: 250 A, 0.59 scmh. Discrete figures denote measurements, lines indicate calculations

IV.A.14. Axial (a) and radial (b) profiles of temperature for case B24: 250 A, 0.83 scmh. Discrete figures denote measurements, lines indicate calculations

IV.A.15. Axial (a) and radial (b) profiles of temperature for case B28: 500 A, 0.83 scmh. Discrete figures denote measurements, lines indicate calculations

IV.A.16. Axial (a) and radial (b) profiles of temperature for case B32: 750 A, 0.59 scmh. Discrete figures denote measurements, lines indicate calculations

IV.B.1. A schematic sketch of the plasma torch and plume

IV.B.2. Current-voltage relationship for the torch used in the BES runs

IV.B.3. Calculated and experimental current-voltage relationships for the argon/nitrogen system

IV.B.4. Calculated temperature contours in the plasma torch and plume for Ar/N_2 and Ar/Ar system (figure is expanded in the radial direction for clarity)

IV.B.5. Experimentally measured (a) and theoretical radial temperature profiles at five axial positions in the plasma plume (solid - Ar/N_2, dash - Ar/Ar)

IV.B.6. Comparison of the experimentally measured and theoretically predicted axial (a) and radial (b) profiles of temperature for run BES25

IV.B.7. Comparison of the experimentally measured and theoretically predicted axial (a) and radial (b) profiles of temperature for run BES30

IV.B.8. Comparison of the experimentally measured and theoretically predicted axial (a) and radial (b) profiles of temperature for run BES34

IV.B.9. Comparison of the concentration contours of argon in the plume for the Ar/N_2 system with and without shroud gas.

IV.B.10. Comparison of the temperature contours of argon in the plume for the Ar/N_2 system with and without shroud gas.

IV.B.11. Comparison of the axial temperature profile in the plume for the Ar/Ar system and the Ar/N_2 system with and without shroud gas.

IV.C.1. Cut-away view of the Metco 7mb plasma torch (courtesy Metco Corp., Westbury, NY)

IV.C.2. Computational domain used in the study of the Metco torch.

IV.C.3. Temperature dependence of the electrical conductivity of argon showing the assumptions used at low temperature and the effect of the constants used in the exponential expression.

IV.C.4. Isotherms (a) and velocity vectors (b) in the Metco plasma torch, (case 12, 450 A, 23.6 lit./min. of argon, Sw=3.0).

IV.C.5. Mass flow (ρu product) vectors (a) and contours of swirl velocity (b) in the Metco plasma torch, (case 12, 450 A, 23.6 lit./min. of argon, Sw=3.0).

IV.C.6. Current density vectors (a) and body force vectors (b) in the Metco plasma torch, (case 12, 450 A, 23.6 lit./min. of argon, Sw=3.0).

IV.C.7. Calculated and experimentally measured current-voltage characteristics of the plasma torch used by Capetti and Pfender[24], calculated (open symbols) and measured (solid symbols).

IV.C.8. Comparison between experimentally measured[24] (symbols) and theoretically predicted (lines) axial profiles of temperature (a) and axial velocity (b) in the plume of the Metco torch for the 450 amp cases.

IV.C.9 Theoretically predicted radial profiles of temperature (a) and axial velocity (b) at a position 1 mm from the nozzle exit for the 450 amp cases.

IV.C.10. Comparison between experimentally measured[24] (symbols) and theoretically predicted (lines) axial profiles of temperature (a) and axial velocity (b) in the plume of the Metco torch for the 600 amp cases.

IV.C.11. Theoretically predicted radial profiles of temperature (a) and axial velocity (b) at a position 1 mm from the nozzle exit for the 600 amp cases.

IV.D.1. Cut-away view of the Miller SG-100 plasma torch (courtesy Miller Thermal, Inc. Tustin, CA)

IV.D.2 Illustration of the swirl ring used in the Miller torch for the experiments represented in this section.

IV.D.3. Isotherms (a) and velocity vectors (b) in the Miller plasma torch, (case 6, 600 A, 75 scfh of argon, Sw=1.22).

IV.D.4. Mass flow (ρu product) vectors (a) and contours of swirl velocity (b) in the Miller plasma torch, (case 6, 600 A, 75 scfh of argon, Sw=1.22).

IV.D.5. Current density vectors (a) and body force vectors (b) in the Miller plasma torch, (case 6, 600 A, 75 scfh of argon, Sw=1.22).

IV.D.6. Calculated and experimental current-voltage characteristics of the Miller SG-100 torch, calculated (solid symbols) and measured (open symbols).

IV.D.7. Comparison of the experimentally measured (circles) and theoretically predicted (squares) center line temperature (a) and velocity (b) at a position 2 mm (case #9, 5 mm) from the exit of the torch nozzle.

IV.D.8. Comparison of the experimentally measured and theoretically predicted radial profile of temperature (a) and axial velocity (b) at a position 2 mm from the nozzle exit for the 300 amp case.

IV.D.9. Comparison of the experimentally measured and theoretically predicted radial profile of argon mole fraction at a position 2 mm from the nozzle exit for the 300 amp case.

IV.D.10. Comparison of the experimentally measured and theoretically predicted axial profile of the center line temperature (a) and axial velocity (b) for the 300 amp case.

IV.D.11. Comparison of the experimentally measured and theoretically predicted axial profile of the argon mole fraction on the center line for the 300 amp case.

IV.D.12. Comparison of the experimentally measured and theoretically predicted radial profile of temperature (a) and axial velocity (b) at a position 2 mm from the nozzle exit for the 400 amp case.

IV.D.13. Comparison of the experimentally measured and theoretically predicted radial profile of argon mole fraction at a position 2 mm from the nozzle exit for the 400 amp case.

IV.D.14. Comparison of the experimentally measured and theoretically predicted radial profile of temperature (a) and axial velocity (b) at a position 2 mm from the nozzle exit for the 500 amp case.

IV.D.15. Comparison of the experimentally measured and theoretically predicted radial profile of argon mole fraction at a position 2 mm from the nozzle exit for the 500 amp case.

IV.D.16. Comparison of the experimentally measured and theoretically predicted radial profile of temperature (a) and axial velocity (b) at a position 2 mm from the nozzle exit for the 600 amp case.

IV.D.17. Comparison of the experimentally measured and theoretically predicted radial profile of argon mole fraction at a position 2 mm from the nozzle exit for the 600 amp case.

IV.D.18. Comparison of the experimentally measured and theoretically predicted axial profile of the center line temperature (a) and axial velocity (b) for the 600 amp case.

IV.D.19. Comparison of the experimentally measured and theoretically predicted axial profile of the argon mole fraction on the center line for the 600 amp case.

IV.D.20. Comparison of the experimentally measured and theoretically predicted radial profile of temperature (a) and axial velocity (b) at a position 2 mm from the nozzle exit for the 700 amp case.

IV.D.21. Comparison of the experimentally measured and theoretically predicted radial profile of argon mole fraction at a position 2 mm from the nozzle exit for the 700 amp case.

IV.D.22. Comparison of the experimentally measured and theoretically predicted radial profile of temperature (a) and axial velocity (b) at a position 2 mm from the nozzle exit for the 900 amp case.

IV.D.23. Comparison of the experimentally measured and theoretically predicted radial profile of argon mole fraction at a position 2 mm from the nozzle exit for the 900 amp case.

IV.D.24. Comparison of the experimentally measured and theoretically predicted axial profile of the center line temperature (a) and axial velocity (b) for the 900 amp case.

IV.D.25. Comparison of the experimentally measured and theoretically predicted axial profile of the argon mole fraction on the center line for the 900 amp case.

IV.D.26. Comparison of the experimentally measured and theoretically predicted radial profiles of temperature at axial positions of 5, 15, 25, 40, and 60 mm from the nozzle exit for the 900 amp case.

IV.D.27. Comparison of the experimentally measured and theoretically predicted radial profiles of axial velocity at axial positions of 5, 15, 25, 40, and 60 mm from the nozzle exit for the 900 amp case.

IV.D.28. Comparison of the experimentally measured and theoretically predicted radial profiles of argon mole fraction at axial positions of 5, 15, 25, 40, and 60 mm from the nozzle exit for the 900 amp case.

IV.E.1. Schematic illustrations of arc heaters with longitudinal-vortex flow from Shaskov et al.:
(a) one-sided outflow, refractory rod electrode and cooled cylindrical electrode,
(b) one-sided outflow, cooled cylindrical electrodes,
(c) dual outflow, cooled cylindrical electrodes.
(1, 2 denote the electrodes)

IV.E.2. Voltage - current characteristics of the torches used in this study correlated using the dimensionless parameters:

Dimensionless Voltage = $\frac{VD\sigma}{I}$, HJ Number = $\frac{\dot{m}D\sigma h}{I^2}$

(a) all cases combined, (b) high argon gas flow cases (c) with mixtures of argon and helium.

IV.E.3. Schematic illustration of the effect the ratio of electromagnetic forces to the swirl momentum forces (as indicated by the ES number) has on the velocity profiles in the torch.

IV.E.4. Calculated radial profile of the axial velocity taken 1 mm from the torch exit, showing the effect of the ES number for (a) increasing inlet swirl numbers (b) increasing flow rates. (Gas flow: CAP12 - 7.01e-4 kg/sec, CAP10 - 1.05e-3 kg/sec, CAP11 - 1.40e-3 kg/sec)

Chapter V

V.A.1. Schematic illustration of particle heat, mass, and momentum transfer phenomena.

V.A.2. Schematic sketch of the model used to describe the plasma plume.

V.A.3. Experimental setup and parameters used in studying the motion of alumina particles in a room-temperature air jet by Lesinski et al.

V.A.4. Computational domain and calculated gas velocity vectors in the air jet.

V.A.5. Comparison of radial profiles of the calculated axial velocity with the experimentally measured axial velocity of Lesinski et. al.

V.A.6. Comparison of the calculated axial velocity profile on the jet axis with measurements.

V.A.7. Comparison of the measured mean particle velocities (shown by the solid lines) with those calculated with the particle model (discrete points) for particles with a mean diameter of 97 microns.

V.A.8. Comparison of the measured mean particle velocities (shown by the solid lines) with those calculated with the particle model (discrete points) for particles with a mean diameter of 13.7 microns.

V.A.9. Calculated trajectories for particles with a mean diameter of 97 microns and a mean injection velocity of 5.0 m/s.

V.A.10. Comparison of the measured mean particle velocities (shown by the solid lines) with those calculated with the particle model (discrete points) for particles with a mean diameter of 97 microns (assuming radial gas velocity is zero).

V.A.11. Comparison of the measured mean particle velocities (shown by the solid lines) with those calculated with the particle model (discrete points) for particles with a mean diameter of 13.7 microns (assuming radial gas velocity is zero).

V.A.12. Schematic of the Miller plasma torch and operating conditions for the spraying of alumina particles (Power: 900 A, 35.4 V @ Efficiency = 69%).

V.A.13. Comparison of measured and calculated axial temperature profiles in the turbulent plasma jet issuing from a plasma torch.

V.A.14. Comparison of measured and calculated radial temperature profiles in a turbulent plasma jet.

V.A.15. Comparison of measured (at the center line) and calculated particle velocities (a) and particle surface temperatures (b) for two different particle sizes and for an injection velocity of 13 m/s.

V.A.16. Calculated particle trajectories in the plasma jet for 27 and 35 μm particles with injection velocities of 13 m/s. The injection point is located 10 mm inside the torch.

V.A.17. Comparison of predictions for particle temperature histories calculated by a lumped parameter model and by the enthalpy method.
(a) 35 μm, and (b) 27 μm.

V.A.18. (a) Calculated mass transfer coefficients due to Langmuir vaporization, diffusion mass transfer and overall (mixed control).
(b) Calculated evaporation rate and particle diameter for 27 and 35 μm particles with injection velocity of 13 m/s.

V.A.19. Effect of vaporization and non-continuum (Knudsen) behavior on the prediction of particle velocities (a), and particle temperatures (b), for alumina particles with a mean diameter of 27 μm in an Ar-He plasma jet. For the limiting case, Knudsen effects are neglected in the calculation, as well as the heat flux terms due to vaporization of the particle.

AI.A.1. Thermodynamic and transport properties of a LTE argon plasma versus temperature (a) density, (b) heat capacity, (c) viscosity, (d) thermal conductivity, (e) radiative loss, and (f) electrical conductivity.

AI.A.2. Thermodynamic and transport properties of a LTE nitrogen plasma versus temperature (a) density, (b) heat capacity, (c) viscosity, (d) thermal conductivity, (e) radiative loss, and (f) electrical conductivity.

AI.A.3. Thermodynamic and transport properties of a LTE air plasma versus temperature (a) density, (b) heat capacity, (c) viscosity, (d) thermal conductivity, (e) radiative loss, and (f) electrical conductivity.

AI.A.4. Thermodynamic and transport properties of a LTE helium plasma versus temperature (a) density, (b) heat capacity, (c) viscosity, (d) thermal conductivity, and (f) electrical conductivity.

ACKNOWLEDGMENTS

I would like to offer my sincere thanks to Prof. Julian Szekely for providing me with support from my first day at MIT. His intuitive and imaginative insight into a wide range of materials processes as well as his enthusiasm for a interesting problems have inspired me through this work.

I owe an immense debt of gratitude to Prof. Amjad H. Dilawari for laying a solid and unique foundation in plasma processing here in the Process Modeling Group at MIT. His meticulous work in this area as well as his helpful advice provided a guiding light to my research throughout my time here.

Many thanks go to all of my office mates in Room 8-135, as well as those in 4-033, whose discussions and insight brought me through a number of seemingly insoluble difficulties. Dr. Roland (Tuck Chow) Choo, and Dr. Luis Gerardo Trapaga-Martinez, gave me valuable counsel and offered their time and energy for fruitful collaboration in research. Dr. Navtej S. Saluja was also a helpful source of insight as well as inspiration. The author is also grateful for the patient ear and helpful advice of Mr. Par Jonsson.

Not unlike many grateful graduate students, I feel compelled to thank the Giver for the gifts which have enabled me to complete my work. I also I want to thank my precious wife Cindy, God's gift to me, without whom I would have certainly misplaced my sanity, perspective and ability to remain human. Her help (cut and paste champ!) and encouragement throughout this project have kept me going. Many thanks to my family (Hi Mom!) and friends in Arizona and Colorado (Thanks Midcaps!) whose prayers and concern encouraged and enabled me to make the best use of the gifts I have.

I would like to acknowledge the Department of Energy for supporting this work under grant #DE-FG02-85ER13331. I would also like to thank Prof. David White at the MIT Energy Lab for his additional support during the final stages of this project.

CHAPTER I: INTRODUCTION

I.A. PLASMA AND ARC PHENOMENA

I.A.1 PLASMAS

A plasma is a gas with a sufficient amount of thermal energy to ionize a significant fraction of its molecules. Such a plasma contains ions and electrons which make it an excellent conductor of both heat and electricity. Within a plasma the process of ionization occurs continuously as does the recombination of electrons and ions. In general then, a plasma is a highly reactive fluid composed of three components: neutral atoms, ions and electrons.

In certain situations, a plasma can reach a state at which the rates of ionization and the rates of recombination in a small control volume are equal. If such is the case, the plasma is said to be in a state of Local Thermodynamic Equilibrium (LTE). In addition, if the collision rate between the heavy particles (ions, neutrals) and the electrons is high enough, they can attain a state of Local Thermal Equilibrium (LTE), so that the electrons and heavy particles may be said to have the same characteristic temperature. In this special case, the properties of the plasma (e.g. heat capacity, viscosity, etc.) can be specified as a unique function of temperature for a given pressure.

Figure I.A.1 shows a plot of the equilibrium diagram for an argon plasma, showing the number densities of total atoms, neutral, singly, doubly and triply ionized atoms and electrons. The method used to calculate this figure is given in Appendix I. Throughout the study presented in this thesis, the special case of Local Thermal and Thermodynamic Equilibrium is assumed to hold, and is labeled LTE. This useful approximation allows the plasma to be treated as an inert gas with strongly non-linear thermodynamic and transport properties. (See appendix I).

It is important to recognize the limitations of this assumption. Figure I.A.2 shows the relative parameter space for two different regions of operation for plasma applications, namely, Thermal Plasma and Non-Equilibrium Plasma. The first is the region in which this study is focussed, while the second is more common in some micro-electronics applications, and other low pressure situations. The reason for this is illustrated in Figure

I.A.3, which shows the respective energies of the electrons and heavy particles in a plasma. (These correspond to temperatures via the relation $E = \frac{3}{2}\frac{k_b}{e}T$ so that 1 eV corresponds to an electron temperature of 7733K). As the operating pressure decreases, it is seen that the heavy and electron particle temperatures diverge. The reason for this is the diminishing rate at which collisions between particles occur as the pressure falls and density decreases. Thus, the LTE plasma assumption is restricted to relatively high pressure applications around atmospheric pressure.

In a non-equilibrium case, it is possible for the plasma to be in a state of chemical or *ionization* equilibrium even though the temperatures of ions and electrons may not be the same. Such a state is often referred to as a "two-temperature" plasma and can be described by an equilibrium model (such as that in Appendix I) with two characteristic temperatures, T_e and T_h, which denote the electron and heavy particle temperatures respectively.

I.A.2 ARC PHENOMENA

If an electrical current passes through a plasma it can be heated and ionized and in some cases become self-sustaining. Figure I.A.4 shows a plot of the current-voltage characteristic of various gaseous discharges. It is seen that an arc is generally a high current/low voltage discharge. In fact a a gaseous discharge is usually classified as an arc if it meets the following criteria[1]:

1. Relatively high current density ($10^4 - 10^7 A/m^2$)
2. Low cathode fall (~10V)
3. The column is highly luminous

Arc phenomena have been known for a long, time and have been studied at length[2], yet because of their complexity, the understanding of them remains incomplete. A schematic sketch of an arc is shown in Figure I.A.5, which notes a number of the physical phenomena which occur.

I.B. PLASMA TORCHES

One very common tool for producing plasma for the purpose of materials processing is a plasma torch. Figures I.B.1-I.B.2 show two different models of torches. These are reasonably complex devices, the heart of which is the arc which strikes between the copper anode and tungsten cathode which are both water cooled. The working gas (usually Argon, Helium, Nitrogen, Hydrogen or mixtures of these) is introduced upstream of the cathode through a gas ring which usually imparts a swirl motion to the gas as it enters the chamber. As it passes through the arc, the gas is heated, ionized and expanded. The resulting plasma leaving the torch nozzle may be 10000–15000 K, making it an excellent source of high intensity, localized heat, useful in a number of materials processes.

Plasma torches may be categorized according to the location of the anode, as illustrated in Figure I.B.3. If the water-cooled nozzle itself acts as the anode the torch is a non-transferred type. On the other hand, if the anode is located outside of the torch nozzle as a water-cooled rod- or ring-shaped electrode or as a flat surface on which the plasma plume impinges, the torch is of the transferred type. The plasma torches addressed in this thesis are all of the non-transferred type.

The design of these devices has up until now been guided largely by intuition and Edisonian methods of development. While such methods have brought the process quite far, it is felt that a more quantitative understanding of the phenomena involved will enable further refinement of these devices.

I.C. APPLICATIONS IN MATERIALS PROCESSING

The plasma torch has many potential applications in materials processing which usually fall into one of the following areas[1,3]:

- Plasma melting, and refining

  This area includes the recycling of scrap metals such as high alloy steel, titanium and superalloys and offers interesting possibilities in metal refining. In general these processes involve the use of plasma torches or arcs to melt the material which is then collected in a suitable crucible for solidification processing. Specific plasma melting and refining operations include the established technology of titanium processing, in either

scrap or sponge form, into usable solid ingots, as well as those in a pilot plant stage such as the melting of high alloy steels and high quality steels.

• Plasma extractive metallurgy

Extractive metallurgy is defined as the winning of metals or alloys from their ores which are found in nature as oxides or sulphides. For metals which require a high smelting or roasting temperature (refractories) or where current processes require a number of complex steps, (such as magnesium or titanium) "plasma-winning" may provide unique opportunities. At present, however, such processes may be limited in a production process by the maximum attainable torch power of about 5 MW, though this may be overcome by designing higher power torches, or by using several in parallel.

• Plasma spray deposition

Plasma spray deposition processing combines the heating, melting, quenching, consolidation of fine particles (metallic or ceramic) into a single step. This is achieved by injecting the particles of a powder in a the plasma jet of a plasma torch. Within the plasma jet the particles are rapidly heated, melted and simultaneously accelerated toward a substrate surface by the hot, (5000-15000 K) high velocity plasma (100-1000 m/s). The particles are rapidly deformed, cooled and solidified upon impacting the substrate and the resulting deposits are characterized by fine, homogeneous microstructures.

Plasma sprayed deposits are very useful as corrosion resistant layers, wear coatings and are widely used as thermal barriers in the turbine engine industry. In addition, plasma spraying has been used for near-net shaping of components such as rocket nozzles, ceramic tubes, crucibles etc.

• Plasma synthesis of materials

Plasmas present useful advantages in the synthesis of refractory materials which require high temperatures and an impurity free environment. The very high heating and cooling rates in these systems allow the production of materials in certain metastable phases which would be difficult to produce by conventional processes. Synthesis operations in plasma include the production of sub-micron ceramic powders, spheroidization, as well as material densification.

The large number of present and potential applications of plasma torches make this an interesting technology. At present, however the scientific understanding of these systems is at best sketchy. The development of new and improved processes will surely benefit from an improved understanding of the phenomena governing their overall behavior.

I.D. SIGNIFICANCE OF THE WORK

To facilitate potential plasma processes and optimize current ones a more complete understanding of the phenomena which occur in plasma torches and plumes is needed. As previously mentioned, the majority of development in these systems to date has been the result of intuition and trial and error. While I have nothing personal at all against the Edisonian method, as it is responsible for most of the modern conveniences which we enjoy, it is well known that a systematic understanding of a physical phenomenon leads to new advances and better processes in that area.

A mathematical model will offer insight into a number of important issues:

- The model will be able to predict the voltage and the overall power level of a torch for a given set of operating parameters (current, gas flow, working gas, etc.). This will provide information which could be useful in torch design as well as process control.

- The model will be able to predict the torch efficiency, which measures the fraction of the torch power which is available as sensible heat in the plume. This will also be useful in process design.

- The model will be able to predict the plasma temperatures, velocities and compositions in the processing zone of the torch. This zone usually includes the plasma plume and may extend some distance inside the torch. For some applications (e.g. plasma synthesis) the arc column may be included. Such information will be useful to process design and optimization.

- The model can be used as a basis for doing further calculations on particle histories in the plasma. It may also form the basis for analysis of chemical reactions occurring in plasma synthesis.

I.E. THESIS ORGANIZATION

The thesis is composed of three chapters which contain material primarily from published papers. A few sections are included to flesh out the details of the work, and some new as yet unpublished work is included. In addition, some of the literature review has been derived from a published review paper written in collaboration Prof. Szekely[4].

Chapter II reviews the work which the author performed in collaboration with Prof. A.H. Dilawari on the modeling of the plume or jet of a plasma torch. This work preceded the later work within the torch itself, and results from two papers which have been published.[5-6]

Chapter III presents more work done in collaboration with Prof. Dilawari. This is on the modeling of transport phenomena in the plasma torch and is based on a simplified model developed as a preliminary step. Again, this work is based primarily on two published papers on which the author collaborated.[7-8]

Chapter IV is the central part of the thesis work, which describes modeling of the fluid flow, heat transfer and electromagnetic phenomena inside plasma torches. It includes work presented in two published papers,[9-10] as well as some later unpublished work.

Chapter V is a case study performed on a plasma spraying process, which was done in collaboration with Dr. Gerardo Trapaga[11-12]. This work models the behavior of single particles immersed in a plasma flame. It is composed of work contained in a published paper, as well as some extensions of the work which are to be published.

I.F. REFERENCES

1. Plasma Processing of Materials, Publication NMAB-415, Committee on Plasma Processing of Materials, National Materials Advisory Board, National Academy Press, Washington, DC. (1985).
2. J. F. Lancaster, ed., The Physics of Welding, 2nd Edition, International Institute of Welding, Pergammon Press, Oxford, (1986).
3. J. Feinman, Ed., Plasma Technology in Metallurgical Processing, Iron and Steel Society,Warrendale, PA. (1987).

4. J. Szekely and R.C. Westhoff "Recent Advances in the Mathematical Modelling of Transport Phenomena in Plasma Systems", Accepted in the Proceedings of the International Symposium: "Thermal Plasma Applications in Materials and Metallurgical Processes", San Diego. (1992).
5. A.H. Dilawari, R. Westhoff, J. Szekely, C. Shaw and B. Detering, "A Comparison of the Experimentally Measured and Theoretically Predicted Temperature Profiles for an Argon Plasma Jet Discharging into a Nitrogen Environment," MRS Symp. on Plasma Processing and Synthesis of Materials III, **190**, 199, San Francisco, CA. (1990).
6. A.H. Dilawari, J. Szekely and R. Westhoff, "A Comparison of Experimental Measurements and Theoretical Predictions Regarding the Behavior of a Turbulent Argon Plasma Jet Discharging into Air," *Plasma Chem. Plasma Process.* 10, (3), 501, (1990).
7. A.H. Dilawari, J. Szekely and R. Westhoff, "An Assessment of Heat and Fluid Flow Phenomena inside Plasma Torches in Non-transferred Arc Systems," *ISIJ International,* 30, (5), 381, (1990).
8. R. Westhoff, A.H. Dilawari and J. Szekely, "A Mathematical Representation of Transport Phenomena inside a Plasma Torch," MRS Symp. on Plasma Processing and Synthesis of Materials III, **190**, 213, San Francisco, CA. (1990).
9. R. Westhoff, and J. Szekely, "A Model of Fluid, Heat Flow and Electromagnetic Phenomena in a Non-Transferred Arc Plasma Torch" Journal of Applied Physics, **70**, (7), 3455-3466, (1991).
10. R. Westhoff, and J. Szekely, "A Model of an Argon Plasma Torch Discharging into Nitrogen", Accepted in the Proceedings of the International Symposium: "Thermal Plasma Applications in Materials and Metallurgical Processes", San Diego. (1992).
11. G. Trapaga, R. Westhoff, J. Szekely, J. Fincke and D. Swank, "Particle and Temperature Histories in a Plasma Plume: A Comparison of Measurements and Predictions," MRS Symp. on Plasma Processing and Synthesis of Materials III, **190,** 191, San Francisco, CA. (1990).
12. R. Westhoff, G. Trapaga, and J. Szekely, "Plasma-Particle Interactions in Plasma Spraying Systems", Accepted in Met. Trans., (1991).

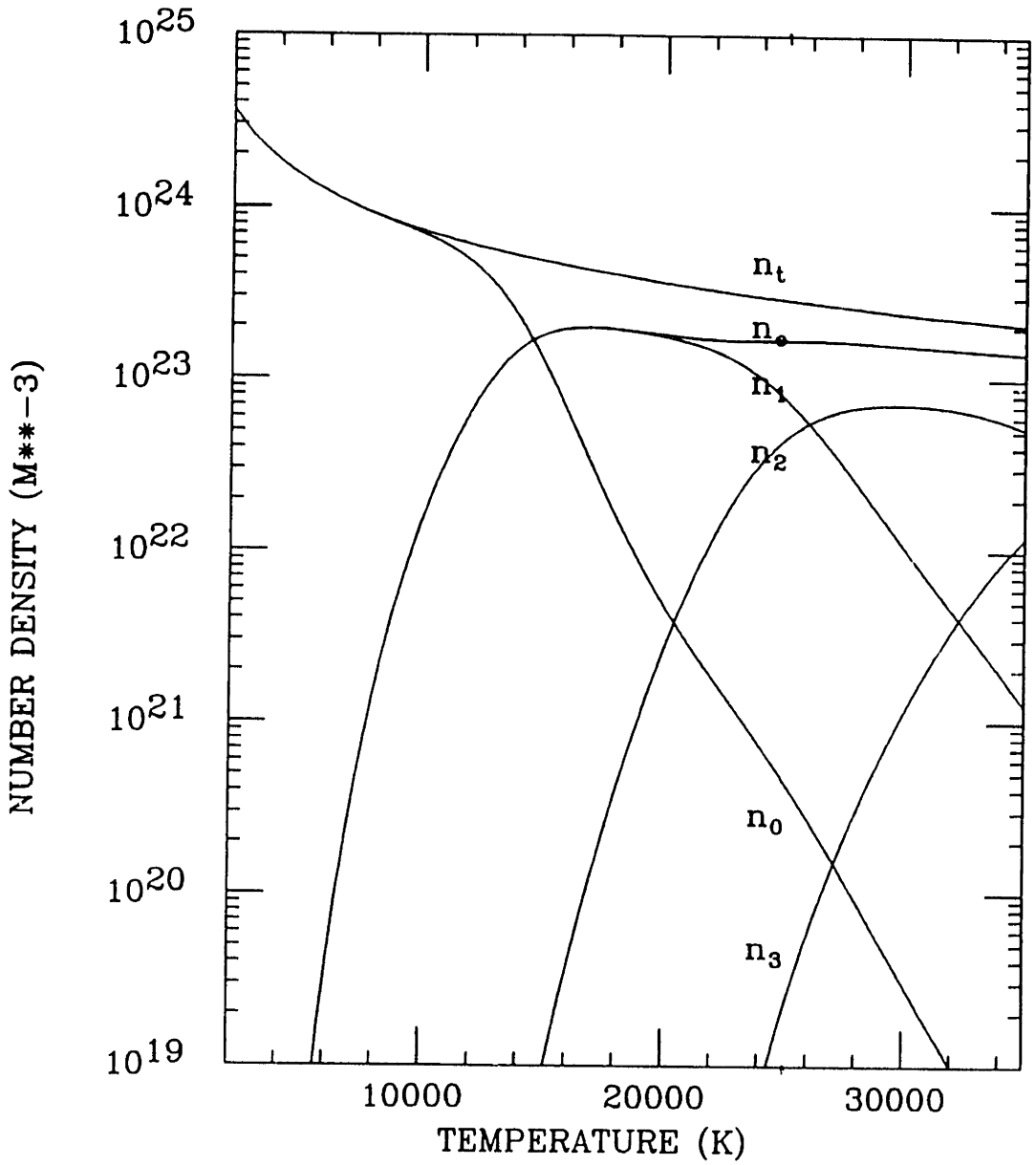

Figure I.A.1 Equilibrium composition of an LTE argon plasma versus temperature.

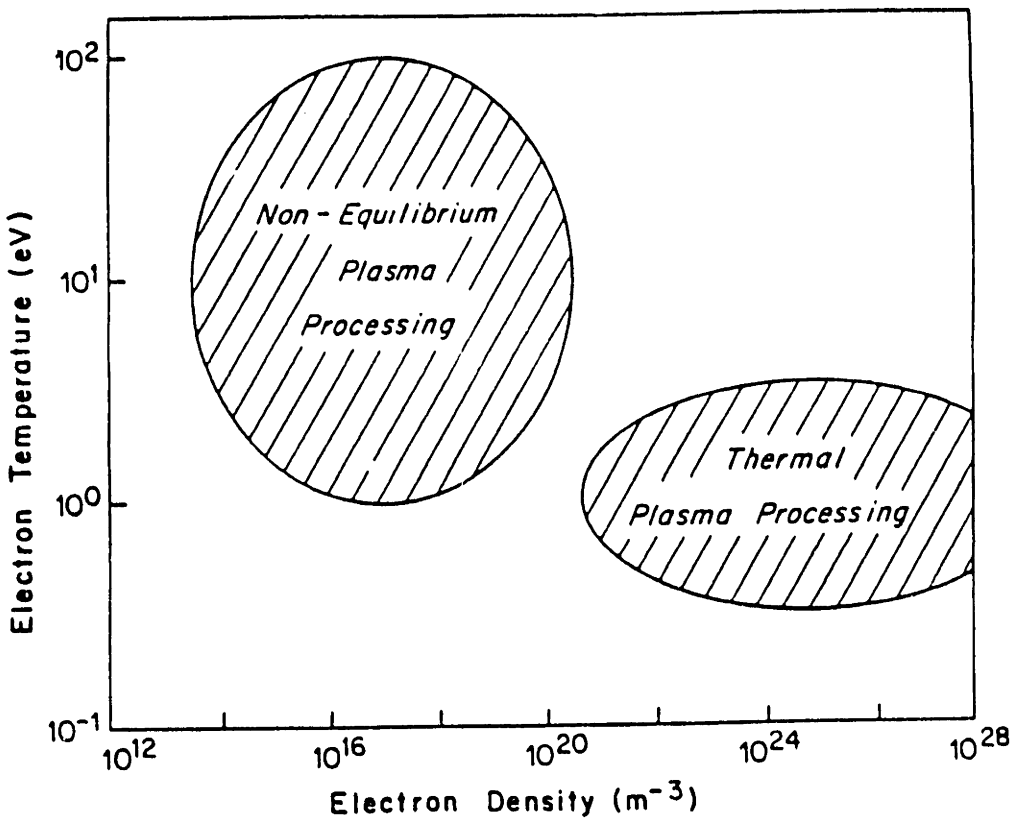

Figure I.A.2 Relative magnitudes of plasma parameters for thermal and non-equilibrium plasma processing of materials.(1)

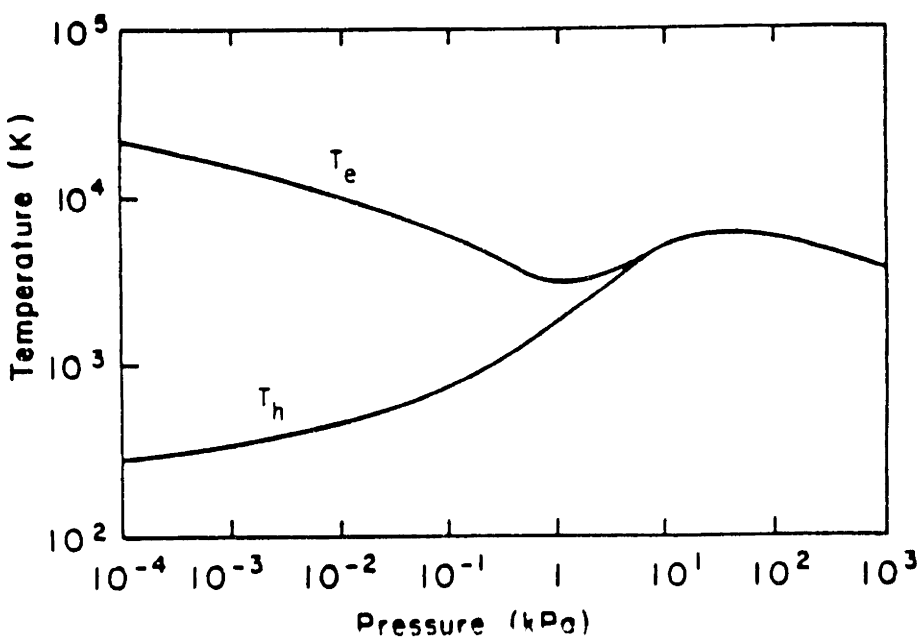

Figure I.A.3 Behavior of the electron temperature (T_e) and the heavy particle temperature (T_h) in an arc plasma.(1)

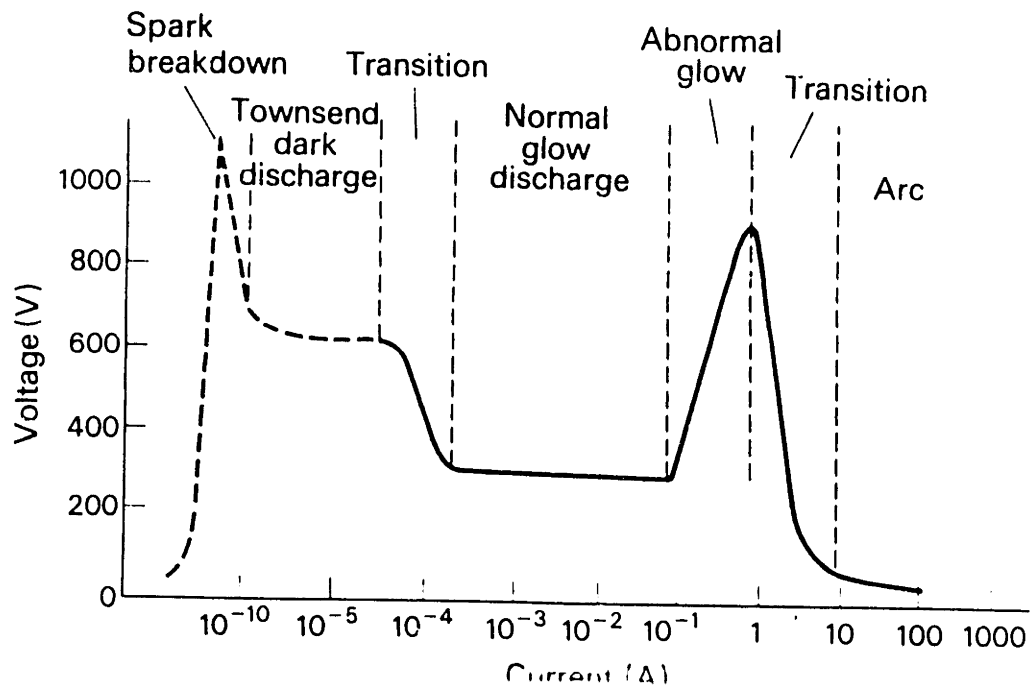

Figure I.A.4 Steady-state voltage -current characteristic of a discharge at about 100 N/m^2, showing order of magnitude values.(2)

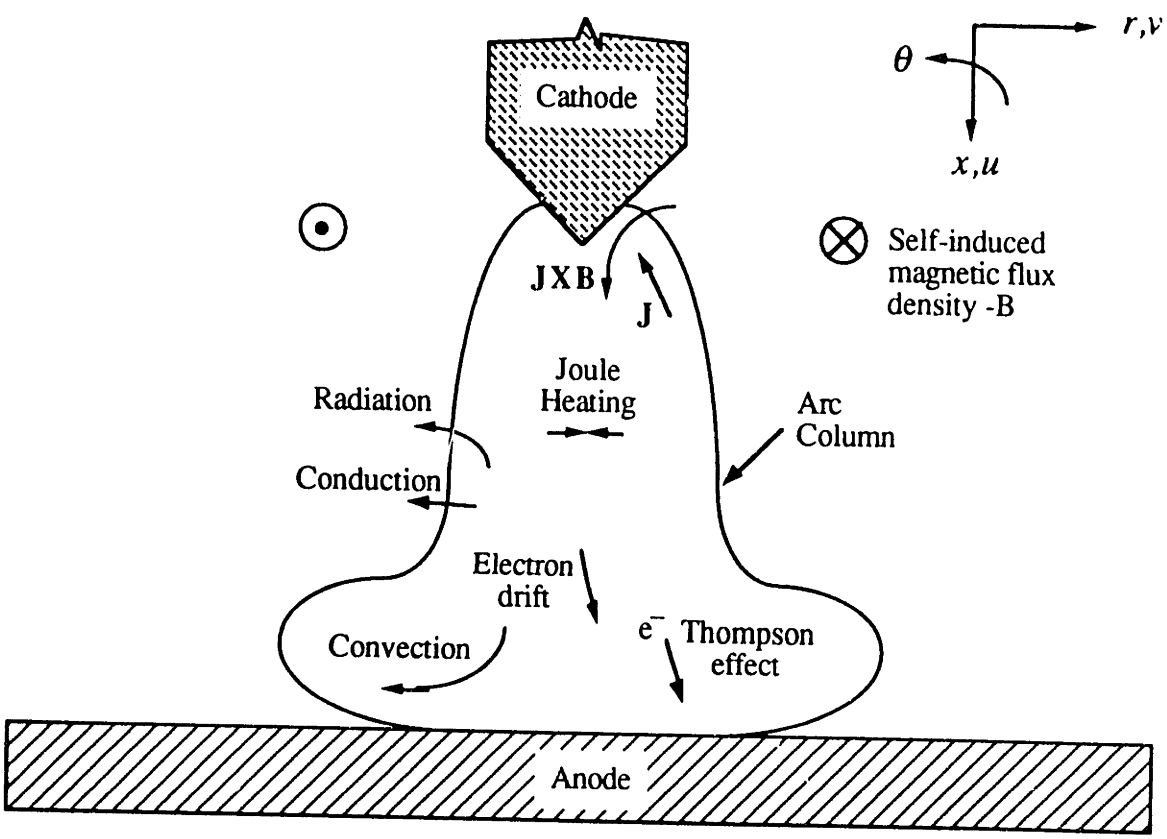

Figure I.A.5 Schematic sketch of an arc illustrating several key phenomena.

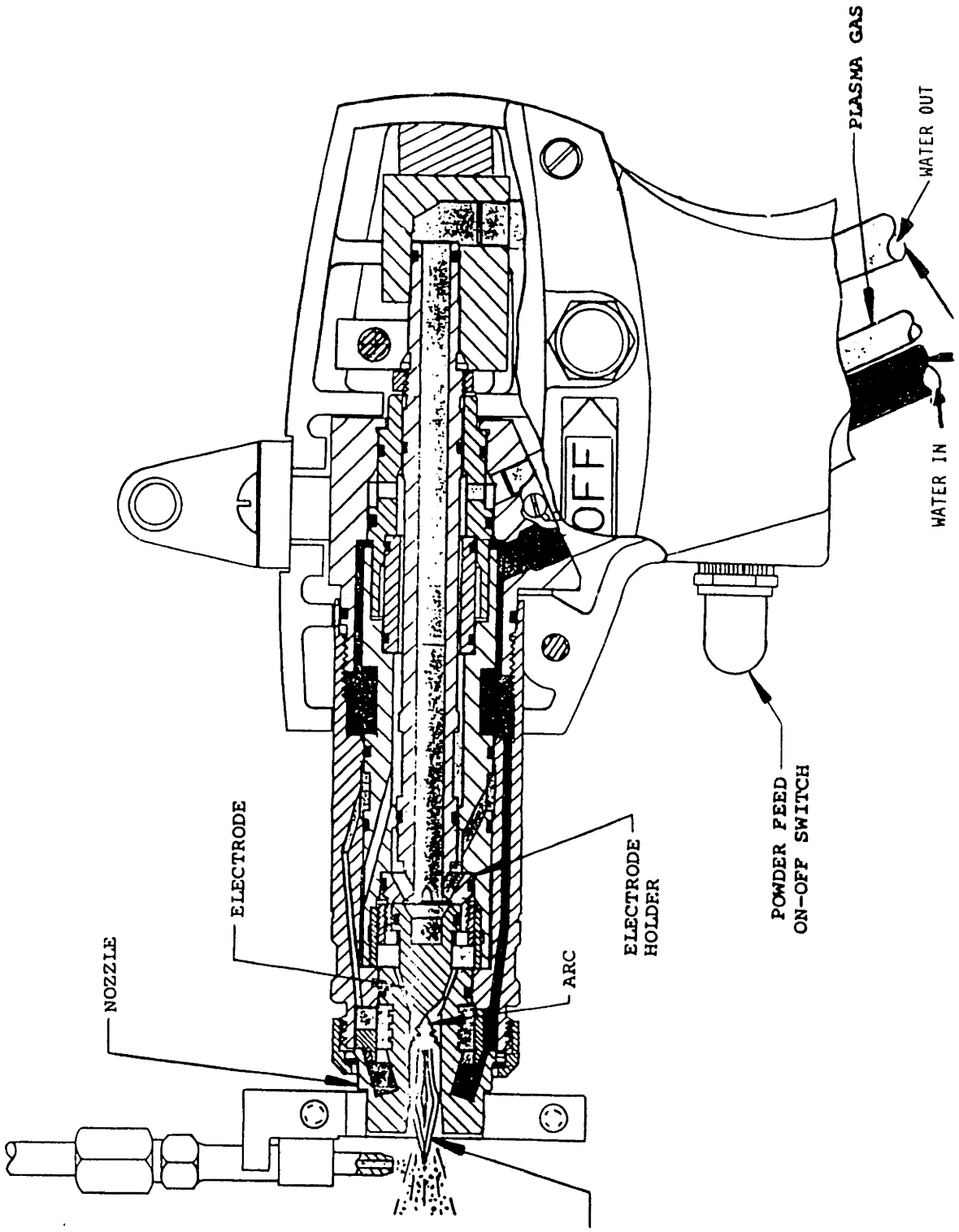

Figure I.B.1 Cut away view of a Metco 7mb plasma torch (courtesy Metco Corp., Westbury, NY)

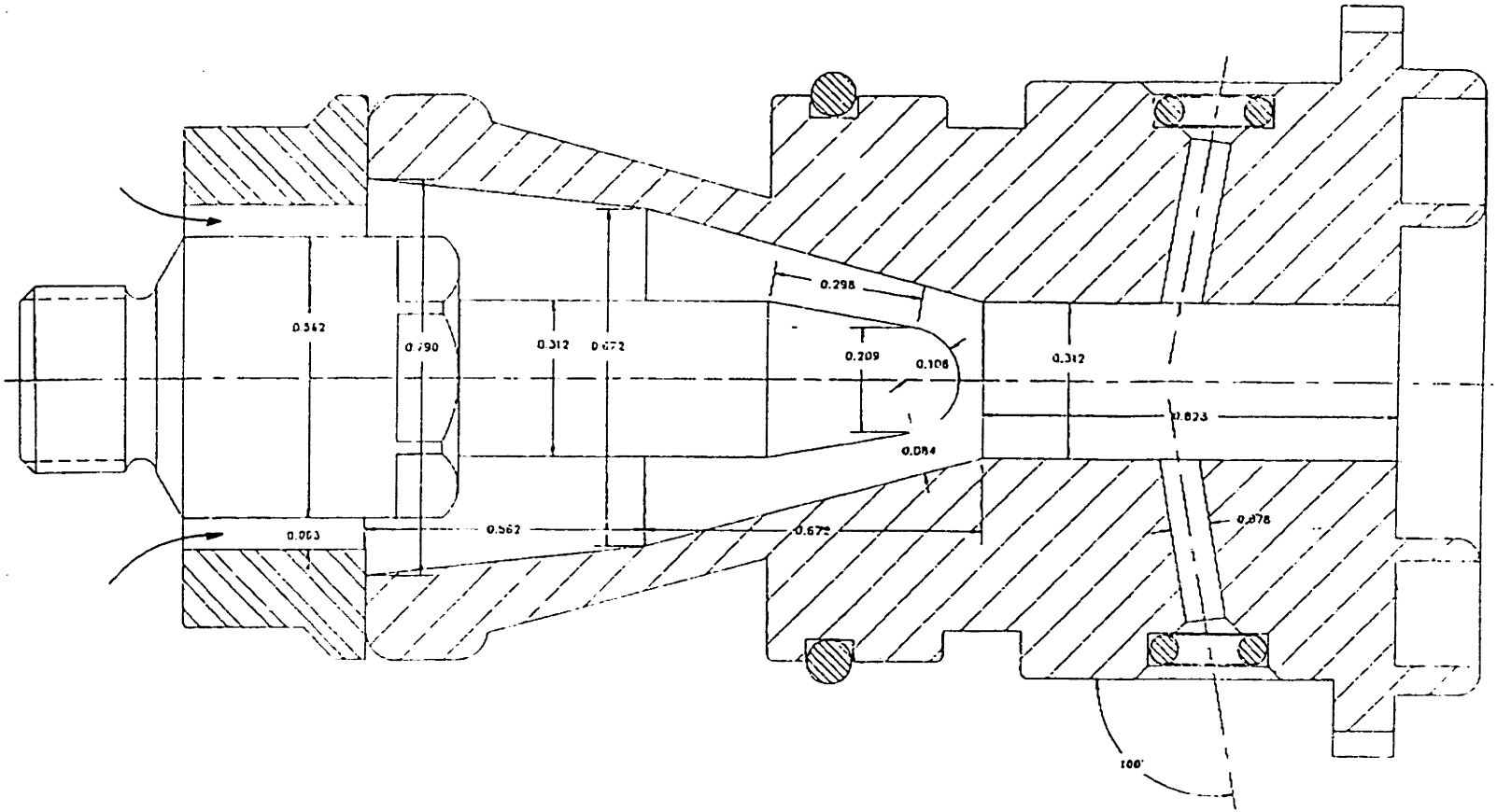

Figure I.B.2 Cutaway view of a Miller SG-100 torch (courtesy Miller Thermal, Inc. Tustin, CA)

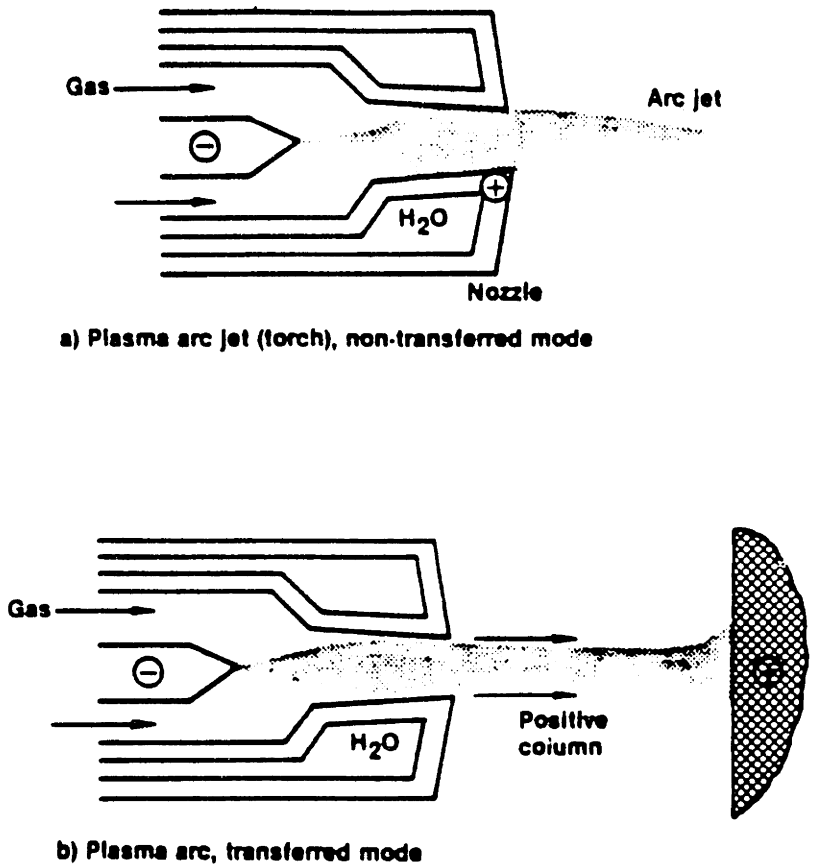

Figure I.B.3 Illustration of plasma torch modes of operation: (a) non-transferred mode. (b) transferred mode.[1]

CHAPTER II. MODELING OF THE PLASMA PLUME

As previously mentioned in Section I.A, the modeling of plasma phenomena has been done by dividing the problem up into separate regions, namely the plasma plume, plasma torch and the treatment of particles immersed in the plasma plume. This chapter deals with the modeling which has been done on the plasma plume alone. Section A is a brief review of the literature (which includes part of the work presented here) while Sections B - D present the modeling work in this specific area which has been done by the author in collaboration with Prof. A.H. Dilawari as well as Prof. J. Szekely. Their assistance is greatly appreciated, especially Prof. Dilawari who developed the plasma model which were used to complete this work.

II. A. LITERATURE SURVEY OF PLASMA PLUME MODELING

II.A.1. INTRODUCTION

Figure II.A.1 shows a schematic sketch of a plasma plume issuing from a plasma torch. It is seen that the hot plasma stream entrains the surrounding gas; the resultant heat and mass exchange has a major effect on the performance of the unit. Most of the phenomena are quite analogous to those well studied in conjunction with combustion processes, except for the much higher temperatures that exist in plasma plumes, particularly in the vicinity of the exit nozzle. These high temperatures and the corresponding ionization, dissociation, radiation and other phenomena are strongly non-linear.

II.A.2. EARLY WORK

The early modeling work on plasma plumes was based on momentum integral techniques of solution[1-3] and later on boundary layer simplifications of the governing equations[4-6]. The momentum integral methods contain numerous simplifications including the reliance on empirically determined velocity profile shapes, which limits their range of application. The boundary layer simplifications, while useful for example for laminar flow in a tube[4], are not applicable to recirculating flows which can occur when a jet impinges against a target or for high swirl cases.

McKelliget et. al[7] first applied the fully elliptic statement of the equations to the plasma jet. This work, however, included a number of simplifications including the assumptions of constant properties, no mixing with surrounding gases and the assumption of flat velocity and temperature profiles at the torch exit. These assumptions limited the accuracy of the numerical predictions significantly.

The later modeling work[8-18] has addressed transport phenomena in the plume based on a fully elliptic statement of the governing equations, including fully temperature dependent properties. This approach has been able to provide a reasonably good understanding of heat transfer and mixing in these systems. The governing conservation equations which describe laminar and turbulent flows are presented in Sections II.B and II.C.

Even at an early stage, however, a number of critical issues have emerged:

1. The computed temperature and velocity profiles in the plume were found to be strongly dependent on the conditions specified at the nozzle exit. In many instances these had to be assumed somewhat arbitrarily, or reliance had to be made on experimental measurements. A full closure of these problems was impossible until the flow issues within the torch could be addressed. This finding has provided additional impetus for the work that will be described in Chapters III and IV.

2. The behavior of laminar plasma jets discharging into a stagnant environment, such that laminar conditions prevail throughout, is readily modeled, since the constitutive equations may be stated unequivocally. Indeed, the quite good agreement between measurements and predictions, illustrated in Figures II.A.2 and II.A.3 further supports this assertion.

3. The situation is much less satisfactory when the plasma jet is turbulent upon exiting the torch or perhaps worse still, when turbulence is established within the plume at some position downstream from the exit nozzle. While the overall behavior of highly turbulent jets may be satisfactorily modeled using the so-called $K-\varepsilon$ model, the $K-\varepsilon$ model has a number of shortcomings. More specifically, it cannot capture the physics inherent in the non-isotropic, transient, fluctuating nature of turbulent flow.

To illustrate, Figure II.A.2 shows a schematic sketch of a short exposure time photograph of a transitional plasma jet[19]; in contrast , the behavior illustrated in Figure II.A.1 is a time smoothed image. The K–ε model can only provide such a time smoothed image. A practical consequence of this behavior is that macroscopic unmixedness, such as sketched in Figure II.A.2, is not readily modeled using this approach.

4. In formulating plasma plume problems, the correct representation of the entrainment boundary was found to be very important.

5. Finally, the critical comparison of measurements and predictions is always essential for testing any model, and relies on the available data base of experimental measurements. In principle we may measure three sets of parameters, namely, the plasma composition, temperature and velocity.

Composition may be measured with an enthalpy probe, which is generally limited to the lower temperature regions for the sake of safety. The velocity measurement techniques (the enthalpy probe, and laser doppler velocimetry) are still problematic at this point, though measurements based on the scattering of incident laser light show some promise[20]. Many temperature data (e.g. those based on emission spectroscopy) are subject to serious discussions, whether local thermodynamic equilibrium (LTE) has indeed been established. As a practical matter the assumption of LTE is thought to be reasonable in the axis of the plasma jet, but serious errors may be introduced upon postulating LTE in the fringe areas.

II.A.3 RECENT WORK

Concerning specific modeling results, some of the most recent work done in the modeling of plasma jets focuses primarily on atmospheric plasma jets, where the LTE assumption is more likely to hold. Some recent low pressure work based on a kinetic model has been done by Chang and Pfender.[17-18] While this work is quite interesting, the high cost of low-pressure spraying relative to atmospheric processes, and the potential of controlled atmosphere and gas shrouded spray torches may make these of more practical interest.

A number of interesting papers have appeared regarding the behavior of both laminar and turbulent plasma jets issuing into similar and dissimilar gas environments.

Chyou and Pfender[13] studied the effect of swirl flow in the plume for both hot and cold flows, and used the K–ε model of turbulence, modified to account for density fluctuations, to study the effect of some of the turbulence parameters. The comparison with experimental measurements was quite reasonable. Some interesting indications were that the exit swirl number was apparently a function of the torch operating conditions, and that a discrepancy in temperatures measured by enthalpy probes and emission spectroscopy could be ascribed to the difference between mass weighted and unweighted temperatures modeled by a probability density function.

A number of papers by Dilawari et al., describe the behavior of laminar, argon plasma jets in an argon and in a nitrogen environment. In both cases the good agreement with experimental data indicate the usefulness of the approach.[17-18] In the case of turbulent plasma jets,[19] however, the model was found to be rather less reliable although the comparison with measurements indicated the ability to represent the trends present in these systems.

II.A.4 DISCUSSION

The modeling work in the plasma plume has offered valuable insights into the effects of gas entrainment or engulfment of similar and dissimilar gases, the effect of the torch exit conditions, the role of swirl in the plume. The work so far provides a valuable tool for the prediction of particle behavior in the plasma plume. The shortcomings present, however, include the lack of knowledge of the turbulent entrainment process, which indicates the need for a more reliable model of the entrainment of ambient gas into the plume, and the uncertainties regarding the nozzle exit conditions, which leads to the investigation of transport phenomena inside plasma torches, a topic which is presented in Chapters III and IV.

Having reviewed the recent work in modeling plasma plumes, the next sections will present the results of the work done by the author in this area.

II. B. LAMINAR PLUME - ARGON IN NITROGEN

II.B.1. INTRODUCTION

Arc plasmas have been used to varying degrees for heating, surface treating, spraying and synthesis of materials. Because of this, much work has been done to generate a quantitative description of non-transferred arc plasma systems.[1-18] While this work has resulted in a good quantitative understanding of these systems, many uncertainties in both the modeling and experiments have not been fully resolved (e.g. the effect of turbulence, mixing with different gases, etc). To do this effectively, an interactive effort was made to compare experiments and measurements in which the number of uncertainties have been reduced, so that a good understanding of the physics can be developed. In an earlier work done in this laboratory,[14] a simple system in which a laminar argon plasma jet discharged into an argon environment was studied so as to eliminate the complexities of turbulence and mixing of dissimilar gases, and the comparison of measurements and predictions was quite good. Further elements of this work introduce additional complexities into the system so the understanding may be developed in a step-wise manner. The purpose then, of this study is to extend the simpler system to a the case of an argon plasma jet mixing into a nitrogen environment. This will allow us to test the validity of the model and measurements to account for the effect of nitrogen which is entrained into a laminar jet.

II.B.2. EXPERIMENTAL WORK

The experimental work was performed by investigators at the Idaho National Engineering Laboratory (INEL). The work of B. A. Detering and C. B. Shaw is specifically acknowledged.[14-15] As the experimental situation is critical to the model, some description of it is given in the following section.

II.B.2.a. Equipment

The experimental apparatus consisted of a non-transferred arc plasma torch (Figure II.B.1) and an atmosphere control chamber (Figure II.B.2). The torch used a 9.5 mm diameter cone-shaped, thoriated tungsten cathode which was mounted in a water-cooled copper support. The working gas entered the cathode region through a distribution ring that provided swirl flow for arc stabilization. The anode was a water cooled copper

cylinder with an inside diameter of 12.7 mm and an overall length of 29 mm. The body of the plasma torch (76 mm diameter) protruded into the atmosphere control chamber as shown in Figure II.B.2. The chamber was approximately a cube with inside dimensions of 0.5 m, which was continuously purged from several locations. As shown in the figure, one purge line supplied gas co-axially with the plasma torch from 19 holes (1.3 mm diameter) equally spaced on a circle of 120 mm diameter. The second purge line supplied gas to distribution tubes which run parallel to the torch axis along four edges of the box. These discharged the gas through 10 equally spaced holes (1 mm diameter) in each of the four tubes so that the gas flowed radially inward toward the torch axis. The total purge flow rate to the chamber was maintained at 1.88 std. m^3/hr or 1.66 std. m^3/hr of nitrogen for all of the runs. The exhaust duct protruded into the chamber and provided baffling to prevent recirculation. View ports on the sides of the box allowed visual observation of the plasma plume at right angles to the torch axis.

II.B.2.b. Temperature Measurements

Several different emission spectroscopy techniques can be used to determine plasma temperatures, including: absolute measurement of continuum emission or a single-line emission, relative measurement of several line emissions, line width measurements, and the Larenz method.(21-24) In these experiments, the absolute intensity of the neutral argon line at 430.01 nm and continuum emission at 430.80 nm were observed with a 1 meter scanning monochrometer, intensified silicon photodiode array detector and optical multichannel analyzer.(25) The photodiode array was calibrated using an NBS calibrated tungsten ribbon lamp. The data processing procedure involved background subtraction, correction for pixel to pixel response, and absolute intensity calibration. The resulting data of emission intensity vs. the transverse coordinate were fit to an equation (which is the product of a second order polynomial and a displaced Gaussian) by a least squares procedure. The resulting equation was used to generate a 100 point data set for input to the discrete Abel inversion procedure.(26) The resulting emissivities are used to determine the plasma temperature via a solution of the Saha equation, the ideal gas law, and the equation describing line emission.(24) Spectral measurements were obtained at 2.0 mm increments from an axial position of 1.0 mm (downstream of the torch exit) to a distance of 49.0 mm.

Data were obtained with the torch operating at the plasma gas flows and power levels shown in Table II.B.I. Operating efficiency was determined by monitoring the input

power (current and voltage at the torch) and the torch coolant energy loss (coolant flow, inlet and outlet temperature).

II.B.2.c. Error Estimates - Net Power

The accuracy of determining the net power to the plasma is determined by the accuracy of the measurements of the current, voltage, coolant flow, and coolant inlet and outlet temperatures. The experimental uncertainties and resulting possible errors in the efficiency for the three currents are summarized in Table II.B.II, which shows that the efficiency (the ratio of net power to input power) is determined to within 11.8-20 percent, resulting in a confidence limit of ±3.8-4.4 percentage points, depending on the power level.

These calculations do not include the loss of radiant energy (from the cathode and plasma column) that is emitted through the exit of the torch. Depending on the location within the torch, the view factor varies from a solid angle of 12 degrees at the cathode to nearly 180 degrees at the exit. The magnitude of this energy loss is strongly dependent on the temperature within the column. For the operating conditions shown in Table II.B.I this could be as large as the measured errors. A model of the plasma column temperature profile is required to obtain a better estimate of this error.

II.B.3. MODEL DESCRIPTION

The mathematical description of an argon plasma jet has previously been described for the case of a laminar jet discharging into an argon atmosphere.(14)

Figure II.B.3 shows the integration domain used in the calculation, which is essentially the plasma jet exiting a nozzle into a large chamber. The flow area in the chamber region is chosen to be large enough to be equivalent to a plasma jet issuing into an infinite nitrogen environment.

Since the Reynolds number in the torch based on the nozzle diameter is well below 2000, the flow in the torch is assumed to be laminar there. Additionally, the nature of flow in the plume may be estimated as follows: The calculations show a velocity of 60 m/s, temperature of 8000 K, density .0.061 kg/m^3 and viscosity of 2.5x10^{-4} kg/m-s at an axial location of 162 mm in the plume, resulting in a Reynolds number (based on axial distance -

z) of 2260. Since the laminar-turbulent transition for a free jet occurs at a Reynolds number of about 100,000, the flow in the plasma jet can reasonably be assumed as laminar. Additionally, the assumptions of local thermal equilibrium in the plasma, and an optically thin plasma are applied. Thus for the axi-symmetric case, the governing conservation equations for the two-gas system are as follows:

Continuity:

$$\frac{\partial(\rho u)}{\partial z}+\frac{1}{r}\frac{\partial(\rho r v)}{\partial r}=0 \qquad [II.B.1]$$

Axial Momentum:

$$\frac{\partial(\rho u^2)}{\partial z}+\frac{1}{r}\frac{\partial(\rho r u v)}{\partial r}=-\frac{\partial P}{\partial z}+2\frac{\partial}{\partial z}\left[\mu\left(\frac{\partial u}{\partial z}\right)\right]+\frac{1}{r}\frac{\partial}{\partial r}\left[r\mu\left(\frac{\partial u}{\partial r}+\frac{\partial v}{\partial z}\right)\right] \qquad [II.B.2]$$

Radial Momentum:

$$\frac{\partial(\rho u v)}{\partial z}+\frac{1}{r}\frac{\partial(\rho r v^2)}{\partial r}=-\frac{\partial P}{\partial r}+\frac{\partial}{\partial z}\left[\mu\left(\frac{\partial v}{\partial z}+\frac{\partial u}{\partial r}\right)\right]+\frac{2}{r}\frac{\partial}{\partial r}\left[r\mu\left(\frac{\partial v}{\partial r}\right)\right]-\mu\frac{2v}{r^2} \qquad [II.B.3]$$

Thermal Energy:

$$\frac{\partial(\rho u h)}{\partial z}+\frac{1}{r}\frac{\partial(\rho r v h)}{\partial r}=\frac{\partial}{\partial z}\left(\frac{k}{C_p}\frac{\partial h}{\partial z}\right)+\frac{1}{r}\frac{\partial}{\partial r}\left(\frac{rk}{C_p}\frac{\partial h}{\partial r}\right)-S_R \qquad [II.B.4]$$

Species:

$$\frac{\partial(\rho r u m)}{\partial z}+\frac{1}{r}\frac{\partial(\rho r^2 v m)}{\partial r}=\frac{\partial}{\partial z}\left(D\frac{\partial(rm)}{\partial z}\right)+\frac{1}{r}\frac{\partial}{\partial r}\left[Dr\left(\frac{\partial(rm)}{\partial r}\right)\right] \qquad [II.B.5]$$

In these equations u, v; t, r are the velocities and coordinates in the axial and radial directions respectively. The plasma properties are ρ, density; μ, viscosity; k, thermal conductivity; C_p, heat capacity; and D, the diffusion coefficient of argon in nitrogen. The other dependent variables are h, enthalpy; P, pressure; m, mass fraction, and T, temperature.

To completely specify the problem the conditions at each boundary in Figure II.B.3 must be specified. These are summarized in Table II.B.III. Two boundaries in the figure are critical to the formulation. The first is at the torch exit, where the chosen velocity and temperature profiles (the second derived from the experiment) must specify the proper amount of mass and enthalpy which exit the torch. This is why the determination of the torch efficiency is so critical to the calculation. The second is the external or "free" boundary at which nitrogen in the chamber is entrained into the jet. At present, the jet is assumed to be entraining pure nitrogen at this boundary, and in fact, gas samples taken at this location have indicated this condition to be reasonable.

The temperature dependent property values for pure argon and nitrogen plasma were taken from the tabulated data of Liu[27] and the radiation loss was adapted from Evans and Tankin.[28] Additionally, the diffusion coefficient for nitrogen in argon was taken from the literature.[29] These were included in the program as tables or equations. The thermodynamic properties of the mixture were estimated by weighting them according to the mass or mole fraction of each component. The transport properties of the mixture were estimated from the properties of the pure components using the equation suggested by Wilke.[30]

The solutions were obtained using a computer model developed by Dilawari and Szekely,[8-12] based on the 2/E/FIX code of Pun and Spalding.[31] The non-uniform grid used in the calculations was concentrated in the area of steepest gradients and used 9X9 grids inside the torch and 21X30 nodes in the plume of the jet. A study on grid refinement showed that the number of grids chosen was sufficient to give adequate numerical accuracy. A typical run required 45 minutes of CPU time on a MicroVax II.

II.B.4. COMPARISON OF MEASUREMENTS AND CALCULATIONS

Figure II.B.4 (a) shows the radial temperature profiles for run BES25 (250 amps, 18.8 volts and .59 scm/hr argon). Note: η_t is the torch efficiency, P_t is the torch power and z is the axial coordinate. Figure II.B.4 (b) shows the comparison between BES25 and BES23 which is performed in a pure argon atmosphere. This figure illustrates the effect of the entrained nitrogen on the plume temperature. Because the dissociation of nitrogen gives it a higher heat capacity than argon (see Figure II.B.9), the plume temperature falls more quickly when the jet issues into nitrogen than when into pure argon. This is seen in both

the experiments and measurements in Figure II.B.4 (b). This figure also shows the calculated argon concentration for BES25.

Figures II.B.5(a) and II.B.5(b) show the radial and axial profiles of temperature in the plume for run BES26 in which the torch current and voltage are 250 amps and 19.1 volts respectively, and the torch flow rate was .83 scm/hr of argon. Both the radial and axial profiles show quite good agreement between the predicted and measured temperatures. Note however, (see Table II.B.1) that the experimental efficiency determined for this case (22.0%) is lower than expected. In the argon atmosphere (run BES24), the measured efficiency is 6.4 points higher. This difference could not be reconciled with the torch exit temperatures (T_{max}), so the efficiency used in the calculation is 28%. This is justified by the fact that in all other cases the difference between the torch efficiency in the nitrogen atmosphere and that in an argon atmosphere was within the range of the experimental error. Additionally, Figure II.B.5(b) shows the calculated concentration of argon, which is seen to vary almost linearly between 1 and .8 over the length of the plume.

Figures II.B.6(a) and II.B.6(b) show the radial and axial temperature profiles for run BES29 (500 amps, 18.6 volts, and 0.59 scm/hr argon). The maximum discrepancy is only about 15% and occurs at the fringes of the temperature measurement where the plume has entrained a significant amount of nitrogen. Additionally, the temperature measurements can be seen (in the axial profile) to be nearly constant near the torch tip, because the experimental technique appears to be unable to measure temperatures above 13,000 K. The variation of argon concentration in the plume is seen to be about the same as in Figure II.B.5 (b).

Figure II.B.7 (a) shows the radial temperature profiles for run BES30 (500 amps, 19.3 volts and 0.83 scm/hr argon). Here again the agreement between measurements and predictions is quite good. Figure II.B.7 (b) shows another comparison between the Ar/N_2 system (BES30), and the pure argon system (BES28). The same trends noted above are seen though the effect of nitrogen entrainment is more apparent in the experimental temperatures. The calculated concentration of argon in the plume is also shown.

Figure II.B.8 (a) shows the radial and axial temperature profiles for run BES34 (750 amps, 20.3 volts and 0.83 scm/hr argon). Figure II.B.8 (b) shows the comparison between BES34 and BES32 which is performed in a pure argon atmosphere. The

agreement between measurement and predictions at temperatures below 13,000 K is good, but as seen in the axial profile the measured temperatures upstream of the 10 mm axial position are seen to flatten out at 13,000 K. Again however, the maximum discrepancy is only about 15%.

II.B.5. CONCLUSIONS

The comparison of measurements and predictions is quite good, with the maximum discrepancy in the 1-17% range. The results show that the model does quite well in predicting the behavior of an argon-nitrogen system for a laminar plasma jet, indicating that the physics of laminar diffusion/mixing are adequately represented by the property values and methods used.

The main source of discrepancies in the results appears to be the inability of the measurements to record temperatures above 13,000 K and the inability of the measurement technique used to account for the changes in emission characteristics of argon when it is diluted by argon. This second problem could also arise from an inability of the model to fully account for the mixing in the jet.

This work has demonstrated the capability of modeling the behavior of a plasma jet which is laminar in nature and issues into a dissimilar gas. The foundation laid here serves as a basis to further explore the nature of turbulence in a plasma jet and eventually to be able to describe a torch well enough to provide useful insight into its use in any given materials process.

II. C. TURBULENT PLUME - ARGON IN AIR

II.C.1. INTRODUCTION

In the previous section, as well as in a number of previous studies, results have been published dealing with a comparison of experimentally measured and theoretically predicted temperature fields in plasma systems.[1-16] In many instances the agreement between measurements and predictions has been quite good, if not fully quantitative, providing a reasonable perspective regarding our ability to represent these phenomena in terms of mathematical models. Most of the measurements pertaining to plasma systems

have been carried out in the high temperature regimes, where spectroscopy has been the logical tool for temperature measurement. At present much less information is available regarding the behavior at lower temperatures, say in the 9000 K – 2000 K range.

The published data of Brossa and Pfender,[32] in which an enthalpy probe was used to measure the temperature, velocity and concentration profiles in an argon plasma discharging into air, provide an excellent basis for performing such a comparison, which is the purpose of this section.

II.C.2. STATEMENT OF THE PROBLEM

II.C.2.a. The Experimental Work.

The experimental measurements were obtained, using a commercial DC plasma torch with a slightly diverging nozzle having an inside diameter of 7.88 mm at the exit. The key parameters of the experimental runs are summarized in Table II.C.I. As discussed in reference 32, the temperature measurements were obtained using an enthalpy probe, while the concentration profiles were determined via chemical analysis of the samples taken from the system. A number of velocity data were obtained when the probe was applied as a Pitot tube. The data thus obtained provided information simultaneously on the temperature and concentration profiles in a turbulent plasma jet. Additionally a limited amount of information was given for velocity in the jet.

II.C.2.b The Modeling Equations.

In the plasma torch, current flows through the plasma from the anode to the cathode; joule heating and electromagnetic forces increase the axial momentum of the gas, resulting in the plasma jet. The calculation domain used is shown in Figure II.C.1. The assumptions used in the model are as follows:

1. The plasma plume is assumed to be in local thermodynamic equilibrium (LTE).
2. The plume is assumed to be symmetric about the torch axis so the problem may be written as 2–D axi-symmetric.
3. The temperature, composition, and velocity profiles at the inlet boundary of the torch are assumed to be known.
4. The plasma plume is assumed to be optically thin to radiation.

5. The flow is turbulent and and the turbulence is assumed to be isotropic.
6. The effects of compressibility are negligible.
7. The density fluctuations due to turbulence are considered to be negligible.

To obtain the theoretical predictions, a previously published model,[8-9] describing the intermixing of a turbulent plasma jet discharging into a large volume of air was used. The statement of the model was made using the axi-symmetric turbulent Navier-Stokes equations, in conjunction with the K-ε model for turbulence,[33] together with the appropriate differential thermal energy balance and mass species conservation relationships. The actual equations used are summarized as follows:

Mass:

$$\frac{\partial(\rho u)}{\partial z}+\frac{1}{r}\frac{\partial(\rho r v)}{\partial r}=0 \qquad [II.C.1]$$

Momentum:

Axial- u

$$\frac{\partial(\rho u^2)}{\partial z}+\frac{1}{r}\frac{\partial(\rho r u v)}{\partial r}=-\frac{\partial P}{\partial z}+2\frac{\partial}{\partial z}\left[\mu_{eff}\left(\frac{\partial u}{\partial z}\right)\right]+\frac{1}{r}\frac{\partial}{\partial r}\left[r\mu_{eff}\left(\frac{\partial u}{\partial r}+\frac{\partial v}{\partial z}\right)\right] \qquad [II.C.2]$$

Radial- v

$$\frac{\partial(\rho u v)}{\partial z}+\frac{1}{r}\frac{\partial(\rho r v^2)}{\partial r}=-\frac{\partial P}{\partial r}+\frac{\partial}{\partial z}\left[\mu_{eff}\left(\frac{\partial v}{\partial z}+\frac{\partial u}{\partial r}\right)\right]+\frac{2}{r}\frac{\partial}{\partial r}\left[r\mu_{eff}\left(\frac{\partial v}{\partial r}\right)\right]$$

$$-\mu_{eff}\frac{2v}{r^2} \qquad [II.C.3]$$

Energy:

$$\frac{\partial(\rho u h)}{\partial z}+\frac{1}{r}\frac{\partial(\rho r v h)}{\partial r}=\frac{\partial}{\partial z}\left(\frac{\mu_{eff}}{\sigma_h}\frac{\partial h}{\partial z}\right)+\frac{1}{r}\frac{\partial}{\partial r}\left(\frac{r\mu_{eff}}{\sigma_h}\frac{\partial h}{\partial r}\right)-S_R \qquad [II.C.4]$$

Species:

$$\frac{\partial(\rho r u m)}{\partial z}+\frac{1}{r}\frac{\partial(\rho r^2 v m)}{\partial r}=\frac{\partial}{\partial z}\left(\frac{\mu_{eff}}{\sigma_m}\frac{\partial(rm)}{\partial z}\right)+\frac{1}{r}\frac{\partial}{\partial r}\left[\frac{\mu_{eff}}{\sigma_m}r\left(\frac{\partial(rm)}{\partial r}\right)\right] \qquad [II.C.5]$$

Kinetic energy of turbulence

$$\frac{\partial(\rho u K)}{\partial z}+\frac{1}{r}\frac{\partial(\rho r v K)}{\partial r}=\frac{\partial}{\partial z}\left(\frac{\mu_{eff}}{\sigma_K}\frac{\partial K}{\partial z}\right)+\frac{1}{r}\frac{\partial}{\partial r}\left(r\frac{\mu_{eff}}{\sigma_K}\frac{\partial K}{\partial r}\right)+G-\rho\varepsilon \qquad [II.C.6]$$

Dissipation of turbulent kinetic energy

$$\frac{\partial(\rho u \varepsilon)}{\partial z}+\frac{1}{r}\frac{\partial(\rho r v \varepsilon)}{\partial r}=\frac{\partial}{\partial z}\left(\frac{\mu_{eff}}{\sigma_\varepsilon}\frac{\partial \varepsilon}{\partial z}\right)+\frac{1}{r}\frac{\partial}{\partial r}\left(r\frac{\mu_{eff}}{\sigma_\varepsilon}\frac{\partial \varepsilon}{\partial r}\right)+\frac{\varepsilon}{K}(C_1 G-\rho\varepsilon C_2) \qquad [II.C.7]$$

In the above equaltions r, v; z, u are the coordinates and velocities in the radial and axial directions, h is the enthalpy, m is the mass fraction of Argon, and K and ε are turbulent kinetic energy and dissipation. μ_{eff} is the effective viscosity given by the sum of the laminar and turbulent viscosity, μ_t.

C_D, C_1, and C_2 are the turbulence constants, σ_h, σ_m, σ_K, σ_ε are the turbulent Prandtl numbers for enthalpy, mass, turbulent kinetic energy and dissipation respectively, and the generation term, G, is given by,

$$G=2\mu_t\left[\left(\frac{\partial u}{\partial z}\right)^2+\left(\frac{\partial v}{\partial r}\right)^2+\left(\frac{v}{r}\right)^2+\frac{1}{2}\left(\frac{\partial u}{\partial r}+\frac{\partial v}{\partial z}\right)^2\right] \qquad [II.C.8]$$

The constants for the K–ε model are the values recommended by Pun and Spalding and are given in Table II.C.II.

In the modeling of plasma jet systems the correct statement of the boundary conditions is perhaps one of the most critical issues. The boundary conditions used are summarized in Table II.C.III. In the present case we postulated power law type profiles for the temperature and the velocity on line GA of Figure II.C.1, ensuring that both the overall energy balance and material balance were satisfied at the torch exit. The actual

computational procedure was identical to that described in earlier papers.[8-9] The modeling equations contained no adjustable parameters; the constants in the K-ε model were the standard values cited in the literature.[31] Legitimate questions may be raised concerning whether this approach should be immediately applicable to plasma systems. However, the accuracy of current available measurements on plasma makes an assessment rather difficult at this time.

The thermodynamic and transport properties of argon and air are taken from the literature.[27-28,34,35] The thermodynamic properties of the argon/air mixture are then calculated using the mass fraction (e.g. for enthalpy) or mole fraction (e.g for density) of each component while the transport properties are calculated using the semi-empirical formula suggested by Wilke.[30] Since the system is turbulent, we expect the turbulent viscosity and thermal conductivity to dominate the molecular values so that the model is not very sensitive to the method of calculating the transport properties of the mixture. For the thermodynamic properties, the method essentially assumes ideal mixing, which holds for most gases. This assumption may be investigated further by solving the equilibrium problem for the composition and properties of the argon/air mixture as outlined by Fauchais et. al.[36]

II.C.3. COMPARISON OF THE MEASUREMENTS WITH PREDICTIONS

Figures II.C.2 - II.C.10 show the comparison between measurements and predictions. Figures II.C.2 - II.C.3 show the comparison between the experimentally measured and the theoretically predicted axial temperature profiles. It is seen that the agreement is quite good, for quite a range of conditions, with the model somewhat over-predicting the experimental data. Three possible explanations for this will be discussed subsequently.

Figures II.C.4 - II.C.5 show a corresponding comparison between the experimentally measured and theoretically predicted mole fraction of argon at the axis. Here again, there is quite good agreement between measurement and predictions, with the experimental points falling somewhat below the theoretically predicted curve.

Figures II.C.6 - II.C.7 compare the experimental and calculated isotherms for one 450 amp and one 600 amp case. The degree of radial spreading of the jet seen in the experiments and calculations is quite comparable for both cases.

Figures II.C.8 - II.C.9 are the corresponding isocontours for argon concentration. Again the model appears to predict the radial distribution of argon quite well.

Figure II.C.10 shows the calculated radial temperature profiles compared against the experimentally measured points taken from Figures II.C.3 and II.C.7. This figure indicates rather good agreement between the two sets of radial profiles. This situation may be seen as somewhat fortuitous, as some other cases not reproduced here show rather poorer agreement.

Figure II.C.11 shows the result of a sensitivity study, in which two different sets of torch exit temperature and velocity profiles were used. The form of the two profiles is taken to be the following:

$$A(r) = A_{max}\left(1 - \left(\frac{r}{r_n}\right)^n\right)$$

In the base case T_{max} , U_{max} , and n are taken to be 11,500 K, 720 m/s and 3.0 respectively. In the next case they are chosen as 10,700 K, 670m/s and 4.0 respectively. The figure shows that while the temperature is affected near the torch exit, those downstream are nearly unchanged.

From this and other sensitivity analyses we determined that within a reasonable range the results far downstream of the exit are not strongly dependent on the postulated profiles. Nearer the exit, the calculations must rely on measurements to correctly prescribe the temperature profile so that the velocity profile may be deduced from the requirements of the heat and mass balance.

In view of the paucity of information on the velocity profiles in plasma jet systems it is desirable to compare the predictions of the model in this regard. This is done in Figure II.C.12 which shows the experimentally measured normalized jet diameter plotted versus the argon gas flow rate for the 400 and 600 amp cases. The jet diameter is defined as the portion of the jet at a given axial location (z =35mm) which has velocities over 100 m/s and is normalized by the nozzle bore diameter. The model tends to under-predict the plasma velocities resulting in a maximum discrepancy of 10% in the normalized jet diameter.

It is seen that the model appears to predict both the absolute values and the observed trends quite well.

II.C.4. DISCUSSION

A comparison is presented between experimentally measured and theoretically predicted axial temperature and concentrations profiles for a turbulent argon jet discharging into air.

The measurements were interesting, because they were obtained using quite straightforward classical means, so that the actual errors would be quite well defined. Indeed, these careful measurements also contained an error assessment, which are given in Figures 12-13 of reference 32. It is seen that both the integrated flow rate and the energy input appear to be less than what was postulated on the basis of the direct measurement of these quantities. Interestingly, the model predictions also appear to follow the same trend, so that the discrepancy between the measurements and the predictions may be partially explained on this basis.

Additional reasons for the discrepancy may include the uncertainties involved in determining the torch efficiency which as was shown in section II.B.2.C may lead to errors in the efficiency in the range of ±2-4 percentage points. This can lead to uncertainties of 5-10% in the enthalpy available in the plasma plume.

Another reason for the disagreement may be the intrusive nature of the enthalpy probe which may very well affect the temperature, velocity and argon concentrations in the plasma plume as measurements are being made.

One may conclude that modeling of these systems has now reached the state that predictions for the temperature profiles and mixing in these systems may be made with a degree of confidence, appropriate at least for engineering purposes. The results presented in this short paper support this contention for turbulent systems – even in the low temperature range.

Clearly a great deal more work needs to be done on these systems, regarding the more micro aspects, such as stability and for defining the conditions in the torch exit region.

II.D. TURBULENT PLUME - ARGON IN ARGON

II.D.1 INTRODUCTION

In the preceeding section the behavior of a turbulent plasma plume discharging into an air atmosphere was addressed. In that case, the plume entrains a large quantity of air which has a higher heat capacity than does argon (see e.g. Figure II.B.9, where this was illustrated for argon-nitrogen systems). This entrainment causes a rapid drop in the plasma temperature which may be undesirable in situations where for instance it is hoped to heat and melt a particle in the plasma plume. For this reason it can be useful to control the atmosphere into which the plasma torch is discharged.

A set of temperature and velocity fields has been obtained experimentally by Capetti and Pfender for a Metco 7MB plasma torch operating in a turbulent mode.(37) These provide another excellent basis for testing the plasma plume model. Such a test is presented in the following section.

II.D.2. EXPERIMENTS

The Metco torch which was used for the turbulent, argon in air experiments of Brossa and Pfender(32) has been used by Capetti and Pfender to obtain a corresponding set of experimental data for the operating conditions shown in Table II.D.1. An enthalpy probe was used to obtain both plasma temperature and velocity in the plume. The experiments and the associated errors are discussed in detail in the aforementioned papers, and so are not detailed here. It is important to note, however, that the experimental errors estimated from an integrated heat balance are in the range of ±10-20%, indicating the accuracy which can be expected of the measurements.

II.D.3. MODELING WORK

The modeling work is essentially the same as that presented in section II.C.2.b except the species equation [Equation II.C.5] can be neglected because a single gas (argon) system is being represented. In addition, the complications introduced by gas mixtures do not appear, although the plume does entrain argon from the controlled atmosphere which will quench the plasma plume somewhat.

The calculation domain is identical to that shown in Figure II.C.1 and the boundary conditions are identical for the remaining equations.

II.D.3.a Torch Exit Conditions - Parametric Study

As shown in Section II.A., the torch exit conditions are an important part of this modeling approach and the need to satisfy the heat and mass balances alone do not enable a unique set of boundary conditions to be defined. For this reason, a parametric study has been done to clearly show the effect the four profile parameters (T_{max}, U_{max}, n_T and n_u) have on the heat and mass output for the torch. Figures II.D.1-II.D.3 show the results of this study.

Figure II.D.1 is a plot of the mass flow and power output versus the maximum velocity, U_{max} for three maximum temperatures, T_{max}. In this case n_u and n_T are both equal to 2.8. No big surprises, mass flow and power output increase linearly with velocity, power output increases with temperature and mass flow decreases with temperature.

Figure II.D.2 shows the effect of the exponents of velocity and temperature profiles, n_u and n_T for constant U_{max} = 700 m/s and T_{max} = 12000k. It is seen that both power output and mass flow increase as n_u is increased. It may also be seen that mass flow decreases and power output increases with increasing temperature exponent n_T. This is more readily apparent in Figure II.D.3 which shows mass flow and power versus the temperature exponent, n_T. The differences in the effect of n_u and n_T on the heat and mass flow allow the boundary conditions to be tuned to match the experimental heat and mass balances.

II.D.3.b Setting up the analysis

Because of the appreciable ability to tune the system shown by Figures II.D.1 - II.D.3, it is necessary to approach the boundary conditions systematically so that a consistent set is generated for the experimental conditions of Table II.D.I.

This systematic approach is based on an analysis of the overall heat and mass balances and is summarized in Table II.D.II. This table shows the net power (leaving the torch nozzle as sensible heat), the mass flow, the overall average enthalpy per unit mass at the exit, the average temperature (found by looking up in the tabulated data for argon), the average density of the plasma (assuming an ideal gas), and the average plasma velocity. It is seen in Table II.D.II that the average temperature at the exit increases with increasing current and decreases with increasing flow rate. This second effect is the result of 10-20% more enthalpy being distributed in 50-100% more plasma.

The table also shows that the average velocity increases as either current or flow rate increase. Based on this analysis, the maximum temperatures and velocities were chosen for the six cases. The exponents of velocity and temperature were then adjusted to match the heat and mass balances.

The parameters used are shown in Table II.D.III. This gave a consistent set of input conditions. It is seen that the exponents of velocity and temperature increase with increasing flow rate indicating the increasing effect of turbulence and momentum forces over the electromagnetic forces (this is addressed more completely in Section IV.E).

II.D.4. RESULTS

These input conditions gave the results which are shown in Figures II.D.4-II.D.7. Figure II.D.4 shows a comparison between the measured and predicted (a) temperature and (b) velocity contours for the 450 amp, 35.4 liter/min case. This shows reasonable agreement with the model tending to over predict the temperatures.

Figure II.D.5 shows a comparison between the measured and predicted (a) temperature and (b) velocity contours for the 600 amp, 35.4 liter/min case. Again the agreement is reasonable with the temperatures being over predicted by the model.

Figure II.D.6 and II.D.7 show the comparison of the experimental and theoretical (a) temperature and (b) velocity profiles on the axis of the plume for the 450 and 600 amp cases. These figures are helpful because they illustrate the trends which are present. For example, the model predicts the trend of the temperatures to decrease with increasing flow rate; this is a direct result of basing the boundary conditions on the overall heat balance. On the other hand, the model predicts that the velocity in the plume will increase with flow rate (a result of the overall mass balance). The experimental data tend to show the opposite trend, though not very clearly. It is believed that this discrepancy is a result of using a fully turbulent model in a transitional regime. Such a model is unable to predict the substantial increase in turbulent energy which occurs between the low flow case (which is laminar in nature) and the high flow case (which is more turbulent).

This effect awaits a laminar-turbulent transitions model of some type before it can be modeled more accurately.

II.D.5 DISCUSSION

This section has illustrated the application of the plume model to a turbulent system in which only a single gas, argon, is present. A systematic approach has been taken to defining the boundary conditions based on the overall balances and the average temperatures and velocities at the exit of the torch. Such a systematic approach leads to a consistent set of boundary conditions.

The calculations generally show reasonable agreement with the measured temperatures and velocities. The model is able to represent the trends present in the temperature and velocity profiles with the exception of the tendency of the velocity on the axis to drop or stay the same with increasing flow rate. It is felt that this is the result of using a high Reynolds number turbulence model for a transitional flow.

II.E. REFERENCES

1. J. Grey, M.P. Sherman, P.M. Williams and D.B. Frodkin, AIAA J. **4**, 986,(1966).
2. C.P. Donaldson and K.E. Gray, AIAA J., **4**, 2017, (1966).
3. T.J. O'Connor, E.H. Comfrot and L.A. Cass, AIAAJ., **4**, 2026, (1966).
4. I.P. Incropera and G. Leppert, Int. J. Heat Mass Transfer, **10**, 1861, (1967).
5. S.M. Correa, 6th Int. Symp. on Plasma Chemistry, Montreal, July 24-28, Vol. 1, (1983).
6. Y.C. Lee and E. Pfender, Plasma Chem. Plasma Proc. **7**, (1), 1, (1987).
7. J. Mckelliget, J. Szekely, M. Vardelle, and P. Fauchais, Plasma Chem. Plasma Plasma Proc., **2**, 317, (1982).
8. A.H. Dilawari, and J. Szekely, Plasma Chem. Plasma Proc. **7**, (3), 317, (1987).
9. A.H. Dilawari, and J. Szekely, Int. J. Heat and Mass Trans. **30**, (11), 2357, (1987).
10. A. H. Dilawari and J. Szekely, Proc. MRS Symposium on Materials Processing in Plasma Systems, **98**, 3, (1987).
11. A. H. Dilawari, J. Szekely, J.F. Coudert, and P. Fauchais, Int. J. Heat and Mass Transfer, **32**, No. 1, 35, (1989).
12. A. H. Dilawari, and J. Szekely, Proc. T.B. King Memorial Symposium, Met. Trans. B, **20B**, April, 243, (1989).
13. Y.P. Chyou, and E. Pfender, Plasma Chem. Plasma Proc. **9**, (2), 291, (1989).
14. A.H. Dilawari, J. Szekely, J. Batdorf, R. Detering, and C.B. Shaw, Plasma Chem. Plasma Proc., 10, (2), 321, (1990).
15. A.H. Dilawari, J. Szekely, R. Westhoff, B.A. Detering, and C.B. Shaw Jr., Mat. Res. Soc. Symp. Proc., **190**, 199, (1991).
16. A.H. Dilawari, J. Szekely, and R. Westhoff, Plasma Chem. Plasma Proc., **10**, (4), 501, (1990).
17. C.H. Chang and E. Pfender, Plasma Chem. Plasma Proc. **10**, (3), 473, (1990).
18. C.H. Chang and E. Pfender, Plasma Chem. Plasma Proc. **10**, (3), 493, (1990).
19. R. Spores, E. Pfender, Proc. of National Thermal Spray Conf., Cincinnati, 85, (1989).
20. J.R. Fincke, R. Rodriquez and C.G. Pentecost, Proc. of National Thermal Spray Conf., Long Beach, 45, (1991).
21. J.F. Coudert, J.F. Baronnet, and P. Fauchais, ISPC-6, Montreal, **1**, 108, (1983).
22. M. Vardelle, Ph.D. Thesis, No. 80-7, Universite de Limoges (1980).

23. D. Gravelle, M. Beaulinieu, C. Carlone, D. Iacocca, and M.I. Boulos, ISPC-8, Montreal, **1**, 108, (1983).
24. M. Boulos, P. Fauchais, and E Pfender, U.S. Department of Energy, Office of Basic Energy Sciences, Washington, D.C., DOE/ER-0270, 190, (1986).
25. OMA III, Model 1460V, Optical Multichannel Analyzer, EG&G Princeton Applied Research, Princeton, N.J.
26. Y. Yasutoma, et. al., IEEE Trans Plasma Sci., PS-9, **1**, 18, (1981)
27. C. H. Liu, Ph.D. Thesis, Department of Mechanical Engineering, Univ. Of Minnesota, Minneapolis, Minnesota (1977).
28. D. C. Evans and R. S. Tankin, *Phys. Fluids* **10**, 1137 (1967).
29. R.B. Bird, et. al., Transport Phenomena, Whiley, N.Y., 511, (1960).
30. C. R. Wilke, *J. Chem Phys.* , **18**, 517-519 (1950).
31. W.M. Pun and D.B. Spalding, Rep. No. HTS/76/2, Heat Transfer Section, Imperial College, London (1976).
32. M. Brossa and E. Pfender, *Plasma Chem. Plasma Proc.*, **8**, 75, (1988).
33. B.E. Launder and D.B. Spalding, Mathematical Models of Turbulence , Academic Press, London, (1972).
34. J. C. Morris, G. R. Bach, and J. M. Yos, Rep. No. ARL-64-180, Aerospace Research Laboratories (1964).
35. J. M. Yos, Technical Memorandum RAD-TM-63-7, Research and Advanced Development Division, AVCO Corporation, Wilmington, Massachusetts (1983).
36. P. Fauchais, M. Boulos and E. Pfender, *Physical and Thermodynamic Properties of Thermal Plasmas*, in Plasma Technology in Metallurgical Processing, 11-26 (1987).
37. A. Capetti and E. Pfender, Plasma Chem Plasma Proc., **9**, (2), 329-341, (1989).

Label	Current (Amps)	Gas Flow (scm/hr)	Chamber gas	Input power (kW)	Cooling loss (kW)	Efficiency (%)	Tmax (K)
BES23	250	0.59	Argon	4.79	3.61	24.6	11131
BES24	250	0.83	Argon	4.86	3.48	28.4	11394
BES25	250	0.59	Nitrogen	4.70	3.59	23.7	11153
BES26	250	0.83	Nitrogen	4.78	3.73	22.0	11255
BES27	500	0.59	Argon	9.86	7.11	27.9	12415
BES28	500	0.83	Argon	9.96	6.99	29.8	12227
BES29	500	0.59	Nitrogen	9.31	6.76	27.4	12404
BES30	500	0.83	Nitrogen	9.65	6.74	30.2	12055
BES31	750	0.59	Argon	15.17	10.77	29.0	12587
BES32	750	0.83	Argon	15.33	10.59	30.9	13075
BES33	750	0.59	Nitrogen	15.68	10.57	32.6	11684
BES34	750	0.83	Nitrogen	15.22	10.53	30.8	12893

Table III.B.I Operating conditions used in the BES experiments at INEL

	250 Amps	500 Amps	750 Amps
Current	2.5%	2.5%	2.5%
Voltage	2.5%	2.5%	2.5%
Input power	3.5% or 0.165-0.170 kW	3.5% or 0.326-0.349 kW	3.5% or 0.531-0.549 kW
Coolant flow	0.5%	0.5%	0.5%
Coolant Temps.	3.0%	2.0%	1.0%
Coolant heat cap.	1.0%	1.0%	1.0%
Cooling loss	3.2% or 0.11 kW	2.3% or 0.15 kW	1.5% or 0.16 kW
Net Power	14.8-19.7% or 0.20-0.21 kW	12.9-14.3% or 0.36-0.39 kW	11.3-12.7% 0.56-0.58 kW
Efficiency	15.3-20.% or ±4.4 percent pts.	13.3-14.4% or ±4.0 percent pts.	11.8-13.2% or ±3.8 percent pts.

Table II.B.II Summary of the uncertainties in the BES experiments

Boundary	u	v	h	m
AB	0	0	$T = 700$ K	$\frac{\partial m}{\partial r} = 0$
BC	0	0	$T = 500$ K	$\frac{\partial m}{\partial z} = 0$
CD	0	$\frac{\partial \rho r v}{\partial r} = 0$	$T = 300$ K	0
DE	$\frac{\partial u}{\partial z} = 0$	$\frac{\partial v}{\partial z} = 0$	$\frac{\partial h}{\partial z} = 0$	$\frac{\partial m}{\partial z} = 0$
EF	$\frac{\partial u}{\partial r} = 0$	0	$\frac{\partial h}{\partial r} = 0$	$\frac{\partial m}{\partial r} = 0$
FA	$u = u(r)$	0	$T = T(r)$	1

Table II.B.III Boundary Conditions used in the plasma plume model with reference to Figure II B.3.

I (A)	Q (l/min)	V (volts)	Power (kW)	Efficiency (%)	Case #
400	23.6	24.0	9.594	41.1	5
400	47.2	27.4	10.880	48.4	6
450	23.6	23.8	10.731	38.9	12
450	35.4	24.8	11.186	47.1	10
450	47.2	27.2	12.238	51.2	11
600	23.6	24.3	14.603	42.8	9*
600	35.4	25.6	15.350	47.1	7
600	47.2	27.0	16.161	51.9	8

*This case (labelled 7 in ref.32) has been re-labelled 9 to be consistent with the order of the 450 amp cases.

Table II.C.I Averaged Torch Conditions during 66 Experimental Runs [32]

C_1	1.43
C_2	1.92
C_D	0.09
σ_K	1.0
σ_ε	1.3
σ_h	0.9
σ_m	0.9

Table II.C.II Constants used in the K–ε turbulence model

	u	v	rw	h	m	K	ε
GA	$u=u(r)$	0	$rw(r)$	$T = 700$	1	$K = .005u^2$	$\varepsilon = \frac{C_D K^{1.5}}{.03\, r_n}$
AB	w.f	w.f.	w.f.	$T = 700$	$\frac{\partial m}{\partial r} = 0$	$\frac{\partial K}{\partial r} = 0$	$\varepsilon = 0$
BC	w.f	w.f.	0	$T = 300$	$\frac{\partial m}{\partial z} = 0$	$\frac{\partial K}{\partial z} = 0$	$\varepsilon = 0$
CD	$\frac{\partial \rho u}{\partial z} = 0$	0	0	$T = 300$	1 or 0	$K \approx 0$	$\varepsilon \approx 0$
DE	$\frac{\partial u}{\partial y} = 0$	$\frac{\partial \rho v}{\partial y} = 0$	0	$T = 300$	1 or 0	$K \approx 0$	$\varepsilon \approx 0$
EF	$\frac{\partial u}{\partial z} = 0$	0	0	$\frac{\partial h}{\partial z} = 0$	$\frac{\partial m}{\partial z} = 0$	$\frac{\partial K}{\partial z} = 0$	$\frac{\partial \varepsilon}{\partial z} = 0$
FG	$\frac{\partial u}{\partial y} = 0$	0	0	$\frac{\partial h}{\partial y} = 0$	$\frac{\partial m}{\partial r} = 0$	$\frac{\partial K}{\partial r} = 0$	$\frac{\partial \varepsilon}{\partial r} = 0$

Table II.C.III. Boundary Conditions used in the model (turbulent case) with reference to Figure II.C.1.

I (A)	Q (l/min)	V (volts)	Power (kW)	Efficiency (%)	Case # *
450	23.6	24.0	10.842	48.2	12
450	35.4	25.5	11.478	50.9	10
450	47.2	27.3	12.265	55.4	11
600	23.6	25.5	15.220	46.4	9
600	35.4	26.8	16.014	53.0	7
600	47.2	28.1	16.813	56.4	8

*These cases are labelled to be consistent with those presented in section II.C.

Table II.D.I. Averaged conditions for the Metco torch experiments of Capetti and Pfender[37].

Case #	Net power (W)	Mass Flow (kg/s)	Average Enthalpy (J/kg)	Average Temperature (K)	Average Density (kg/m^3)	Average Velocity (m/s)
12	5226	7.01e-4	7.45e6	10575	0.0460	312
10	5842	1.05e-3	5.56e6	9454	0.0515	418
11	6795	1.40e-3	4.85e6	8794	0.0554	519
9	7062	7.01e-4	1.01e7	11466	0.0425	339
7	8502	1.05e-3	8.10e6	10876	0.0448	481
8	605	1.40e-3	6.77e6	10255	0.0475	605

Table II.D.II. Summary of the analysis of the overall heat and mass balances performed on the Metco torch

Case #	U_{max} (m/s)	T_{max} (K)	N_u	N_T	Net Power (W)	Efficiency (%)
12	500	13000	1.95	4.46	6561	43.1
10	750	12000	2.56	5.33	7556	47.1
11	850	11000	3.8	7.43	8780	52.2
9	500	12500	2.4	3.6	4809	44.4
7	600	11500	2.95	3.56	5503	47.9
8	700	10500	3.67	4.3	6317	52.2

Table II.D.III. Parameters used in the model to represent the Metco torch (argon in argon)

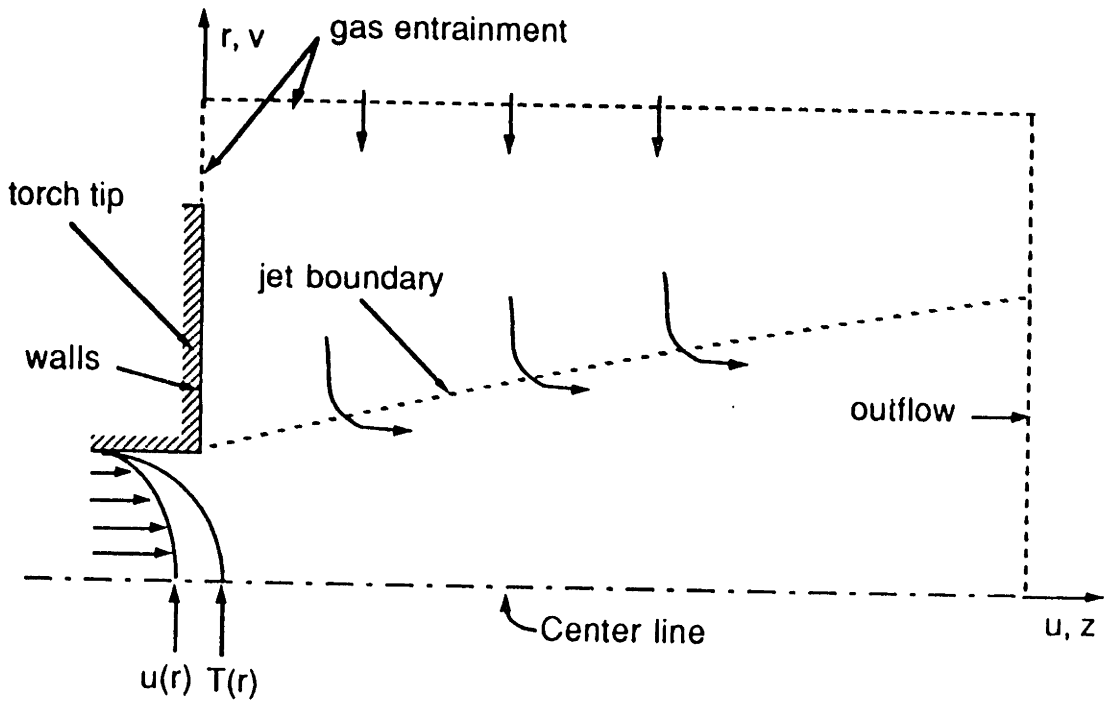

Figure II.A.1 Sketch of the phenomena associated with a plasma plume issuing from a plasma torch.

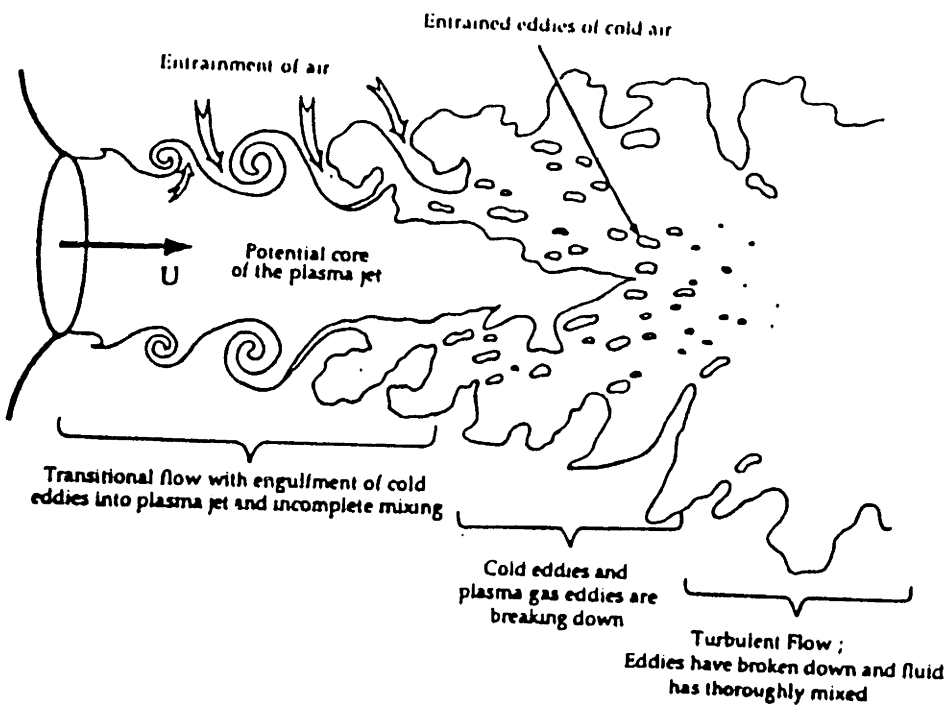

Figure II.A.2 Schematic illustration of transitional flow in a plasma jet (19).

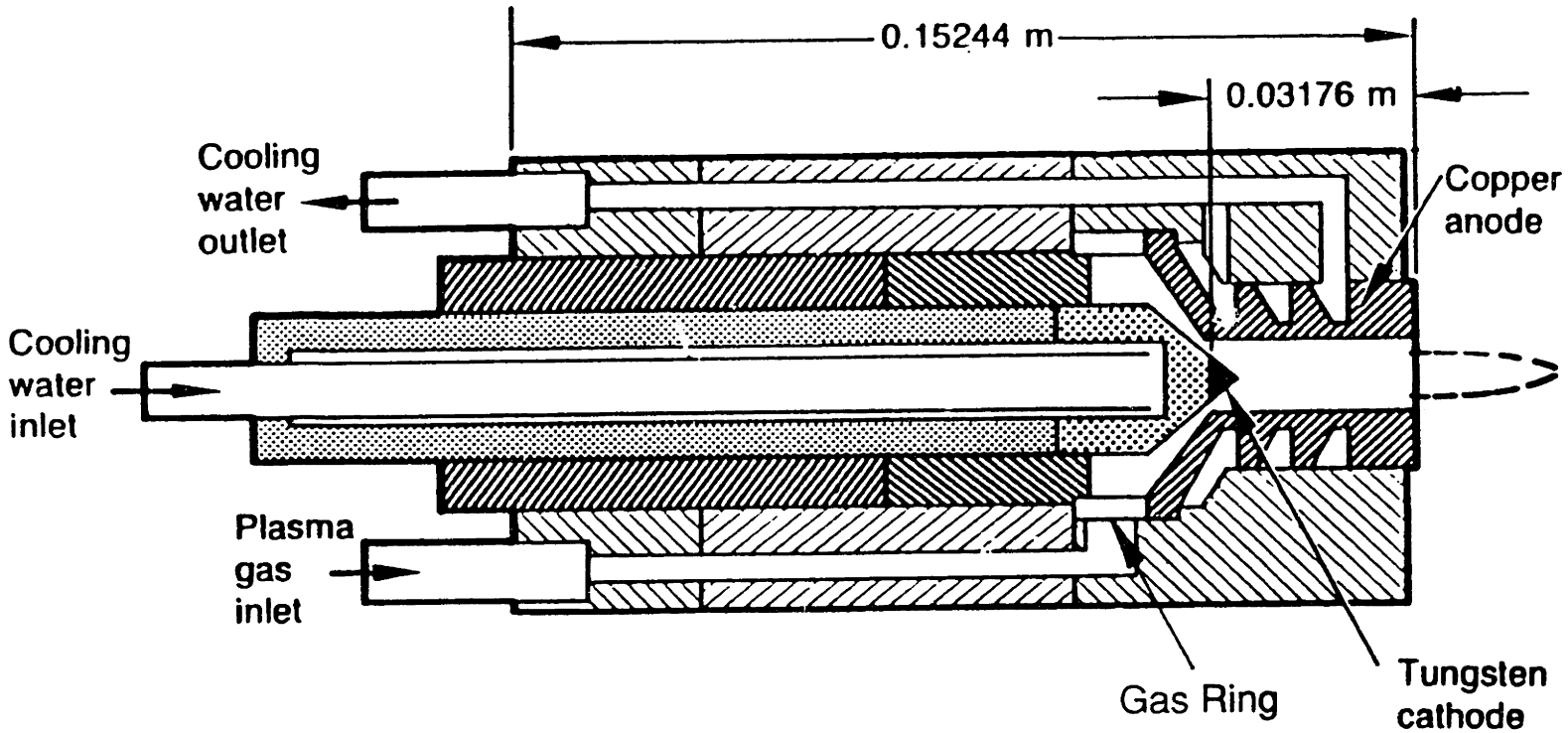

Figure II.B.1 Cut-away view of the non-transferred arc plasma torch used in the BES experiments (17-18).

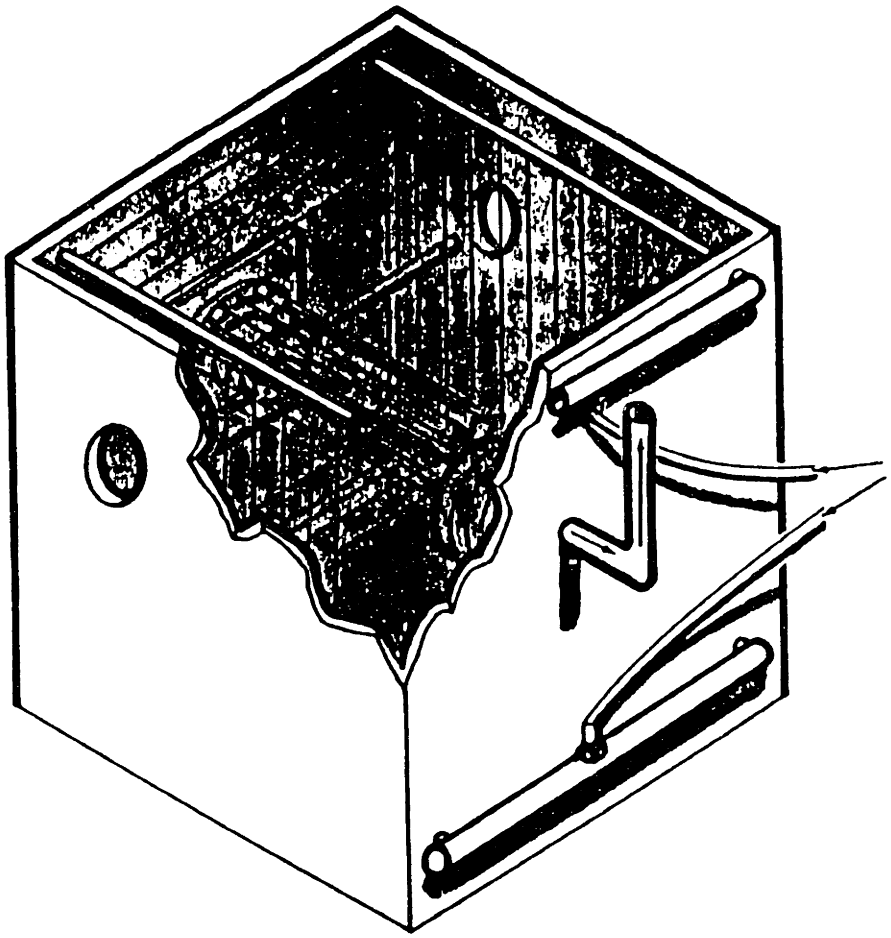

Figure II.B.2 Atmosphere control chamber used in the BES experiments [14-15].

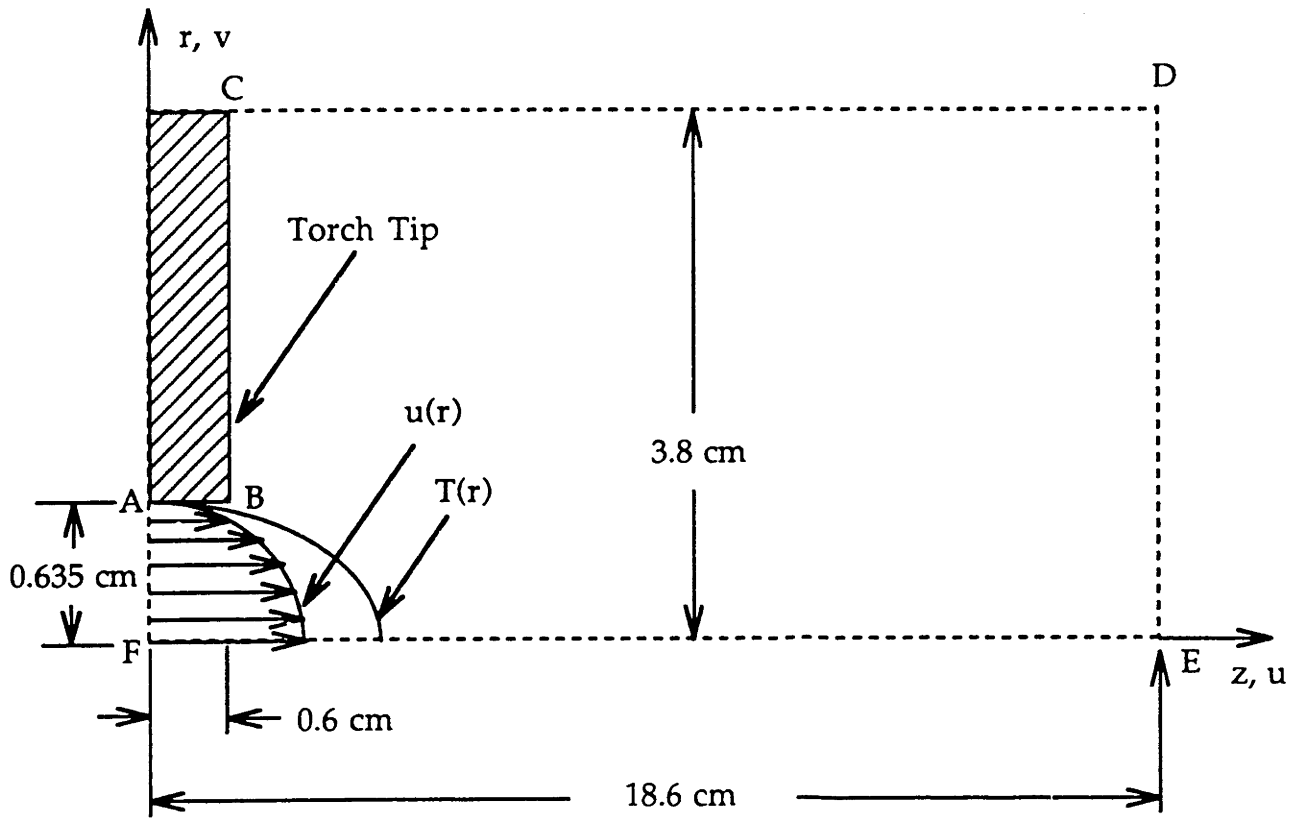

Figure II.B.3 Integration domain used in the BES calculations [14-15].

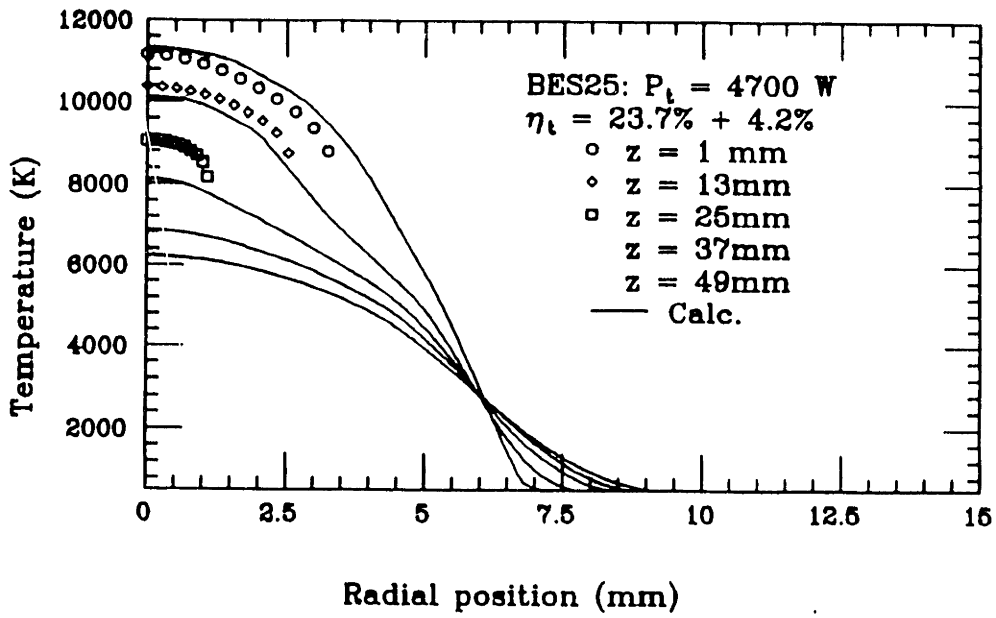

(a)

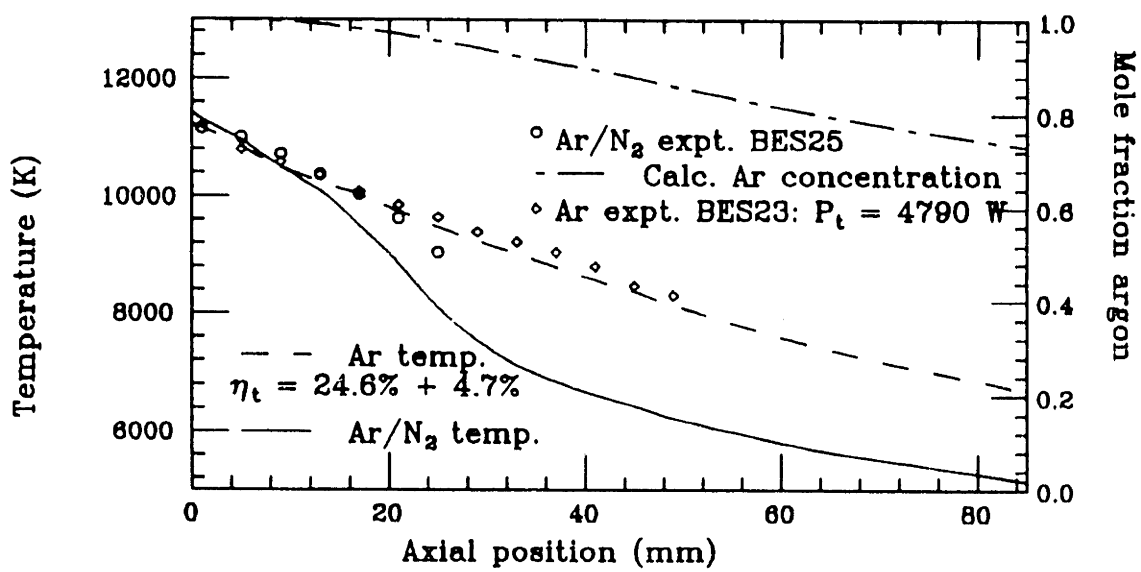

(b)

Figure II.B.4 Comparison of calculated and experimental data for run BES25.
(a) Radial temperature profiles at several axial positions.
(b) Temperature profile and calculated argon concentration profile on the axis.

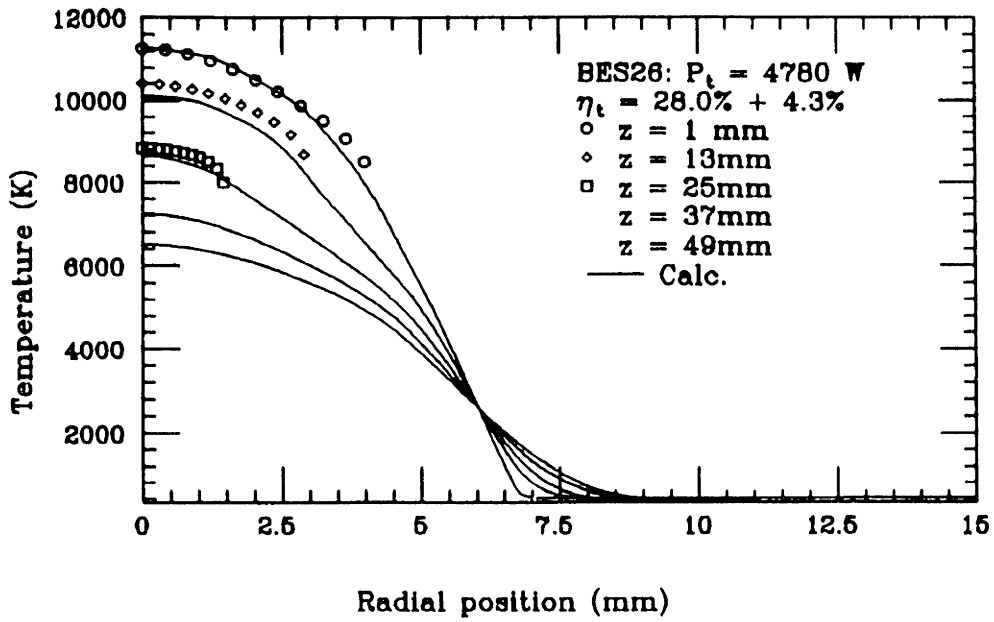

(a)

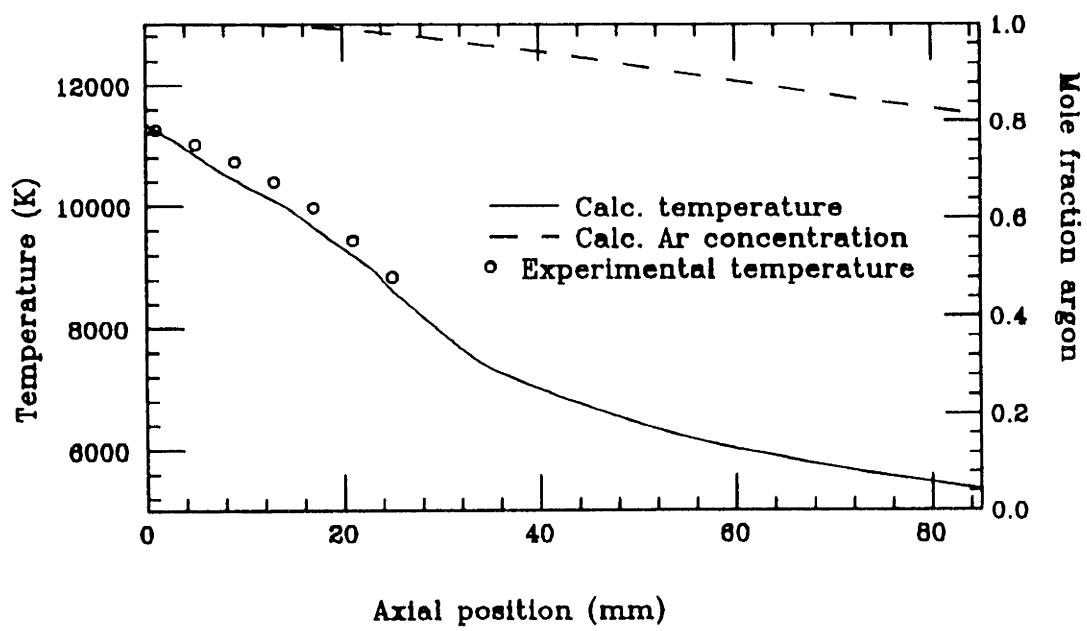

(b)

Figure II.B.5 Comparison of calculated and experimental data for run BES26.
(a) Radial temperature profiles at several axial positions.
(b) Temperature profile and calculated argon concentration profile on the axis.

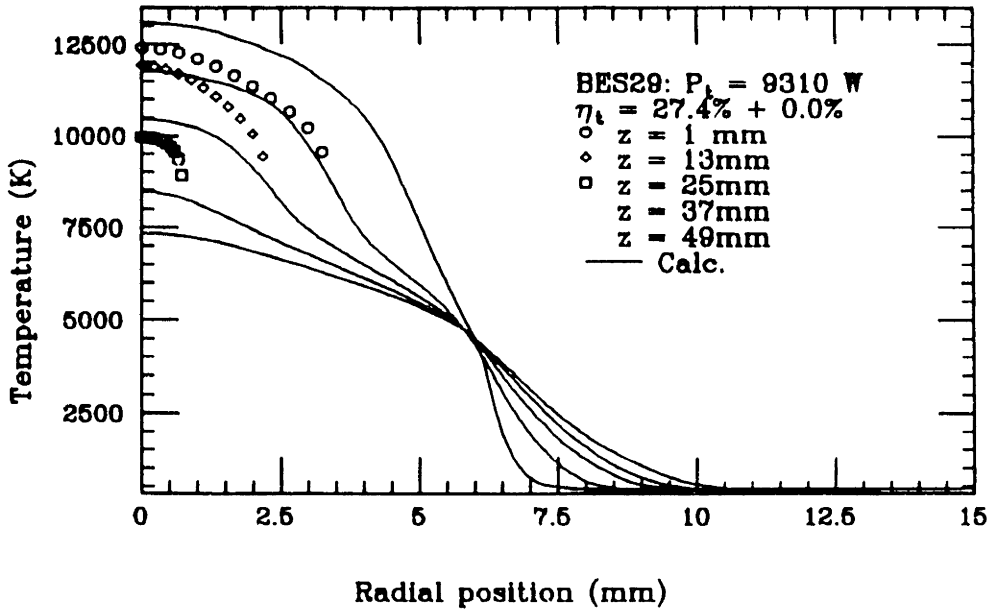

(a)

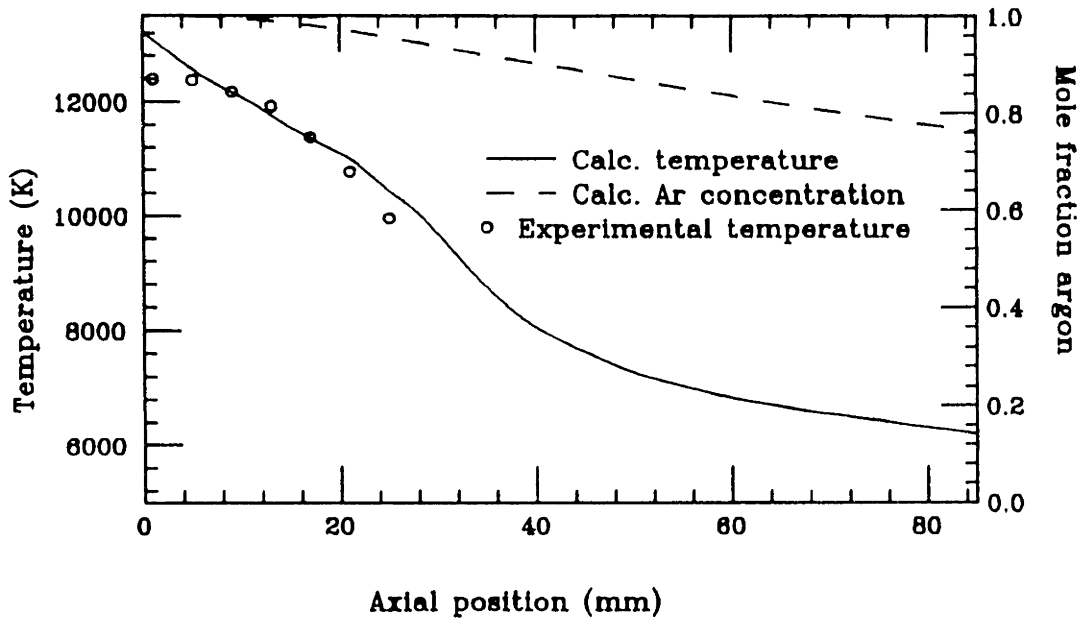

(b)

Figure II.B.6 Comparison of calculated and experimental data for run BES29.
(a) Radial temperature profiles at several axial positions.
(b) Temperature profile and calculated argon concentration profile on the axis.

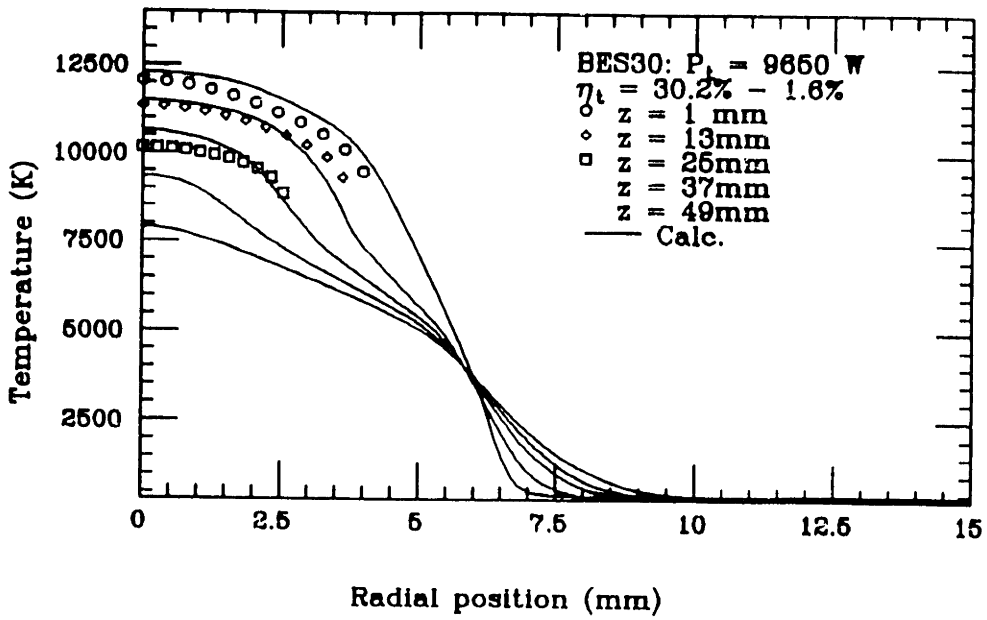

(a)

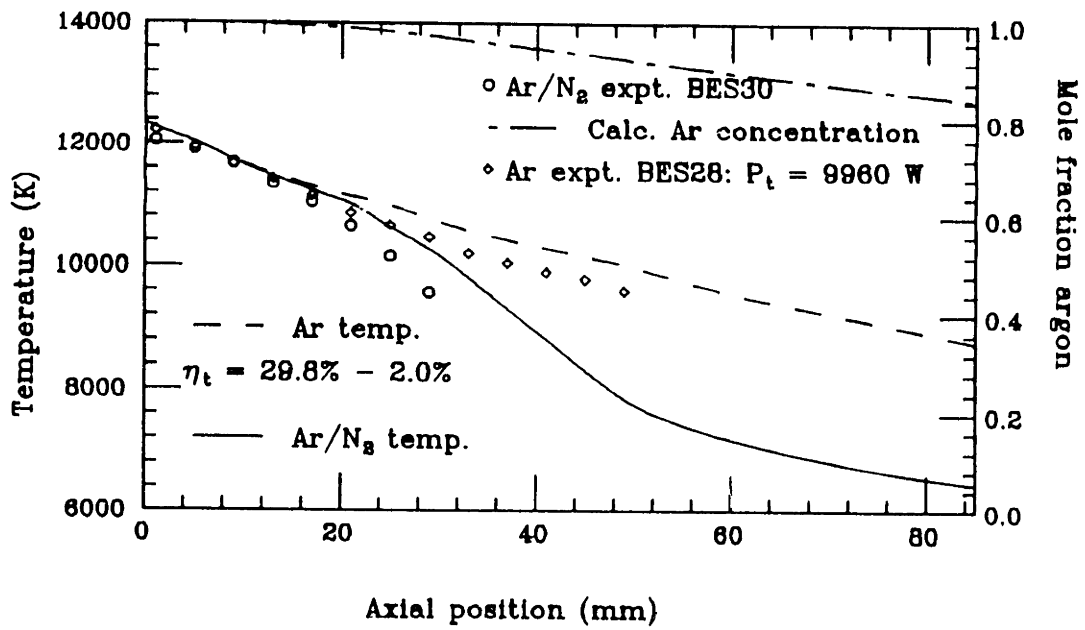

(b)

Figure II.B.7 Comparison of calculated and experimental data for run BES30.
(a) Radial temperature profiles at several axial positions.
(b) Temperature profile and calculated argon concentration profile on the axis.

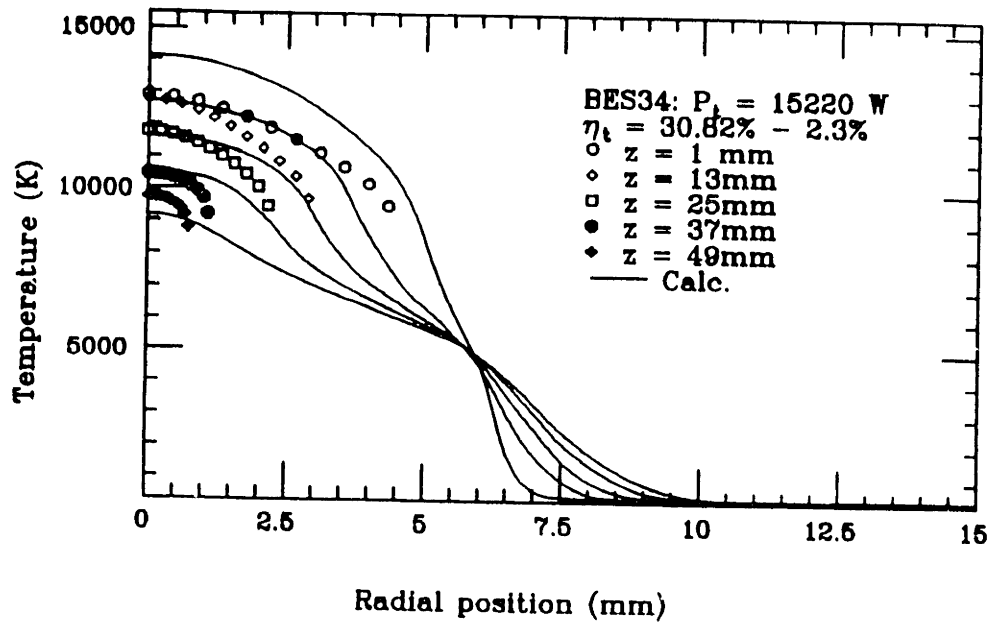

(a)

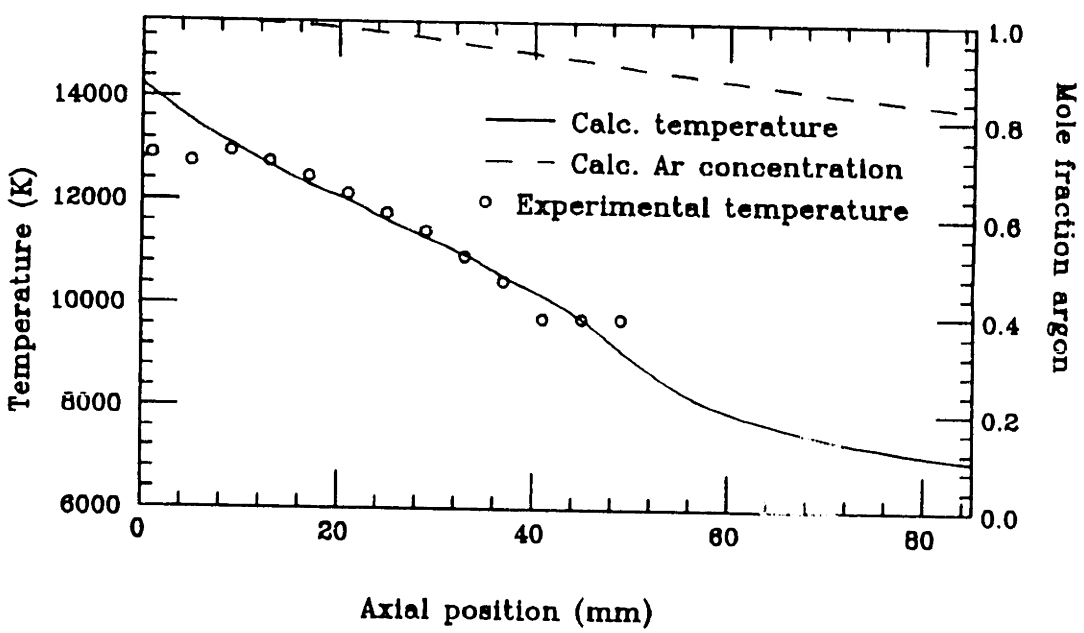

(b)

Figure II.B.8 Comparison of calculated and experimental data for run BES34.
(a) Radial temperature profiles at several axial positions.
(b) Temperature profile and calculated argon concentration profile on the axis.

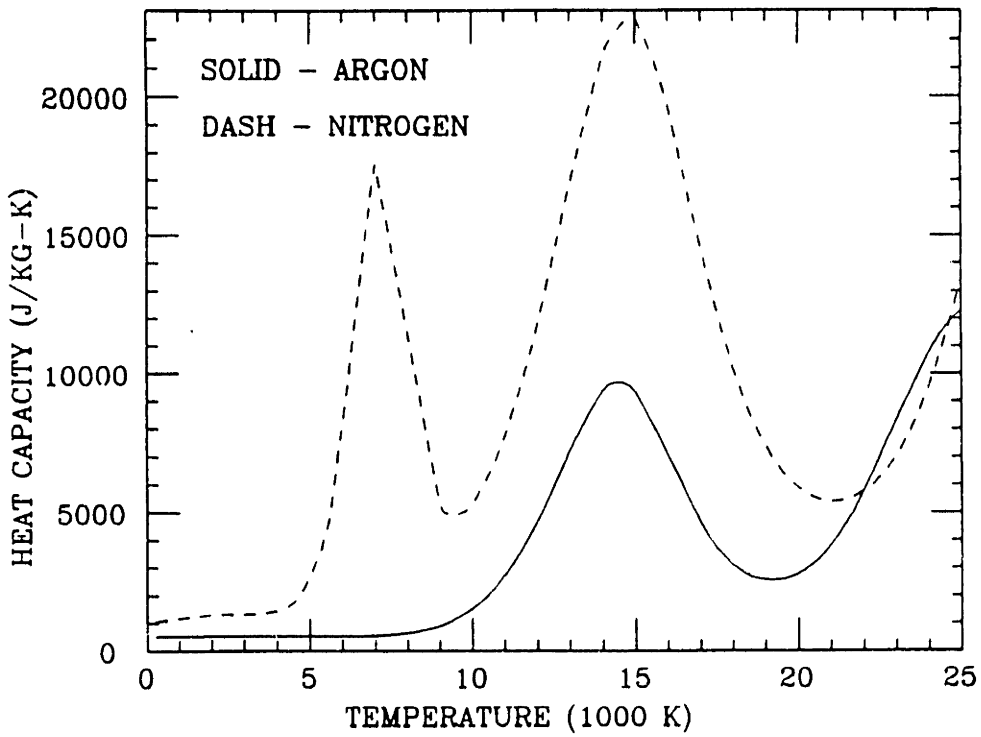

Figure II.B.9 Comparison of the temperature dependence of the heat capacity of argon and nitrogen plasma.

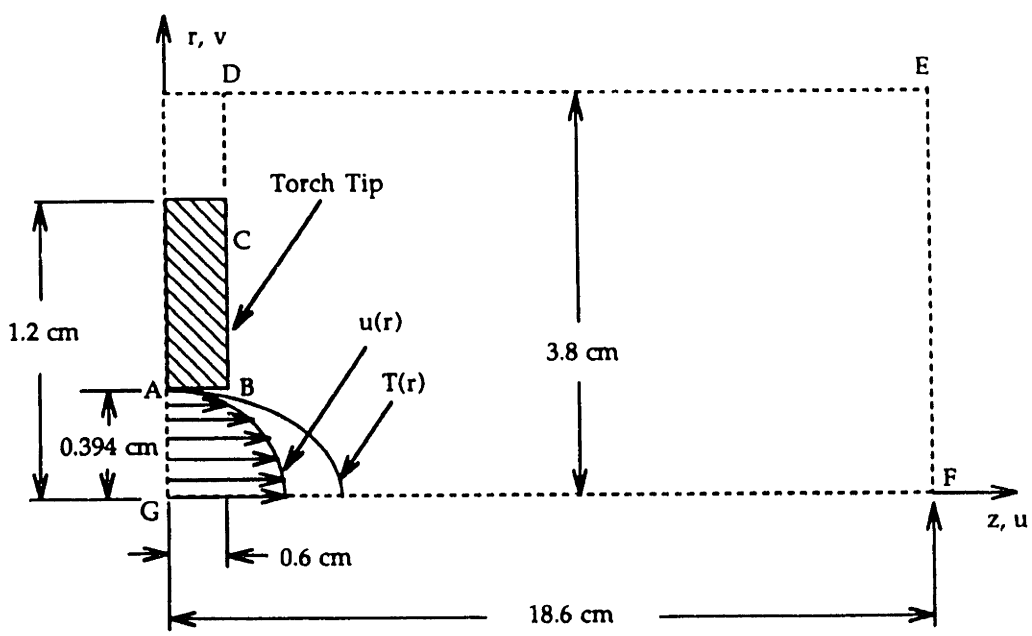

Figure II.C.1 Calculation domain used in modeling the experiments of Brossa and Pfender (32).

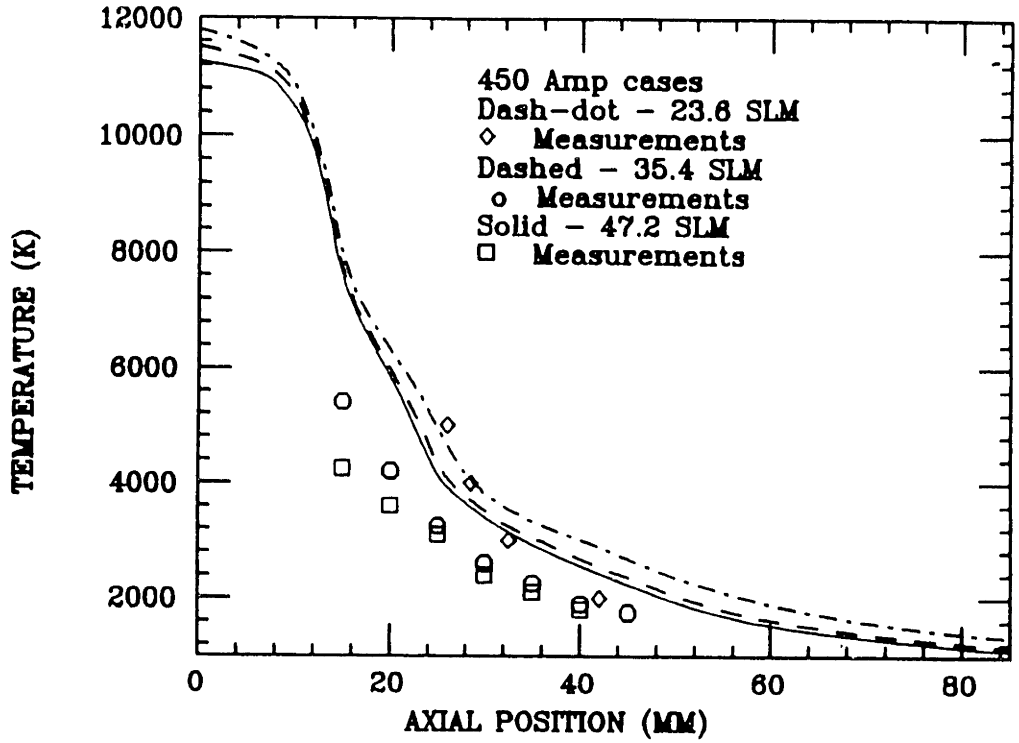

Figure II.C.2 Temperature profiles on the axis of the plume - 450 amp cases.

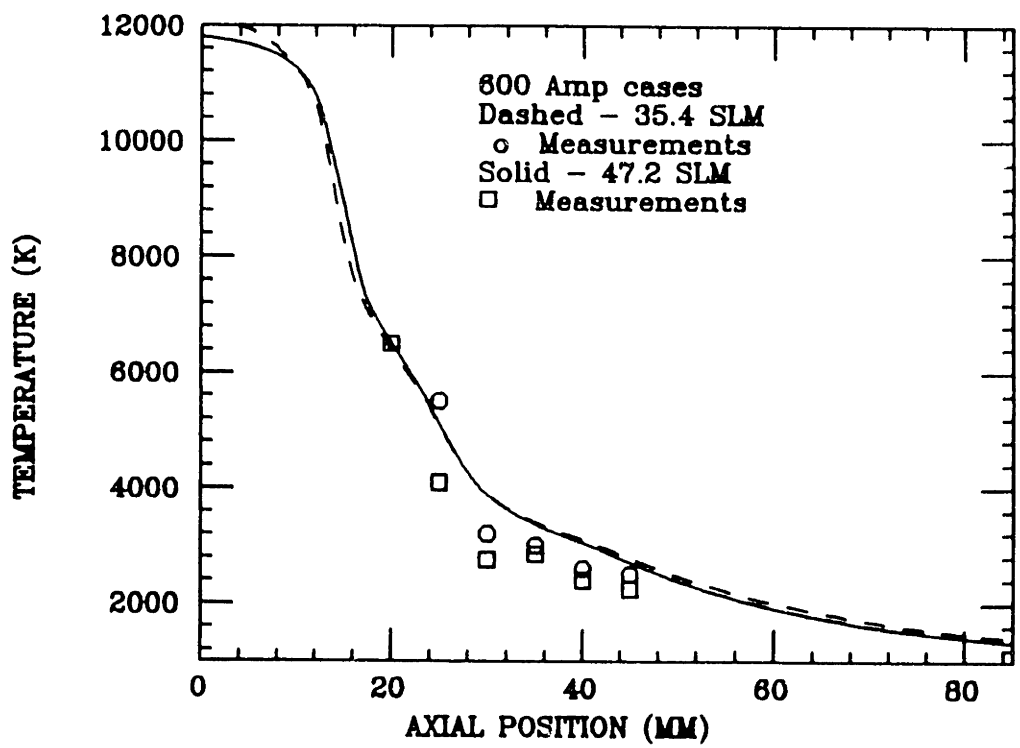

Figure II.C.3 Temperature profiles on the axis of the plume - 600 amp cases.

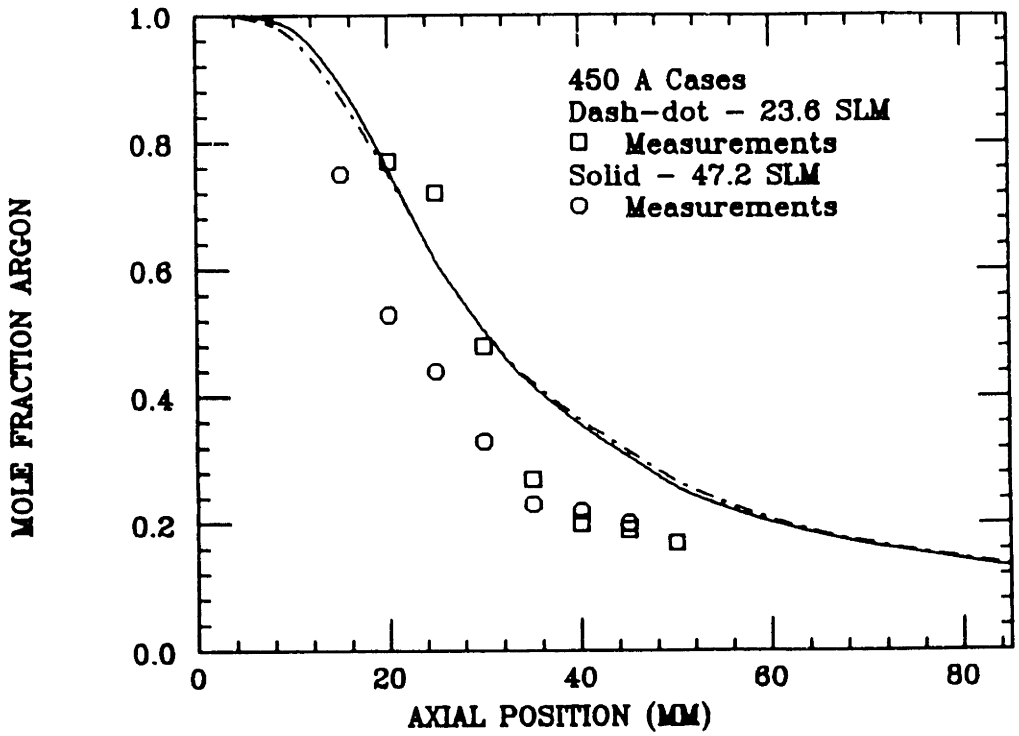

Figure II.C.4 Argon concentration profiles on the axis of the plume - 450 amp cases.

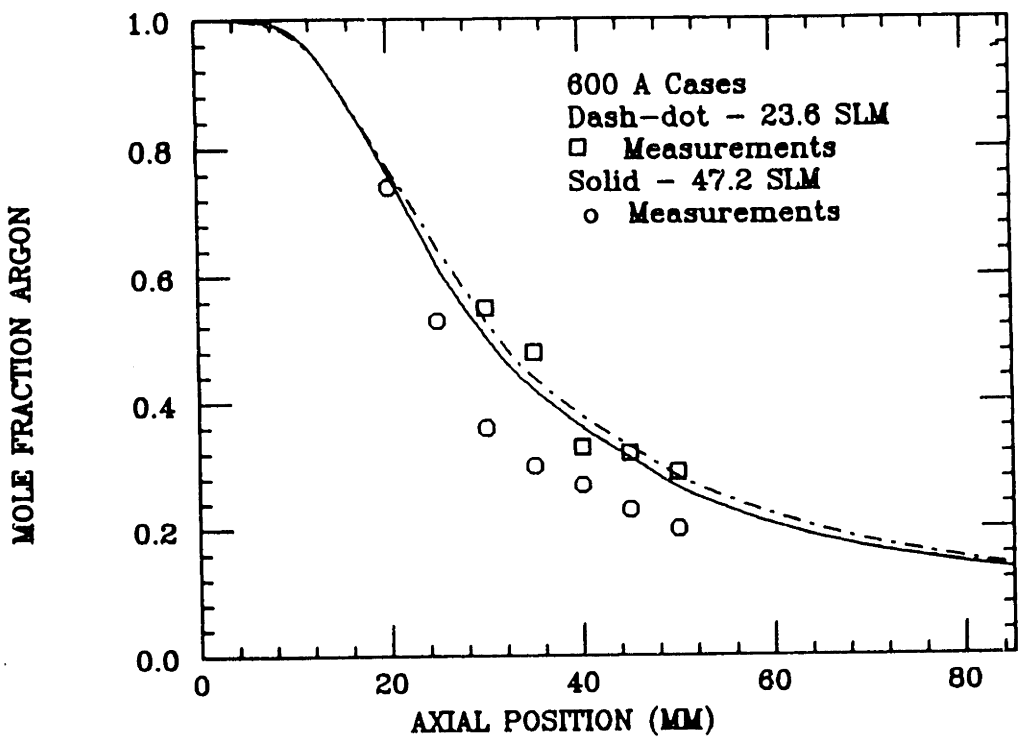

Figure II.C.5 Argon concentration profiles on the axis of the plume - 600 amp cases.

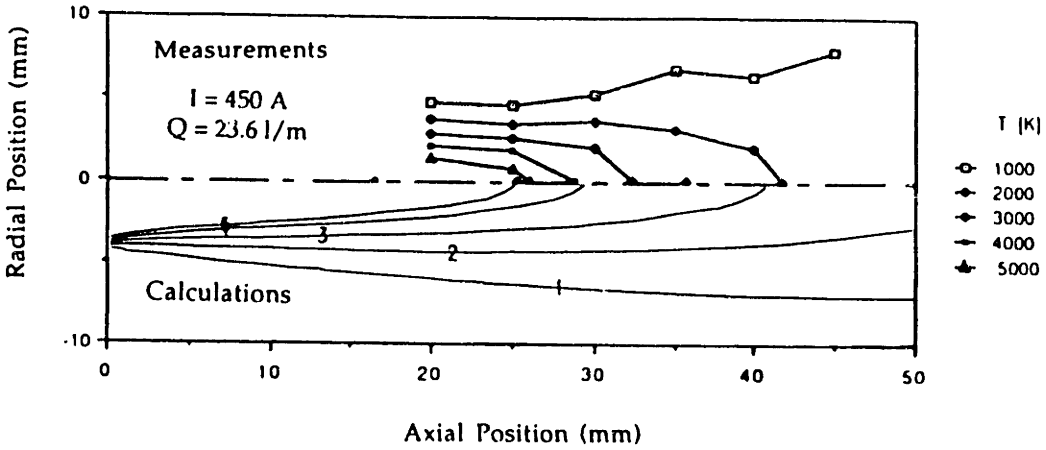

Figure II.C.6 Comparison of calculated and measured temperature contours in the plume - Case #12.

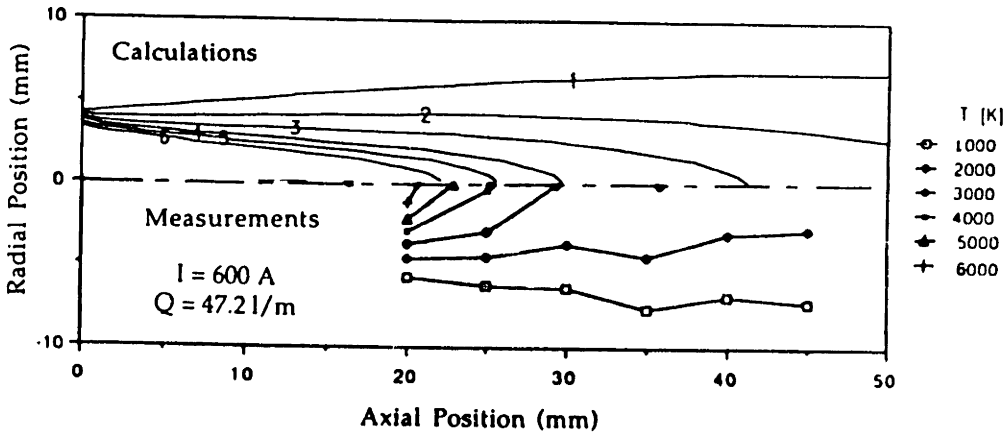

Figure II.C.7 Comparison of calculated and measured temperature contours in the plume - Case #8.

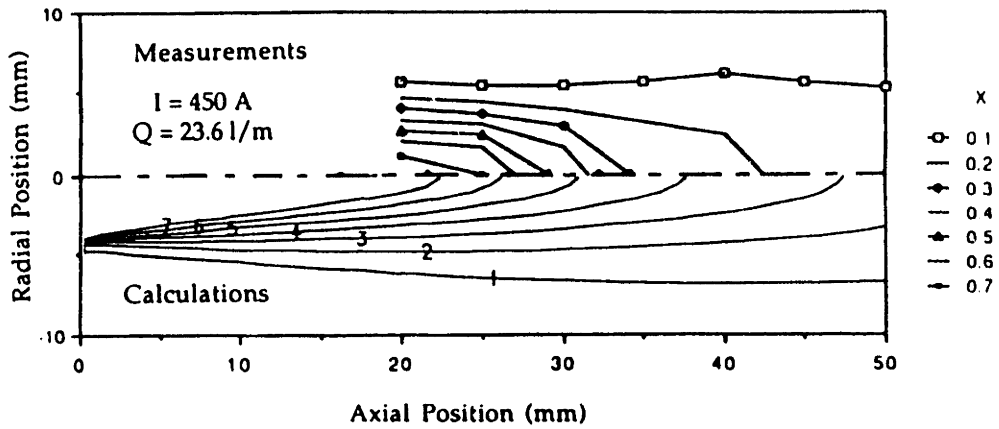

Figure II.C.8 Comparison of calculated and measured argon mole fraction contours in the plume - Case #12.

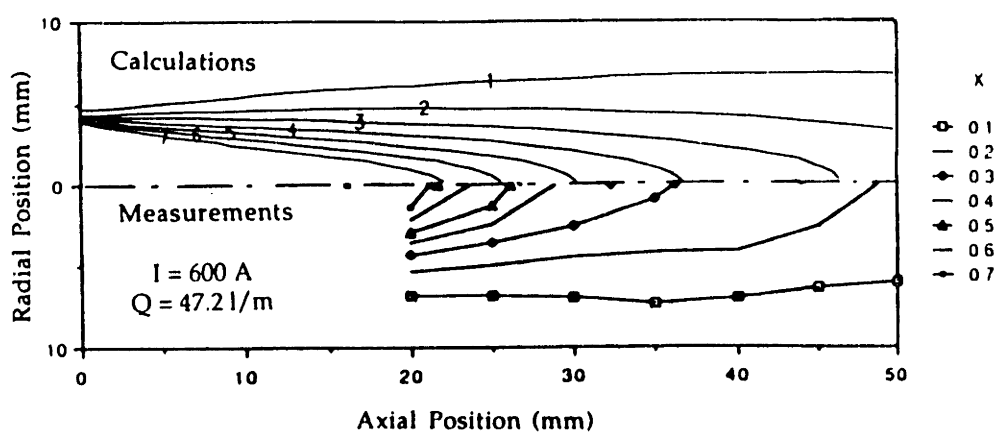

Figure II.C.9 Comparison of calculated and measured argon mole fraction contours in the plume - Case #8.

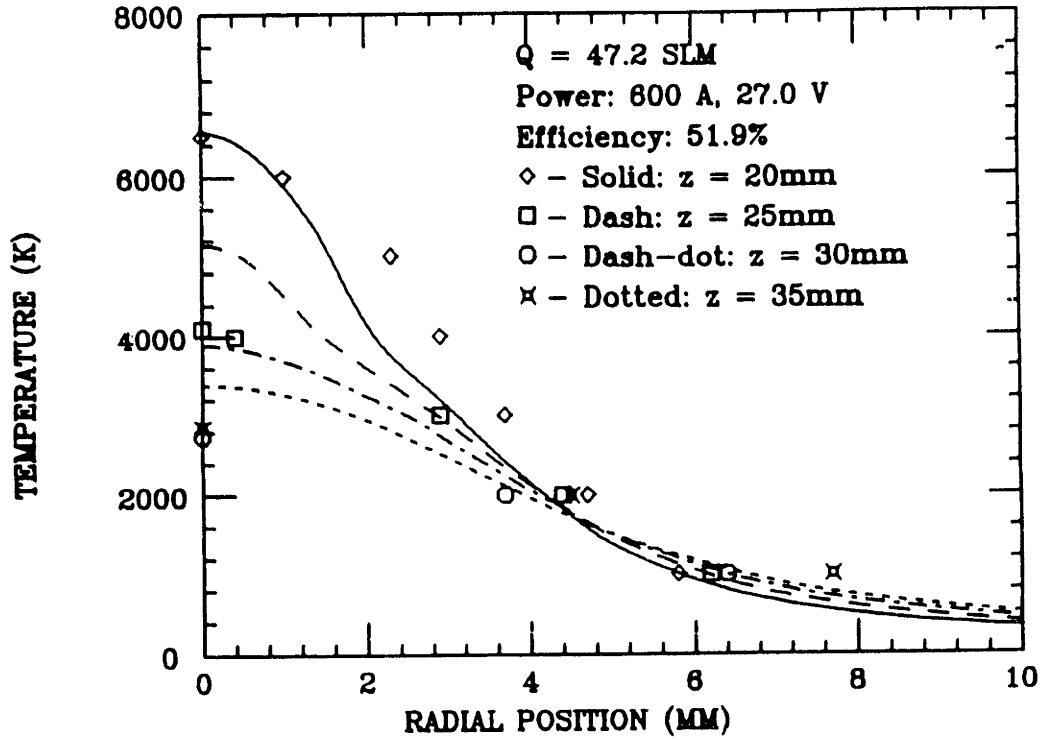

Figure II.C.10 Comparison of calculated and measured radial temperature profiles in the plume at several axial positions - Case #8.

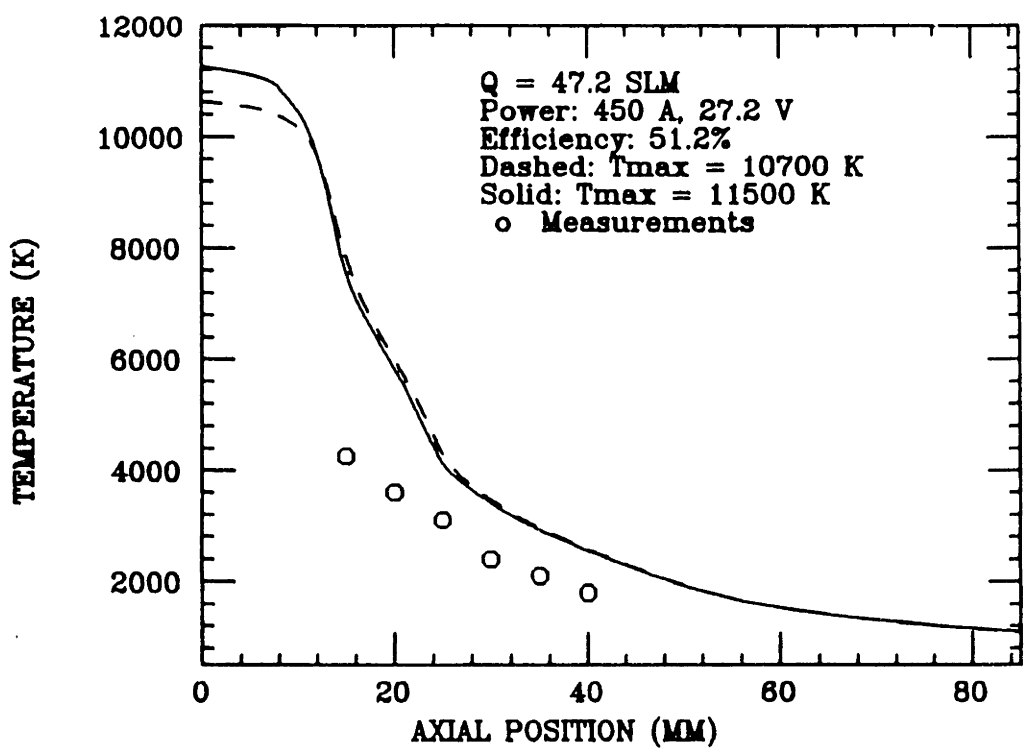

Figure II.C.11 Temperature profiles on the plume axis illustrating the insensitivity of the experimental vs. calculated discrepancies to the torch exit temperature profile.

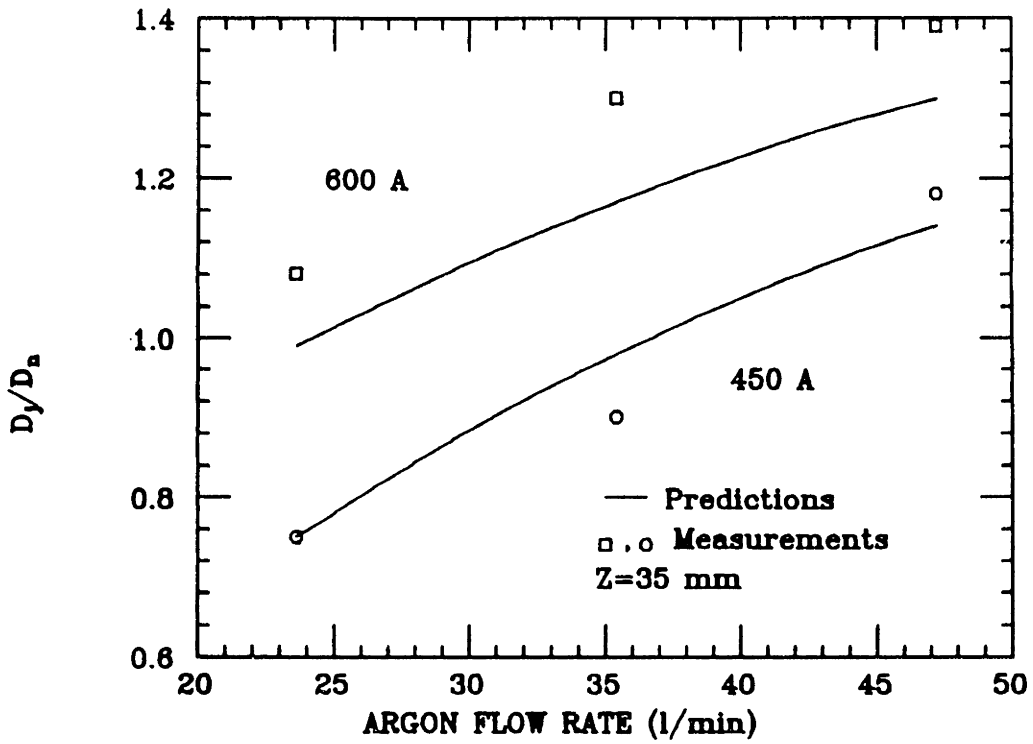

Figure II.C.12 Normalized jet diameter (radial position at which U=100 m/s) versus the torch flow rate and current - comparison of calculated and experimental data.

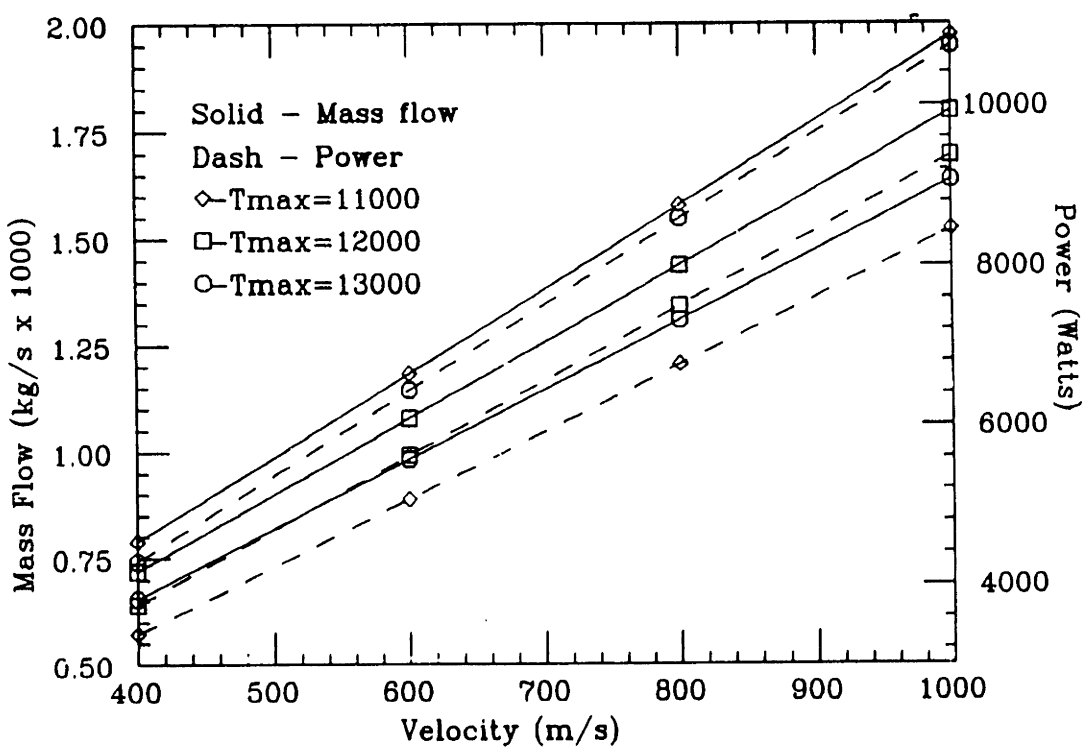

Figure II.D.1 Mass flow and power from the torch exit versus the maximum velocity, for three different maximum temperatures ($n_u = n_t = 2.8$).

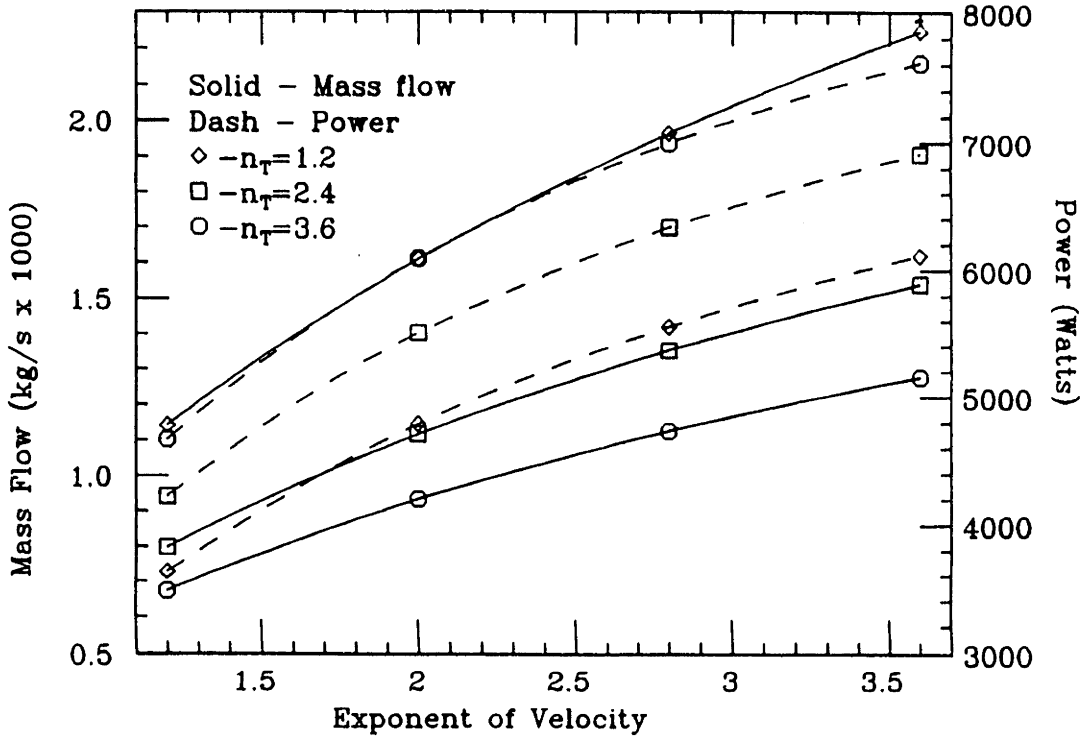

Figure II.D.2 Mass flow and power from the torch exit versus the exponent of velocity for three different temperature exponents (U_{max} = 700 m/s, T_{max} = 12,000k).

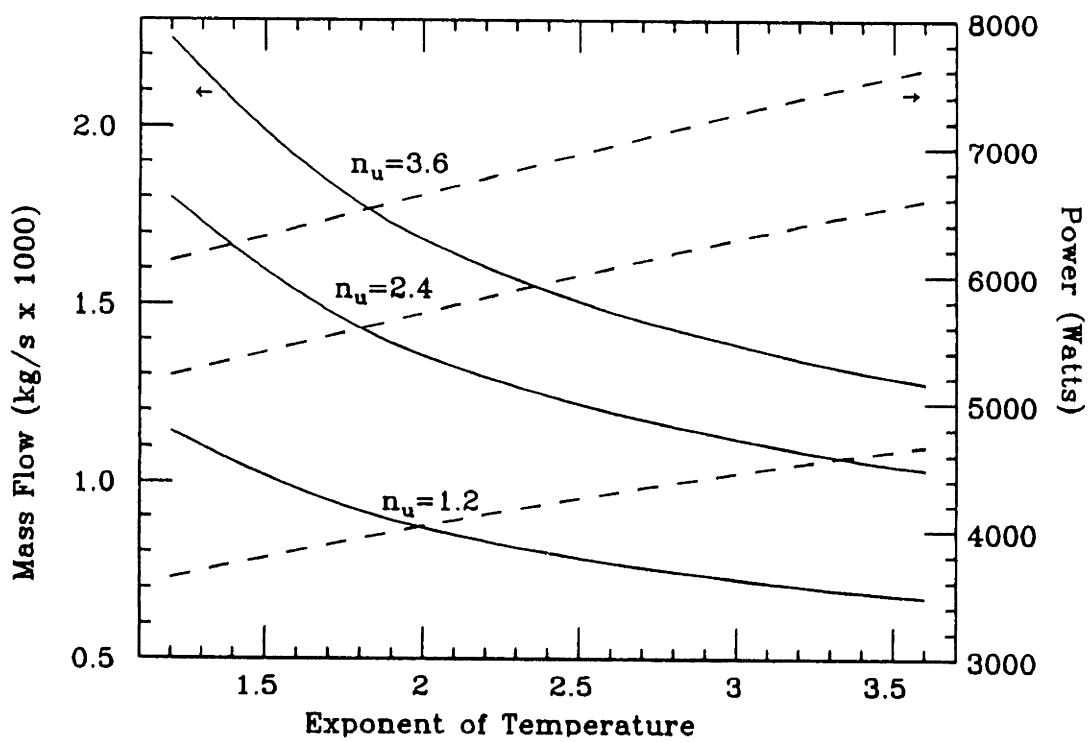

Figure II.D.3 Mass flow and power from the torch exit versus the exponent of temperature for three different velocity exponents (U_{max} = 700 m/s, T_{max} = 12,000k).

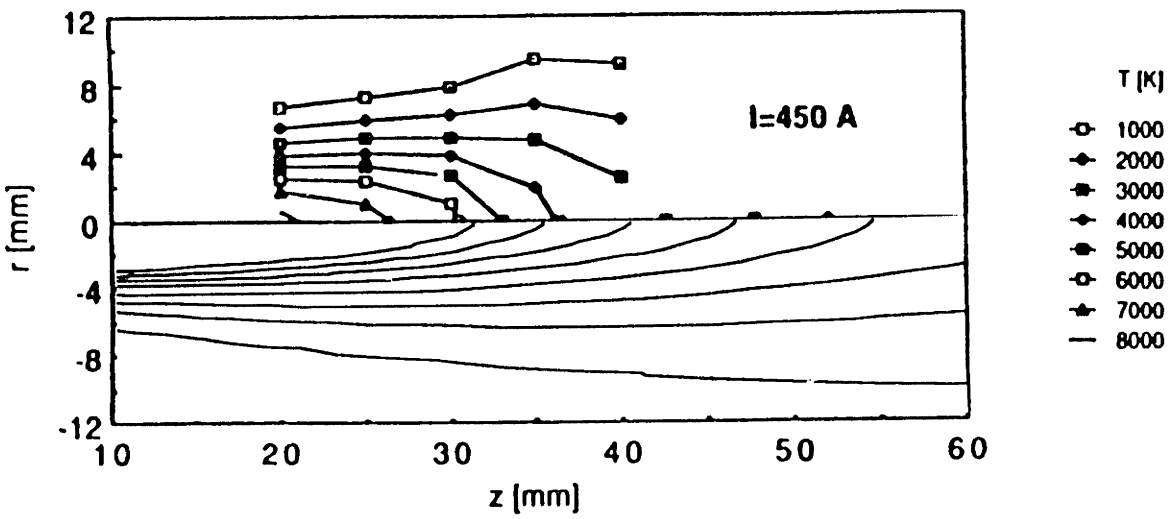

(a)

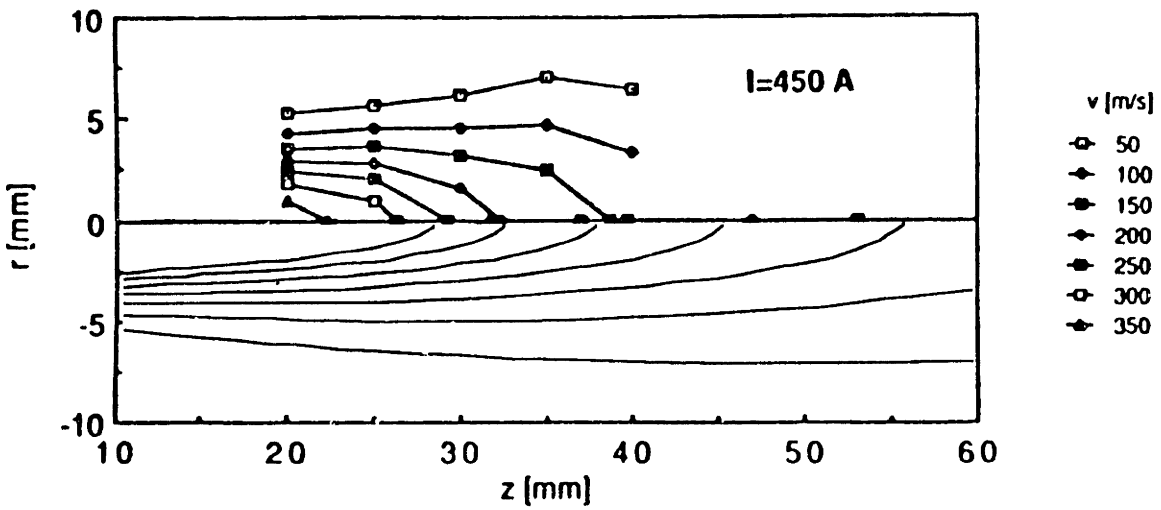

(b)

Figure II.D.4 Comparison of the measured and calculated
(a) temperature and
(b) velocity contours (450 amp, 35.4 lit/min).

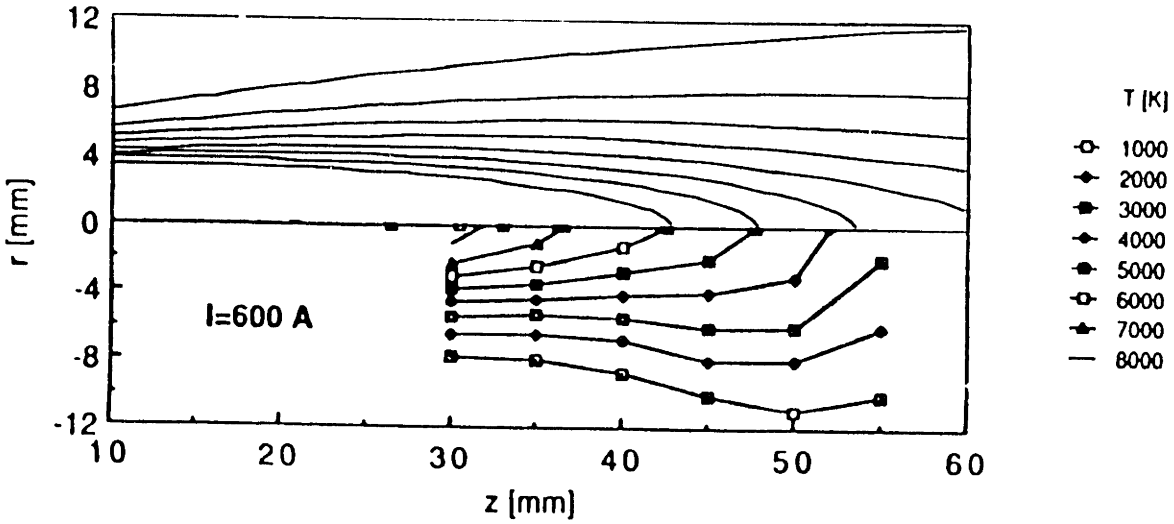

(a)

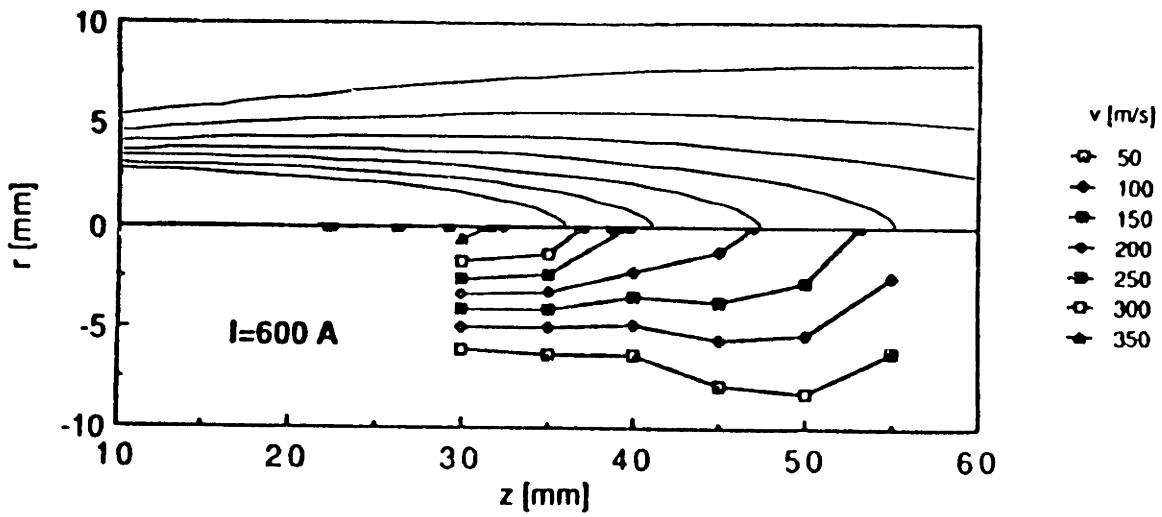

(b)

Figure II.D.5 Comparison of the measured and calculated
(a) temperature and
(b) velocity contours (600 amp, 35.4 lit/min).

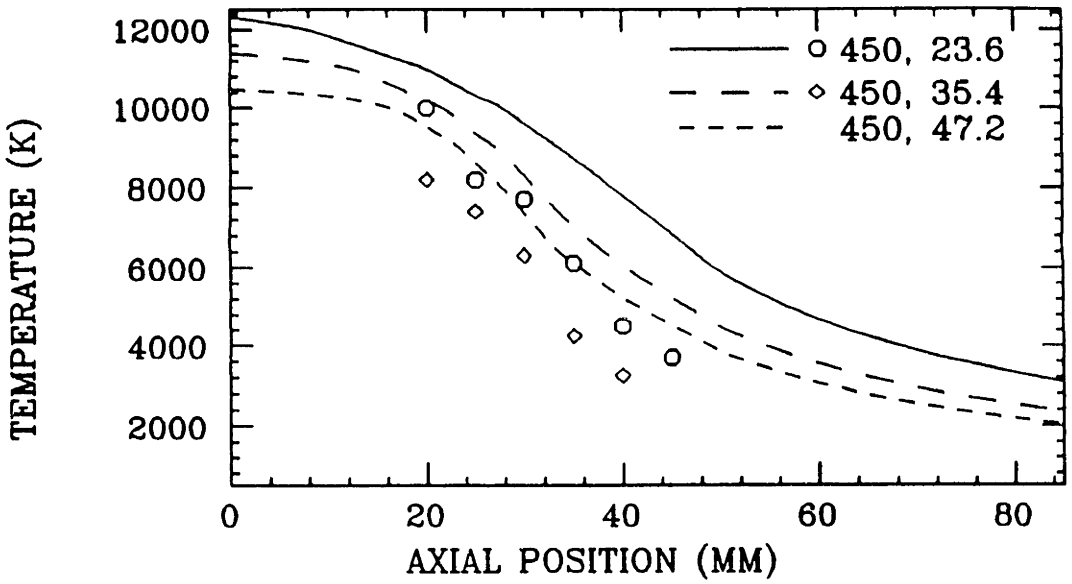

(a)

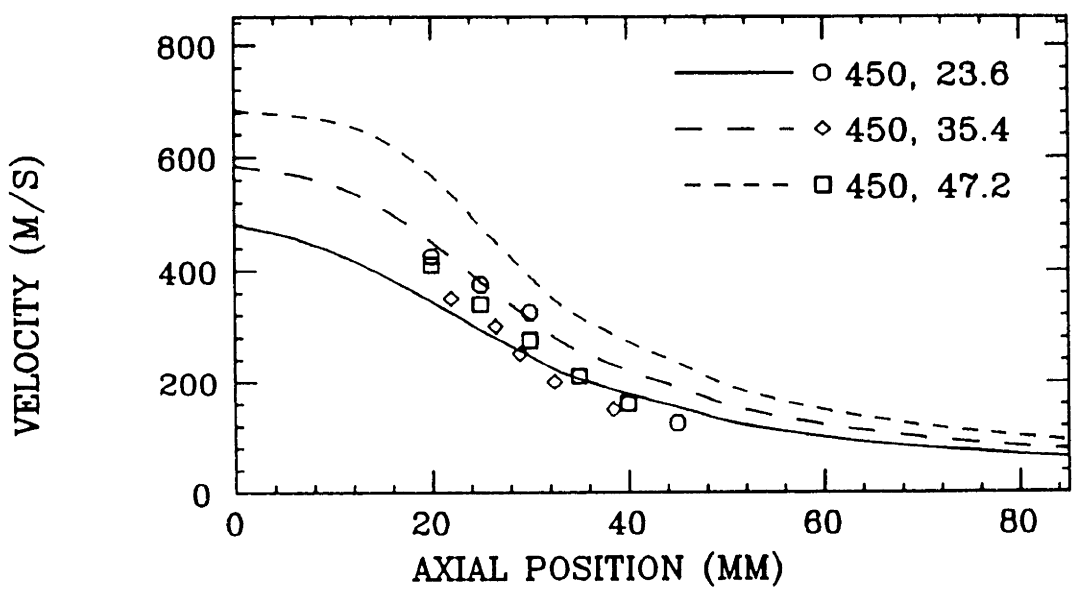

(b)

Figure II.D.6 Comparison of the experimental and theoretical
(a) temperature and
(b) velocity profiles on the plume axis (450 amp cases).

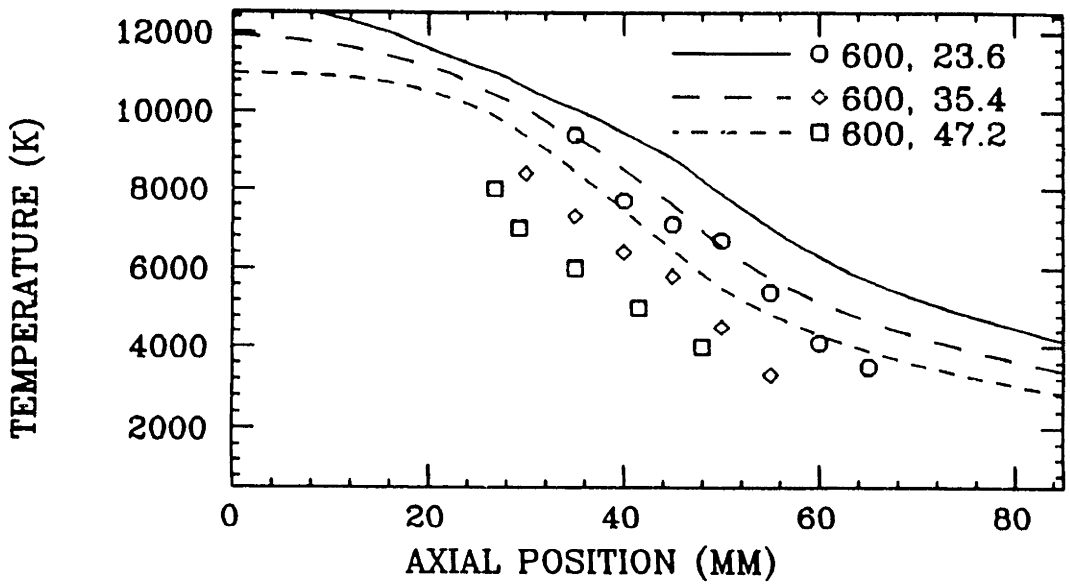

(a)

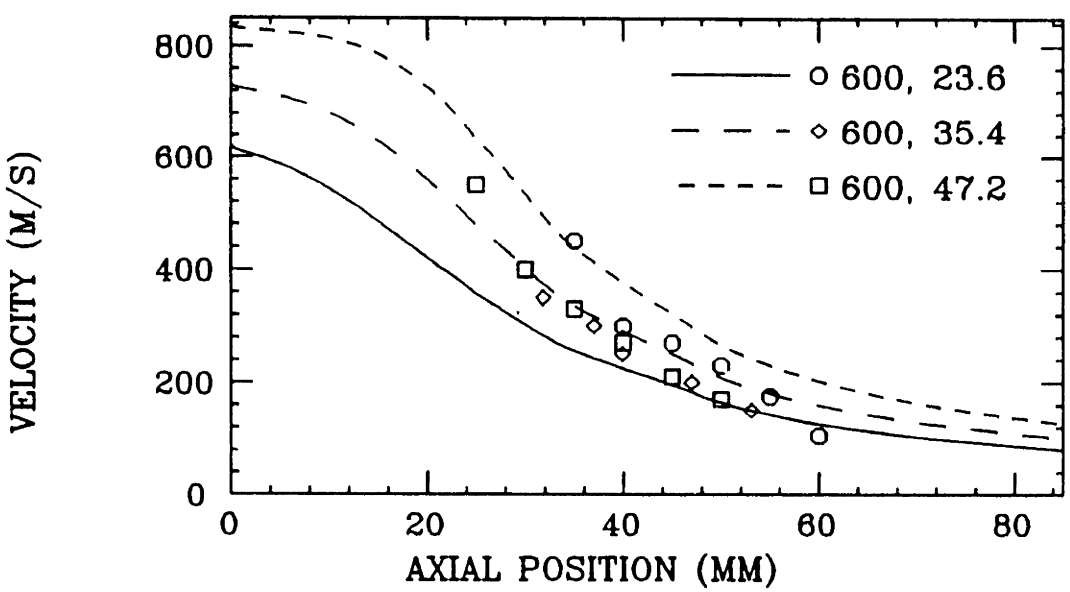

(b)

Figure II.D.7 Comparison of the experimental and theoretical
(a) temperature and
(b) velocity profiles on the plume axis (600 amp cases).

CHAPTER III. MODELING THE PLASMA TORCH - A SIMPLIFIED APPROACH

Up to the present time most modelers of plasma plumes and plasma-particle interactions regarded the plasma torch as a "black box" and had to rely on experimental measurements, or worse still, "educated guesswork" to specify the temperature and the velocity fields, including the swirl profiles, in the torch exit region. This situation was highly unsatisfactory, because any set of modeling and experimental results were specific to a given torch and given operating conditions.

While the transport phenomena inside torches are very complex, quite useful advances have been made in this area. Figure III.A.1 shows a schematic sketch of the key phenomena that have to be addressed in modeling the behavior inside plasma torches. These include such complex issues as the effect of arc attachment, and electromagnetic forces as well as fluid flow and heat transfer phenomena.

The next section presents a review of the modeling of plasma torches. It examines two types of work, namely that related to constricted or wall stabilized arcs which can operate in a transferred mode and that related more strictly to non-transferred plasma torches.

III.A LITERATURE REVIEW OF PLASMA TORCH MODELS

III.A.1. CONSTRICTED ARCS

The constricted, or wall stabilized arc shown in Fig III.A.2 has been of interest both as a heat source and as a laboratory tool for studying plasma for quite some time. Constricted arc phenomena may be described by the conservation equations given in section IV.A. The earliest attempts at representing constricted arc phenomena (up to 1973) are documented in a review by Incropera.(1) The attempts at solving these equations date from the early 1930's and fall into three categories based on the simplifications included in the problem description.

III.A.1.a Fully developed region

The earliest references in the literature (1934-1964) address primarily the fully developed region of the arc in which the heat losses to the walls balance the joule heating in the arc. In this region the temperature is only a function of the radial coordinate. Despite its limitations, the fully developed arc assumption was pursued because it presented the only means of tackling the complex nature of arc phenomena in plasma torches.[2-3]

III.A.1.b Entrance region: decoupled parabolic equations

The second set of references (1962-1965) deal with the next level of complexity which describes both the fully developed and the arc entrance regions using the continuity equation, and the (laminar) momentum and energy conservation equations. The electromagnetic forces are neglected, as are the enthalpy transport due to electron drift and any swirling velocity component. These equations are further simplified using boundary layer approximations, which eliminate the momentum equation for the radial component of velocity. Further simplifications are introduced to decouple the energy equation from the continuity and momentum equations so they can be transformed into a set of ordinary differential equations for numerical solution such as that by Stine and Watson.[4]

III.A.1.c Entrance region: coupled parabolic equations

The next development in the literature (1964-1983) is the solution of the same equations accounting for the coupling and non-linear nature of properties. The coupled equations in boundary layer form have been solved analytically[5] and using finite difference approaches[6-7] but provided about the same useful information as the Stine-Watson solution.

The finite difference solution of Watson and Pegot[8] was the first to solve the coupled set of boundary layer type equations which included a careful allowance for the transport and thermodynamic properties of the gas. Though it includes assumptions which are not necessarily valid for non-transferred arc torches, (e.g. arbitrary assumptions for the inlet boundary conditions, and negligible radial current density). This work continues to be one of the most commonly cited descriptions of plasma torch modeling. A representative example of a three-dimensional plot of the enthalpy within the torch is shown in Figure III.A.3.

A few more recent studies (1969-1981) have expanded on the boundary layer approach by including the effect of swirl flow, turbulence, radiation transport, and secondary gas injection. The work in the 1970's is summarized in a culminating work by Schaeffer,[9] which takes account of all these phenomena. In general though, these all assumed an electric field which is parallel to the axis and uniform along the radius, which is a severe limitation, and the effect of the electromagnetic forces has also been neglected.

Some of this work indicated that departures from local thermal equilibrium (LTE) may become significant in these types of arcs.[10] Such studies indicate that a complete description of the plasma phenomena in a constricted arc should ideally use two-temperature forms of the energy equation.

Mazza and Pfender[11] (1983) used an LTE model to approximate a transferred-arc torch, indicating that it is still a useful approximation. This model, however, is limited by the use of idealized conditions at the upstream and fully developed conditions at the downstream boundaries, and its neglect of electromagnetic forces. A typical set of temperatures inside the torch is shown in Figure III.A.4.

III.A.1.d Fully elliptic equations:

Earlier, (1980-1981) Chen, et al.[12-13] used both the LTE and two-temperature descriptions of a plasma to model plasma reactors. In these models the fully elliptic form of the governing equations were applied and the electromagnetic forces in the momentum equations and the transport of thermal energy by electron drift in the energy equation were included. The main limitations of these studies again are their use of fully developed conditions at the upstream and downstream boundaries. Additionally, this work was aimed at modeling the constriction of an arc due to radial gas injection. Temperature contours in the constriction zone are shown in Figure III.A.5.

III.A.2 TRANSPORT PHENOMENA INSIDE PLASMA TORCHES.

While some of the older models have been developed which may be used to describe transport phenomena in plasma torches, e.g. Watson and Pegot,[8] Schaeffer,[9] and Mazza and Pfender,[11] in general these contained a large number of assumptions about

the electromagnetic phenomena which limited their usefulness, and for the most part, they were not actually used for generating direct comparisons between measurements and predictions in the plasma plume. Some recent plume work has been based on the application of the model of Mazza and Pfender to approximate the nozzle exit conditions of a plasma torch.(14) In this case, however, the behavior of the torch and that of the plume were not represented in a fully coupled manner.

A few of the latest (1973-1991) works do take into account the non-transferred mode of torch operation, although each does so in an approximate manner.

The first is some interesting work done in the U.S.S.R.(15-16) which involves the use of approximate similarity in correlating the characteristics of arcs in several torch configurations. This approach may perhaps provide useful guidelines to torch design, but cannot give the detailed information sought here.

The second is an interesting work done to study a plasma thruster.(17) While this work solves the complete set of LTE governing equations and includes some electrode effects, the geometry (seen in Figure III.A.6, which shows the plasma velocity vectors) is significantly different than the plasma torch studied in this research.

More recent work by this author in collaboration with others(18-19) also made some rather sweeping assumptions about the arc attachment and dimensions, but focussed on what the model could explain about swirl phenomena, as well as how the model could predict the temperature in a laminar argon plasma plume. The model shows excellent agreement when compared to measurements(18) and gives important insights into torch behavior, especially regarding swirling flow in the plasma torch. One or two drawbacks can be pointed out in this model; it necessarily relies on the experimentally determined power level in the torch, (i.e it cannot predict torch V-I characteristics), it requires the arc length and radius to be specified and it may introduce some errors in the computation because of the neglect of electromagnetic forces.

Later this work was extended to other torches operating at higher flow rates in which the flow was assumed to be turbulent, but the results were less satisfactory, possibly due to the neglect of electromagnetic forces in the simplified model.(19)

Other work has improved on the models of the magneto-fluid-dynamic phenomena within the torch, and their effect on the plasma plume. Scott et al.[20] studied a non-transferred arc plasma torch both experimentally and using a model which accounted for electromagnetic phenomena, heat transfer, fluid flow, (including swirl) and turbulence. Some simplifications (e.g. modeling a single gas system, though the experiments were not performed in a controlled atmosphere) and oversights (e.g. the boundary conditions used have not been presented), however, limit the range of practical application of this work.

Recent work by the author and Szekely,[21-22] which is described in section IV.A-B, has taken a more realistic account of the boundary conditions used to describe the torch. This includes an approximate method for estimating the swirl generated by a given injection scheme, examines the effect of the electromagnetic forces, studies the effect of the cathode current density boundary condition, and accounts for the presence or absence of dissimilar gases. The study of swirl gives an indication of the competing roles which the swirl and the electromagnetic forces play in determining the nozzle exit profiles. This work, while far from complete, adds to the data base regarding the behavior of non-transferred arc plasma torches. A comparison with previously mentioned experimental temperature measurements provides useful support for the validity of the model.

III.B APPLICATION OF THE SIMPLIFIED MODEL OF THE PLASMA TORCH TO A LAMINAR ARGON - ARGON SYSTEM

III.B.1. INTRODUCTION

The use of both transferred and non–transferred arcs is of considerable interest in steel processing, in smelting, melting, heating and surface treatment applications.[23-26] In recent years there has been considerable effort in the modeling of plasma systems which has been reviewed in Section II.A., which focused on the plasma plume.

The input into these calculations, pertaining to plume behavior, in addition to the system geometry, the power input and the gas flow rate necessarily had to involve specifying the temperature and the velocity profiles at the torch exit. In the early work this could serve as an adjustable parameter, to bring about "agreement" between measurements and predictions. In more recent work the present authors[27-28] and others[29] have shown the need to simultaneously satisfy the overall heat and mass balances in defining the torch

exit conditions (i.e. the starting point of the integration of the governing equations) which has provided a highly desirable constraint and at the same time conferred more credibility on the modeling effort.

A serious conceptual problem remains, however, that up to the present time any plume calculation had to rely on experimental input and there existed no fundamental way of incorporating the torch characteristics into such modeling efforts. This was a major difficulty, because it would be highly desirable to develop a predictive capability for the torch efficiency and to be able to do plasma plume calculations without prior measurements.

The main motivation for undertaking this work was to initiate research into the understanding of flow phenomena inside the torch and to explore the sensitivity of the plume behavior to the heat and fluid flow phenomena postulated inside the plasma torch. The ultimate, long term, objective of the research is to develop a comprehensive understanding of transport phenomena inside plasma torches and thus to provide guidelines toward optimal torch design.

III.B.2 STATEMENT OF THE PROBLEM.

Figure III.B.1 shows a schematic sketch of a typical non–transferred arc plasma torch. It is seen that the torch consists of a pointed cathode (often made of tungsten or thoriated tungsten) and a water cooled anode (often made of copper or of copper alloys). An arc is struck between the cathode and the anode and part of the thermal energy generated in the arc (due to Joule heating) is being transferred to the plasma gas (often argon, argon–nitrogen or argon–hydrogen mixtures). The hot (e.g. 10,000–15,000 K) gases emerging from the torch constitute the plasma plume, which is then used to perform the metallurgical work, that is heating, melting or surface treatment.

As a matter of fact only a fraction (e.g. 25 - 35%) of the total energy generated in the torch modeled here is available in the plume, the remainder being lost to the water cooled anode by convection, the Thompson effect, electron condensation at the anode and by thermal radiation.

The principal issue that one needs to address here is how the shape and properties of the plasma column formed inside the torch will affect the heat and fluid flow phenomena and hence the velocity and temperature distribution of the plasma gases exiting the torch.

If this problem could be solved rigorously a complete closure could be obtained and all the currently invoked empiricism in plume modeling could be eliminated.

Certain qualitative observations may be readily made at this point.

(i) As the gas is heated up during its passage through the torch a significant incremental axial momentum will be generated and hence any initially introduced azimuthal momentum will be overwhelmed.

(ii) If a short arc is being produced this will lead to a loss in thermal efficiency, for two reasons:

(a) the initially hot gases will have a longer residence time in contact with the water cooled anode

(b) the higher temperatures generated in the smaller arc volume (under the condition of constant input power) will lead to increased radiation losses.

(iii) A long, thin arc column would lead to a higher maximum exit temperature and a higher thermal efficiency, than would a broad, shorter arc column.

These essentially "common sense" observations are qualitative at this stage; the specific purpose of the paper is to quantify these relationships by performing parametric calculations to explore the effect of the arc column dimensions on the temperature and the velocity profiles and on the torch efficiency. These theoretical predictions will be compared with experimental measurements.

III.B.3 FORMULATION.

Figure III.B.2 provides a sketch of the idealized system considered for the formulation. It is seen that the section of the torch downstream from the cathode is

approximated as a cylinder into which an argon gas stream is being fed at a fixed temperature (700 K in the present instance); this argon stream has both axial and swirl components. The plasma column is approximated as being of cylindrical shape, with the attachment occurring at the end of the column. The actual volume of the attachment tail is considered to be small. The volume of the column, that is, its length and diameter, are parameters in the calculation.

Then in essence the formulation has to represent the following:

(i) the velocity and temperature field inside the torch by solving the axi-symmetric heat flow and fluid flow equations, with a specified heat generation .

(ii) an overall heat balance on the system, with due allowance for the losses due to the behavior of electrons and ions at the cathode and anode, and the radiative and convective heat transfer between the plasma gas and the water cooled walls–to obtain information on the torch efficiency.

Thus we have:

Continuity of mass:

$$\frac{\partial(\rho u)}{\partial z}+\frac{1}{r}\frac{\partial(\rho r v)}{\partial r}=0 \qquad [III.B.1]$$

Conservation of axial momentum:

$$\frac{\partial(\rho u^2)}{\partial z}+\frac{1}{r}\frac{\partial(\rho r u v)}{\partial r}=-\frac{\partial P}{\partial z}+2\frac{\partial}{\partial z}\left[\mu\left(\frac{\partial u}{\partial z}\right)\right]+\frac{1}{r}\frac{\partial}{\partial r}\left[r\mu\left(\frac{\partial u}{\partial r}+\frac{\partial v}{\partial z}\right)\right] \qquad [III.B.2]$$

Conservation of radial momentum:

$$\frac{\partial(\rho u v)}{\partial z}+\frac{1}{r}\frac{\partial(\rho r v^2)}{\partial r}=-\frac{\partial P}{\partial r}+\frac{\partial}{\partial z}\left[\mu\left(\frac{\partial v}{\partial z}+\frac{\partial u}{\partial r}\right)\right]+\frac{2}{r}\frac{\partial}{\partial r}\left[r\mu\left(\frac{\partial v}{\partial r}\right)\right]$$
$$-\mu\frac{2v}{r^2}+\frac{\rho w^2}{r} \qquad [III.B.3]$$

Conservation of azimuthal momentum:

$$\frac{\partial(\rho ruw)}{\partial z}+\frac{1}{r}\frac{\partial(\rho r^2 vw)}{\partial r}=\frac{\partial}{\partial z}\left(\mu\frac{\partial(rw)}{\partial z}\right)+\frac{1}{r}\frac{\partial}{\partial r}\left[\mu r\left(\frac{\partial(rw)}{\partial r}\right)\right]-\frac{2}{r}\frac{\partial(\mu rw)}{\partial r} \qquad [III.B.4]$$

Conservation of energy:

$$\frac{\partial(\rho uh)}{\partial z}+\frac{1}{r}\frac{\partial(\rho rvh)}{\partial r}=\frac{\partial}{\partial z}\left(\frac{k}{C_p}\frac{\partial h}{\partial z}\right)+\frac{1}{r}\frac{\partial}{\partial r}\left(\frac{rk}{C_p}\frac{\partial h}{\partial r}\right)+S_j-S_R \qquad [III.B.5]$$

An approximate allowance must be made for the loss of electrical energy to the electrodes. These losses at the anode may be described approximately by the following equation:

$$Q_{e,a}=I\left[\left(\frac{5}{2}+\frac{e\Phi_d}{k_b\sigma}\right)\frac{k_bT_e}{e}+\phi_a\right] \qquad [III.B.6]$$

The first term is the Thompson effect and the second is the contribution from electron condensation at the anode. This is energy in the arc that is unavailable for joule heating. For an argon plasma with an electron temperature of 10000 K in the boundary layer (the work function of the copper anode is taken to be 4.0) this may be approximated as follows:[30]

$$Q_{e,a}=(2.76+4.0) \qquad [III.B.7]$$

At the cathode, ion bombardment of the surface imparts some of the thermal energy which causes evaporation of electrons. This phenomena is quite complex, with radiation and convection also heating the cathode surface. Some of this heat is lost by conduction, as the cathode is water cooled. The model makes allowance for radiation and convection, but it assumes that the energy of ion bombardment is approximately equal to the energy required for electron evaporation, so no further allowance is made for energy lost to the cathode. Thus, an approximate estimate of the energy available in the arc for joule heating is given by the following:

$$Q_j=Q_{tot}-Q_{e,a}=VI-6.76I \qquad [III.B.8]$$

As noted in Table III.B.IV, this leaves 3.10 kW of the total torch power (4.79 kW) available for joule heating. The heating is assumed to be distributed uniformly through the cylindrical arc column so that the Joule heating source can be estimated:

$$S_j = \frac{Q_j}{\pi r_a^2 l_a} \qquad \text{[III.B.9]}$$

In this way the governing equations are fully defined and may be solved when the boundary conditions and gas properties are specified.

The boundary conditions are summarized in Table III.B.I with reference to Figure III.B.II. At the inlet (AB) the axial velocity is a parabolic function of radius while the swirl velocity is prescribed as that of solid body rotation. This set of equations is readily solved numerically, using a procedure described in earlier papers;[27-28] in essence a modification of the 2-EFIX code was employed[31] and typically a 17 x 25 grid was employed within the torch and a 23 x 40 grid in the plume region. The properties of the argon plasma are taken from the literature.[32-33]

The solution of this set of equations then provided information on the temperature and velocity profiles inside the torch and at the plane of the torch exit. This information could then be used in principle to integrate the heat flow and fluid flow equations describing the plume. In fact these two sets of equations were solved together as a continuum. It follows that the computed results given in subsequent sections will provide information on temperature and velocity data both inside and outside the torch (the plume region). A selection of the computed results is given in the following.

III.B.4 COMPUTED RESULTS

In generating the computed results, the input parameters were so selected to allow a global comparison with experimental data reported by researchers at the Idaho National Engineering Laboratory (INEL).[28] The computed results will be presented in the following two sections which describe the effect of inlet swirl on torch behavior and the effect of arc column characteristics on the temperature and velocity profiles in the torch and in the plume:

III.B.4.a The effect of swirl on the torch behavior.

It is a well established fact that swirling flows, with the greatly enhanced entrainment they produce, may markedly modify the behavior of the plume. For this reason it is of interest to examine how a given inlet swirl condition is modified as the gas passes through the torch.

The swirl may be quantified using the swirl number, *Sw*, which is defined as the ratio of the axial flux of the azimuthal momentum to the axial flux of the axial momentum, normalized by an appropriate radius R_0 (taken here as the nozzle radius). This is given by the following expression:

$$\frac{G_\theta}{G_z R_0} = Sw \qquad [III.B.10]$$

where the axial flux of the azimuthal momentum is

$$G_\theta = \int_0^\infty \rho u w r^2 dr \qquad [III.B.11]$$

and the axial flux of axial momentum (neglecting the pressure term) is

$$G_z = \int_0^\infty \rho u^2 r dr \qquad [III.B.12]$$

In order to define the swirl boundary condition at the inlet of the torch (line AB of Figure III.A.3) the specified velocity profiles are integrated numerically over the radius to evaluate the swirl number. The specified azimuthal velocity, w is then adjusted to give the desired inlet swirl number. After the calculation of the flow field has been completed, the above expressions are integrated numerically at the exit of the torch to determine the exit swirl number.

The computed results in this regard are summarized in Tables III.B.II and III.B.III and in Figures III.B.3 and III.B.4.

Table III.B.II shows the behavior of an unheated system. It is see[illegible] the initially imposed swirl is largely maintained, although some decay in the swirl m[illegible] occur

due to transfer of azimuthal momentum to the wall of the torch. The computed axial position of the centerline velocities is shown in Figure III.B.3, where it is seen that a very sharp decay of the axial velocity occurs throughout the whole axial distance travelled along the torch and the plume for swirl number equal to one.

Table III.B.III and Figure III.B.4 show the corresponding results, but now for a heated torch. It is seen that notwithstanding the very high value assigned to the swirl number at the inlet, the flow field is overwhelmed by the expansion of the gas, brought about by the arc heating, so that the swirl number at the exit is quite small. A logical consequence of this behavior is that the previously observed reduction in the gas velocity at the centerline does not occur in this instance. Indeed, as observed in Figure III.B.4, the computed axial variation in the centerline temperatures is essentially identical for all the cases considered here.

The important practical point to be made here is that the generation of highly swirling flows in plasma torches is far from straight forward.

Table III.B.4 summarizes the input conditions in the computations. The base case corresponds to a specific well documented experimental run, carried out at the INEL. The input power and the gas flow rate were accordingly fixed and the parameters varied, as seen in the table, were the dimensions of the arc column.

As limiting cases the arc column occupied as little as 4.5% of the torch volume (run #B23E) and as much as 77% of the torch volume (run #B23M).

Examination of this table is quite instructive, because it reveals the following key points:

(i) In spite of the vary large variations in the volume of the arc column that have been explored, the overall arc efficiency varied only between 29% and 40% ; the experimentally observed arc efficiency for this run by the INEL researchers was 24.6% ± 4.4%.

(ii) The variation in the maximum torch exit temperatures (from 10,446 K to 12,569 K) was even smaller in percentage terms, notwithstanding the large range of arc column volumes that has been explored.

(iii) It is of interest to note that for an identical power input the maximum exit temperature did not correspond to the highest thermal efficiency. In fact a thin, long arc column gave the maximum temperature, but because of the enhanced radiation losses from such a system, this did not correspond to the highest thermal efficiency.

Let us now examine these results in a graphical form. In the plots that follow the experimentally measured temperatures are shown with the discrete symbols, while the computed results are depicted by continuous or broken lines.

Figure III.B.5 (a) and (b) show the effect of the arc radius on the computed axial and radial temperature profiles, for a fixed arc length of 6.1 mm, which is about 1/5 of the torch length (i.e. the distance from the cathode tip to the torch exit.

Inspection of Figure III.B.5 (a) shows that while the maximum temperatures inside the torch will depend markedly on the arc column diameter, the temperature profiles outside the torch, i.e. in the plume would be much less affected. Perhaps fortuitously, the smallest arc column diameter would give the best agreement with the experimental measurements, but this is not a critical issue here. As seen in Figure III.B.5 (b) the effect on the radial profile (computed 1 mm from the torch exit) is quite similar.

Figure III.B.6 (a) and (b) depict the behavior of a 13.7 mm long arc column again exploring the effect of the arc column diameter. In a qualitative sense these results are again quite similar to those seen earlier in Figure III.B.5, showing relative insensitivity to the arc dimensions chosen.

Figure III.B.7 (a) and (b) depict the behavior of the longest (24.5 mm) arc column which appears to over-estimate the temperatures (and the arc efficiency) quite consistently– although not by a very wide margin. This finding appears to be consistent with physical reasoning, because one would expect the length of the arc column to be consistently shorter than the distance between the cathode tip and the torch exit.

Figure III.B.8 (a) and (b) represent the data given earlier for the smallest arc radius, 2.95 mm, but now with the arc length as a parameter. The conclusions that may be drawn are quite similar in that the experimental results are quite well represented using intermediate or shorter arc column lengths.

Up to the present point we examined only the axial or single radial temperature profiles in the system. The following discussion describes the comparison of three sets of experimental data from INEL[28] to calculations; these are summarized in Table III.B.5.

Figure III.B.9 is a plot of the temperature contours in the torch and 50mm of the plume for run B28. The maximum temperature is over 24000 K and occurs at the end of the arc column (see Table III.B.V). This figure gives a good overall picture of the temperatures in the system but is difficult to use for direct comparison with the measurements. For this reason, the figures that follow will consist of axial and radial temperature profiles of the system.

Figure III.B.10 (a) shows a set of radial temperature profiles taken at five axial positions measured from the torch tip. Figure III.B.10 (b) shows the axial temperature profile, again for the same INEL run that has been considered previously. It it seen that the agreement between measurements and predictions is quite good.

Figures III.B.11 (a) and (b) and III.B.12 (a) and (b) show a comparison between the experimentally measured and the theoretically predicted radial and axial temperature profiles for two other experimental runs reported by the INEL researchers (see Table III.B.5). The arc column dimensions were so selected to provide arc efficiencies that fall within the experimental range. (By analyzing the cumulative experimental errors, the postulated error limits for the torch efficiency were put at about ±3.8-4.4 percentage points).

It is seen that the agreement seems quite reasonable. Possibly the computed results could have been "tuned" within the margin of the experimental error of efficiency to bring about a better agreement between measurements and predictions of the temperatures in the plasma plume.

III.B.5 DISCUSSION

In this section a new technique has been presented for calculating the temperature and velocity distribution in the plume region of plasma jets in non–transferred arc systems. This approach postulated the dimensions of the arc column inside the torch and then used

this as a specified heat source in the solution of the heat flow and fluid flow equations–both inside the torch and in the plume.

In this representation allowance has been made for convective heat transfer between the hot plasma gases and the water cooled anode and for radiative heat losses. Additionally, an approximate allowance is made for the Thompson effect and for electron condensation at the anode. Thus one could represent the different thermal efficiencies that may be attained for different arc column dimensions. In particular one could show that shorter arcs inside the torch would give rise to lower arc efficiencies.

Perhaps the most interesting finding of this work was that (for a given input power and flow rate) the overall torch performance was not very sensitive to the arc column dimensions chosen. Indeed a 2–fold variation in the column radius, a 4–fold variation in the column length, corresponding to a 17–fold variation in the column volume produced only an 11 percentage point difference in the overall arc efficiency and only a 13.5% difference in the maximum exit temperatures.

It was found that by making "reasonable estimates" of the arc column dimensions one could provide an adequate representation of experimental data.

These calculations, while primarily scoping in nature, have nevertheless provided very useful insight into plasma torch behavior. More specifically, it has been shown that:

- much of the initially imposed swirl is overwhelmed by the expansion of the plasma gas due to heating by the arc column and corresponding increase in axial momentum, so that high swirl at the exit would be difficult to sustain using conventional torch design.

- the calculations have shown that the actual shape of the plasma column will have an effect on the temperature and the velocity profiles of the plasma jet exiting the torch. The fact that shorter arcs would lead to a lower thermal efficiency and also to a lower maximum exit temperature is an essentially expected result. However, the finding that under certain circumstances a long narrow arc column can provide the highest exit temperature, but not necessarily the highest arc efficiency is perhaps less expected, but apparently consistent with experience.[34]

It is felt that several important lessons may be learned from these simple scoping calculations:

- for a given power input and plasma gas flow rate the flow phenomena inside the torch will have a subtle, rather than overwhelming effect on the temperature profiles in the plasma plume. This finding explains the apparent success of many modeling efforts.

- the actual dimensions of the plasma column will affect both the arc efficiency and the nature of the temperature (and velocity) distribution of the plasma jet exiting the torch.

- the maximum temperature of the plasma jet exiting the torch is not necessarily a good measure of the arc efficiency; indeed using this maximum temperature to fit measurements and predictions may not be the ideal way to proceed in the light of the present work.

- the rapid expansion of the plasma gas inside the torch will tend to overwhelm any swirl that has been imposed at the inlet to the torch.

At this point some comment should be made on the shortcomings of the present treatment. In the model proposed here the dimensions of the arc column had to be specified a priori, at present in a somewhat arbitrary manner.

Clearly, both the length and the diameter of the arc column will have to depend on the specific operating conditions; higher currents will lead to a constriction of the column, for otherwise identical conditions, while flow instabilities or the onset of turbulence should lead to shorter arcs within the torch. These aspects of the problem will have to be addressed by considering the actual arc formation within the torch. Such work is presented in Chapter IV; nevertheless, it is thought that the scoping studies presented in the present paper should provide helpful, previously unavailable insights into torch behavior. Furthermore, by making "reasonable" assumptions for the arc column dimensions, it should be possible to estimate plume behavior even in the absence of experimentally measured torch exit temperatures.

III.C. APPLICATION OF THE SIMPLIFIED MODEL TO TURBULENT SYSTEMS

III.C.1 INTRODUCTION

In the vast majority of practical applications of plasma torches, the flow rates in the system are much higher than those used in Section III.B. The resulting flows in the plume are either fully turbulent or make a transition to turbulence as they exit the torch. These types of flows have been addressed based on a model of the plasma plume as described in Section II.C-D, which required that assumptions be made about the velocity and temperature profiles of the gas exiting the torch. However, work presented in Chapter II has shown that the computed results for the plume may be very markedly affected by these assumptions. It follows that it would be highly desirable to predict, on a fundamental basis, the parameters that characterize the gas exiting the torch. This is the ultimate purpose of the work to be described in the following.

III.C.2 DESCRIPTION OF THE MODEL FOR TURBULENT CASES

Figure III.C.1 shows a schematic sketch of a given non-transferred arc plasma torch, which has been studied in this work. A complete description of the phenomena inside the torch required the solution of a complex set of coupled partial differential equations which govern fluid and heat flow, turbulence, electromagnetic phenomena, and species conservation. The approach taken here was to simplify the problem by neglecting the electromagnetic effects namely: current flow, magnetic field and the **JXB** or Lorentz forces. The remaining equations are the continuity equation, the axial and radial momentum equations, the equations for turbulent kinetic energy and turbulent energy dissipation, the heat equation and the species balance, as follows:

Continuity

$$\frac{\partial(\rho u)}{\partial z}+\frac{1}{r}\frac{\partial(\rho r v)}{\partial r}=0 \qquad [III.C.1]$$

Axial Momentum

$$\frac{\partial(\rho u^2)}{\partial z}+\frac{1}{r}\frac{\partial(\rho r u v)}{\partial r}=-\frac{\partial P}{\partial z}+2\frac{\partial}{\partial z}\left[\mu_{eff}\left(\frac{\partial u}{\partial z}\right)\right]+\frac{1}{r}\frac{\partial}{\partial r}\left[r\mu_{eff}\left(\frac{\partial u}{\partial r}+\frac{\partial v}{\partial z}\right)\right] \qquad [III.C.2]$$

Radial Momentum

$$\frac{\partial(\rho u v)}{\partial z}+\frac{1}{r}\frac{\partial(\rho r v^2)}{\partial r}=-\frac{\partial P}{\partial r}+\frac{\partial}{\partial z}\left[\mu_{eff}\left(\frac{\partial v}{\partial z}+\frac{\partial u}{\partial r}\right)\right]+\frac{2}{r}\frac{\partial}{\partial r}\left[r\mu_{eff}\left(\frac{\partial v}{\partial r}\right)\right]$$
$$-\mu_{eff}\frac{2v}{r^2}+\frac{\rho w^2}{r} \qquad [III.C.3]$$

Azimuthal Momentum

$$\frac{\partial(\rho r u w)}{\partial z}+\frac{1}{r}\frac{\partial(\rho r^2 v w)}{\partial r}=\frac{\partial}{\partial z}\left(\mu_{eff}\frac{\partial(rw)}{\partial z}\right)+\frac{1}{r}\frac{\partial}{\partial r}\left[\mu_{eff}r\left(\frac{\partial(rw)}{\partial r}\right)\right]$$
$$-\frac{2}{r}\frac{\partial(\mu_{eff}rw)}{\partial r} \qquad [III.C.4]$$

Thermal Energy Conservation

$$\frac{\partial(\rho u h)}{\partial z}+\frac{1}{r}\frac{\partial(\rho r v h)}{\partial r}=\frac{\partial}{\partial z}\left(\frac{\mu_{eff}}{\sigma_h}\frac{\partial h}{\partial z}\right)+\frac{1}{r}\frac{\partial}{\partial r}\left(r\frac{\mu_{eff}}{\sigma_h}\frac{\partial h}{\partial r}\right)-S_R+S_J \qquad [III.C.5]$$

If the plasma torch is discharging into a gas which is different from the gas in the plasma jet, it may entrain large amounts of the ambient gas. In such cases it is necessary to solve the appropriate equation for the mass fraction of the working gas.

Species Conservation

$$\frac{\partial(\rho r u m)}{\partial z}+\frac{1}{r}\frac{\partial(\rho r^2 v m)}{\partial r}=\frac{\partial}{\partial z}\left(\frac{\mu_{eff}}{\sigma_m}\frac{\partial(rm)}{\partial z}\right)+\frac{1}{r}\frac{\partial}{\partial r}\left[\frac{\mu_{eff}}{\sigma_m}r\left(\frac{\partial(rm)}{\partial r}\right)\right] \qquad [III.C.6]$$

Turbulent kinetic Energy:

$$\frac{\partial(\rho u K)}{\partial z}+\frac{1}{r}\frac{\partial(\rho r v K)}{\partial r}=\frac{\partial}{\partial z}\left(\frac{\mu_{eff}}{\sigma_K}\frac{\partial K}{\partial z}\right)+\frac{1}{r}\frac{\partial}{\partial r}\left(r\frac{\mu_{eff}}{\sigma_K}\frac{\partial K}{\partial r}\right)+G-\rho\varepsilon \qquad [III.C.7]$$

Turbulent energy dissipation:

$$\frac{\partial(\rho u\varepsilon)}{\partial z}+\frac{1}{r}\frac{\partial(\rho rv\varepsilon)}{\partial r}=\frac{\partial}{\partial z}\left(\frac{\mu_{eff}}{\sigma_\varepsilon}\frac{\partial\varepsilon}{\partial z}\right)+\frac{1}{r}\frac{\partial}{\partial r}\left(r\frac{\mu_{eff}}{\sigma_\varepsilon}\frac{\partial\varepsilon}{\partial r}\right)+\frac{\varepsilon}{K}(C_1G-\rho\varepsilon C_2) \quad [III.C.8]$$

Where:

$$G=\mu_t\left\{2\left[\left(\frac{\partial u}{\partial z}\right)^2+\left(\frac{\partial v}{\partial r}\right)^2+\left(\frac{v}{r}\right)^2\right]+\left[\left(\frac{\partial w}{\partial z}\right)^2+\left(\frac{\partial u}{\partial r}+\frac{\partial v}{\partial z}\right)^2+\left(\frac{\partial w}{\partial r}-\frac{w}{r}\right)^2\right]\right\} \quad [III.C.9]$$

And:

$$\mu_t=\frac{C_D\rho K^2}{\varepsilon} \quad [III.C.10]$$

The constants for the K–ε model are the values recommended by Pun and Spalding and are given in Table III.C.I.

The boundary conditions for these conservation equations are summarized in Table III.C.II. In the table, "w.f." for the u and v equations indicates that the boundary conditions at all the walls are derived using the standard wall function approach as used by Dilawari and Szekely(35). Note also that even though the model was general, the swirl velocity in the calculations performed here was assumed to be zero, as was done for the experimental comparisons of Section III.B.

To approximate the effects of the arc, the joule heating was estimated from the total power level, discounting the electrical energy carried by the arc, which was estimated from the total electronic heat flux at the anode. The joule heat was included in the energy equation as a constant heat density source term within the region of an idealized cylindrical arc. The procedure employed is identical to that described in the previous section (III.B.). The set of equations, together with the fully temperature dependent equilibrium properties of the plasma were solved using the method described by Pun and Spalding (31), using the approach taken by Dilawari et. al. (35-36).

III.C.3 TURBULENT ARGON/AIR SYSTEM

The set of calculations presented in this section were performed based on a turbulent argon plasma torch issuing into an air atmosphere. Temperature and concentration measurements were taken by Brossa and Pfender using an enthalpy probe.(37) These experiments and the associated operating conditions have been presented in Table II.C.I of Section II.C. In addition, other, still earlier measurements using an enthalpy probe were made on a U-51 Thermal Dynamics plasma torch by Lewis and Gauvin.(38) In both of these cases the plume is turbulent, and so the full set of equations is required for solution, namely, turbulence and species balance equations must be included. Additionally, as a means of investigating discrepancies, a comparison is made with calculations done based on the earlier model presented in Section II.C.

Figure III.C.2(a) and III.C.2(b) illustrate the results of a comparison between two calculations and the experimentally determined temperatures and argon mole fraction for a single case. As seen in the figures the present model which includes the inside of the torch (represented by the solid line) markedly over predicts the temperature, showing poorer agreement with measurement than the previous model. The possible explanation for this is shown in Figure III.C.3, which shows the axial variation of velocity in the two models, in which the torch model shows a much lower maximum velocity at the torch exit.

Figure III.C.4 again illustrate the comparison between the measured and calculated (two models) temperature on the axis of the plume, which shows the model over predicting the temperatures. Figure III.C.5 again illustrates the velocity predicted by this model and the earlier one. Again the velocity predicted by the "inside torch' model is lower than that predicted by the "plume model". This trend is the same for all the runs modeled for this torch, at a range of flow rates and power levels.

Figure III.C.6 illustrates a comparison between the radial temperature and velocity profiles calculated in the "inside torch" model and those specified in the plume model at a position 6mm inside the torch nozzle. It is seen that the temperature profile is not very different, and in fact has the same type of shape, while the velocity profile is much different, being much flatter for the inside torch model.

Figures III.C.7(a) and III.C.7(b) illustrate another comparison with the experimental results of Lewis and Gauvin(38) on the U-51 Thermal Dynamics torch shown

in Fig. III.C.1. Figure III.C.7(a) and Figure III.C.7(b) compares the calculated and experimental temperature, (a) and argon mole fraction, (b) on the centerline of the plume. It is seen in this case that the agreement is reasonable especially noting that the torch efficiency is not even given in the literature. The calculated value is 34.3%, which is reasonable considering the power level, and relatively low flow rate and length of the torch nozzle (30 V, 650 A, 5.937×10^{-4} kg/s, and approximately 35 mm respectively). If comparison of the measured and calculated velocity on the axis of the plume is made as is shown in Figure III.C.8, it is seen that the model again underestimates the velocity in the plume significantly in the region near the torch exit.

From these comparisons we may reasonably conclude that the disagreement between the torch model and the measurements is apparently caused by the prediction of a torch exit velocity which is too low. This leads to a lower level of turbulence in the plume and less turbulent entrainment of the surrounding air. With less air entrainment the plume is not quenched as quickly, resulting in temperatures which are higher than those measured. This discrepancy again underscores the need for knowing the torch exit velocity profiles, especially in these turbulent systems.

The reason for the torch model under predicting the exit velocity may be the neglect of the **JXB** or Lorentz forces. An order of magnitude analysis may be performed to see if these body forces can reasonably affect the exit velocity profile. What is needed is to compare the relevant source terms in the momentum equations, namely the pressure gradient and Lorentz force. The maximum axial pressure gradient calculated in these systems is estimated from the model results as follows:

$$\frac{DP}{Dz} \sim \frac{10 \text{ N/m}^2}{0.001 \text{ m}} = 10^4 \text{ N/m}^3$$

The order of magnitude of the JXB force for a 100 Amp free arc is estimated from the work of Mckelliget and Szekely .[30]

$$j_r B_\theta \sim 10^7 \text{ A/m}^2 \times 10^{-2} \text{ Wb/m}^2 = 10^5 \text{ N/m}^2$$

From this analysis it appears that the Lorentz forces in the arc may indeed affect the shape of the velocity profile that results at the torch exit. Thus, while this simplified model may be adequate to describe the temperature behavior of laminar systems in which

entrainment occurs via laminar diffusion, it may not adequately describe the velocities in these systems. It follows that a fully comprehensive model will necessarily include the electromagnetic forces.

III.C.4 CONCLUSIONS

Experimental measurements of both temperature and velocity are important for comparison with models, as it may be possible in some systems to have agreement with temperatures and not such good agreement with velocities.

The model indicates, and an order of magnitude analysis strongly suggests that the Lorentz or **JXB** forces in the torch are comparable to pressure gradient forces. They must be included in a more complete model as they will effect the velocities in the torch and plume.

III.D. REFERENCES

1. F. P. Incropera, "Procedures for Modeling Laminar Cascade Arc Behavior", IEEE Trans. Plasma Sci., **PS-1**, No. 3, 3-9, (1973).
2. W. Elenbaas, "Die Quecksilber–Hochdruckentladung", Physica, **1**, 635, (1934).
3. "Dynamic Similarity Laws of the Mercury High Pressure Discharge", Physics, **6**, 390, (1935).
4. H. A. Stine and V.R. Watson, "The Theor. Enthalpy Distrib. of Air in Steady Flow Along the Axis of a Direct Current Electric Arc", NASA TN D-1331, (1962).
5. J. G. Skifstad, Review of Theoretical Analyses of Arc Heating In a Tube", ARL 65-207, Oct. (1965).
6. P.S. Masser, "Arc Jet Design", ARS Paper, 2352-62, (1962).
7. D.J. Norton and S.N.B. Murthy, "An Investigation of Energy Transfer in a Tube Arc Heater", ARL 65-54, (1965).
8. V.R. Watson and E.B. Pegot, "Numerical Calculations for the Characteristics of a Gas Flowing Axially Through a Constricted Arc", NASA TN D-4042, (1967).
9. J.F. Schaeffer, "Swirl Arc: A Model for Swirling, Turbulent, Radiative Arc Heater Flowfields", AIAA J., **16**, (10), 1068-1075, (1978).

10. K.J. Clark and F.P. Incropera, "Thermochemical Non-Equilibrium in an Argon Constricted Arc Plasma", AIAA J., **10**, No. 1, 17, (1972).
11. A. Mazza and E. Pfender, "Modeling of an Arc Plasma Reactor for Thermal Plasma Synthesis", Symp. Proc. Int. Symp. Plasma Chem. 6th, **1**, 41-50, (1983).
12. D.M. Chen, K.C. Hsu and E. Pfender, "The Effects of Cold Gas Injection on a Confined Arc Column", IEEE Trans. Plasma Sci., **PS-8**, No. 4, 425, (1980).
13. D.M. Chen, K.C. Hsu and E. Pfender, "Two Temperature Modelling of an Arc Plasma Reactor", Plasma Chem Plasma Proc., **1**, No. 3, 295-314, (1981).
14. D.J. Varacalle, Jr., J.R. Fincke, G.D Lassahn, B.A. Detering, and J.A. Batdorf., Proc. of National Thermal Spray Conf., Cincinnati, 93, (1989).
15. A.G. Shashkov and O.I. Yasko, "Applic. of Approx. Similarity for Correlating Arc Characteristics", IEEE Trans Plasma Sci., **PS-1**, No. 3, 21-37, (1973).
16. V.A. Vashkevich, S.K. Kravchenko, T.V. Laktyushina, and O.I. Yasko, "On the Allowance for the Temperature Dependence of Plasma Properties for Selection of Dimensionless Numbers to Correlate Characteristics of Electric Arcs", Mater. Res. Soc. Symp. Proc., **30**, 255-61, (1984).
17. W.T. Park and D.I, Choi, "Two Dimensional Model of the Plasma Thruster", J. of Propulsion and Power, **4**, No. 2, 127-32, (1988).
18. A.H. Dilawari, J. Szekely and R. Westhoff, "An Assessment of the Heat and Fluid Flow Phenomena Inside Plasma Torches in Non-Transferred Arc Systems", ISIJ International, **30**, (5), 381-389, (1990).
19. R. Westhoff, A.H. Dilawari and J. Szekely. Mat. Res. Symp. Proc. **190**, 213, (1990).
20. D.A. Scott, P. Kovitya, and G.N. Haddad, J. Appl. Phys. **66**, (11), 5232, (1989).
21. R. Westhoff, and J. Szekely, J. Appl. Phys. **70**, (7), 3455-3466, (1991).
22. R. Westhoff and J. Szekely, Proc. of TMS Conf. on Plasma Processing of Materials, San Diego, (1992).
23. J. Feinman, Ed., Plasma Technology in Metallurgical Processing, Iron and Steel Society,Warrendale, PA. (1987).
24. Plasma Processing of Materials, Publication NMAB-415, Committee on Plasma Processing of Materials, National Materials Advisory Board, National Academy Press, Washington, DC. (1985).
25. V. Dembovsky, Plasma Metallurgy: The Principles, Materials Science Monographs, **23**, Elsevier, New York (1985).
26. J. Kubel Jr., *Advanced Materials and Processes*, **132**, No. 6 (1987), 69.
27. A.H. Dilawari and J. Szekely, *Plasma Chem. Plasma Proc.*, **7** (1987), 317.

28. A.H. Dilawari, J. Szekely, J.Batdorf, and C.B. Shaw, *Plasma Chem. Plasma Proc.*, in press **10**, No. 2, (1989).
29. Y.P Chyou and E. Pfender, *Plasma Chem. Plasma Proc.*, **9**, No. 2, (1989), 291.
30. J. McKelliget and J. Szekely, Met. Trans A, **17A**, 1139-1148, (1986).
31. W.M. Pun and D.B. Spalding, Rep. No. HTS/76/2, Heat Transfer Section, Imperial College, London (1976).
32. C.F. Liu, Ph.D. Thesis, Dept. of Mechanical Engineering, University of Minnesota, Minneapolis, MN. (1977).
33. D.L. Evans and R.S. Tankin, *Phys. Fluids* **10**, (1967), 1137.
34. Professor P. Fauchais, Universite de Limoges, 123 Avenue Albert-Thomas, 87060 Limoges CEDEX, France, Private Communications, (1989).
35. A.H. Dilawari and J. Szekely, *Int. J. Heat and Mass Transfer*, **30**, No. 11, (1987), 2357.
36. A.H. Dilawari and J. Szekely, Mat. Res. Symp. Proc., **98**, (1987), 3.
37. M. Brossa and E. Pfender, Plasma Chem. Plasma Process., **8**, (1), 75, (1988).
38. Lewis and Gauvin, AIChE. J., 19, (5), 982-990, (1973).
38. A.H. Dilawari, J. Szekely and R. Westhoff, Plasma Chem. Plasma Process. **10**, (3), 501, (1990).

Boundary	u	v	rw	h
AB	$u(r)$	0	$rw(r)$	$T = 700$ K
BC	0	0	0	$T = 700$ K
CD	0	0	0	$T = 500$ K
DE	0	$\frac{\partial \rho r v}{\partial r} = 0$	$rw = 0$	$T = 300$ K
EF	$\frac{\partial u}{\partial z} = 0$	$\frac{\partial v}{\partial z} = 0$	$\frac{\partial rw}{\partial z} = 0$	$\frac{\partial h}{\partial z} = 0$
FA	$\frac{\partial u}{\partial r} = 0$	$v = 0$	$\frac{\partial rw}{\partial r} = 0$	$\frac{\partial h}{\partial r} = 0$

Table III.B.I. Boundary conditions used in the simplified plasma torch model (laminar case)

Run No.	Swirl No. at Inlet	Swirl No. at Exit	Gas Velocity at Exit (m/s)
1	0.0	0.00	4.48
2	0.5	0.35	4.09
3	1.0	0.68	0.59

Argon Gas Flow Rate = 0.62 SCMH

Torch Inside Diam. = 12.7 mm

Max. Gas Velocity = 4.50 m/s

Torch Length = 29 mm

Table III.B.II. Effect of swirl number on cold flow in a plasma torch

Run No.	Swirl No. at Inlet	Swirl No. at Exit	Gas Veloc. at Exit (m/s)	Heat Output (kw)	Temp. at Exit (axis) (K)
1	0.0	0.0	71.09	1.592	11193
2	0.5	0.01	71.00	1.592	11195
3	1.0	0.02	70.81	1.589	11201
4	1.5	0.03	70.52	1.584	11208
5	2.0	0.04	70.06	1.576	11214
6	5.0	0.11	64.21	1.497	11211

Argon Gas Flow Rate = 0.62 SCMH
Max. Inlet Gas Velocity = 4.50 m/s
Torch Inside Diam. = 12.7 mm
Torch Length = 29 mm
Joule Heating = 4.79 kW

Table III.B.III. Effect of Swirl Number on Hot Flow in INEL Plasma torch

Run No.	Arc Length (mm)	Arc Radius (mm)	Thermal Efficiency (%)	Max. Temp at Exit (K)	Reynolds No. at Exit
B23E	6.1	2.95	29.23	11133	99.4
B23F	13.7	2.95	30.61	11573	98.3
B23G	24.5	2.95	35.91	12569	95.9
B23H	6.1	4.55	30.40	10885	98.8
B23I	6.1	6.05	28.02	10446	100.0
B23J	13.7	4.55	34.20	11323	96.0
B23K	13.7	6.05	32.19	10864	97.6
B23L	24.5	4.55	40.11	11912	96.8
B23M	24.5	6.05	38.78	11213	96.2

Torch Power = 4.79 kW Joule Heating = 3.10 kW

Argon Gas = 0.59 SCMH Torch Length = 29 mm

Table III.B.IV. Operating Conditions for Studying the Effect of Arc Dimensions on Transport Phenomena in the Plasma Torch

Run No.	Argon Gas (scmh)	Torch Power (kW)	Cur. (A)	Therm. Effic. Exper. (%)	Therm. Effic. Calc. (%)	Exit Temp. Exper. (K)	Exit Temp. Calc. (K)	Arc Radius (mm)	Arc Length (mm)
B23	0.59	4.79	250	24.64 (±4.4)	28.73	11131	11118	2.65	4.40
B28	0.83	9.96	500	29.82 (±4.0)	28.51	12227	12882	2.65	10.50
B32	0.83	15.33	750	30.92 (±3.8)	27.82	13075*	15306	2.35	19.95

*The temperature measuring technique used seems to give constant temperatures above 13,000 K.

Table III.B.V. Simulation of a System Studied Experimentally at INEL

C_1	1.43
C_2	1.92
C_D	0.09
σ_K	1.0
σ_ε	1.3
σ_h	0.9
σ_m	0.9

Table III.C.I. Constants used in K–ε turbulence model

	u	v	rw	h	m	K	ε
AB	$u=u(r)$	0	$rw(r)$	$T = 700$	1	$K = .005u^2$	$\varepsilon = \frac{C_D K^{1.5}}{.03\, r_n}$
BC	w.f	w.f.	w.f.	$T = 700$	$\frac{\partial m}{\partial r} = 0$	w.f.	w.f.
CD	w.f	w.f.	0	$T = 300$	$\frac{\partial m}{\partial z} = 0$	w.f.	w.f.
DE	$\frac{\partial u}{\partial y} = 0$	$\frac{\partial \rho v}{\partial y} = 0$	0	$T = 300$	*1 or 0*	$K \approx 0$	$\varepsilon \approx 0$
EF	$\frac{\partial u}{\partial z} = 0$	0	0	$\frac{\partial h}{\partial z} = 0$	$\frac{\partial m}{\partial z} = 0$	$\frac{\partial K}{\partial z} = 0$	$\frac{\partial \varepsilon}{\partial z} = 0$
FA	$\frac{\partial u}{\partial y} = 0$	0	0	$\frac{\partial h}{\partial y} = 0$	$\frac{\partial m}{\partial r} = 0$	$\frac{\partial K}{\partial r} = 0$	$\frac{\partial \varepsilon}{\partial r} = 0$

Table III.C.II. Boundary Conditions for the Turbulent Case

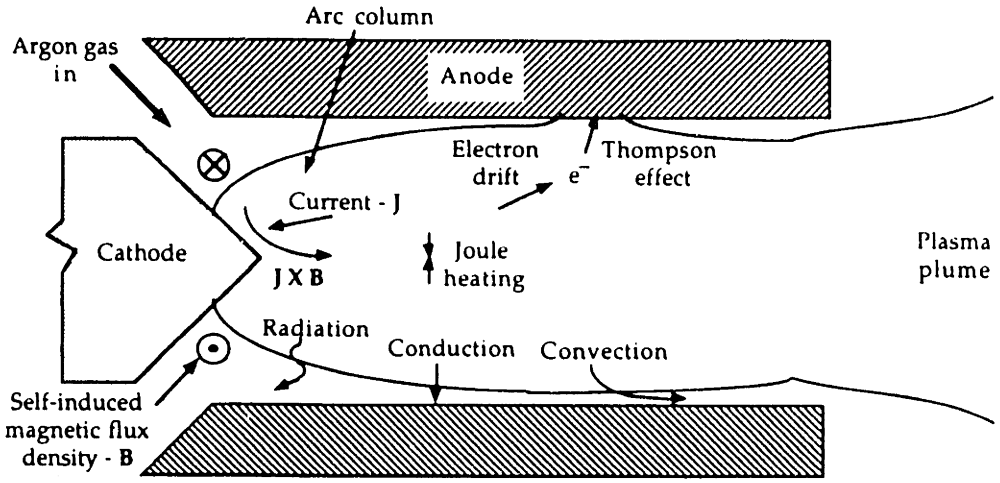

Figure III.A.1. Schematic illustration of the key phenomena in a plasma torch.

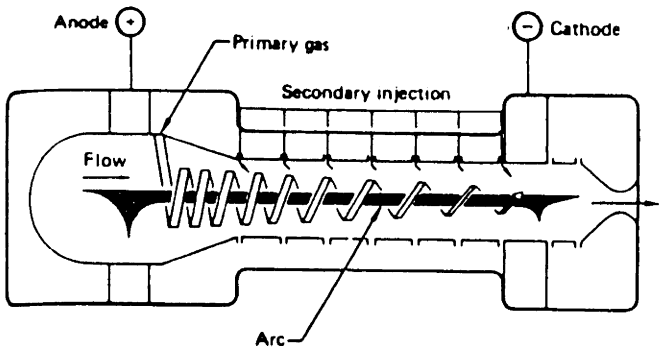

Figure III.A.2. Schematic sketch of a wall stabilized constricted arc after Schaeffer.[9]

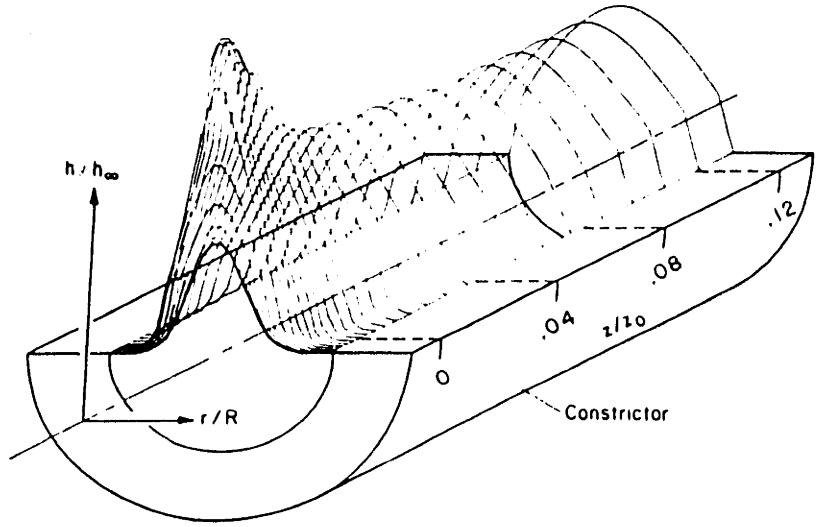

Figure III.A.3. Normalized plasma enthalpy for the calculations of Watson and Pegot.(8)

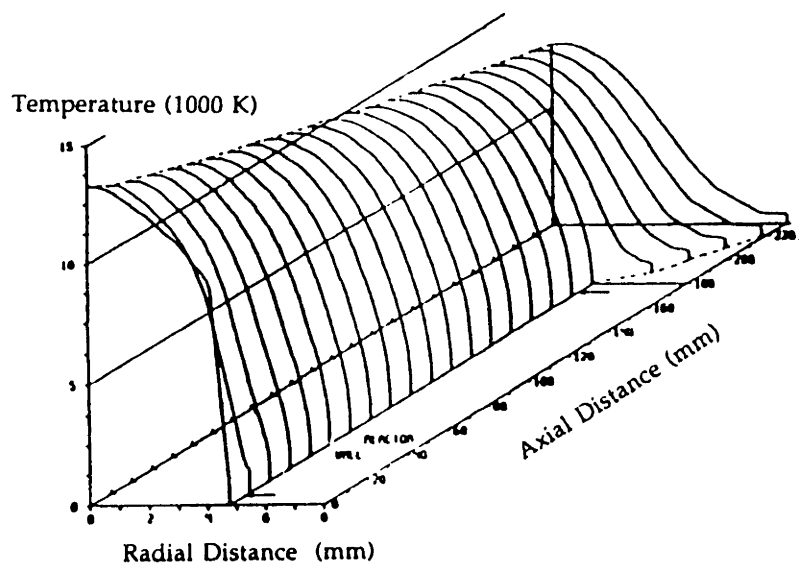

Figure III.A.4. Temperature distribution in a non-transferred arc reactor by Mazza and Pfender.(11)

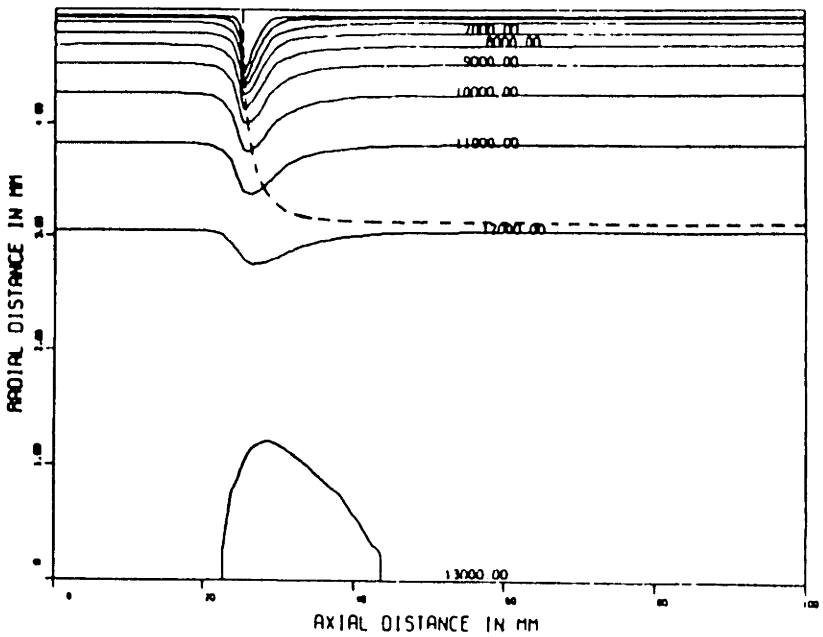

Figure III.A.5. Temperature contours in a confined arc plasma with injected cold gas from Chen et. al.(12) Dashed line indicates the penetration of the injected flow.

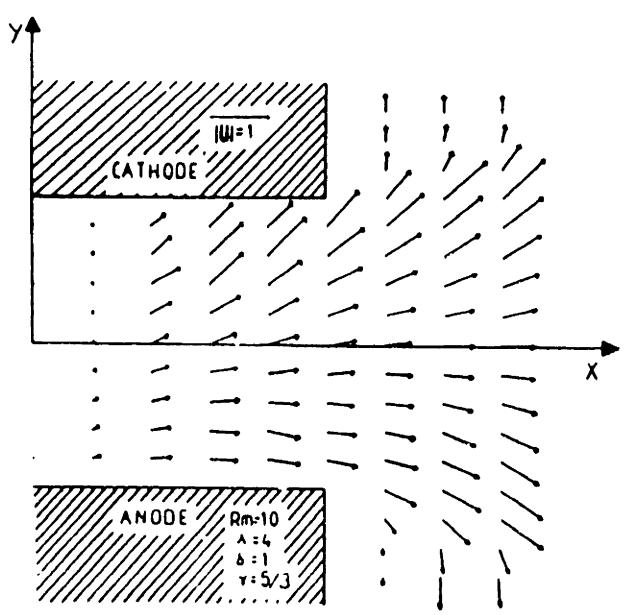

Figure III.A.6. Velocity vectors and configuration in a plasma thruster from Park and Choi.(17)

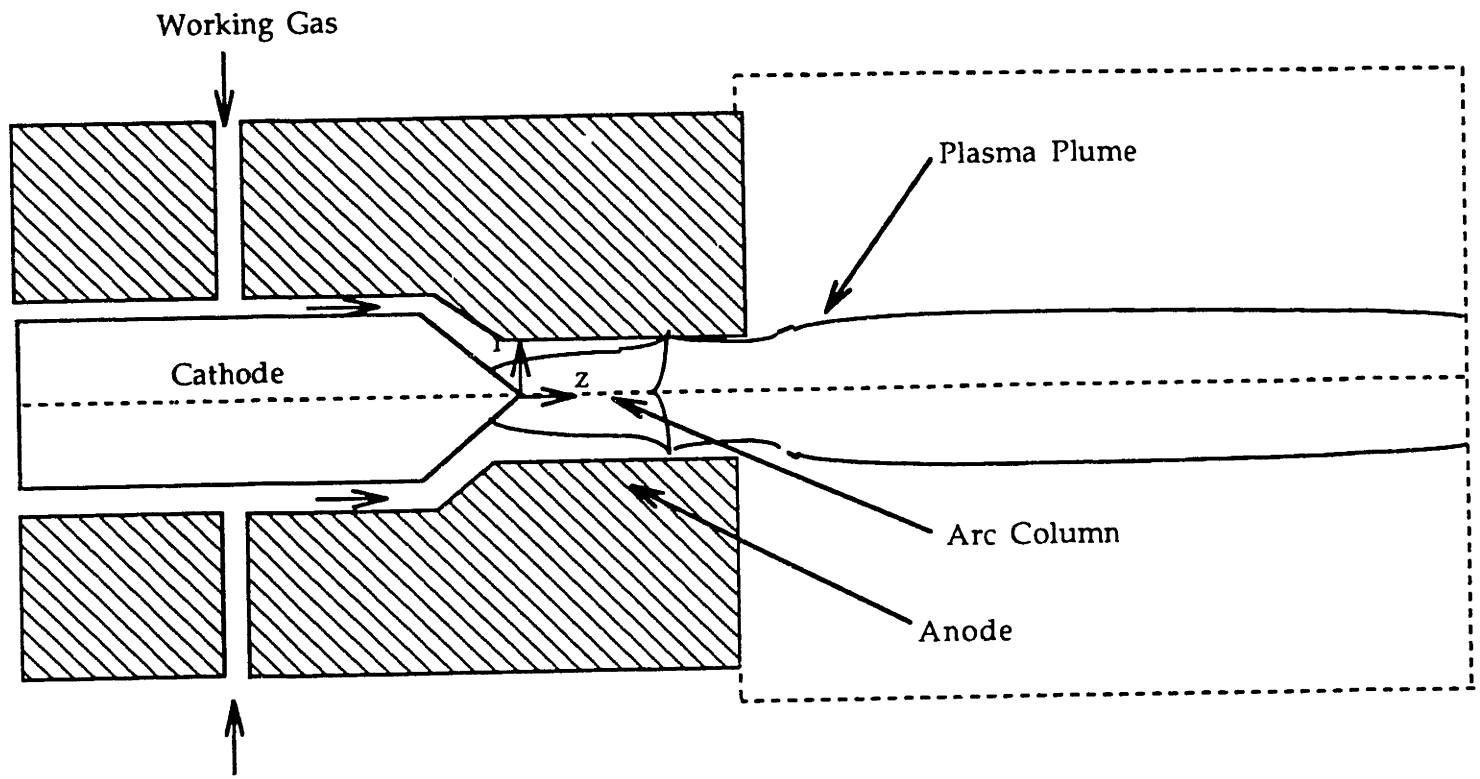

Figure III.B.1. Schematic of a plasma torch.

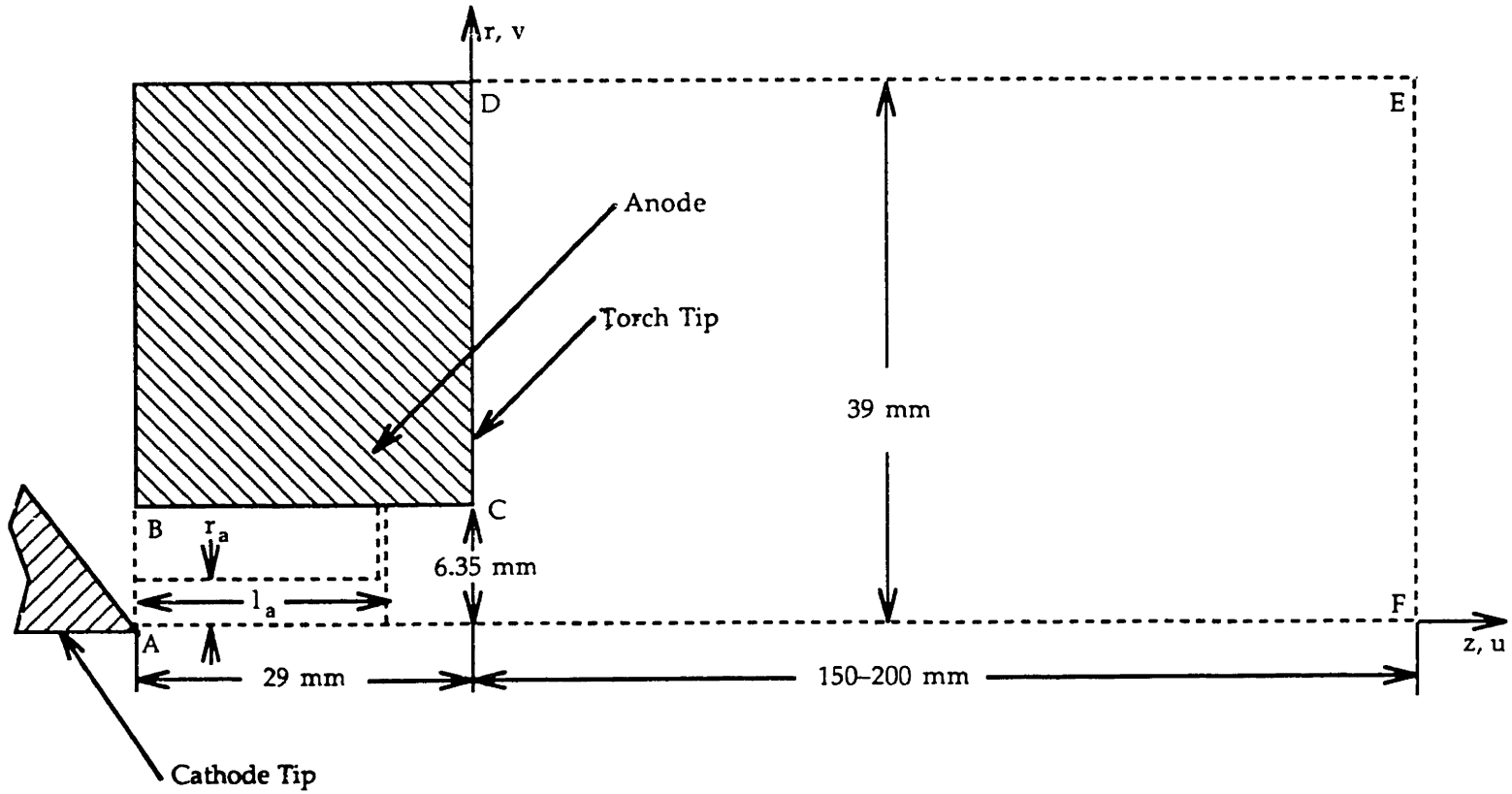

Figure III.B.2. Calculation domain used in the simplified modeling approach.

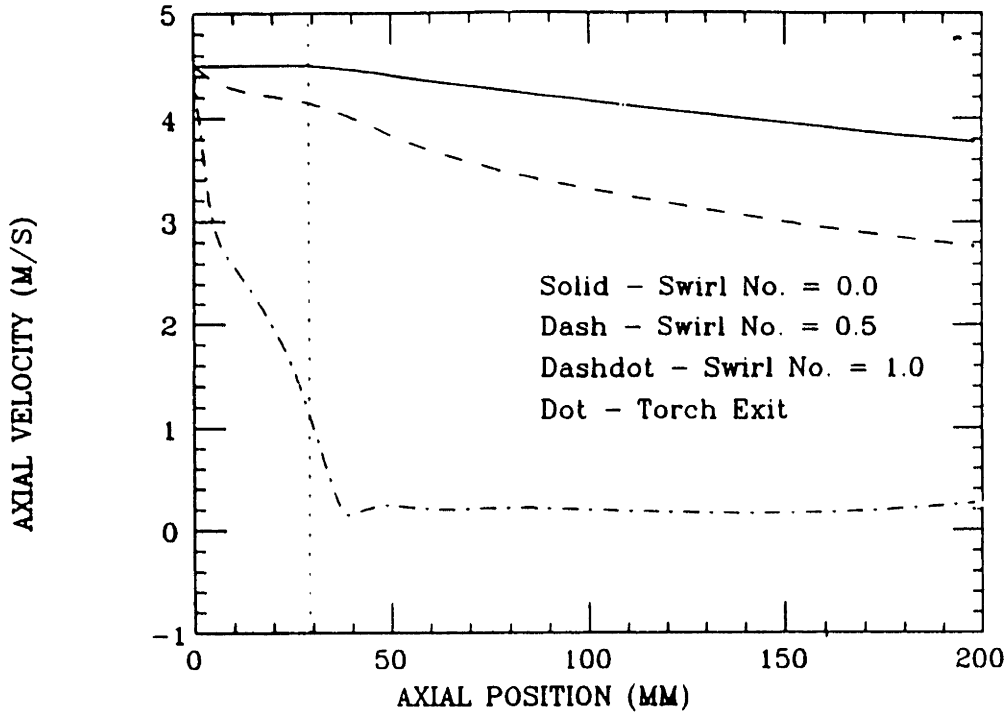

Figure III.B.3. Effect of swirl on axial velocity decay for an unheated torch.

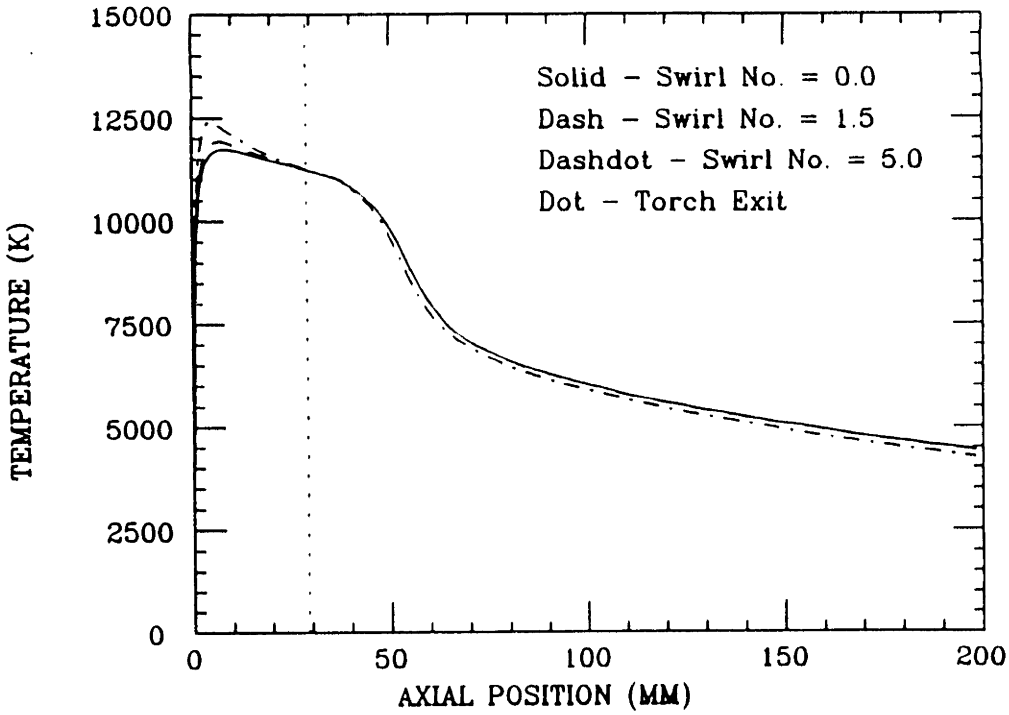

Figure III.B.4. Effect of swirl on axial temperature decay for a heated torch.

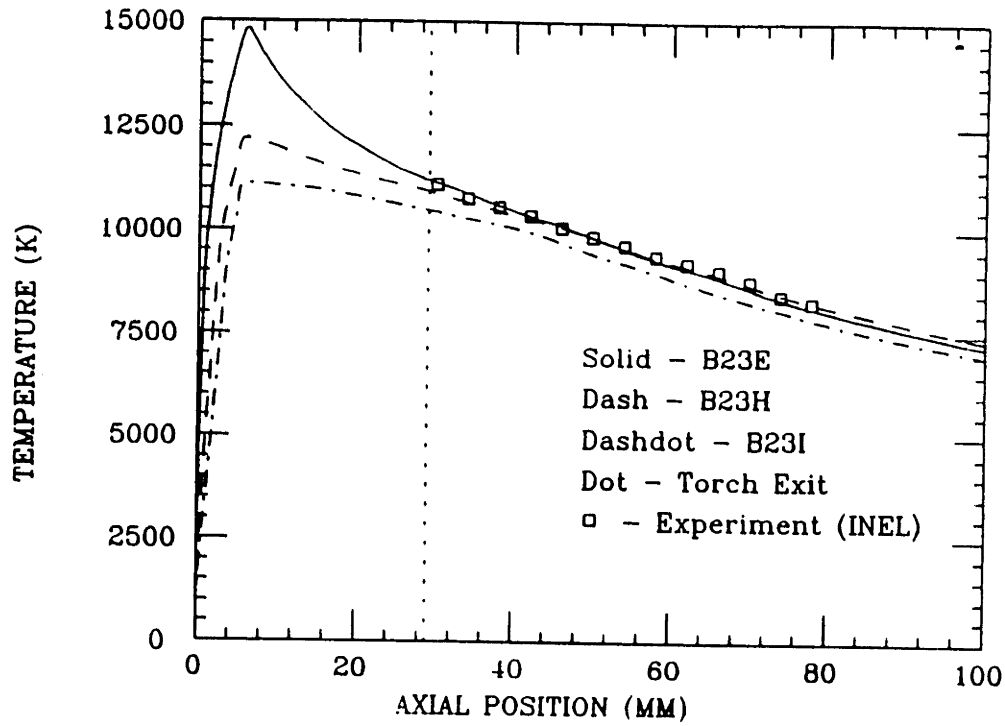

(a)

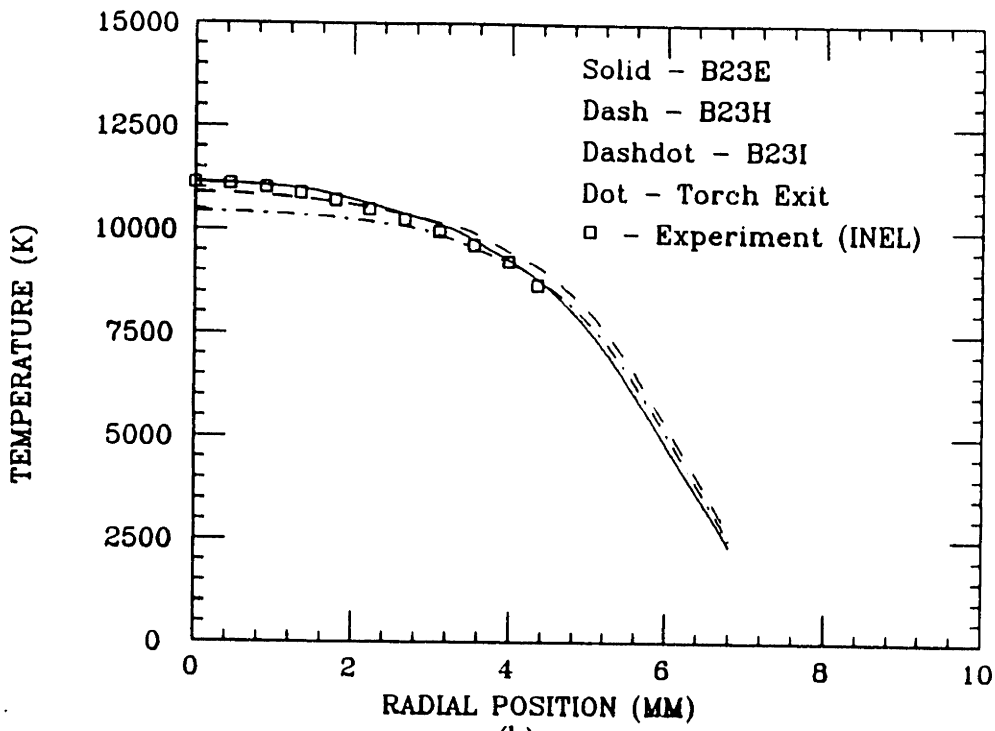

(b)

Figure III.B.5. Effect of arc radius on the (a) axial temperature profile and (b) radial temperature profiles for 6.1 mm Long Arcs.

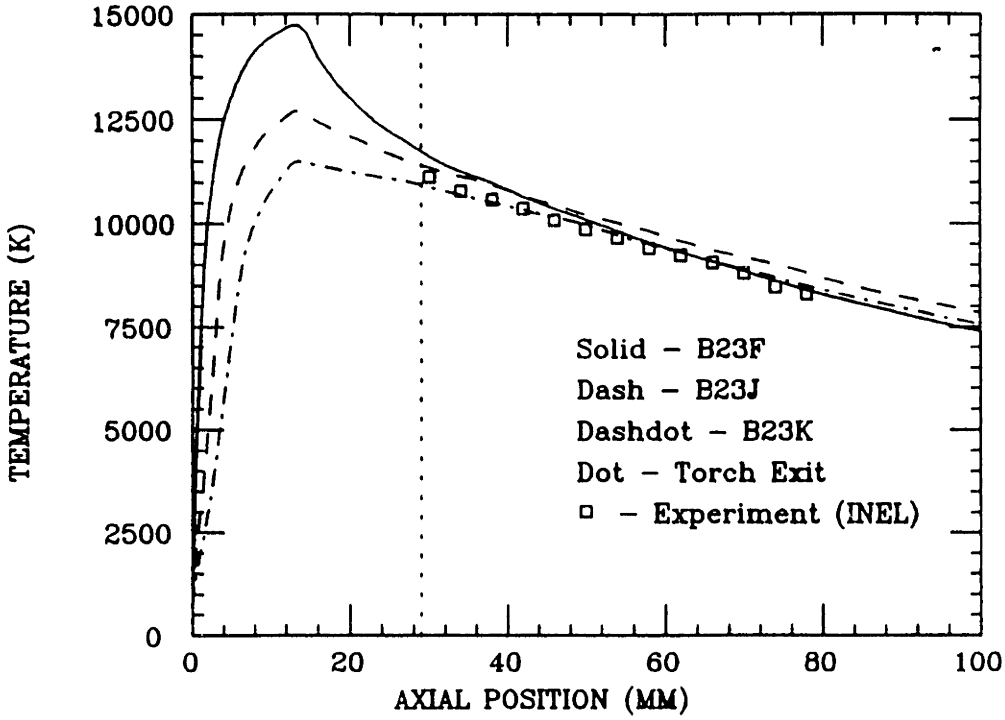

(a)

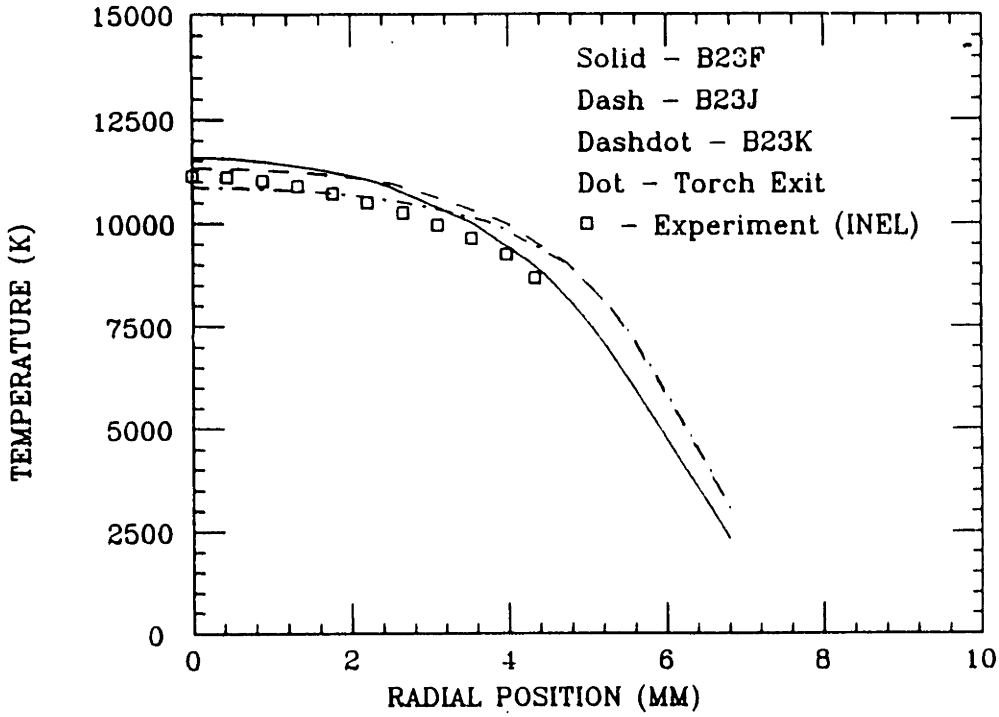

(b)

Figure III.B.6. Effect of arc radius on the (a) axial temperature profile and (b) radial temperature profiles for 13.7 mm Long Arcs.

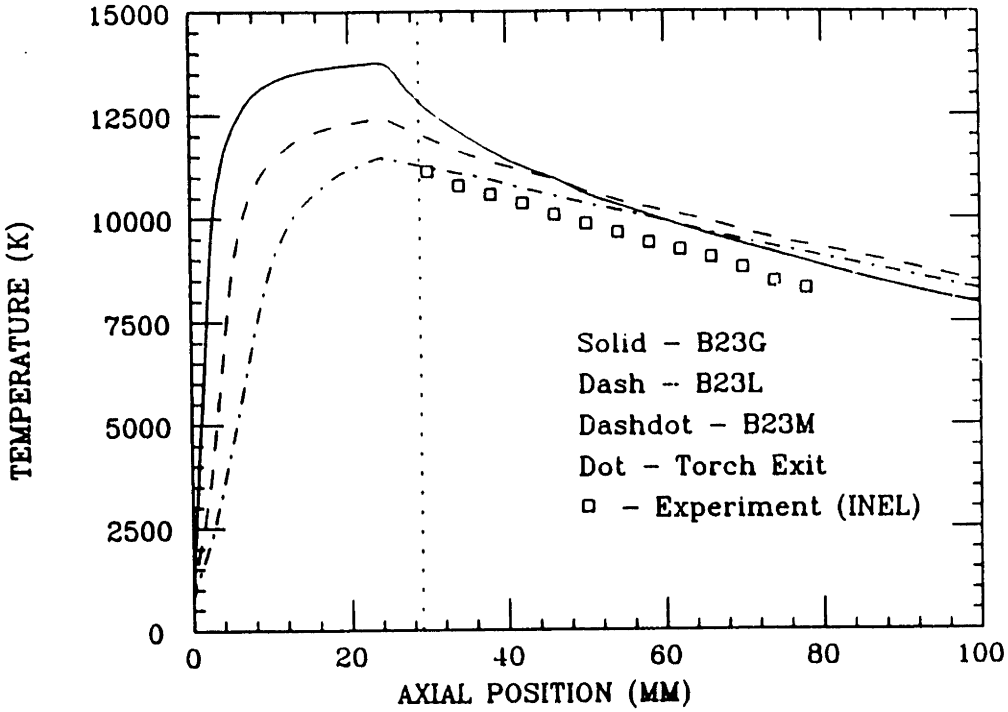

(a)

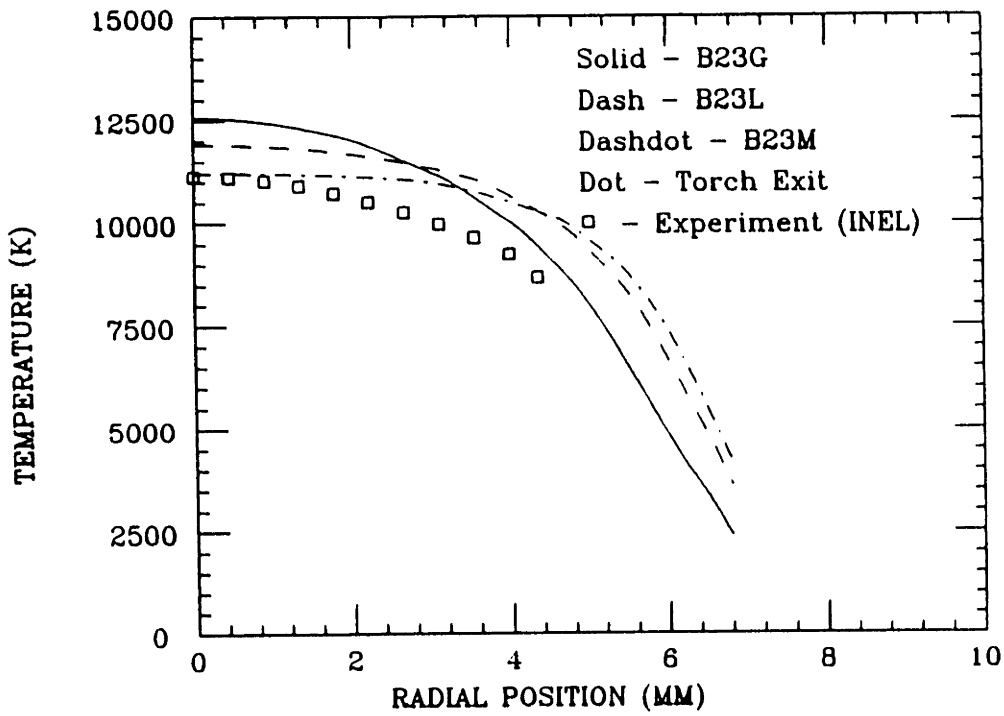

(b)

Figure III.B.7. Effect of arc radius on the (a) axial temperature profile and (b) radial temperature profiles for 24.5 mm Long Arcs.

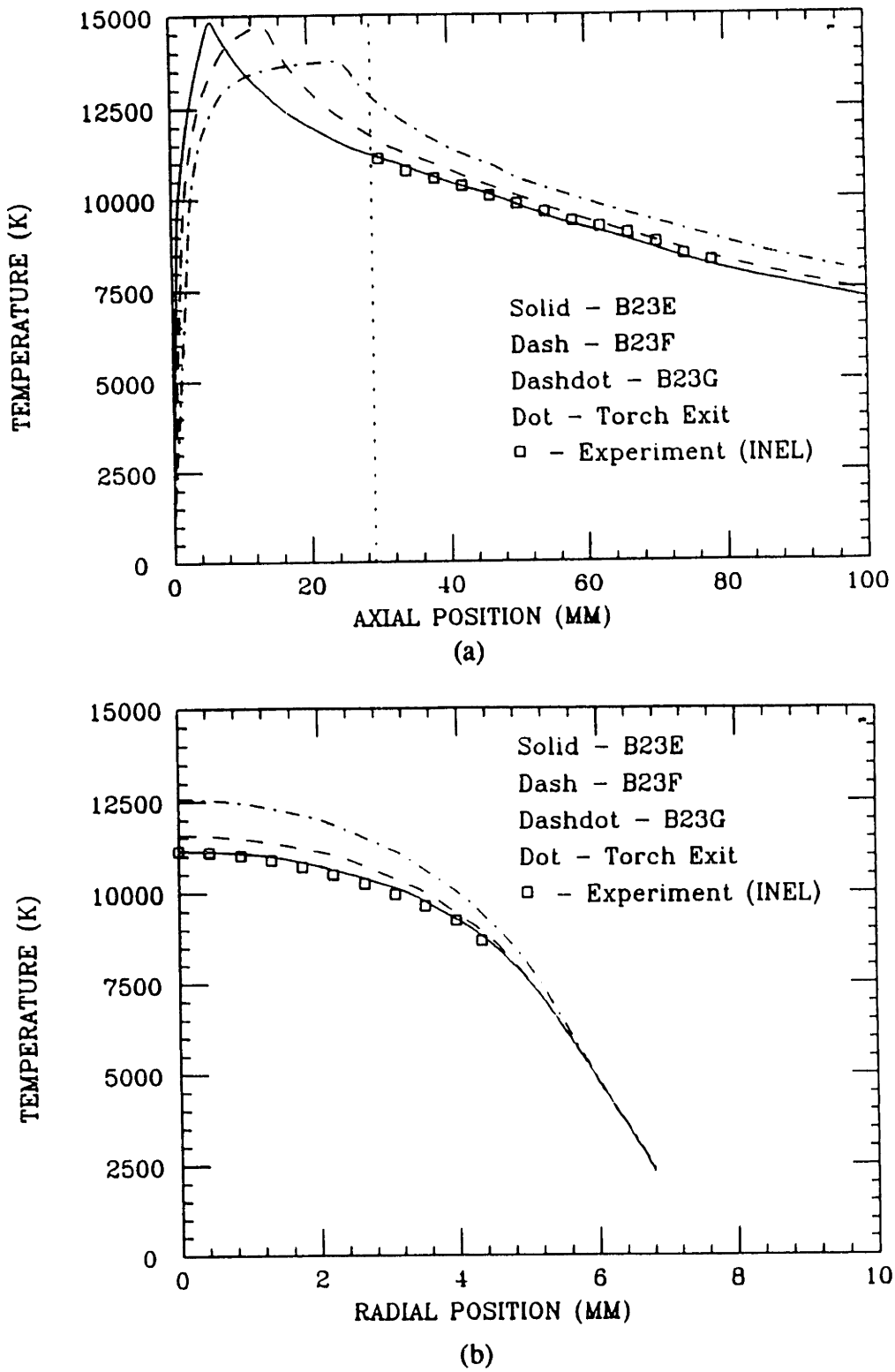

Figure III.B.8. Effect of arc length on the (a) axial temperature profile and (b) radial temperature profiles for 2.9 mm Radius Arcs.

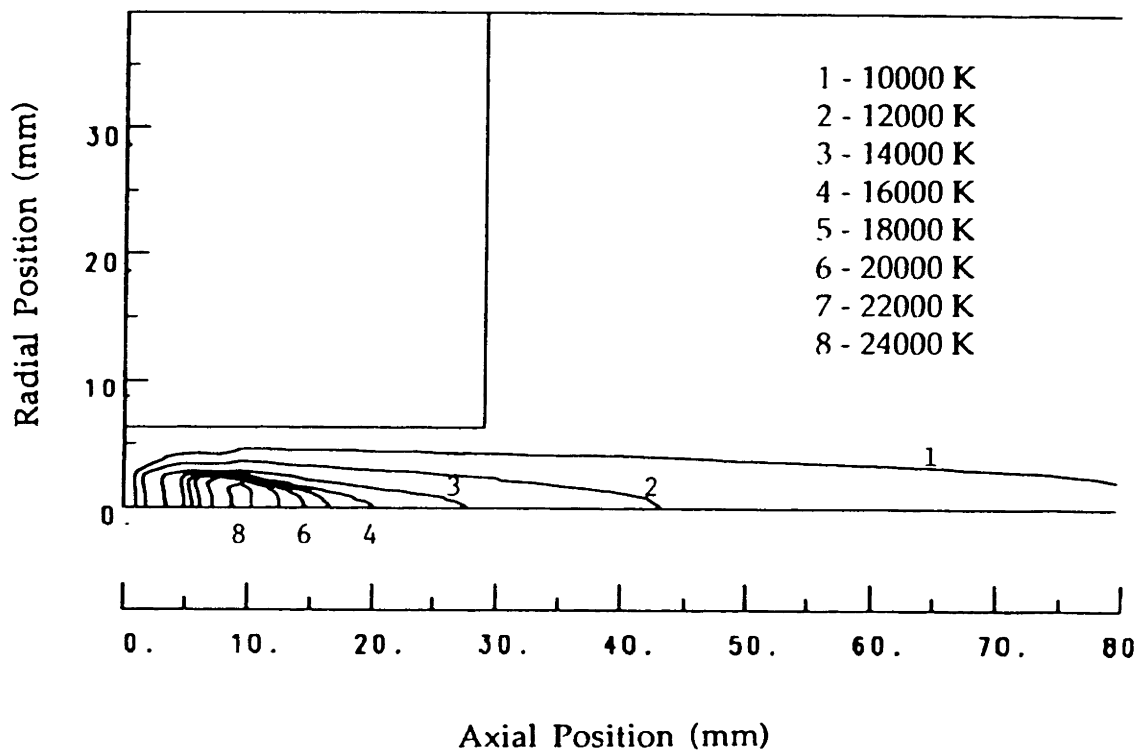

Figure III.B.9. Temperature contours for case B28.

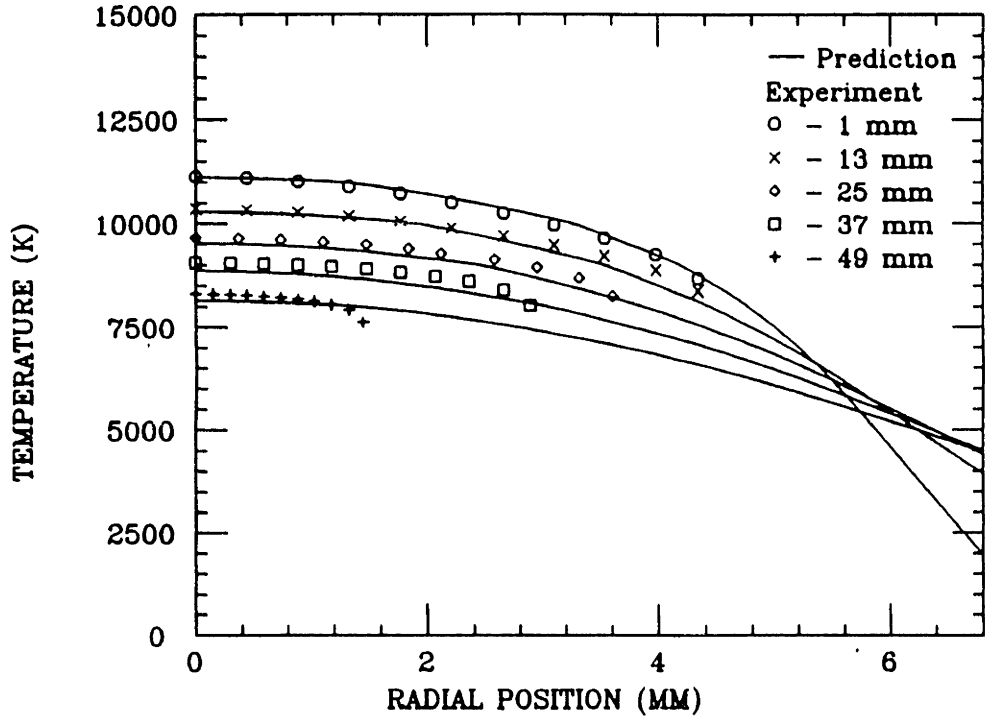

(a)

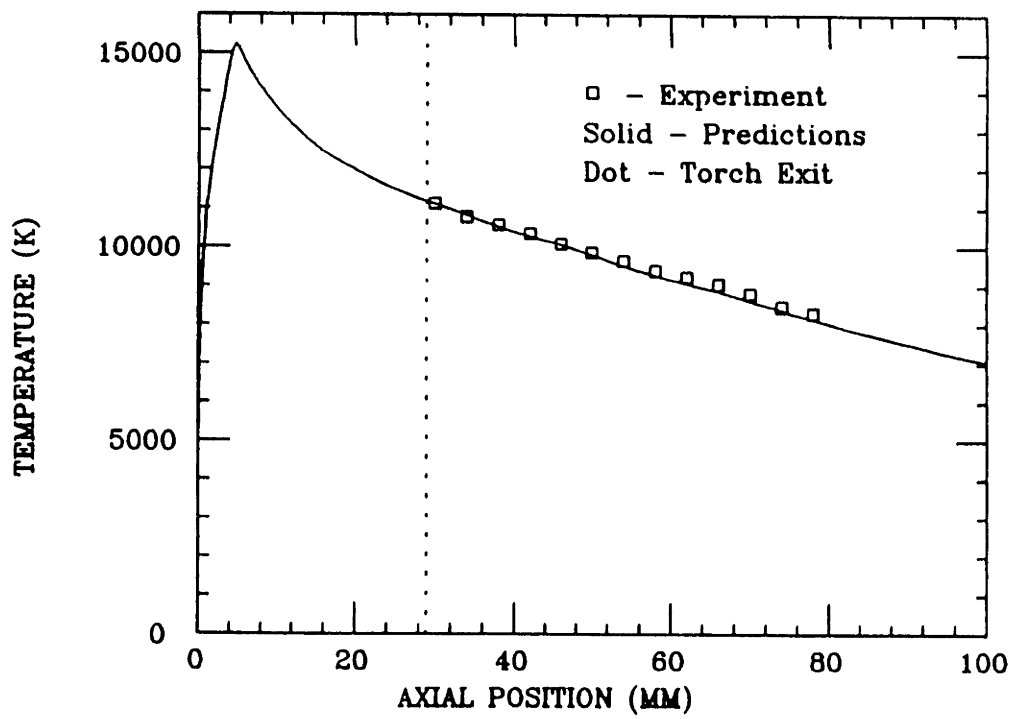

(b)

Figure III.B.10. The radial temperature profiles (a) at five axial positions and (b) the axial temperature profile – B23

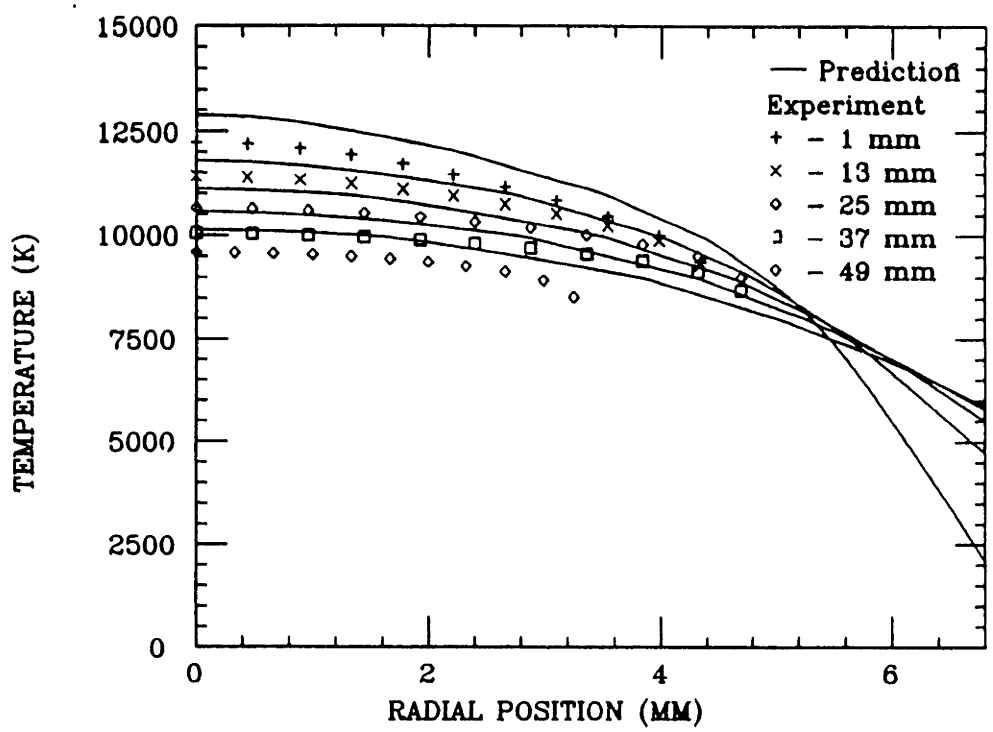

(a)

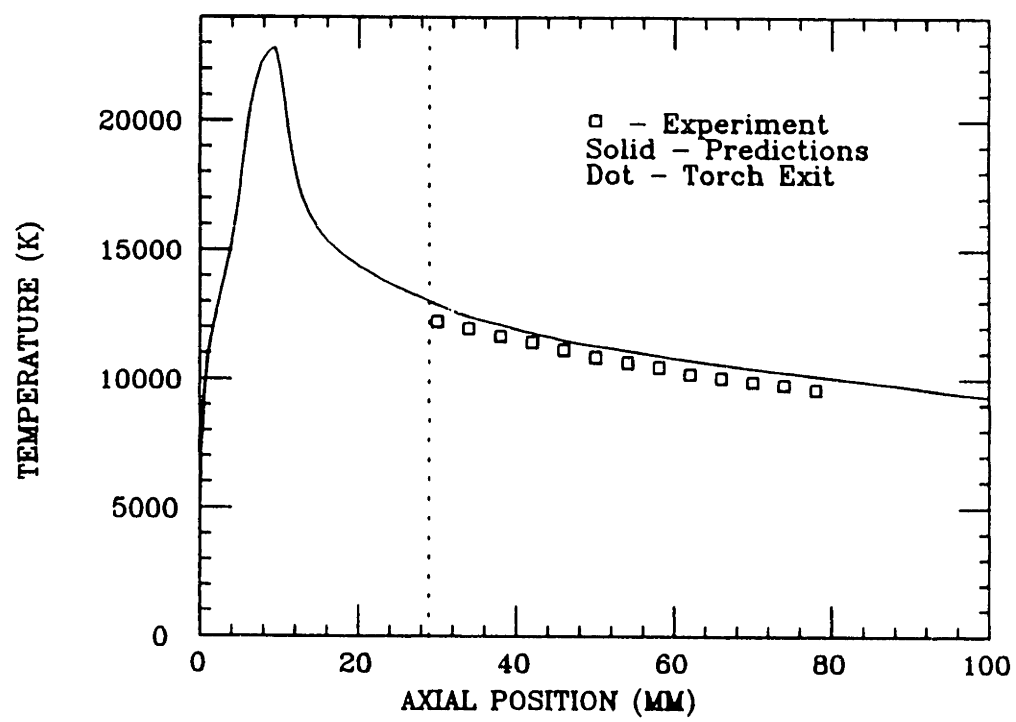

(b)

Figure III.B.11. The radial temperature profiles (a) at five axial positions and (b) the axial temperature profile – B28

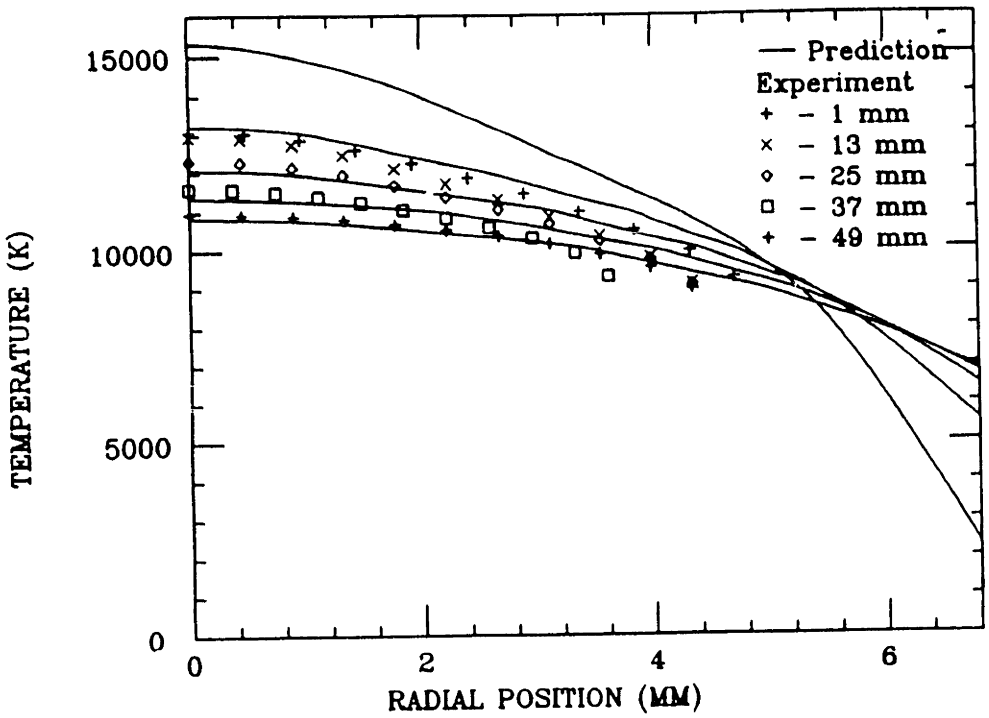

(a)

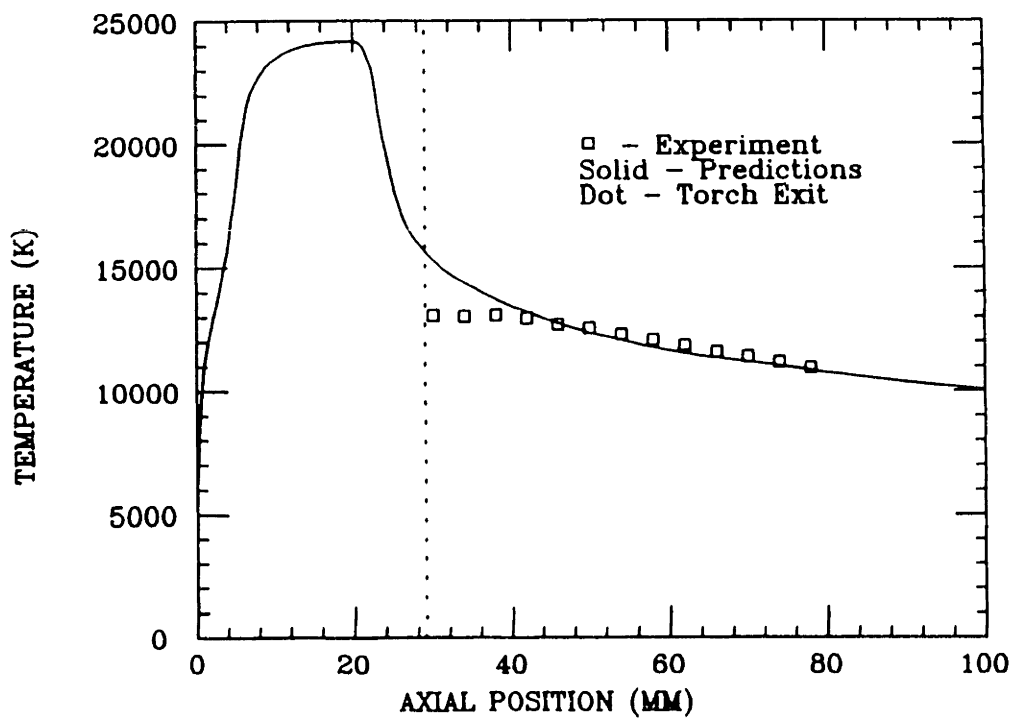

(b)

Figure III.B.12. The radial temperature profiles (a) at five axial positions and (b) the axial temperature profile – B32

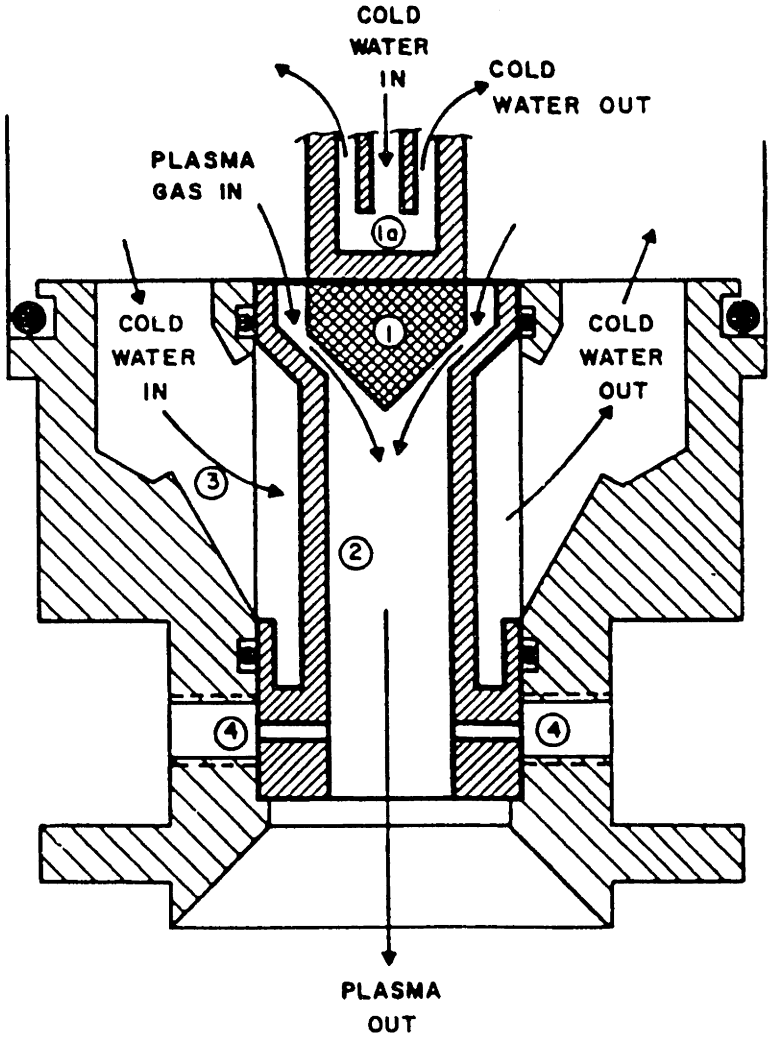

Figure III.C.1 Cutaway view of the plasma torch in the experimental study of Lewis and Gauvin.[38]

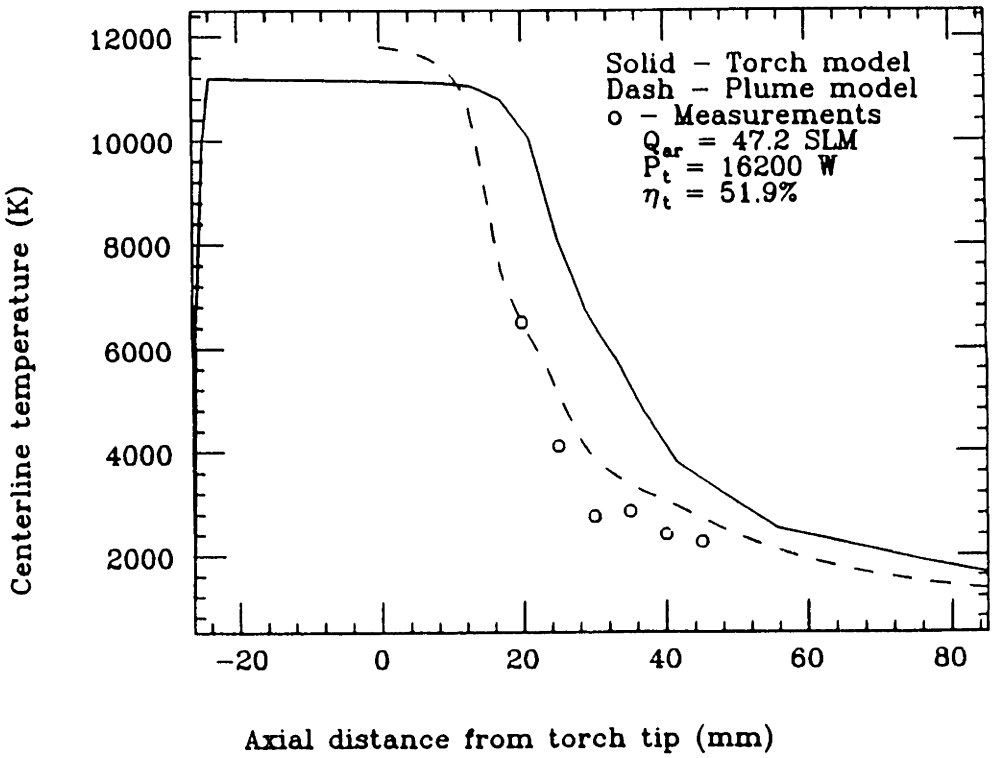

Figure III.C.2.(a) Axial temperature profile calculated using the inside torch and plume models compared to measurements by Brossa and Pfender, 600 amp case.[37]

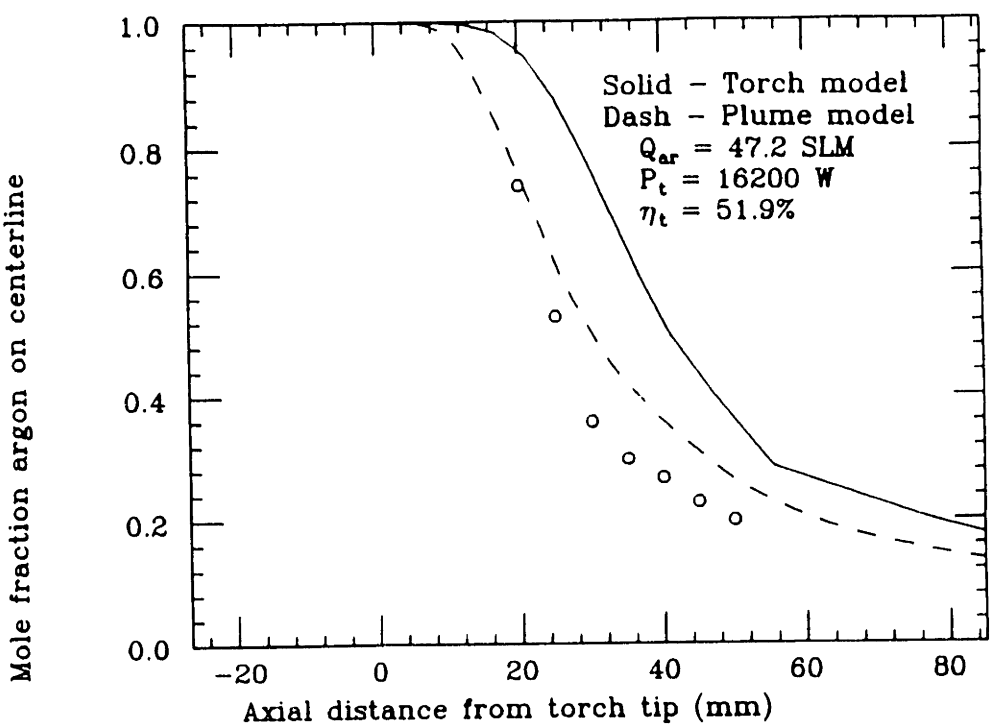

Figure III.C.2.(b) Axial concentration profile calculated using the inside torch and plume models compared to measurements by Brossa and Pfender, 600 amp case.[37]

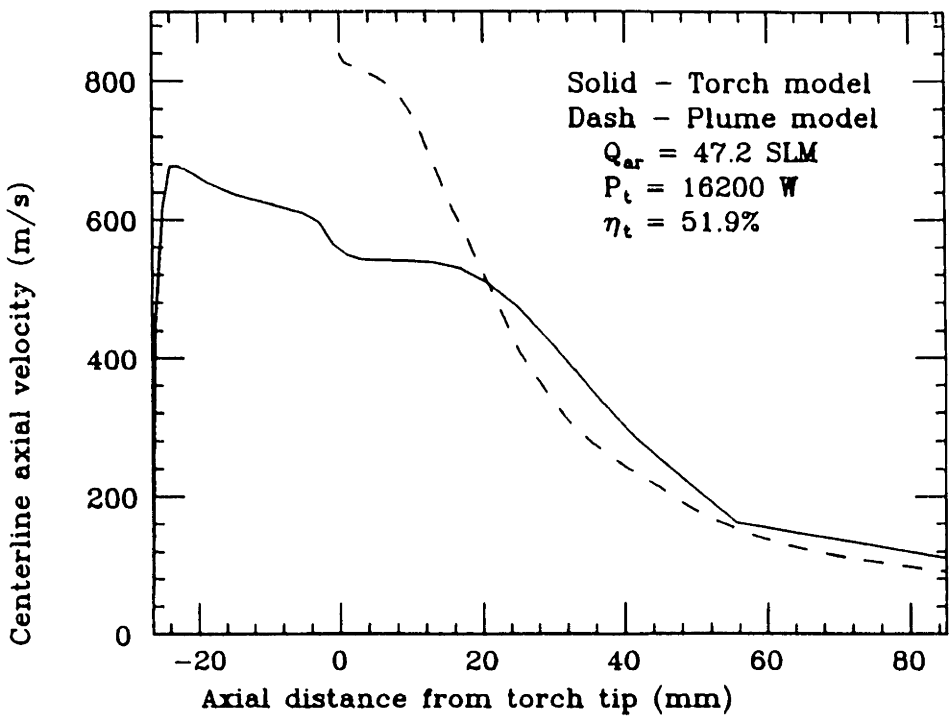

Figure III.C.3. Plasma velocity on the torch axis calculated by the inside torch model and the plume model, 600 amp case.[37]

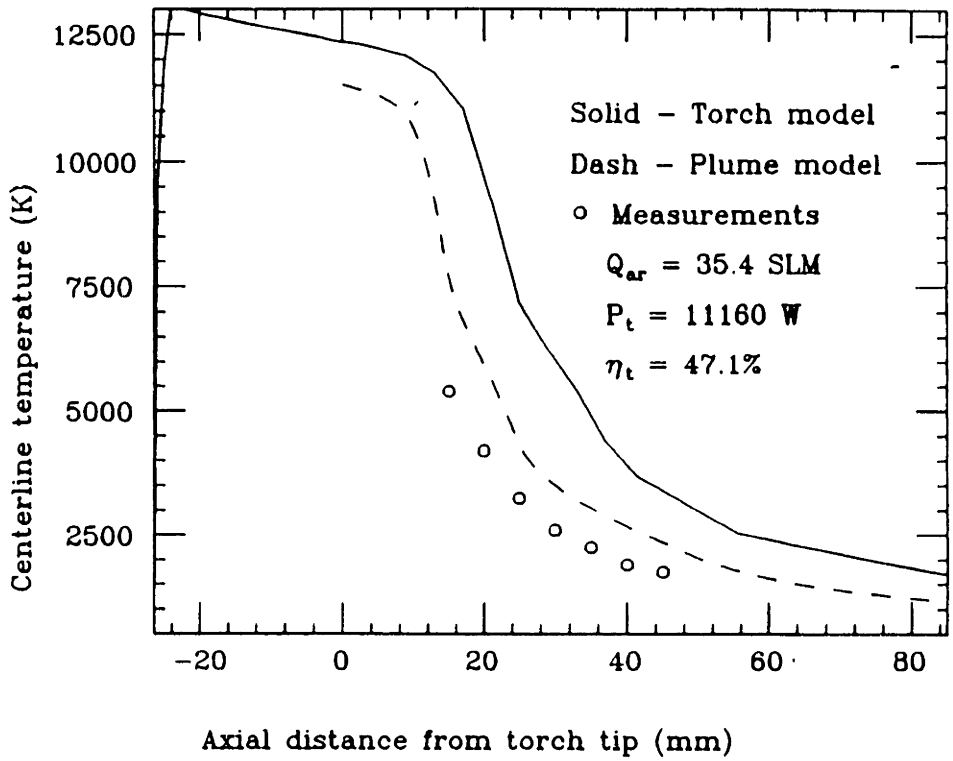

Figure III.C.4. Plasma temperature calculated with the inside torch model and the plume model compared to measurements by Brossa and Pfender, 450 amp case.[37]

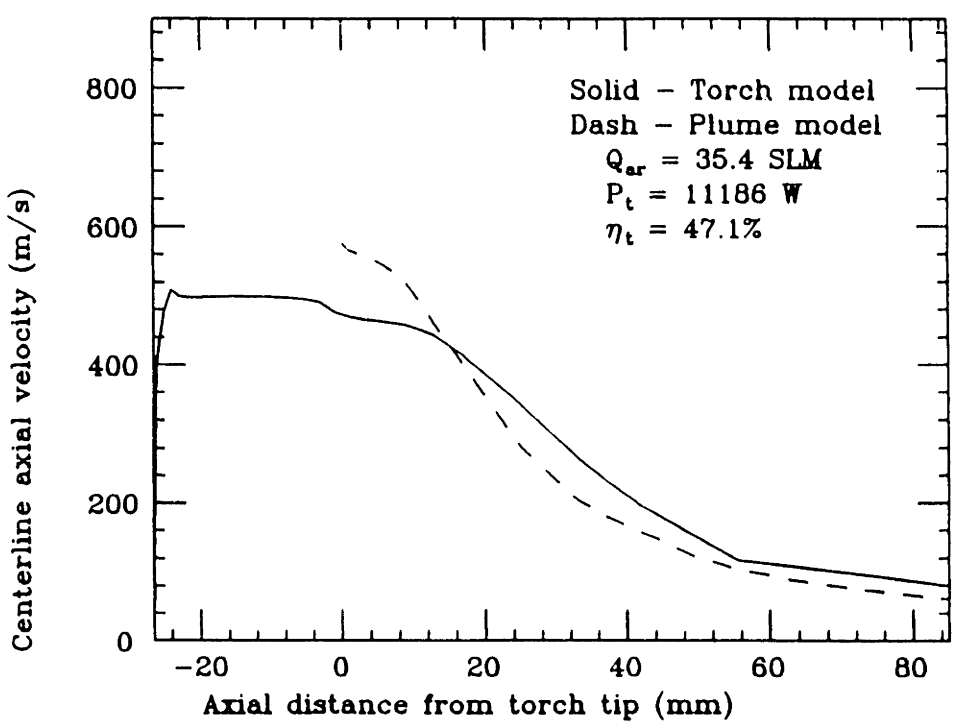

Figure III.C.5. Plasma velocity on the torch axis calculated by the inside torch model and the plume model, 450 amp case.[37]

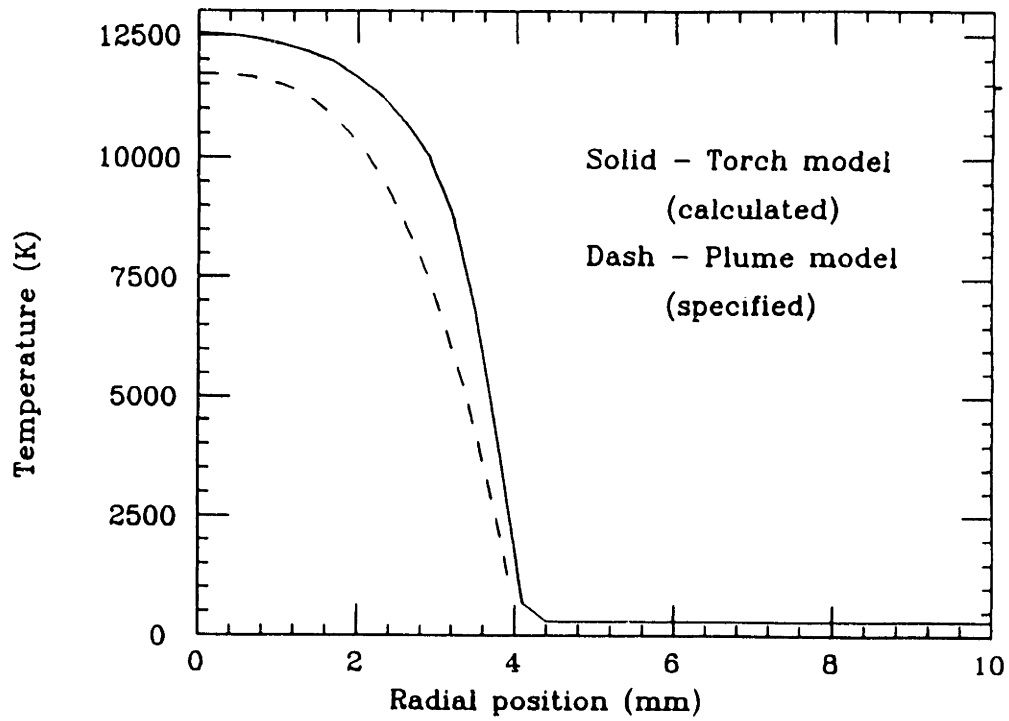

(a)

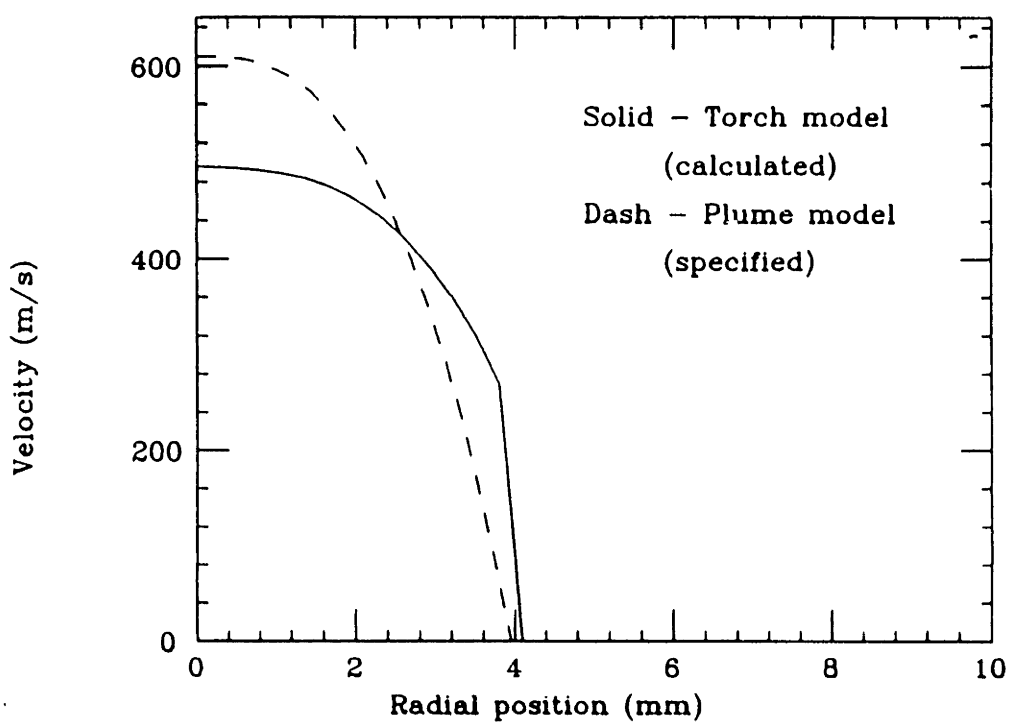

(b)

Figure III.C.6. Comparison of the radial profiles of (a) temperature and (b) velocity at a position 6 mm inside the torch nozzle for the plume and the simplified torch models.

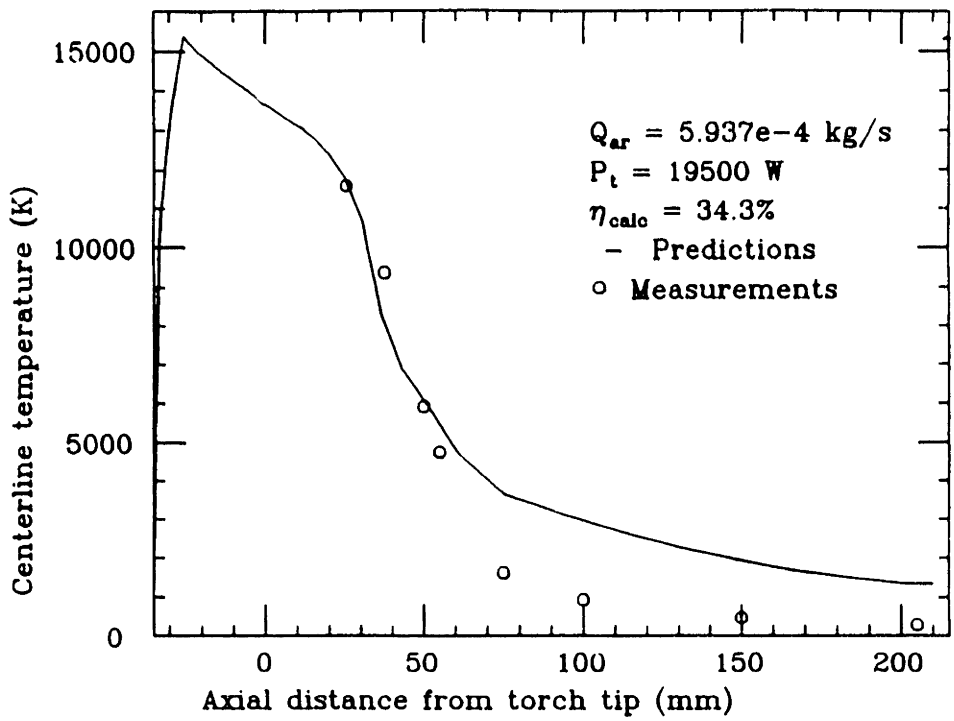

Figure III.C.7. Comparison of experimental and calculated axial temperature profile for the U-51 Thermal Dynamics torch studied by Lewis and Gauvin, operating at 650 amps.(38)

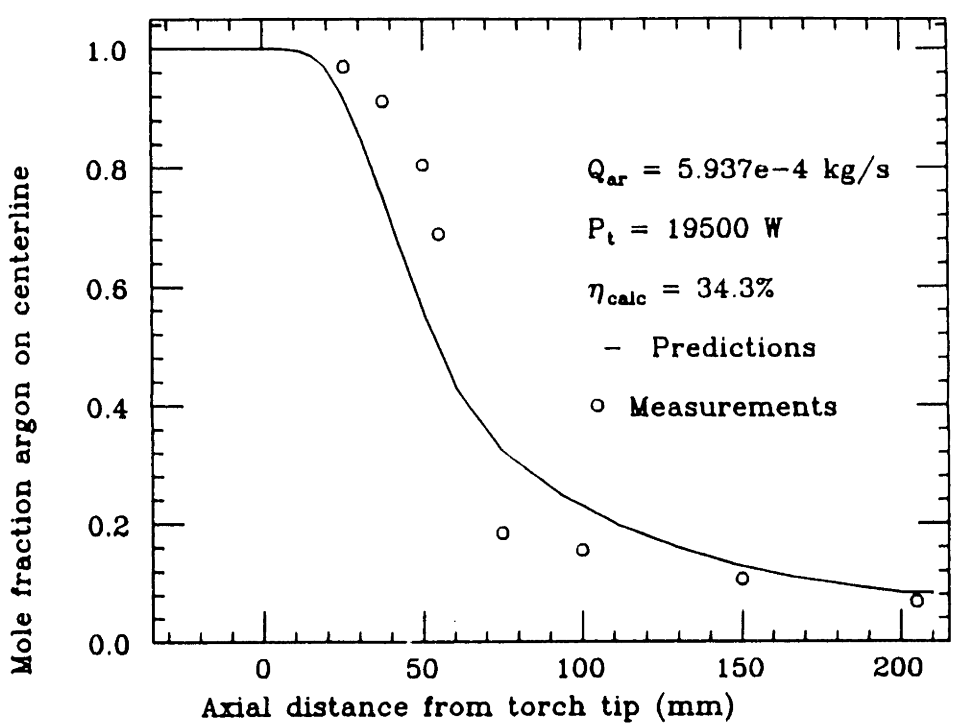

Figure III.C.8. Comparison of experimental and calculated axial profile of argon concentration for the U-51 Thermal Dynamics torch studied by Lewis and Gauvin, operating at 650 amps.(38)

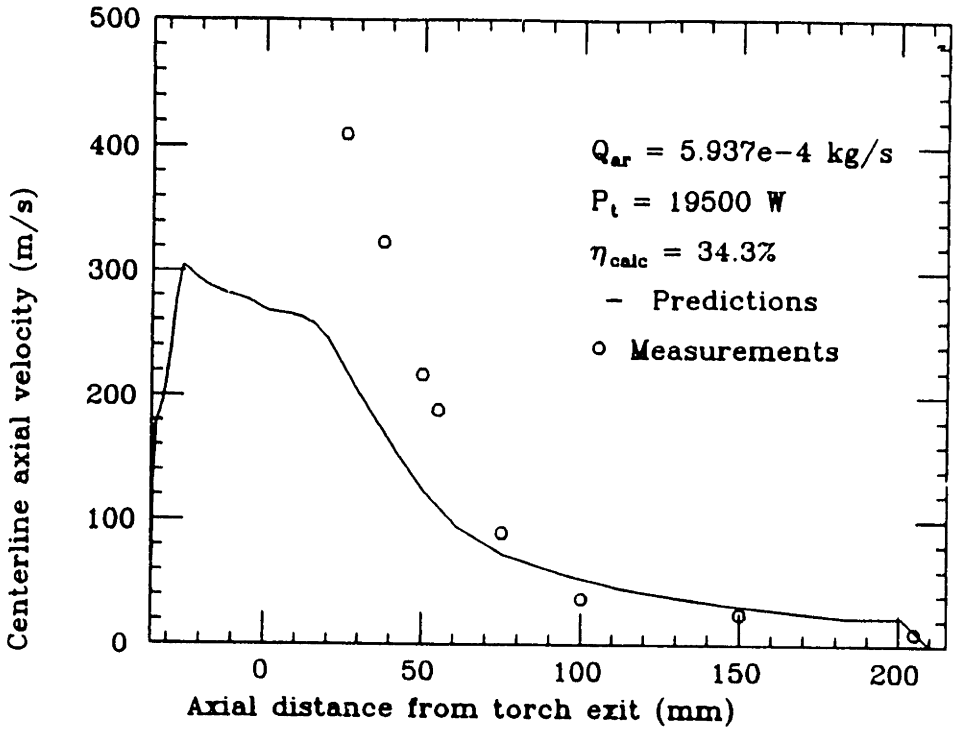

Figure III.C.9. Comparison of experimental and calculated axial velocity profile for the U-51 Thermal Dynamics torch studied by Lewis and Gauvin, operating at 650 amps.[38]

CHAPTER IV. A MODEL OF THE PLASMA TORCH INCLUDING ELECTROMAGNETIC PHENOMENA

IV. APPLICATION TO A LAMINAR, ARGON IN ARGON SYSTEM

IV.A.1. INTRODUCTION

The work to be described in this section is part of an investigation aimed at the development of a comprehensive mathematical model of transport phenomena in non-transferred arc systems, such that the behavior of the torch and the plume are fully coupled. During the past decade a great deal of work has been done, aimed at representing heat flow, fluid flow, and mass transfer in plasma plumes and this work has been summarized in Section II.A. A major drawback of most of the older work has been the fact that the modeling work has concentrated on the plume and that all these calculations had to rely on boundary conditions needed to specify conditions at the torch exit. In some instances these could be deduced from experimental measurements, but in others somewhat arbitrary postulates had to be made.

These circumstances made the results specific to certain torch designs and operating conditions and could not allow the generalization of the research findings.

The work done aimed at modeling transport phenomena inside plasma torches has been rather more limited and recent vintage. It has been discussed in Section III.A.

The work to be presented in the following also seeks to represent the transport and the electromagnetic phenomena inside a non-transferred arc torch. Attention is focused on a laminar system involving a single gas (argon discharging into argon) and comparison is made between predictions and measurements. The effect of the various boundary conditions is also explored explicitly..

IV.A.2. STATEMENT OF THE PROBLEM

The following presents a mathematical statement of the problem, but logically this has to be preceded by a discussion of the process physics. An important feature of the work will be a comparison with specific measurements; the characteristic features of these

measurements will have to be introduced through the boundary conditions. For this reason some experimental details will be given within this section.

IV.A.2.9.a. Description of the phenomena

A schematic sketch of a non-transferred arc plasma torch is shown in Figure IV.A.1. The primary elements include the thoriated tip tungsten cathode, and the copper anode. The voltage difference imposed between the cathode and anode gives rise to an arc in the channel between the two. The arc's natural tendency is to take the shortest path between the cathode and anode, resulting in a short arc and low torch voltage. The working gas (argon in this case), however, is introduced near the cathode and is forced to flow through the channel, which stretches the arc so that a longer arc and higher voltage results under normal operating conditions. The current in the arc causes Joule heating which heats and ionizes the gas. This transition to the plasma state is accompanied by a rapid expansion and a large resulting increase in the gas/plasma velocity. Additionally, the arc current interacts with its own induced magnetic field, and the resulting Lorentz forces accelerate the gas. The fluid dynamic, heat flow, and electromagnetic effects interact to give a torch its natural voltage-current versus flow rate characteristics.

In developing a mathematical statement of this physical picture, the fluid flow phenomena are represented by the laminar Navier-Stokes equations for an axi-symmetric system, but with due allowance for the temperature dependence of the gas density and viscosity and for the electromagnetic forces. Heat transfer is represented by the axi-symmetric convective heat flow equation with allowances for Joule heating in the arc, thermal transport due to electron drift, thermal radiation, and energy change due to pressure variations.

As far as the electrodynamic equations are concerned, we solve the electric potential equation and the self induced magnetic field is found using Ampere's Law. Assumptions are made regarding the cathode spot and the water cooled copper anode is considered to be an isopotential surface. The very steep temperature gradients in the plasma system result in sharp variations in most property values, which requires special precautions in the numerical procedures.

IV.A.2.b. Experimental system

A schematic sketch of the torch studied is shown in Figure IV.A.2. and a detailed description of the experiments which were performed at the Idaho National Engineering Laboratory (INEL) has been presented in an earlier article.(1) The experimental parameters of the chosen cases are shown in Table IV.A.I, where the torch efficiency is defined as the ratio: (1– cooling losses /torch power)x100%. The torch operates in a low flow, low power, laminar mode so that the flow both in the torch and in the plume near the torch may be assumed to be laminar, since the Reynolds number at the exit is in the range 100-200. Additionally, the torch discharges into a controlled atmosphere chamber so that the system may be treated as pure argon to eliminate the complication of intermixing of dissimilar gases. The swirl introduced upstream of the cathode in this torch is not addressed in Reference (4) and so is discussed here:

The injection of gas is done through the gas ring (41.30 mm I.D.) shown in Figure IV.A.2 through twelve holes, 0.94 mm in diameter, drilled such that they are tangential to the inside diameter of the ring. For 0.53 scmh of argon at 300 K, the resulting azimuthal velocity through the holes is 19.3 m/s. At the narrowest point between the anode and cathode the cathode radius is 5.85 mm, and the nozzle radius is 6.35mm, so that the resulting gas velocity through that annulus (for the same cold flow) is 8.42 m/s. These values will allow us to better quantify the swirl within the torch.

IV.A.2.c. Assumptions used in the model

The following assumptions will be made in the analysis:

1. The arc within the torch, and the heat and fluid flow inside and outside the torch are assumed to be axially symmetric, so that the governing equations can be written in two-dimensional cylindrical coordinates. In addition, the fluid flow is assumed to be laminar, which is reasonable for the operating conditions considered.

2. The operation of the arc is assumed to be steady-state so the governing equations are not time dependent.

3. The arc is assumed to be in local thermodynamic equilibrium (LTE), which is taken to mean that the electron and heavy particle temperatures are not significantly different.

Pfender and co-workers[2-3] showed this to be true through most of a free-burning arc except in the fringes and very near the cathode and anode surfaces. This assumption has been reasonably questioned in the constricted arc,[4-5] but still serves as a reasonable basis for developing a working model.

4. The plasma is assumed to be optically thin so that radiation may be accounted for using an optically thin radiation loss per unit volume.

5. The heating effects of viscous dissipation, compressibility effects and buoyancy forces due to gravity are neglected.

6. The cathode tip is assumed to be flat rather than pointed.

IV.A.2.d. Governing Equations:

Using the above assumptions the governing equations for the laminar plasma torch with swirl may be written as follows:

Continuity of mass:

$$\frac{\partial(\rho u)}{\partial z}+\frac{1}{r}\frac{\partial(\rho r v)}{\partial r}=0 \qquad [IV.A.1]$$

In these equations z, u; r,v and θ, w are the coordinates and velocities in the axial, radial and azimuthal directions respectively, as shown in Figure IV.A.3, and ρ is the density of the gas.

Conservation of axial momentum:

$$\frac{\partial(\rho u^2)}{\partial z}+\frac{1}{r}\frac{\partial(\rho r u v)}{\partial r}=-\frac{\partial P}{\partial z}+2\frac{\partial}{\partial z}\left[\mu\left(\frac{\partial u}{\partial z}\right)\right]+\frac{1}{r}\frac{\partial}{\partial r}\left[r\mu\left(\frac{\partial u}{\partial r}+\frac{\partial v}{\partial z}\right)\right]+j_r B_\theta \quad [IV.A.2]$$

In the above, P denotes the pressure, μ is the gas viscosity, j_r is the radial component of the current density, and B_θ is the azimuthal magnetic flux density.

Conservation of radial momentum:

$$\frac{\partial(\rho uv)}{\partial z}+\frac{1}{r}\frac{\partial(\rho rv^2)}{\partial r}=-\frac{\partial P}{\partial r}+\frac{\partial}{\partial z}\left[\mu\left(\frac{\partial v}{\partial z}+\frac{\partial u}{\partial r}\right)\right]+\frac{2}{r}\frac{\partial}{\partial r}\left[r\mu\left(\frac{\partial v}{\partial r}\right)\right]$$

$$-\mu\frac{2v}{r^2}+\frac{\rho w^2}{r}-j_z B_\theta \qquad [IV.A.3]$$

In the above, j_Z is the axial component of the current density vector. The terms $j_r B_\theta$, and $j_Z B_\theta$ are the electromagnetic or **J X B** forces, where **J** is the current density vector, and **B** is the magnetic flux density vector.

Conservation of azimuthal momentum:

$$\frac{\partial(\rho ruw)}{\partial z}+\frac{1}{r}\frac{\partial(\rho r^2vw)}{\partial r}=\frac{\partial}{\partial z}\left(\mu\frac{\partial(rw)}{\partial z}\right)+\frac{1}{r}\frac{\partial}{\partial r}\left[\mu r\left(\frac{\partial(rw)}{\partial r}\right)\right]$$

$$-\frac{2}{r}\frac{\partial(\mu rw)}{\partial r} \qquad [IV.A.4]$$

Conservation of Energy:

$$\frac{\partial(\rho uh)}{\partial z}+\frac{1}{r}\frac{\partial(\rho rvh)}{\partial r}=\frac{\partial}{\partial z}\left(\frac{k}{C_p}\frac{\partial h}{\partial z}\right)+\frac{1}{r}\frac{\partial}{\partial r}\left(\frac{rk}{C_p}\frac{\partial h}{\partial r}\right)+\frac{j_z^2+j_r^2}{\sigma}$$

$$-S_R+\frac{5}{2}\frac{k_b}{e}\left(\frac{j_z}{C_p}\frac{\partial h}{\partial z}+\frac{j_r}{C_p}\frac{\partial h}{\partial r}\right) \qquad [IV.A.5]$$

The terms in this equation represent the transport of enthalpy by convection and diffusion, joule heating, radiation losses, electron drift, and finally a term which accounts for energy changes due to pressure variations. Symbols used in the above denote the thermal conductivity, k, heat capacity, C_p, electrical conductivity, σ, specific enthalpy, h, Boltzmann's constant, k_b, the electric charge, e, and the volumetric radiative loss term, S_R.

Current continuity in terms of electric potential:

$$\frac{\partial}{\partial z}\left(\sigma\frac{\partial\phi}{\partial z}\right)+\frac{1}{r}\frac{\partial}{\partial r}\left(\sigma r\frac{\partial\phi}{\partial r}\right)=0 \qquad [IV.A.6]$$

where ϕ, is the electric potential.

The plasma properties are taken from the tabulated data of DeVoto,(6) and the radiation loss is adapted from the measurements of Evans and Tankin,(7) and measurements of Fauchais.(8) Additionally, at temperatures below 9000 K the plasma electrical conductivity is given by the expression of Scott et al.(9)

IV.A.2.e Auxiliary Equations

If the current distribution is axi-symmetric, the self induced magnetic field may be calculated by the following relation from Amperes law:

$$B_\theta=\frac{\mu_o}{r}\int_0^r j_z\zeta d\zeta \qquad [IV.A.7]$$

where μ_O, is the magnetic permeability of free space, and ζ is a dummy variable of integration.

The current density is calculated from the definition of electric potential:

$$\bar{J}=-\sigma\nabla\phi \qquad [IV.A.8]$$

IV.A.2.f. Boundary Conditions:

The integration region is sketched in Figure IV.A.3, and the corresponding boundary conditions are given in Table IV.A.II.

These conditions specify zero velocities at all solid boundaries, and zero fluxes at the axis of symmetry. Constant temperatures of all solid boundaries and at the outer

entrainment boundary are assumed. Additionally, zero gradients are assumed at the downstream boundary, and zero currents are assumed on all boundaries except on the cathode (where a current density is specified) and at the anode (where a constant electric potential is assumed). The anode and cathode surfaces may require special treatment since deviations from LTE occur in these regions.

Inlet boundary

At the inlet boundary (line DE of Figure IV.A.3) the axial velocity is assumed to have a parabolic profile with its maximum halfway between the anode and cathode wall. The radial velocity is assumed to be zero. Additionally, it is important to be able to quantify the degree of swirl at the inlet boundary. The values given in the first section may be used to estimate swirl.

As discussed by Dilawari and Szekely,[10] the swirl number, Sw, which is the ratio of the axial flux of the azimuthal momentum to the axial flux of the axial momentum, normalized by an appropriate radius R_0 (taken here as the nozzle radius) is given by

$$\frac{G_\theta}{G_z R_0} = Sw \qquad [IV.A.9]$$

where the axial flux of the azimuthal momentum is

$$G_\theta = \int_0^\infty \rho u w r^2 dr \qquad [IV.A.10]$$

and the axial flux of axial momentum (neglecting the pressure term) is

$$G_z = \int_0^\infty \rho u^2 r dr \qquad [IV.A.11]$$

If we assume characteristic values for u and w as constants, denoting them as U and W, we can derive an approximate relation for the swirl number:

$$Sw \approx \frac{\frac{1}{3}\rho U W r^3}{\frac{1}{2}\rho U^2 r^2 R_0} = \frac{2 W r_{inj}}{3 U R_0} = \frac{2\left(1/A_{inj}\right) r_{inj}}{3\left(1/A_{an}\right) R_0} \qquad [IV.A.12]$$

Here r_{inj} is the radius at which the swirling flow is injected in a purely tangential direction, A_{inj} is the total area of the injection holes, and A_{an} is the area of the annular slot between the cathode and the nozzle. The values of the appropriate velocities and radii are given in the first section of this paper; for this torch: W = 19.3 m/s at r_{inj} = 0.0206 m, U = 8.4 m/s and R_0 = 0.00635 m, so that Sw = 5.0. The type of swirl introduced is assumed to be that of solid body rotation at the inlet boundary.

The latter form of Equation IV.A.12 is of interest because it shows that in this approximation, the inlet swirl number is a characteristic of the torch, independent of the flow rate, and can be calculated from the torch configuration. For this reason, the swirl number is assumed to be constant for a given torch configuration, because the characteristic velocities U and W will both be proportional to the flow rate.

Cathode Region

Between the arc column and the cathode surface is a thin transition layer in which steep gradients occur; it supports several of the physical processes that sustain the arc. Positive ions are accelerated toward the cathode surface and provide energy for the thermal emission of electrons. The emitted electrons either combine with the positive ions or are accelerated away from the cathode. Additionally, the plasma is ionized in this layer, causing a substantial potential drop called the cathode fall. This cathode boundary layer has been investigated by Hsu and Pfender(11) who showed that as the cathode surface is approached the heavy particle temperature approaches the cathode surface temperature while the electron temperature remains much higher (~17000 K). This state of thermal non-equilibrium cannot be represented using an LTE model. In addition, the thickness of the cathode boundary layer is of the order 0.1 mm, which presents some practical problems in being resolved using a 2-D finite-difference approximation.

The contribution of the cathode fall is accounted for approximately using a "free fall" type of expression for the cathode fall voltage, V_C as was done by McKelliget and Szekely(12) for a free-burning arc:

$$V_c = \frac{5}{2}\frac{k_b T_{elec}}{e} \qquad [IV.A.13]$$

In this expression, V_C is the cathode fall voltage, and T_{elec} is the electron temperature, which is approximated as the maximum plasma temperature in the column adjacent to the cathode (~20000 K), so that $V_C \sim 4.3\ V$. In Table IV.A.II, the torch current is denoted by I, and Q_C is a positive source to the plasma column at the cathode boundary which approximates the energy used in the cathode boundary layer to ionize the plasma.

The boundary condition for electric potential is approximated assuming that the cathode current density, j_C which is emitted from the cathode normal to the surface is constant inside the cathode spot radius, R_C and is zero outside:

$$j_c = \frac{I}{\pi R_c^2} \quad ; \quad r < R_c \ \ and \ \ j_c = 0 \ ; \quad r > R_c \qquad [IV.A.14]$$

The unknown parameter j_C must be specified by giving the cathode spot radius. A value of 3×10^7 A/m^2 was chosen for this study based on experiments performed on thoriated tungsten cathodes in transferred argon arcs at atmospheric pressure which show j_C to vary between 3.8×10^7 to 2.5×10^7 A/m^2 as current varies between 300 - 700 amps (j_C decreases as I increases).[13] This assumption will be examined by doing a parametric study.

Anode Region

Three principal modes of heat transfer at the anode contribute to the loss of energy from the arc: conduction/convection from the plasma, electron flow due to the current, and radiation from the plasma.

The boundary layer which exists between the anode and the arc column is of some interest as the processes which occur there govern the current density and the resulting heat flux to the anode. Dinulescu and Pfender[14] presented a model of the anode boundary layer for a transferred arc in which the anode is perpendicular to the arc axis. This boundary layer region is approximately 0.1-1.0 mm thick and presents the same problems to an LTE model as does the cathode boundary layer. At present, to calculate the heat losses, we will choose to take the same approach as Dilawari, et al.[15] who showed that the LTE model can, at least approximately, estimate the convective losses to the torch wall.

IV.A.2.g. Method of Solution

The governing equations and boundary conditions are solved using a finite-volume approach described by Pun and Spalding[16] which is implemented using a modified version of the 2/E/FIX code. The difference equations are solved by iteration until they are satisfied within approximately 99%. A typical run uses a 35X23 grid inside the torch and a 32X45 grid in the plume region (total number of grids is 67X45), and requires 3-7 hours of CPU time on a Microvax 3100. Grid dependence was tested using a 35X23 grid, and the difference between the two was only 10-15%. The finer grid was used for generating the results to be presented in the following.

IV.A.3. CALCULATED RESULTS

In the following we shall present a selection of the experimental results, together with a comparison of the computed results with experimental measurements. In the organization of this material our main motivation is to provide insight regarding the torch operation and also to highlight areas where further understanding would be desirable.

IV.A.3.a. Temperature, Current Density, and Mass Flow in the Torch

Figures IV.A.4 (a), (b) and (c) show the temperature contours, current density vectors and mass flow vectors (ρu product) for the current and fluid flow within the torch. The operating conditions are those of case B23 of Table IV.A.I. The swirl number at the inlet is assumed to be 5.0. The resulting isotherms show a maximum temperature near the cathode tip where the current density is a maximum. The maximum current density occurs at the cathode tip where it is two orders of magnitude larger than it is at the anode surface. As a result of this large variation, the distribution of current density at the anode surface must be shown in a different form (see Figure IV.A.9). The mass flow vectors show a significant difference between these results and what might be expected for a simple isothermal flow, namely a separation zone downstream of the flat cathode tip. The difference is a combined result of the high temperature region near the cathode tip, and the electromagnetic forces, which eliminate the separation. The mass flow is nearly uniform from the torch exit in this case. The results shown in Figure IV.A.4 may be regarded as a baseline case.

IV.A.3.b. Effect of Electromagnetic Forces

An important feature of the present model is that an assessment can be made for the role played by the electromagnetic, or "JXB" forces in driving or at least modifying the flow. In previous work (Section II.A), this was not the case and postulates had to be made regarding the velocity fields exiting the torch. A potential problem with this approach was that changes in operating conditions that could affect the relative importance of the electromagnetic forces could not be adequately represented. On the other hand, the previous approach allowed one to satisfy the overall heat balances explicitly, which could aid us in obtaining a reasonably good agreement between the measurements and the predictions. In the calculations to be presented in the following we shall address the effect of the electromagnetic forces explicitly.

In examining the effect of the electromagnetic forces we shall consider five cases, as summarized in Table IV.A.III. These runs correspond to a situation where swirl is absent. The "simple model", which has been described in Chapter III, postulates certain heat generation patterns inside the torch and makes no allowance for the electromagnetic forces. Cases two and three involve the solution of the equations presented in Section IV.2.d, with the calculation of the distributed heat generation pattern, but in one case the electromagnetic force field has been neglected. Finally, cases four and five compare the response of this model to the presence and absence of JXB forces at a higher current level.

Figures IV.A.5 (a) and (b) show the radial profiles of temperature and velocity one millimeter from the torch exit for the three cases, as well as the experimentally measured temperature data. While the electromagnetic forces have a significant effect on the temperature profile, the velocity profile is modified in a more dramatic manner. It is of interest to note that case 1 and 2 give remarkably similar results. We should note that even for the relatively low currents employed the allowance for the JXB forces will increase the centerline velocity by as much as 67%.

It should be noted that the heat balance is not "automatically" satisfied in these calculations; as discussed earlier, we specify the current and then *calculate* the corresponding voltage. It follows that the accuracy with which we predict the actual heat release in the plasma will necessarily depend on the similarity of the specified conditions (swirl number, cathode current density, presence or absence of JXB) to the actual

experimental conditions. It should be stressed though, that all these calculations are energetically self-consistent, meeting all the physical balance criteria, but need not match the experimentally determined heat balance, based on the torch efficiency, η. The reasonable agreement between the measured and the predicted temperatures, which will be presented subsequently, provides a good test of the model. This point will be addressed further.

Figure IV.A.6 (a) and (b) illustrate the effect of the JXB forces for a higher current of 750 amps. It is seen that the electromagnetic forces are very important; indeed the calculated centerline exit velocity is four times higher with JXB than without!

The important point to be made here is that the electromagnetic forces will have a significant effect on the shape of the velocity profiles at the torch exit, an effect which becomes more important with increasing current. Thus, only with a model which makes allowance for JXB forces can we hope to develop a general, predictive representation of the velocity and temperature fields of the plasma gas exiting the torch.

IV.A.3.c. Effect of Swirl

In many plasma torches the gas is introduced with a significant degree of swirl to stabilize the arc and reduce the rate of anode erosion by rotating the arc root. Additionally, studies by Dilawari et al.[10] have shown that a significant swirl in the plume of a torch would promote mixing to aid chemical reactions for synthesis of materials. This finding closely parallels the well documented experience in combustion.

A study was performed to determine the effect of swirl on the arc in the torch and on the resulting plume, and the results are shown in Table IV.A.IV and illustrated in Figures IV.A.7-IV.A.9. In the table, L_{arc} denotes the calculated arc length, and V_{arc} the calculated torch voltage (which includes the approximate cathode fall voltage).

It may be seen from Table IV.A.IV that it is rather difficult to get a significant degree of swirl in the plume, due to the large increase in axial momentum within the torch. This is in agreement with the results of Section III.B shown with the simpler torch model. Furthermore, these results show that the presence of swirl causes the arc attachment point to move upstream, thereby reducing the torch voltage. By comparing Figures IV.A.4 (swirl number = 5.0) and IV.A.7 (swirl number = 0.0), it may be seen that swirl causes the

arc to spread more in the radial direction, thus allowing it to strike the wall at a shorter distance from the cathode; the resulting arc voltage is lower by 1.4 volts.

The resulting temperature fields in the plume are illustrated in Figure IV.A.8, which shows the axial profiles and radial profiles at the torch exit. The curves with $Sw = 0$ and $Sw = 1.0$ nearly coincide indicating that a rather significant swirl is required to modify the arc behavior. The results indicate that swirl "flattens out" both the temperature and the velocity profiles, which is illustrated by the decreasing maximum temperature and velocity with increasing swirl number seen in Table IV.A.IV.

Figure IV.A.9 shows the distribution of the radial current density at the anode for the cases of different swirl numbers. It can be seen that each of the profiles exhibits a sharp maximum at some intermediate point between the cathode tip and the nozzle exit. We may use the plots shown in Figure IV.A.9 to define an effective arc length by taking the axial position of the centroid of the current distribution curves. This effective arc length (relative to the cathode tip, z = 4.2 mm in the figure) is a useful parameter for characterizing the behavior of the torch.

The decrease of the arc length with increasing swirl is illustrated in this figure. It is also seen that upon increasing the swirl number the maximum value of the current density is decreased; this seems consistent with physical reasoning because swirl will tend to spread out the arc. Furthermore, this behavior is also consistent with practical experience in that swirl has been found useful to increase the anode life.

IV.A.3.d. Current - Voltage Characteristics of the Torch

Figure IV.A.10 and Table IV.A.V show a comparison between the experimentally measured and the theoretically predicted current - voltage relationship. It is seen that the agreement is quite reasonable, which provides an important proof for the basic concept of the model. The agreement is not perfect, however, which will lead to some discrepancy between the experimentally measured and the theoretically predicted temperature profiles in the plume. The discrepancy may be at least partially explained by the uncertainty in the cathode spot current density as will be shown in Section IV.A.3.e.

Figure IV.A.11 shows the computed current density distribution at the anode surface for various total current and gas flow rates. This plot indicates that upon

increasing the total current, rather sharp maxima are established in the local current density. This figure also indicates that upon increasing the flow rate of the plasma gas, the arc length (defined in conjunction with Figure IV.A.9) will also increase. Both these findings appear to be consistent with physical reasoning and with operating experience. Indeed, it has been found that anode erosion may increase dramatically upon increasing the current. The plots shown in Figure IV.A.11 also indicate that the arc length is reduced upon increasing the current. This is also reasonable on physical grounds, because at the higher current levels the arc will tend fill the channel more completely and hence will be able to strike closer to the cathode.

IV.A.3.e. Effect of Cathode Spot Current Density

In this model it was assumed that the current density within the cathode spot is constant over a range of currents. Table IV.A.VI summarizes the results of a parametric study done to test this assumption. The study shows that at constant inlet swirl number, the arc voltage, net power, maximum velocity inside and at the exit, and maximum temperature inside and at the exit all increase with increasing cathode current density. The exit swirl number decreases with increasing cathode current density, due to the increased enthalpy and momentum imparted to the plasma. The study shows that this variation in the cathode current density ($\pm 1 \times 10^7$) leads to variations in the calculated arc voltage of ±2.6 - 4.2 volts, which is large enough to explain the discrepancy in the current - voltage characteristics mentioned above. This is illustrated in Figure IV.A.12, which shows the current - voltage characteristics calculated for three cathode current densities, compared with the experimentally measured values at a flow rate of 0.83 scmh. The higher and lower current density cases bracket the experimental measurements, illustrating the sensitivity of the arc voltage to the current density at the cathode.

The sensitivity of these and other important quantities (e.g. exit velocity) to the cathode current density illustrates the importance of the cathode phenomena in affecting the behavior of the torch. This point deserves further attention in future research.

IV.A.3.f. Comparison with Experimental Temperature Measurements

Figures IV.A.13-IV.A.16 show a comparison of the theoretically predicted temperature profiles with those measured experimentally for a range of operating conditions. The general impression that these plots create is that one can predict the

experimentally measured temperatures reasonably well, but not necessarily any more accurately than was the case with the previous models. A major point should be made here, however. In the previous modeling efforts a suitable adjustable parameter was always present, through the need to specify the temperature and the velocity fields at the torch exit. The fact that the prescription of these profiles was constrained by the need to meet the experimentally obtained heat and mass balances obviously helped the agreement between the measurements and the predictions. In the present case the actual net heat generation in the torch is calculated rather than postulated, so that the agreement between measurements and predictions is a direct indication of the integral errors involved the the whole model.

One other point should be made in examining these figures; the experimental measurements were found to be less than accurate above 12,500 K; indeed the instrumentation employed could not measure temperatures above 13,000 K, so that the apparent discrepancy between the measurements and the predictions seen in Figures IV.A.15 and IV.A.16 may at least in part be attributable to experimental difficulties within the high temperature range.

IV.A.4. DISCUSSION.

In this section a comprehensive mathematical model has been presented which describes the electromagnetic, heat flow, and fluid flow phenomena in a non-transferred arc plasma torch and in the plume that emerges from it. This is perhaps the first time that such a comprehensive representation has been developed, where account has been taken of swirl and a great deal of information has been developed on the detailed behavior of the system.

Using this approach, it was possible to predict the temperature and the velocity profiles in the plume, without making any arbitrary assumptions or relying on adjustable parameters. The theoretically predicted temperature profiles were found to be in good agreement with the measurements over a range of experimental conditions; furthermore, the computed current-voltage relationships also agreed quite well with the measurements, which should provide good experimental support for this approach.

The principal findings of the work may be summarized as follows:

The electromagnetic forces that exist within the torch cavity may play a very important role in determining both the velocity and the temperature profiles in the plasma stream exiting the torch. The important practical consequence of this finding is that even for the same torch, when changing the current, the resultant velocity and temperature fields may be markedly affected in a manner, that could not be predicted, without considering the electromagnetic forces in the system. The JXB forces may provide a sharply peaked velocity distribution and corresponding changes in the temperature profile.

The model was able to account for the effect of the swirl, which may be directly related to the torch geometry and to the way in which the gases are introduced into the torch. This is an important point, because swirl has been found to play a very significant role in affecting the arc and the resulting velocity and temperature fields within the gas stream exiting the torch. The effect of swirl is to reduce the maximum current density at the anode as well as to reduce the arc length. It follows that the torch voltage will decrease with increasing swirl.

The computed results have shown that there is an interesting interplay between the swirl, the applied current, and the gas flow rate. Increasing the current will tend to reduce the swirl at the exit, because of the increase in the axial momentum due to both higher torch power (i.e. greater gas expansion) and greater electromagnetic forces, which are the strongest on the axis of the torch. In addition, the swirl at the exit will increase with an increasing gas flow rate at a constant current level for two physical reasons; one being that the JXB forces will remain essentially constant, and the other is that at constant current level the thermal generation of axial momentum, due to the expansion of the gas will be somewhat reduced. The important consequence of these findings is that one cannot associate a given swirl number at the exit with a particular torch, without specifying the current and the flow rate; indeed changing the current level or gas flow will affect the swirl at the exit for a given device.

In conclusion it has to be stressed that this is an initial effort at representing the complex electromagnetic, heat flow, and fluid flow phenomena inside plasma torches and their effect on the plasma plume behavior. These initial results seem very promising and the computed results appear to be quite consistent with physical reasoning and with the available experimental plume measurements and torch data. In its present state it would be prudent to use the model in conjunction with measurements, but for the longer term it offers a real promise of predicting torch behavior almost entirely from first principles.

IV.B APPLICATION TO A LAMINAR, ARGON IN NITROGEN SYSTEM

IV.B.1. INTRODUCTION

In this section we will address the operation of a non-transferred arc argon plasma torch which is operating in an environment of nitrogen. While this system has been addressed in Section II.B., it has not been examined using a complete model of the torch which accounts for the electromagnetic phenomena within the torch, as well as the mixing with a different gas.

The extension to gas mixtures is important, because for instance, in the case of plasma spraying, it is often the case that a plasma torch is operating in an environment of air. In such a case, the air is entrained into the plasma jet and causes significant cooling of the jet (due to dissociation of the diatomic gases), as well as possible reactions with the ambient gas which may be undesirable.

IV.B.2. STATEMENT OF THE PROBLEM

IV.B.2.a. Description of the phenomena

Figure IV.A.1 shows a schematic sketch of the system considered, highlighting the important phenomena represented. These include the arc within the torch (which is idealized as being axi-symmetric in the model), the formation of the plasma jet at the torch exit, and notably the entrainment of nitrogen at the outer part of the region of interest. Also shown is the injection of a shroud gas, which was not done in the experiments but is considered in Section IV.B.3.d. Downstream, the plasma jet exits the region of interest at the outflow boundary.

IV.B.2.b. The experimental work

The experimental work was performed at the Idaho National Engineering Laboratory and is described in Section II.B. In these experiments a controled atmosphere of either argon or nitrogen was maintained within an enclosed chamber, into which the

torch discharged. The temperature measurements were performed using optical spectroscopy on the plasma plume. The inside diameter of the torch nozzle was 12.7 mm, and the length of the nozzle (from the cathode tip to the exit) was 29 mm. The experimental conditions are summarized in Table II.B.I.

A very important aspect of the experimental procedure was to estimate the range of experimental uncertainties present in the measured torch efficiency which is given by:

$$\eta_t = 1 - \left(\frac{cooling\ \ loss}{torch\ \ power} \right) \qquad [IV.B.1]$$

where η_t is the torch efficiency. The experimental uncertainties are summarized in Table II.B.II which gives an estimate of the error in the torch efficiency at the three different power levels. This table indicates the accuracy to which the net power (or energy in the plasma at the torch exit) can be known. It is seen that in the present case the error bars on the experimental efficiency are about ±3.8 - ±4.4 percentage points. As discussed in earlier publications, the precise knowledge of the torch efficiency is quite critical in making any comparison between measurements and predictions.[10] Up to the present, these torch efficiencies could only be determined experimentally. In this work, we will be able to make predictions of the torch efficiency on a fundamental basis.

IV.B.2.c. The modeling equations

The model is based on the solution of the appropriate conservation equations, namely the conservation of mass, momentum and energy as well as electric charge. In addition, Ampere's law is used to calculate the magnetic field, and Ohm's law gives the current densities. These equations, the boundary conditions and the associated assumptions have been described in Section IV.A. As in that Section, the swirl number at the inlet (upstream of the cathode tip) is taken as 5.0, based on the torch configuration.

In essence, the assumptions made are as follows: that the system is steady-state, and axi-symmetric; that the plasma is in local thermodynamic equilibrium (LTE), and is optically thin to radiation; that the flow is laminar and incompressible; and that heating due to viscous dissipation may be neglected.

In this Section, the additional complexity is introduced by the presence of nitrogen in the controlled atmosphere chamber. To describe the intermixing of the dissimilar gases, an additional conservation equation must be solved for the mass fraction of the primary gas (argon). This is written as follows:

$$\frac{\partial(\rho r u m)}{\partial z}+\frac{1}{r}\frac{\partial(\rho r^2 v m)}{\partial r}=\frac{\partial}{\partial z}\left(D\frac{\partial(rm)}{\partial z}\right)+\frac{1}{r}\frac{\partial}{\partial r}\left[Dr\left(\frac{\partial(rm)}{\partial r}\right)\right] \qquad [IV.B.2]$$

where ρ is the density of the plasma, D is the diffusivity of argon in nitrogen, m is the mass fraction of argon, and z,u, and r,v are the coordinates and velocities in the axial and radial directions respectively as shown in Figure IV.B.1.

The boundary conditions which are applied to this equation include specifying the mass fraction of argon at the inlet ($m = 1$) and at the outer entrainment boundary ($m = 0$). At all other boundaries the diffusional flux of species is assumed to be zero, (i.e. $\frac{\partial m}{\partial n} = 0$, where n denotes the normal to the boundary).

To complete the description of the problem, the thermodynamic and transport properties of the two pure plasma components are taken from the literature,[6-7,17] and included in the program in tabular form. The thermodynamic properties of the mixture are then estimated by weighting them according to the mass or mole fraction of each component present. The transport properties of the mixture are estimated from the properties of the pure components using Wilke's equation.[18] The diffusion coefficient of nitrogen in argon was estimated using Chapman-Enskog theory.[19]

The solution of the equations was obtained using a modified and extended version of the code developed by Dilawari et al.[10,15] based on the 2/E/FIX code of Pun and Spalding.[16] The code, which has been modified to include the electromagnetic phenomena, was executed in a mode which includes the solution of the species equation. The grid system was previously found to give sufficient numerical accuracy, and uses a 67X45 mesh, with 35X23 grids inside the torch and 32X45 grids outside.

IV.B.3. RESULTS OF CALCULATIONS

In the following we present some results of calculations performed using the experimental conditions listed in Table II.B.I.

IV.B.3.a Current-voltage characteristics

Figure IV.B.2 shows the experimentally measured current-voltage characteristics of the torch in a pure argon system and in the argon/nitrogen system. The relationship between current and voltage appears to be quite different for the two cases; in the Ar/Ar case it is linear while in the Ar/N_2 system it appears to be rather non-linear over this current range. The reasons for this behavior are not clear, although the following three explanations may be offered.

It is possible that the intermixing with nitrogen, which causes some turbulence in the fringes of the jet, may change the pressure distribution upstream (i.e within the nozzle of the torch), and consequently affect the arc behavior. If this is the case, it was not seen to any significant degree in the results of the model.

It is also possible that some localized change in the anode composition may have changed the behavior of the torch. For example, it is known that the extent of oxidation can significantly change the work function of a copper anode,[20] and thus modify the arc voltage. It would seem, however, that such an effect would have made a constant change in the arc voltage over the range of current values.

Finally, it is quite possible that small changes in the cathode shape or composition may affect the value of the current density at the cathode. This will cause the torch voltage to vary, even for a constant current, as was shown in Section IV.A.3. It may be that the variations in the torch characteristics seen in Figure IV.B.2 are the result of these shape or composition changes rather than the change in the controled atmosphere from argon to nitrogen. In fact, the experiments have shown that the torch behavior can change over time as the cathode is eroded.

Figure IV.B.3 shows a comparison of the theoretically predicted current-voltage plot with that measured experimentally. It is seen that the agreement is reasonable, and in

fact may be quite good considering the nature of the experimental variations as seen in Figure IV.B.2.

In order to provide a perspective of the behavior of the system it is of interest to examine in a general way how the behavior of the Ar/Ar and Ar/N_2 systems may differ. Then we will examine a direct comparison between measurements and predictions as they pertain to the latter system.

IV.B.3.b Comparison of Ar/Ar with Ar/N_2

It has been observed that the behavior of an argon plasma jet is quite different depending on whether it exits into argon, or into ambient air or nitrogen.(21) Figures IV.B.4-IV.B.5 illustrate the nature of this difference.

Figure IV.B.4 illustrates a comparison of the temperature contours in the jet for the Ar/Ar and the Ar/N_2 system. It is seen that the hot plasma jet extends further in both the axial and radial directions in the pure argon system than in the two gas system. This is readily explained by the fact that the diatomic nitrogen dissociates when it is entrained by the plume. The energy involved in heating and dissociation is much greater than that required only to heat the monatomic argon. Thus, while the energy of the two plumes may be nearly the same, the one which entrains nitrogen will have a much lower temperature.

Figure IV.B.5 shows a comparison of the temperature profiles of an argon plasma jet in an argon atmosphere with those in a nitrogen atmosphere, with (a) measurements, and (b) theoretical predictions. The trends are consistent; in both cases the temperature falls more steeply in both the axial and radial directions when the jet issues into a nitrogen atmosphere.

IV.B.3.c Comparison with experimentally measured temperatures.

Figures IV.B.6-IV.B.8 show the comparison between experimentally measured and theoretically predicted axial and radial temperature profiles in the plasma plume over the range of conditions covered by the experiments. In all cases the agreement is quite reasonable, considering the difficulties involved (e.g. the uncertainty in the temperature measurements, the assumption of LTE, as well as the assumptions in the model). In fact,

the agreement is not as good as Section II.B which addressed only the plasma plume, because in that work, the enthalpy at the torch exit could be adjusted in the model (within the range of the experimental uncertainty) to bring about a closer agreement. In this model, in which the energy generated in the arc is calculated from first principles, the only such parameter available is the current density at the cathode, which was not adjusted in in this paper, but was chosen as a constant value of 3×10^7 A/m^2.

IV.B.3.d Effect of a shroud gas

One method of reducing the effect of the surrounding environment on the gas plume is to inject argon parallel to the torch axis through an annular region as illustrated in Figure IV.B.1. Intuitively, one can expect that the argon flow should act as a shroud to prevent the entrainment of nitrogen (or air) into the hot plume; then the plume will entrain primarily monatomic argon and will behave more like that in the argon-in-argon controlled atmosphere experiments of the previous section.

Calculations have been performed using case BES25 listed in Table II.B.I, including a shroud gas injected at 0.5 m/s through an annular slot of inner radius 40 mm and outer radius 48 mm. The shroud gas flow was 4.0 scmh, and the results are illustrated in Figures IV.B.9-IV.B.11. Figure IV.B.9 shows a comparison of the contours of the argon mass fraction, for the shrouded and unshrouded cases. It is seen that the shroud gas dramatically reduces the concentration of nitrogen in the hot region of the plume. The resulting plume temperatures are higher and the hot plume region is larger as illustrated in Figure IV.B.10. Figure IV.B.11 shows a comparison of the calculated temperatures in the plume for the three cases: Ar/Ar, Ar/N_2 and Ar/N_2 with a shroud gas. As expected, the axial temperature profile falls more steeply in the Ar/N_2 system than in the Ar/Ar system, while the shrouded case falls between the two.

IV.B.4 DISCUSSION

In this section, a formulation and computed results have been presented describing the behavior of an argon jet discharging into a nitrogen atmosphere. An important new feature of the calculations has been the fact that in the calculations we have been able to examine the transport phenomena inside the plasma torch. A comparison with experimental measurements provided an additional means for testing the appropriateness of our previously published "inside torch" model.

In general the theoretical predictions were found to be in quite reasonable agreement with the measurements. We have been able to predict the fact that the Ar/Ar and the Ar/N_2 systems behave in a markedly different manner. with a rather sharper drop in temperature in the latter case.

The theoretical predictions agreed quantitatively with the experimentally measured temperature profiles; furthermore, we have been able to provide at least a semi-quantitative representation of the experimentally determined current-voltage relationships. Finally, we have also examined the effect of using an argon shroud surrounding the plasma jet. The predictions regarding this arrangement were in accordance with the expected behavior in that the presence of an argon shroud would reduce the intermixing with the surrounding gas and hence lead to the less rapid cooling of the plasma jet than would have been the case in the absence of the shroud. This quantitative description of the effects produced by the presence of the shroud may be quite helpful in many materials processing applications where we may wish to separate the plasma regions from the surrounding gas.

IV.C. TURBULENT ARGON-ARGON SYSTEM - METCO TORCH

In the following section the model of the plasma torch which has been presented in sections IV.A-B will be extended to torches of more practical interest, namely torches for which the plume becomes turbulent. These torches include most systems of practical interest in plasma spraying, for instance. The torch to be addressed in this section is the Metco 7MB torch which is shown schematically in Figure IV.C.1 and has previously discussed in section II.C-D, with regard to the modeling of the plasma plume.

IV.C.1 MODEL DESCRIPTION

The model developed for the cases involving turbulence is essentially a combination of the turbulent plume model with the model of the phenomena inside the plasma torch. For the sake of completeness, the model will be presented here in its entirety.

The governing equations are written applying the same set of assumptions as used in section IV.A.2 except the assumption of laminar flow has been relaxed. Turbulence is represented using a K-ε model. The resulting equations which describe the time averaged behavior of the system include the following:

IV.C.1.a Governing Equations

Continuity of mass:

$$\frac{\partial(\rho u)}{\partial z}+\frac{1}{r}\frac{\partial(\rho r v)}{\partial r}=0 \qquad [IV.C.1]$$

In these equations z, u; r,v and θ, w are the coordinates and velocities in the axial, radial and azimuthal directions respectively, as shown in Figure IV.C.2, and ρ is the density of the gas.

Conservation of axial momentum:

$$\frac{\partial(\rho u^2)}{\partial z}+\frac{1}{r}\frac{\partial(\rho ruv)}{\partial r}=-\frac{\partial P}{\partial z}+2\frac{\partial}{\partial z}\left[\mu_{eff}\left(\frac{\partial u}{\partial z}\right)\right]+\frac{1}{r}\frac{\partial}{\partial r}\left[r\mu_{eff}\left(\frac{\partial u}{\partial r}+\frac{\partial v}{\partial z}\right)\right]$$
$$+j_r B_\theta \quad [IV.C.2]$$

In the above, P denotes the pressure, μ_{eff} is the effective viscosity, j_r is the radial component of the current density, and B_θ is the azimuthal magnetic flux density.

Conservation of radial momentum:

$$\frac{\partial(\rho uv)}{\partial z}+\frac{1}{r}\frac{\partial(\rho rv^2)}{\partial r}=-\frac{\partial P}{\partial r}+\frac{\partial}{\partial z}\left[\mu_{eff}\left(\frac{\partial v}{\partial z}+\frac{\partial u}{\partial r}\right)\right]+\frac{2}{r}\frac{\partial}{\partial r}\left[r\mu_{eff}\left(\frac{\partial v}{\partial r}\right)\right]$$
$$-\mu_{eff}\frac{2v}{r^2}+\frac{\rho w^2}{r}-j_z B_\theta \qquad [IV.C.3]$$

In the above, j_z is the axial component of the current density vector. The terms $j_r B_\theta$, and $j_z B_\theta$ are the electromagnetic or **J X B** forces, where **J** is the current density vector, and **B** is the magnetic flux density vector.

Conservation of azimuthal momentum:

$$\frac{\partial(\rho ruw)}{\partial z}+\frac{1}{r}\frac{\partial(\rho r^2vw)}{\partial r}=\frac{\partial}{\partial z}\left(\mu_{eff}\frac{\partial(rw)}{\partial z}\right)+\frac{1}{r}\frac{\partial}{\partial r}\left(\mu_{eff}r\frac{\partial(rw)}{\partial r}\right)$$
$$-\frac{2}{r}\frac{\partial(\mu_{eff}rw)}{\partial r} \qquad [IV.C.4]$$

Conservation of Energy:

$$\frac{\partial(\rho uh)}{\partial z}+\frac{1}{r}\frac{\partial(\rho rvh)}{\partial r}=\frac{\partial}{\partial z}\left(\frac{\mu_{eff}}{\sigma_h}\frac{\partial h}{\partial z}\right)+\frac{1}{r}\frac{\partial}{\partial r}\left(\frac{r\mu_{eff}}{\sigma_h}\frac{\partial h}{\partial r}\right)+\frac{j_z^2+j_r^2}{\sigma}$$
$$-S_R+\frac{5}{2}\frac{k_b}{e}\left(\frac{j_x}{C_p}\frac{\partial h}{\partial z}+\frac{j_r}{C_p}\frac{\partial h}{\partial r}\right) \qquad [IV.C.5]$$

The terms in this equation represent the transport of enthalpy by convection and diffusion, joule heating, radiation losses, electron drift, and finally a term which accounts for energy changes due to pressure variations. Symbols used in the above denote the turbulent Prandtl number for enthalpy, σ_h, heat capacity, C_p , electrical conductivity, σ, specific enthalpy, h, Boltzmann's constant, k_b, the electric charge, e, and the volumetric radiative loss term, S_R.

In the case of a two gas system (e.g. an argon gas passing through a torch into an environment of air) then the species balance must also be included in the governing equations.

Species Balance:

$$\frac{\partial(\rho u m)}{\partial z}+\frac{1}{r}\frac{\partial(\rho r v m)}{\partial r}=\frac{\partial}{\partial z}\left(\frac{\mu_{eff}}{\sigma_m}\frac{\partial m}{\partial z}\right)+\frac{1}{r}\frac{\partial}{\partial r}\left(\frac{r\mu_{eff}}{\sigma_m}\frac{\partial m}{\partial r}\right) \qquad [IV.C.6]$$

Current continuity in terms of electric potential:

$$\frac{\partial}{\partial z}\left(\sigma\frac{\partial\phi}{\partial z}\right)+\frac{1}{r}\frac{\partial}{\partial r}\left(\sigma r\frac{\partial\phi}{\partial r}\right)=0 \qquad [IV.C.7]$$

whereσ_m is the turbulent Schmidt number, m is the mass fraction of argon and ϕ is the electric potential.

In addition, two equations are solved for the kinetic energy of turbulence, K and for the turbulent energy dissipation, ε.

Turbulent Kinetic Energy

$$\frac{\partial(\rho u K)}{\partial z}+\frac{1}{r}\frac{\partial(\rho r v K)}{\partial r}=\frac{\partial}{\partial z}\left(\frac{\mu_e}{\sigma_K}\frac{\partial K}{\partial z}\right)+\frac{1}{r}\frac{\partial}{\partial r}\left(r\frac{\mu_e}{\sigma_K}\frac{\partial K}{\partial r}\right)+G-\rho\varepsilon \qquad [IV.C.8]$$

Turbulent Energy Dissipation

$$\frac{\partial(\rho u \varepsilon)}{\partial z}+\frac{1}{r}\frac{\partial(\rho r v \varepsilon)}{\partial r}=\frac{\partial}{\partial z}\left(\frac{\mu_e}{\sigma_\varepsilon}\frac{\partial \varepsilon}{\partial z}\right)+\frac{1}{r}\frac{\partial}{\partial r}\left(r\frac{\mu_e}{\sigma_\varepsilon}\frac{\partial \varepsilon}{\partial r}\right)+\frac{\varepsilon}{K}(C_1G-C_2\rho\varepsilon) \qquad [IV.C.9]$$

where σ_K and σ_ε are the turbulent Prandtl numbers for the K and e respectively and the generation term G is given by

$$G = \mu_t \left\{ 2\left[\left(\frac{\partial u}{\partial z}\right)^2 + \left(\frac{\partial v}{\partial r}\right)^2 + \left(\frac{v}{r}\right)^2 \right] + \left[\left(\frac{\partial w}{\partial z}\right)^2 + \left(\frac{\partial u}{\partial r} + \frac{\partial v}{\partial z}\right)^2 + \left(\frac{\partial w}{\partial r} - \frac{w}{r}\right)^2 \right] \right\} \qquad [IV.C.10]$$

and the effective viscosity is given by the sum of the laminar and turbulent components, $\mu_{eff} = \mu_{lam} + \mu_t$ where the turbulent viscosity is given by

$$\mu_t = \frac{C_D \rho K^2}{\varepsilon} \qquad [IV.C.11]$$

The plasma properties are taken from the sources detailed in Sections IV.A-B and Section II.C. The electrical conductivity is modified using an exponential expression below a certain cutoff temperature as noted in Section IV.A. This is more fully described here.

As suggested by Scott et al.(9) the electrical conductivity has been modified below a certain cutoff value using the expression $\sigma = A \exp(T/B)$. In the expression used in Reference (9), A = 20 and B = 2000. These are the values used in Sections IV.A-B. However, a parametric study indicated that more realistic values might be chosen to better represent the voltage versus flow rate behavior of the system. The constants chosen were those for which the theoretical current versus flow rate relationship (shown in Figure IV.C.7) would have the same slope as that demonstrated experimentally. Thus for this section, the values of the constants have been modified to A = 300 and B = 4364.42. Three relations of the type chosen, together with the LTE values are plotted in Figure IV.C.3. In addition, the cathode current density used has been increased to $j_c = 6.5 \times 10^7$ A/m^2 based on experimental observations which indicate that higher values than previously used may be more representative of the conditions inside plasma torches.(23)

Casting the Equations

It is important to note here that because of the transitional nature of the phenomena, care is required in casting the equations in a form which most accurately represents the system. In a large number of plasma torches, because of the high viscosity of the plasma,

the flow within the torch will remain essentially laminar. This has been illustrated by high speed photographs and shadowgraphs which indicate laminar flow exiting the torch with a rather sudden transition to turbulent flow.[27] In this version of the model, this behavior is represented by assuming laminar flow ($\mu_{eff} = \mu_{lam}$) inside the torch while fully turbulent flow is assumed at the nozzle exit.

IV.C.1.b. Auxiliary Equations

If the current distribution is axi-symmetric, the self induced magnetic field may be calculated by the following relation derived from Amperes law:

$$B_\theta = \frac{\mu_o}{r}\int_0^r j_z \zeta d\zeta \qquad [IV.C.12]$$

where μ_O, is the magnetic permeability of free space, and ζ is a dummy variable of integration.

The current density is calculated from the definition of electric potential:

$$\vec{J} = -\sigma \nabla \phi \qquad [IV.C.13]$$

IV.C.1.c. Boundary Conditions:

The integration region is sketched in Figure IV.C.2, and the corresponding boundary conditions are given in Table IV.C.I.

These conditions specify zero velocities at all solid boundaries, and zero fluxes at the axis of symmetry. Constant temperatures of all solid boundaries and at the outer entrainment boundary are assumed. Additionally, zero gradients are assumed at the downstream boundary, and zero currents are assumed on all boundaries except on the cathode (where a current density is specified) and at the anode (where a constant electric potential is assumed). The anode and cathode surfaces may require special treatment since deviations from LTE occur in these regions.

Inlet boundary

At the inlet boundary (line DE of Figure IV.C.2) the axial velocity is assumed to have a flat profile. The radial velocity is assumed to be zero. Additionally, it is important to be able to quantify the swirl at the inlet boundary. The values given in the first section may be used to estimate swirl number. This is done in the same way as outlined in Section IV.A.

For the torch in this section the injection is done in the upstream region through two tangentially directed holes 1.6 mm in diameter. The annulus upstream of the arc has an approximate inside diameter of 7 mm and and outer diameter of 8 mm, which gives a cross-sectional area of 1.178×10^{-5} m^2. The resulting values of the average velocities and required radii are the following: W = 99 m/s at r_{inj} = 0.0075 m, U = 33.4 m/s and R_0 = 0.0035 m, so that Sw = 4.0. The type of swirl introduced is assumed to be that of solid body rotation at the inlet boundary.

Electrodes

The regions near the electrodes are represented as they are in section IV.A. The contribution of the cathode fall is given approximately by the "free fall" type of expression for the cathode fall voltage, V_C as was done by McKelliget and Szekely(12) for a free-burning arc:

$$V_c = \frac{5}{2}\frac{k_b T_{elec}}{e} \qquad [IV.C.14]$$

In this expression, V_C is the cathode fall voltage, and T_{elec} is the electron temperature, which is approximated as the maximum plasma temperature in the column adjacent to the cathode (~20000 K), so that $V_C \sim 4.3\ V$. In Table IV.C.I, the torch current is denoted by I, and Q_C is a positive source to the plasma column at the cathode boundary which approximates the energy used in the cathode boundary layer to ionize the plasma.

The boundary condition for electric potential is approximated assuming that the cathode current density, j_C which is emitted from the cathode normal to the surface is constant inside the cathode spot radius, R_C and is zero outside:

$$j_c = \frac{I}{\pi R_c^2} \quad ; \quad r < R_c \ \ and \quad j_c = 0 \ ; \quad r > R_c \qquad [IV.C.15]$$

Nozzle Exit

At the nozzle exit, where transition from laminar to turbulent flow is assumed to occur, the values of K and ε must be set. The default values would be zero, but this was seen to grossly underestimate the turbulent mixing which occurs in the plume. For this reason, the values were calculated using the expressions in Table IV.D.I for the inlet flow. This leads to somewhat of a paradox at the nozzle exit, namely, assuming laminar flow, but specifying values of K and ε (for use in the plume) which correspond to turbulent flow. If this is not done, however, the turbulence develops much too slowly to represent the plume behavior.

IV.C.1.d Solution Method

The solution is done using a finite volume technique using a modified and extended version of the code developed by Dilawari et al.[10,15] based on the 2/E/FIX code of Pun and Spalding.[16] The code, which has been modified to include the electromagnetic phenomena, was executed in a mode which includes the solution of the turbulence equations. The grid system was previously found to give sufficient numerical accuracy, and uses a 67X40 mesh, with 33X15 grids inside the torch and 34X40 grids outside. The solution requires about 4.5 hours of CPU time on a Vaxstation 3100 for three thousand iterations.

IV.C.2. RESULTS OF CALCULATIONS

In the following we shall present some results of calculations performed using the experimental conditions listed in Table IV.C.II which were taken by Capetti and Pfender[24].

Figure IV.C.4 (a-b) shows a set of representative temperature contours and velocity vectors in the system (for case 12, 450 amps, 23.6 liters/min). The maximum temperature is higher than in the previous systems of section IV.A-B due to the higher cathode current density. The resulting maximum velocity of 1159 m/s is also much higher than in the section IV.A-B because of the higher flow rate and current density.

Figure IV.C.5 (a-b) shows the mass flow (ρu product) vectors and the contours of the swirl velocity in the system. The mass flow vectors show a maximum near the walls because of the high mass density in those lower temperature regions. This is in agreement with the results shown by previous investigators[25-26]. The swirl isocontours show a maximum (901 m/s) on the center line as a result of the combination of decreased density and the conservation of angular momentum (swirl velocity tends to increase as 1/r).

Figure IV.C.6 (a-b) shows the electric current density vectors and the resulting body forces in the flow. The maximum current density is 6.3×10^7 A/m^2 which occurs near the cathode tip. The body forces result from the interaction of the current density with the self-induced magnetic field according to the right-hand rule, (maximum $= 2.5 \times 10^6$ N/m^3). As a result, the body forces act toward the center line of the system which tends to increase the pressure on the axis, and away from the cathode tip. These forces lead to the well known "cathode jet" effect.

Figure IV.C.7 shows a comparison of the calculated and experimentally measured voltage characteristics of the torch as a function of the gas flow rate for the two different currents. The calculations represent the experiments rather well, however the calculation neglects to include any allowance for the anode fall, which could lead to the observed discrepancy of some 2 volts.

Figures IV.C.8-11 (a-b) illustrate the behavior of the plasma plume as it exits the nozzle of the torch. Figures IV.C.8 and IV.C.10 show the comparison between the measured and calculated profiles of the temperature and velocity on the center line of the plume versus axial position for two different current levels and three different flow rates. The discrepancies are partly due to the limitations of switching from a laminar model inside the torch to a fully turbulent model at the torch exit.

While the comparison is not as good as that shown in the "plume only" section, corresponding to Figures II.D.6-7, at least one of the trends shown may prove to be more realistic. The observation in question, is that with an increase in flow rate, the velocities on the axis of the plume do not change appreciably[24]. This is contrary to what may be expected from a simple mass balance as previously shown in Section IV.D and summarized in Table II.D.II. The model, however, suggests an explanation for this trend. It appears

that the high flow case may be more "swirl dominated" at the nozzle exit, which leads to a wider jet spreading and thus comparable velocities on the center line.

This effect is further illustrated in Figures IV.C.9 (a-b) and IV.C.11 (a-b) which show the radial profiles of temperature and velocity at a position 1 mm from the nozzle exit. The figures show that while the temperature profile is relatively unchanged as the flow rate is increased, the velocity profile may change significantly, even exhibiting a bi-modal distribution at higher flow rates. This occurs because the larger flow of gas receives a relatively smaller increase in axial momentum due to expansion forces than the smaller gas flow, resulting in a higher swirl number at the nozzle exit as seen in Table IV.C.III. The enhanced spread of the jet may lead to lower velocities in the plume, which is seen for example in Figure IV.C.8 over the section of the plume nearest the nozzle exit

IV.C.3 CONCLUSIONS

This section has illustrated the applicability of the model to a plasma torch operating at high flows like those which are usually used in practical applications. The model shows some significant limitations, tending to over-predict the temperatures and under predict the velocities. It is felt that these shortcomings stem from a number of simplifications and assumptions, including the swirl number at the entrance of the torch, the assumption of LTE, the assumption of axial symmetry, which necessitates the use of an artificially high electrical conductivity, and finally the simplifications made regarding the transition from laminar flow in the torch to fully turbulent flow in the plume.

The model, however, has provided some important insights into the behavior of the torch, including an inside look into the role and persistence of swirl in the torch nozzle. This is explored in some more detail in Section IV.E, and is further quantified using dimensional analysis.

IV.D. TURBULENT ARGON-AIR SYSTEM - MILLER TORCH

In this section, the model of the plasma torch will be applied to another commercially available torch made by Miller-Thermal, Inc. operating at reasonably high flows so that the torch is operating in the turbulent mode. This torch is illustrated in Fig. IV.D.1, and was also used in doing the plasma spray measurements which are presented in Chapter V. In order to provide a good test of the model, the temperature, velocity and the composition of the plasma must be measured as near as possible to the torch exit. This provides the best test of the model that can be done in the absence of measurements inside the torch.

Measurements of this type have been made at the Idaho National Engineering Laboratory by Fincke and co-workers[27]. The measurements were made on a Miller SG-100 torch with pure argon as the working gas, which exited the torch nozzle into ambient air. Measurements of the radial profiles of plasma temperature, velocity and concentration were made at an axial position 2 mm from the torch exit. In addition, the axial profiles of these variables was taken for two cases (300 and 600 amps). Finally, at a current level of 900 amps a full map of the radial profiles was taken at axial positions of 5, 10, 15, 20, 25, 30, 40, 50, 60 and 70 mm. The experimental conditions are shown in Table IV.D.I.

IV.C.1 TORCH SPECIFICS

In this torch the injection of the working gas is done through a swirl ring shown in Figure IV.D.2 which injects the gas though four 1.98 mm (5/64 in) diameter holes. As seen in the figure, the holes are not tangential to the inner diameter of the ring as in previous arrangements, so it was approximated that the injection is tangential at a radius of 4.19 mm (0.165 in). The resulting velocity of 0.00059 m^3/s (75 std.cu.ft./hr) of argon passing through four holes is 47.85 m/s. The inner and outer radii of the annulus between the cathode and anode are 5.31 mm (0.209 in) and 7.44 mm (0.293 in) respectively, resulting in a cross-sectional flow area of 2.14×10^{-5} m^2. The resulting axial velocity of the gas in the annulus is 27.6 m/s. Applying equation [IV.A.12] with W = 47.85 m/s, r_{inj} = 0.00419, U = 27.6 m/s, and R_0 = 0.00396 m gives a swirl number of 1.22.

It should be noted that this analysis alone is quite enlightening, indicating why particles in the plume of this torch may appear to have little swirling or angular motion, while particles in the plume of the Metco torch of section IV.C may show a visible angular motion.

IV.D.2. DETAILS OF THE CALCULATION

The calculations performed are quite similar to those done in Section IV.C. The additional complexity is brought in by the fact that the torch exits into an air atmosphere. This requires that the species equation [IV.C.6] be included in the solution. This has been previously described in Section II.C.

In addition, the Miller torch is assumed (based on cut-away views of the two torches) to have a more blunt cathode tip than the Metco torch. As seen from measurements and models of gas tungsten welding arcs, this should tend to produce lower cathode current densities[28-29], and hence the value of 5.0×10^7 A/m^2 is used in modeling this torch. The assumed temperature dependence of the electrical conductivity is identical to that used in Section IV.C., namely an exponential relationship with the constants A = 300 and B = 4364.42, as shown in Figure IV.C.3.

The calculation domain used for the Miller torch has the same dimensions as used in the Metco torch (Figure IV.C.2) except the length of the nozzle is 0.0216 m (0.850 in).

IV.D.3. RESULTS OF CALCULATIONS

Calculations were performed and comparisons made for all the cases shown in Table IV.D.I. A characteristic set of results are plotted inside the torch in Figures IV.D.3-IV.D.5.

Figure IV.D.3 (a-b) shows a set of representative temperature contours and velocity vectors in the system (for case 6, 600 amps, 75 scfh). The region of maximum temperature is somewhat smaller than in the previous section IV.C (Figure IV.C.4) because of the lower cathode current density used. The resulting maximum velocity of 1189 m/s is nearly the same as in Figure IV.C.4 because of the ofsetting effect of the

higher flow rate and lower current density used here. The velocity distribution at the nozzle exit is more peaked in this case because of the gas is introduced with a lower swirl number.

Figure IV.D.4 (a-b) shows the mass flow (ρu product) vectors and the isocontours of the swirl velocity in the system. The mass flux again assumes a maximum in the low temperature regions near the walls. The swirl contours are similar to the previous case, except the maximum swirl velocity (622 m/s) is lower.

Figure IV.D.5 (a-b) shows the electric current density vectors and the resulting body forces in the flow. The maximum current density is 5.0×10^7 A/m^2 near the cathode tip. The maximum body force is 2.2×10^6 N/m^3, slightly lower than in the previous case, again due to the lower current density.

Figure IV.D.6 shows a comparison of the calculated and experimentally measured voltage characteristics of the torch as a function of the current. The experiments and calculations are in reasonable agreement, however the calculation neglects to include any allowance for the anode fall, which could explain the observed discrepancy.

Figure IV.D.7 shows a comparison between the experimentally measured and theoretically predicted center line temperature (a) and axial velocity (b) at a position 2 mm from the torch exit (except case 9 which is shown at 5 mm). The trends are represented rather well, though the maximum temperature is over predicted by about 25%. It is felt that this disagreement is caused by the over prediction of the torch efficiency which is most likely due to the simplified treatment of the non-equilibrium anode boundary layer. The presence of non-thermal equilibrium will likely produce higher thermal conductivities in that region (relative to LTE values) which should increase the conductive losses to the anode, leading to the lower than predicted thermal efficiencies which have been measured.

Figures IV.D.8 - IV.D.28 show the detailed comparison of the experimental measurements with the calculated results. Cases 3, 6 and 9 (300, 600, 900 amps) have the most complete sets of data. Thus for example at 300 amps Figures IV.D.8 - IV.D.9 illustrate the radial profiles of temperature, velocity and argon mole fraction at an axial position 2 mm from the nozzle exit. Figures IV.D.10 - IV.D.11 show the axial profile on the center line of the temperature, velocity and argon mole fraction.

In the cases for which the axial profiles were not measured, namely cases 4, 5, 7 and 8, only the radial profiles of temperature, velocity and argon mole fraction are compared at an axial position 2 mm from the exit (note, no profiles were measured for case 8). These are illustrated for example in Figures IV.D.10 - IV.D.11, for case 4.

Finally, Figures IV.D.26 -IV.D.28 show three dimensional plots of the calculated and measured radial profiles of temperature, velocity and argon mole fraction at five different axial positions for the 900 amp case. This gives an overall picture of the comparison between the measured and predicted data in the plume.

On the whole the agreement seen in the comparison is reasonably good, and the discrepancies where they appear are consistent, and reasonable.

In general, the temperatures in the core of the jet are over predicted by as much as 25% at the nozzle exit (e.g. Figure IV.D.8 (a)). This over prediction persists throughout most of the length of the jet to an axial position of about 70 mm (Figure IV.D.10 (a)).

The velocity profiles are remarkably well predicted by the model with the errors being in the 5-10% range (Figure IV.D.8 (b)). The agreement is nearly as good over the length of the plume (with the exception of case 9), giving confidence in the model's ability to predict the axial velocity in the plume (Figure IV.D.10 (b)).

Finally, the predicted concentration of argon at the nozzle exit tends to be two low in the fringes of the jet (Figure IV.D.9) and too high on the center line as the axial distance increases (Figure IV.D.11). Perhaps this indicates that the turbulence model is limited in its ability to predict the plume behavior.

IV.D.4 CONCLUSIONS

The comparison between experimental measurements and theoretical predictions presented in this section has provided the most rigorous test of the model to date. The simultaneous comparison with temperature, velocity and concentration data in the plume and especially near the torch exit, and the resulting agreement (or predictable discrepancy) between measurements and predictions lends added credibility to the model.

To summarize, the model predicts current voltage characteristics reasonably well, though the predictions are low, perhaps due to the neglect of the anode fall voltage. The model over predicts the torch efficiency or net power, probably because of the presence of non-equilibrium in the narrow torch nozzle. Finally the predictions of the temperatures, velocities and concentrations in the plume are consistent, and the errors reasonable and predictable. In general, the temperature is about 25% too high in the core of the jet, while the velocity is within 5-10% of the measured values. The concentration of argon tends to be low in the jet fringes and to a lesser degree, too high on the axis with increasing distance from the nozzle.

IV.E. DIMENSIONAL ANALYSIS

While rigorous numerical models can provide insight into the operation of plasma torches, it is highly desirable to develop an understanding which is based on dimensional analysis. In this way, knowledge gained in one system or by modeling may be transferred to another system.

This section will examine some dimensionless numbers which apply to plasma torches to see what information can be obtained in this way. The dimensionless numbers of interest are given in Table IV.E.I, together with their definitions, descriptions and approximate ranges of values in plasma systems. In addition Tables IV.E.II - IV.E.IV summarize the values of these parameters for the systems represented in this thesis.

IV.E.1 DIMENSIONLESS NUMBERS OF GENERAL INTEREST

Reynolds Numbers:

Two Reynolds numbers are of interest in plasma torch/plume systems. They are based on the nozzle diameter, Re_D and the local position in the plume, Re_Z. The first indicates whether the flow in the nozzle is laminar or turbulent (laminar for $Re_D < 2000$) while the second indicates whether the plume is laminar or turbulent (transition to turbulence occurs at $Re_Z \sim 100{,}000$ for a free jet).

As seen in Tables IV.E.II - IV.E.IV the majority of the systems studied in this thesis have been essentially laminar at the torch exit. It must be noted that the steep velocity and temperature gradients present in plasma torches may cause the critical Reynolds for transition to turbulence to be lower than 2000. Even so, it is to be expected that many of these systems make a transition to turbulent flow in the plume region.

Mach Number:

The Mach number is the ratio of the flow velocity to the velocity of sound in a medium, as seen in Table IV.E.I This dimensionless variable indicates the type of flow (subsonic, sonic or supersonic) and whether it is incompressible.

The sonic velocity in an ideal gas is given by the following relation:

$$U_s = \sqrt{\frac{\gamma R T}{M}} \qquad [IV.E.1]$$

where γ, is the ratio of specific heat at constant pressure, C_p to that at constant volume, C_v, R is the universal gas constant and M is the molecular weight.

Using this expression the Mach numbers in the cases studied here may be calculated and are summarized in the tables. These indicate that the cases are all subsonic and for the most part incompressible.

IV.E.2 DIMENSIONLESS NUMBERS SPECIFIC TO ARC SYSTEMS

In electromagnetic systems such as these, a number of other dimensionless numbers characterize the interaction between the arc and the plasma.

Magnetic Reynolds Number:

The magnetic Reynolds number indicates the relative importance of magnetic diffusion to magnetic convection. As seen in Table IV.E.I it retains small values in plasma systems. This enables the equations describing the electromagnetic phenomena to be greatly simplified by neglecting the convective terms. Note, however, that the fluid flow, thermal and electromagnetic field equations are still coupled through the strongly non-linear, temperature dependent electrical conductivity.

Dimensionless Torch Parameters:

It has been suggested by Shashkov, et al.[22] that several other dimensionless numbers may be used to characterize torch behavior. Two of these numbers included in Table IV.E.1 and have been labeled EM and HJ for the sake of brevity.

The EM number is the ratio of the Electromagnetic force to the plasma Momentum force. It gives an indication of the importance that the JXB forces have in determining the velocity profiles. Since the electromagnetic force tends to be concentrated on the axis of the torch, higher EM numbers will have more peaked velocity distributions.

The HJ number is the ratio of the Heat capacity of the plasma to the Joule heating which occurs in the torch. In fact, Shashkov uses this as the principal parameter to correlate the Voltage-Current characteristics of torches of the type illustrated in Figure IV.E.1(c). It has been attempted to use this parameter to correlate the current-voltage characteristics of the type (a) torches in this study.

This correlation was performed using an overall enthalpy balance on each of the torches. To evaluate the HJ number, the plasma properties σ and h must be evaluated at some characteristic temperature. The temperature used is an average based on the an adjusted torch power. As in the simplified torch model presented in Chapter III, the electrical energy in the arc, which heats the anode directly, is subtracted from the torch power $(V \times I)$. It is given by Equation III.B.7 as

$$Q_{e,a} = I\,(2.76+V_w) = I\,(2.76 + 4.0) \qquad \text{[IV.E.1]}$$

The remaining energy is the "Joule heat" which is given in column 2 of Tables IV.E.II - IV.E.IV. Dividing this power by the mass flow rate of gas, $\dot{m}$ gives an average specific enthalpy for the gas in the arc. This is used to look up the average temperature using tables of argon plasma properties.

When this is done, the dimensionless voltage can be calculated from the expression

$$\text{Dimensionless Voltage} = \frac{VD\sigma}{I} \qquad \text{[IV.E.2]}$$

and the HJ number, given by

$$HJ = \frac{\dot{m}Dh\sigma}{I^2} \qquad \text{[IV.E.3]}$$

can be calculated for all the cases shown in Tables IV.E.II - IV.E.IV. This may be done using a spread sheet or a simple program like that presented in Appendix II which contains the tables for the thermodynamic and transport properties of the plasma.

The results are shown in Figure IV.E.2 (a) which shows a remarkably good correlation over a rather wide range of torch variables including gas flow rate, torch current and nozzle diameter. Figure IV.E.2 (b) shows a more detailed plot of the high flow rate cases taken with the Metco and Miller torches. While the experimental scatter is significant, the linear relationship is quite good.

This method of correlating the torch characteristics was further extended to the Miller torch operating with different mixtures of argon and helium, based on the experimental conditions shown in Table IV.E.V. The properties of the mixture were determined using the same mixing rules as in the numerical model, and which are incorporated into the program in Appendix II. Using the mixture properties, the dimensionless voltage for this torch could also be plotted as a straight line versus the HJ number. Such an ability to correllate (and hence predict) the torch behavior could be extremely valuable for process design and control.

The next dimensionless parameter which is of interest is the CJ number, which is the ratio of Conduction to Joule heating. Again Tables IV.E.2 - IV.E.4 summarize this number for the systems studied. It is seen that conduction is a significant heat transfer mode, but that it is generally less than the convective mode indicated by the HJ number.

Finally, in dealing with swirling flows, it is suggested that another number labeled the ES number will provide still more information about the velocity profiles. This is the product of the EM number and the reciprocal of the swirl number (which has been introduced in Section IV.A.) This gives the ratio of Electromagnetic forces to the Swirl forces. It is expected that high ES cases will have very peaked velocity distributions while low ES cases will have bimodal distributions with a peak off axis and perhaps even a reverse flow zone on the axis. ES numbers of around 1.0 should demonstrate intermediate situations. These cases are sketched schematically in Figure IV.E.3.

In performing the work on the Metco torch presented earlier, a parametric study was done to illustrate the effect of the ES number on the velocity profiles at the torch exit. The results are shown in Figure IV.E.4 (a)-(b).

Figure IV.E.4 (a) illustrates the the effect of increasing the swirl number, which decreases the ES number, leading to the bimodal velocity profile. While this may be expected, the effect shown in Figure IV.E.4 (b) is less obvious. It is seen that increasing

the gas flow, which decreases the EM number, at a constant swirl also tend to change the velocity profile into a bimodal shape. Thus the ES number includes the effect of gas flow on the system, indicating how increased flow tends to preserve swirl through the torch. This is true because the higher gas flow case has a lower specific enthalpy than the lower flow case which leads to a smaller incremental increase in the axial momentum due to expansion of the gas, thus preserving the swirl.

IV.E.3 CONCLUSIONS

It has been illustrated that dimensional analysis can indeed give new insight into the behavior of plasma torches. This is important because these type of calculations can be done using a very simple spreadsheet or program (such as that given in Appendix II). The resulting information may be very useful to the experimentalist or plasma spray shop.

The principal items of importance demonstrated are

(1) the ability to correlate the torch current - voltage characteristics of three different torches using the HJ number and
(2) the ability to qualitatively predict the shape of the velocity profiles at the exit of the torch.

These represent a significant contribution to the understanding of torch behavior.

IV.F. REFERENCES

1. A.H. Dilawari, J. Szekely, J. Batdorf and C.B. Shaw, Plasma Chem. Plasma Proc., **10**, No. 2., (1990).
2. K.C. Hsu, K. Etemadi, and E. Pfender, J. Appl. Phys. **54**, No. 3, 1293-1301, (1983).
3. K.C. Hsu and E. Pfender, J. Appl. Phys. **54**, No. 8, 4359-66, (1983).
4. K.J. Clark and F.P. Incropera, AIAA J., **10**, No. 1, 17, (1972).
5. D.M. Chen, K.C. Hsu and E. Pfender, Plasma Chem Plasma Proc., **1**, No. 3, 295-314, (1981).
6. R.S. DeVoto, Phys. Fluids, **16**, No. 5, 616, (1973).
7. D.L. Evans and R.S. Tankin, Phys.Fluids **10**, No. 6, 1137-44, (1967).
8. P. Fauchais, Private Communication.

9. D.A. Scott, P. Kovitya, and G.N.Haddad, J. Appl. Phys., **66**, No. 11, 5232, (1989).
10. A.H. Dilawari and J. Szekely, Int. J. Heat and Mass Transfer, **30**, No. 11, 2357, (1987).
11. K.C. Hsu and E. Pfender, J. Appl. Phys. **54**, No. 7, 3818-24, (1983).
12. J. McKelliget and J. Szekely, Met. Trans. A, **17A**, 1139-48, (1986).
13. J.F. Lancaster, Ed. The Physics of Welding, 2nd Ed., p.166, International Institute of Welding, Pergammon Press, Oxford, (1986).
14. H.A. Dinulescu and E. Pfender, J. Appl. Phys. **51**, No. 6, 3149-57, (1980).
15. A.H. Dilawari, J. Szekely and R. Westhoff, ISIJ International, **30**, No. 5, (1990).
16. W. Pun and D.B. Spalding, Report No. HTS/76/2, Heat Transfer Section, Imperial College, London, (1976)
17. C.H. Liu, Ph.D. Thesis, Department of Mech. Eng., Univ. of Minnesota, Minneapolis (1977).
18. C. R. Wilke, J. Chem Phys. , **18**, 517-519 (1950).
19. R. B. Bird, W. E. Stewart, and E. W. Lightfoot, Transport Phenomena, Wiley, N.Y., 511, (1960).
20. O.H. Nestor, Journal Appl. Phys. **33**, 1638, (1962).
21. M. Brossa, and E. Pfender, Plasma Chem. Plasma Proc. **8**, 75, (1988).
22. A.G. Shashkov and O.I. Yasko, "Applic. of Approx. Similarity for Correlating Arc Characteristics", IEEE Trans Plasma Sci., **PS-1**, No. 3, 21-37, (1973).
23. P. Fauchais, Comment on the authors paper made in the sessions of the TMS meeting on Plasma Processing. San Diego, (1992)
24. A. Capetti and E. Pfender, Plasma Chem Plasma Proc., **9**, (2), 329-341, (1989).
25. V.R. Watson and E.B. Pegot, "Numerical Calculations for the Characteristics of a Gas Flowing Axially Through a Constricted Arc", NASA TN D-4042, (1967).
26. A. Mazza and E. Pfender, "Modeling of an Arc Plasma Reactor for Thermal Plasma Synthesis", Symp. Proc. Int. Symp. Plasma Chem. 6th, **1**, 41-50, (1983).
27. J. Fincke, T.E. Repetti, S.C. Snyder, G.D. Lassahn, B.A. Detering, Proceedings of the TMS International Symposium: "Thermal Plasma Applications in Materials and Metallurgical Processing", 85-94, San Diego (1992).
28. N. Tsai, Ph.D. Thesis, Dept. of Materials Science and Engineering, Massachusetts Institute of Technology, Cambridge, MA. (1983).
29. R. Westhoff, Masters Thesis, Dept. of Materials Science and Engineering, Massachusetts Institute of Technology, Cambridge, MA. (1989).

Label	Current (Amps)	Gas Flow (scmh)	Input power (kW)	Cooling loss (kW)	Efficiency (%)	T_{max} (exit) (K)
B23	250	0.59	4.79	3.61	24.6	11131
B24	250	0.83	4.86	3.48	28.4	11394
B27	500	0.59	9.86	7.11	27.9	12415
B28	500	0.83	9.96	6.99	29.8	12227
B31	750	0.59	15.17	10.77	29.0	12587
B32	750	0.83	15.33	10.59	30.9	13075

Table IV.A.I. Operating conditions for plasma torch experiments at INEL

	u	v	rw	h	ϕ
AB	0	0	0	$T = 3000$ K $Q_c = I j_c / V_c$	$j_c = \frac{I}{\pi R_c^2}$
BC	0	0	0	$T = 3000$ K	$\frac{\partial \phi}{\partial z} = 0$
CD	0	0	0	$T = 3000$ K	$\frac{\partial \phi}{\partial r} = 0$
DE	$u = u(r)$	0	$rw(r)$	$T = 1000$ K	$\frac{\partial \phi}{\partial z} = 0$
EF	0	0		$T = 1000$ K	$\phi = \phi_a$
FG	0	0	0	$T = 500$ K	–
GH	0	$\frac{\partial \rho r v}{\partial r} = 0$	0	$T = 300$ K	–
HI	$\frac{\partial u}{\partial z} = 0$	$\frac{\partial v}{\partial z} = 0$	0	$\frac{\partial h}{\partial z} = 0$	–
IA	$\frac{\partial u}{\partial r} = 0$	0	0	$\frac{\partial h}{\partial r} = 0$	–
FJ	-	-	-	-	$\frac{\partial \phi}{\partial z} = 0$
JA	-	-	-	-	$\frac{\partial \phi}{\partial r} = 0$

Table IV.A.II. Boundary conditions for the solution of the governing equations of a non-transferred arc plasma torch.

Run No.	Identifier	Heat Output (W)	Gas Veloc. at Exit (m/s)	Temp. at Exit (axis) (K)
B23 - 250 A				
1	Simple model [9]	1376	62.3	11118
2	This model no **JXB**	1217	57.1	10900
3	This model with **JXB**	1557	105	11780
B31 - 750 A				
4	This model no **JXB**	1875	94.0	12210
5	This model with **JXB**	3772	421	14340

Table IV.A.III. Effect of electromagnetic forces on fluid flow in plasma torch used at INEL, case B23 and B31 (calculations done without swirl).

Run No.	Inlet Swirl No.	Exit Swirl No.	L_{arc} (mm)	V_{arc} (calc.) (V)	Net Power (W)	Max Temp. in Torch (K)	Max Temp. at exit (K)	Max Veloc. in torch (m/s)	Max Veloc. at exit (m/s)
B23									
1	0.0	0.0	12.24	20.1	1557	18690	11780	217	105
2	1.0	0.051	12.23	20.0	1545	18620	11760	215	103
3	3.0	0.160	12.16	19.4	1472	18120	11610	209	91.2
4	5.0	0.297	12.04	18.7	1338	17530	11340	201	67.9
5	7.0	0.463	11.87	17.9	1143	17000	10810	186	38.3

Table IV.A.IV. Operating conditions and results of the study concerning the effect of swirl number on the arc behavior in the plasma torch for case B23, (Current = 250 Amps, Gas flow = 0.59 scmh Argon).

Run No.	Current (Amps)	Gas Flow (scmh)	Experimental Voltage (V)	Experimental Net Power (W)	Calculated Voltage (V)	Calculated Net Power (W)
B23	250	0.59	19.16	1180	18.7	1338
B24	250	0.83	19.44	1380	19.6	1749
B27	500	0.59	19.72	2750	20.3	2439
B28	500	0.83	19.92	2970	21.6	3178
B31	750	0.59	20.22	4400	20.2	3517
B32	750	0.83	20.44	4740	21.6	4501

Table IV.A.V. Experimental and calculated current-voltage characteristics of the INEL plasma torch.

Run No.	V_{arc} (calc.) (V)	L_{arc} (mm)	Exit Swirl No.	Net Power (W)	Max. Temp. in torch (K)	Max. Temp. at exit (K)	Max. Velocity in torch (m/s)	Max. Velocity at exit (m/s)
$j_c = 2x10^7$								
B23A	17.3	11.9	0.310	1269	15660	11120	140	57.7
B24A	18.3	12.8	0.447	1684	15510	11170	139	57.6
B27A	18.0	8.2	0.185	2120	17860	12640	280	155
B28A	19.4	9.3	0.283	2864	17990	12890	312	170
B31A	17.9	6.4	0.151	2927	19400	13510	384	250
B32A	19.3	7.3	0.241	3917	20060	13820	458	284
$j_c = 3x10^7$								
B23	18.7	12.0	0.297	1338	17530	11340	201	67.9
B24	19.6	13.0	0.439	1749	17370	11370	202	66.1
B27	20.3	8.7	0.156	2439	21940	13300	404	234
B28	21.6	9.8	0.255	3178	22000	13480	439	249
B31	20.2	6.6	0.106	3517	23110	14210	533	384
B32	21.6	7.6	0.177	4501	23470	14420	596	420
$j_c = 4x10^7$								
B23B	19.9	12.2	0.287	1393	20220	11540	265	78.7
B24B	20.8	13.1	0.432	1803	20080	11570	273	75.8
B27B	21.7	8.9	0.139	2638	24120	13680	504	301
B28B	23.0	10.0	0.237	3374	24120	13830	536	317
B31B	22.1	7.0	0.090	4015	25420	14730	685	521
B32B	23.5	8.0	0.156	4995	25660	14900	733	554

Table IV.A.VI. Operating conditions used for studying the effect of cathode spot current density, j_c on transport phenomena in the plasma torch (all values calculated using a constant inlet swirl number of 5.0).

	u	v	rw	h	ϕ	m	K	ε
AB	w.f	w.f.	w.f.	$T = 3000$	$j_c = \frac{I}{\pi R_c^2}$	$\frac{\partial m}{\partial z} = 0$	$\frac{\partial K}{\partial z} = 0$	$\varepsilon = 0$
BC	w.f	w.f.	w.f.	$T = 3000$	$\frac{\partial \phi}{\partial z} = 0$	$\frac{\partial m}{\partial z} = 0$	$\frac{\partial K}{\partial z} = 0$	$\varepsilon = 0$
CD	w.f	w.f.	0	$T = 3000$	$\frac{\partial \phi}{\partial n} = 0$	$\frac{\partial m}{\partial n} = 0$	$\frac{\partial K}{\partial n} = 0$	$\varepsilon = 0$
DE	$u=u(r)$	0	$rw(r)$	$T = 1000$	$\frac{\partial \phi}{\partial z} = 0$	1	$K = .005u^2$	$\varepsilon = \frac{C_D K^{1.5}}{.03\, r_n}$
EF	w.f	w.f.	0	$T = 1000$	$\frac{\partial \phi}{\partial n} = 0$	$\frac{\partial m}{\partial n} = 0$	$\frac{\partial K}{\partial n} = 0$	$\varepsilon = 0$
FG	w.f	w.f.	w.f.	$T = 700$	-	$\frac{\partial m}{\partial z} = 0$	$\frac{\partial K}{\partial z} = 0$	$\varepsilon = 0$
GH	$\frac{\partial u}{\partial r} = 0$	$\frac{\partial \rho v}{\partial r} = 0$	0	$T = 300$	-	1 or 0	$K \approx 0$	$\varepsilon \approx 0$
HI	$\frac{\partial u}{\partial z} = 0$	0	0	$\frac{\partial h}{\partial z} = 0$	-	$\frac{\partial m}{\partial z} = 0$	$\frac{\partial K}{\partial z} = 0$	$\frac{\partial \varepsilon}{\partial z} = 0$
IA	$\frac{\partial u}{\partial r} = 0$	0	0	$\frac{\partial h}{\partial r} = 0$	$\frac{\partial \phi}{\partial r} = 0$	$\frac{\partial m}{\partial r} = 0$	$\frac{\partial K}{\partial r} = 0$	$\frac{\partial \varepsilon}{\partial r} = 0$

Table IV.C.I. Boundary Conditions used in the model (turbulent case) with reference to Figure IV.C.2.

I (A)	Q (l/min)	V (volts)	Power (kW)	Efficiency (%)	Case # *
450	23.6	24.0	10.842	48.2	12
450	35.4	25.5	11.478	50.9	10
450	47.2	27.3	12.265	55.4	11
600	23.6	25.5	15.220	46.4	9
600	35.4	26.8	16.014	53.0	7
600	47.2	28.1	16.813	56.4	8

*These cases are labelled to be consistent with those presented in section II.C.

Table IV.C.II. Averaged conditions for the Metco torch experiments of Capetti and Pfender[37].

Run No.	V_{arc} (calc.) (V)	Exit Re No.	Exit Swirl No.	Net Power (W)	Axis Temp. in torch (K)	Axis Temp. at exit (K)	Axis Velocity in torch (m/s)	Axis Velocity at exit (m/s)
12	22.2	416	0.236	4993	25600	14030	1159	563
10	23.8	621	0.315	6332	24970	14160	1661	545
11	25.1	849	0.381	7384	24750	14180	1297	492
9	23.0	439	0.197	6580	26580	14770	1300	748
7	24.8	632	0.257	8468	25910	14920	1853	744
8	26.3	830	0.305	9938	25410	14890	2406	625

Table IV.C.III Summary of calculated results for the Metco torch.

Case # *	I (A)	V (volts)	Net Power (kW)	Efficiency (%)	$U_{m\text{-}ex}$ (m/s)	$T_{m\text{-}ex}$ (K)
3	300	24.8	3.870	52.0	461	10481
4	400	25.4	4880	48.0	568	11192
5	500	25.4	6060	47.4	733	11757
6	600	25.0	7030	46.9	885	12335
7	700	25.0	7920	45.3	918	12051
8	800	25.6	~9216	~45	1021	12742
9	900	26.3	10470	44.2	1033	12660

All cases taken with a flow rate of 75 scfh of argon

Table IV.D.I. Averaged conditions for the Miller torch experiments at INEL.

Run No.	V_{arc} (calc.) (V)	Exit Re No.	Exit Swirl No.	Net Power (W)	Axis Temp. in torch (K)	Axis Temp. at exit (K)	Axis Velocity in torch (m/s)	Axis Velocity at exit (m/s)
12	22.2	416	0.236	4993	25600	14030	1159	563
10	23.8	621	0.315	6332	24970	14160	1661	545
11	25.1	849	0.381	7384	24750	14180	1297	492
9	23.0	439	0.197	6580	26580	14770	1300	748
7	24.8	632	0.257	8468	25910	14920	1853	744
8	26.3	830	0.305	9938	25410	14890	2406	625

Table IV.D.II Summary of calculated results for the Metco torch.

Dimensionless Number	Definition	Description	Region of Application	Range of Values
Re_D	$\frac{\rho U D}{\mu}$	$\frac{\text{Momentum forces}}{\text{Viscous forces}}$	Nozzle	100 - 5000
Re_z	$\frac{\rho U z}{\mu}$	$\frac{\text{Momentum forces}}{\text{Viscous forces}}$	Plume	$0 - 10^5$
Ma	$\frac{U}{U_s}$	$\frac{\text{Velocity}}{\text{Sonic Velocity}}$	All	0.03 - 1.0 (or higher)
Re_M	$\frac{U D \sigma}{\mu_0}$	$\frac{\text{Magnetic convection}}{\text{Magnetic diffusion}}$	Arc	$10^{-4} - 10^{-1}$
EM	$\frac{\mu_0 I^2}{\rho U^2 D^2}$	$\frac{\text{Electromagnetic force}}{\text{Axial momentum force}}$	Arc	$10^{-1} - 40$
HJ	$\frac{\sigma h \dot{m} D}{I^2}$	$\frac{\text{Convection}}{\text{Joule heating}}$	Nozzle	0.5 - 5.0
CJ	$\frac{\sigma k T D^2}{I^2}$	$\frac{\text{Conduction}}{\text{Joule Heating}}$	Nozzle	0.001 - 0.3
ES	$\frac{EM}{Sw}$	$\frac{\text{Electromagnetic force}}{\text{Swirl momentum force}}$	Arc	$10^{-2} - \infty$

Table IV.E.I Dimensionless numbers of interest in plasma torch systems

Label	Joule heat (W)	T_{avg} (K)	Re_D	Ma	EM	HJ	CJ	ES
BES23	3100	11860	114	0.030	4.47	3.24	0.221	0.893
BES24	3170	11008	140	0.041	2.42	2.68	0.108	0.484
BES25	3010	11771	112	0.030	4.50	3.08	0.207	0.900
BES26	3090	10915	139	0.041	2.44	2.54	0.101	0.488
BES27	6480	13772	219	0.032	15.38	2.41	0.130	3.076
BES28	6580	12899	216	0.044	8.26	2.12	0.089	1.653
BES29	5930	13516	195	0.032	15.67	2.12	0.117	3.135
BES30	6270	12758	206	0.044	8.36	1.96	0.084	1.671
BES31	10100	15278	454	0.034	31.20	1.98	0.083	6.239
BES32	10260	14123	365	0.046	16.98	1.78	0.065	3.396
BES33	10610	15499	501	0.034	30.75	2.12	0.085	6.150
BES34	10150	14092	360	0.046	17.02	1.75	0.065	3.404

Table IV.E.II Characteristic dimensionless numbers for the experiments at INEL

Label	Joule heat (W)	T_{avg} (K)	Re_D	Ma	EM	HJ	CJ	ES
CAP12	7800	11744	474	0.207	0.806	1.503	0.024	0.201
CAP10	8436	10846	629	0.298	0.389	1.285	0.011	0.097
CAP11	9223	10167	821	0.384	0.233	1.122	0.006	0.058
CAP9	11164	12642	599	0.215	1.330	1.458	0.021	0.333
CAP7	11985	11820	719	0.311	0.634	1.323	0.014	0.159
CAP8	12757	11204	870	0.403	0.376	1.209	0.009	0.094
BRO12	7689	11702	471	0.206	0.808	1.466	0.023	0.202
BRO10	8144	10715	627	0.296	0.393	1.189	0.010	0.098
BRO11	9196	10158	820	0.384	0.233	1.116	0.006	0.058
BRO9	10547	12491	570	0.213	1.346	1.337	0.020	0.337
BRO7	11294	11646	699	0.308	0.644	1.194	0.012	0.161
BRO8	12105	11078	853	0.401	0.381	1.111	0.008	0.095

Table IV.E.III Characteristic dimensionless numbers for the experiments on the Metco torch at the University of Minnesota.

Label	Joule heat (W)	T_{avg} (K)	Re_D	Ma	EM	HJ	CJ	ES
MIL3	5412	9510	562	0.247	0.243	1.144	0.001	0.199
MIL4	7456	10717	565	0.236	0.383	1.399	0.013	0.314
MIL5	9320	11364	602	0.270	0.564	1.343	0.014	0.462
MIL6	10944	11813	648	0.276	0.781	1.225	0.014	0.640
MIL7	12768	12198	706	0.280	1.030	1.142	0.013	0.844
MIL8	15072	12601	797	0.285	1.302	1.115	0.012	1.067
MIL9	17586	13038	926	0.290	1.593	1.116	0.011	1.306

Table IV.E.IV Characteristic dimensionless numbers for the experiments on the Miller torch at INEL

Current (A)	Voltage (V)	T_{avg} (K)	Re_D	Ma	EM	HJ	CJ	ES
100 scfh Ar - 47 scfh He								
500	36.0	11236	742	0.532	0.217	2.127	0.017	0.181
600	35.2	11736	795	0.559	0.291	1.942	0.016	0.242
700	31.8	11830	805	0.565	0.390	1.496	0.013	0.325
800	31.4	12175	862	0.588	0.482	1.382	0.012	0.402
900	31.6	12520	944	0.616	0.575	1.319	0.010	0.479
1000	31.5	12840	1038	0.644	0.670	1.248	0.009	0.559
1100	31.7	13147	1148	0.673	0.767	1.201	0.009	0.639
125 scfh Ar - 47 scfh He								
500	36.6	10649	899	0.596	0.159	1.830	0.010	0.133
600	36.6	11289	943	0.631	0.210	1.823	0.012	0.175
700	33.6	11437	962	0.640	0.280	1.458	0.009	0.233
800	34.0	11925	1033	0.675	0.340	1.447	0.010	0.283
900	34.5	12283	1123	0.705	0.406	1.406	0.009	0.338
1000	34.0	12521	1199	0.727	0.481	1.297	0.008	0.401
1100	36.6	13088	1433	0.790	0.524	1.421	0.008	0.437
85 scfh Ar - 47 scfh He								
500	35.0	11550	652	0.488	0.274	2.227	0.021	0.229
600	31.5	11720	668	0.497	0.385	1.690	0.016	0.321
700	31.8	12230	735	0.527	0.484	1 627	0.016	0.403
800	32.2	12668	826	0.559	0.586	1.563	0.014	0.488
900	33.0	13134	956	0.597	0.681	1.544	0.013	0.567
1000	32.9	13426	1060	0.623	0.797	1.445	0.012	0.664
1100	31.8	13588	1129	0.639	0.935	1.288	0.010	0.779
100 scfh Ar - 60 scfh He								
500	37.8	11270	737	0.573	0.201	2.294	0.018	0.168
600	37.6	11874	799	0.610	0.265	2.184	0.018	0.221
700	33.7	11945	807	0.614	0.357	1.660	0.014	0.297
800	34.0	12347	885	0.645	0.437	1.585	0.013	0.364
900	34.8	12804	1004	0.687	0.510	1.568	0.012	0.425
1000	34.8	13132	1114	0.720	0.593	1.486	0.011	0.494
1100	34.1	13332	1193	0.741	0.692	1.356	0.010	0.577
500	32.5	11078	738	0.471	0.246	1.777	0.014	0.205
600	30.8	11404	773	0.486	0.339	1.504	0.012	0.283
700	30.8	11895	831	0.513	0.429	1.444	0.013	0.357
800	31.3	12298	913	0.539	0.524	1.398	0.012	0.437
900	31.5	12646	1009	0.565	0.624	1.335	0.010	0.520
1000	30.7	12871	1083	0.584	0.739	1.208	0.009	0.616
1100	30.4	13109	1173	0.604	0.856	1.128	0.008	0.713

Table IV.E.V Characteristic dimensionless numbers for the experiments on the Miller torch at INEL (with mixtures of argon and helium as the working gas)

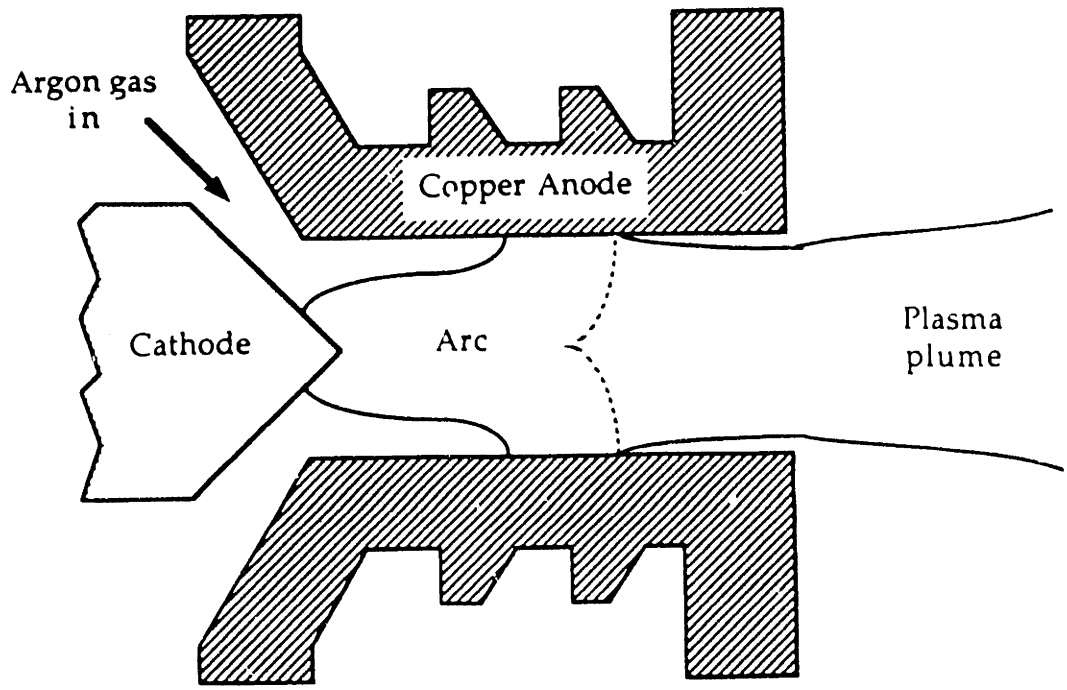

Figure IV.A.1. Schematic of an axi-symmetric arc in a non-transferred plasma torch.

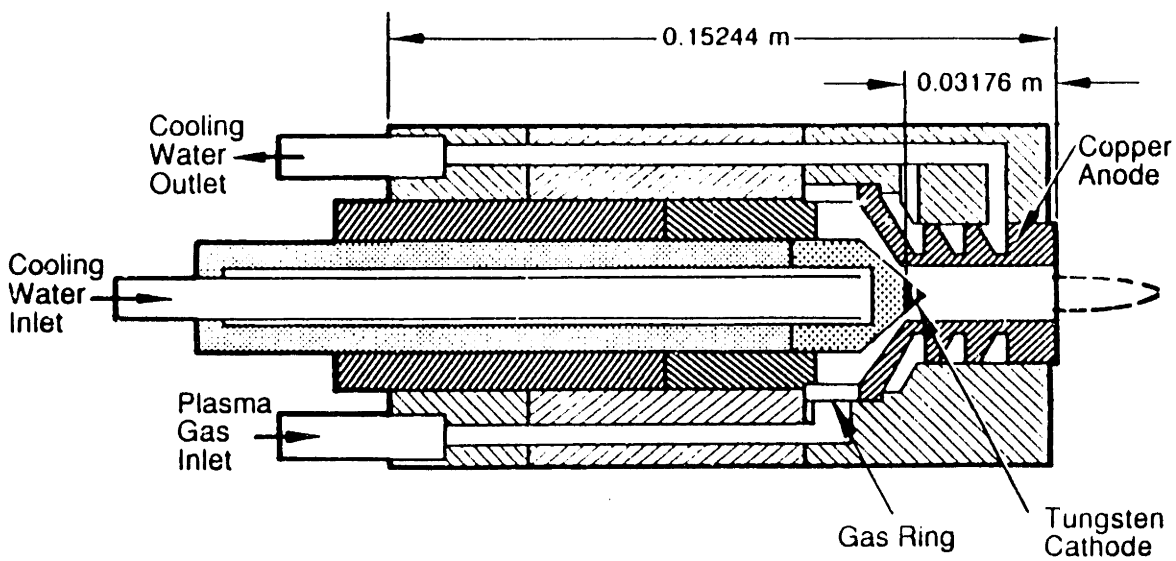

Figure IV.A.2. Schematic of the non-transferred arc plasma torch used at INEL.

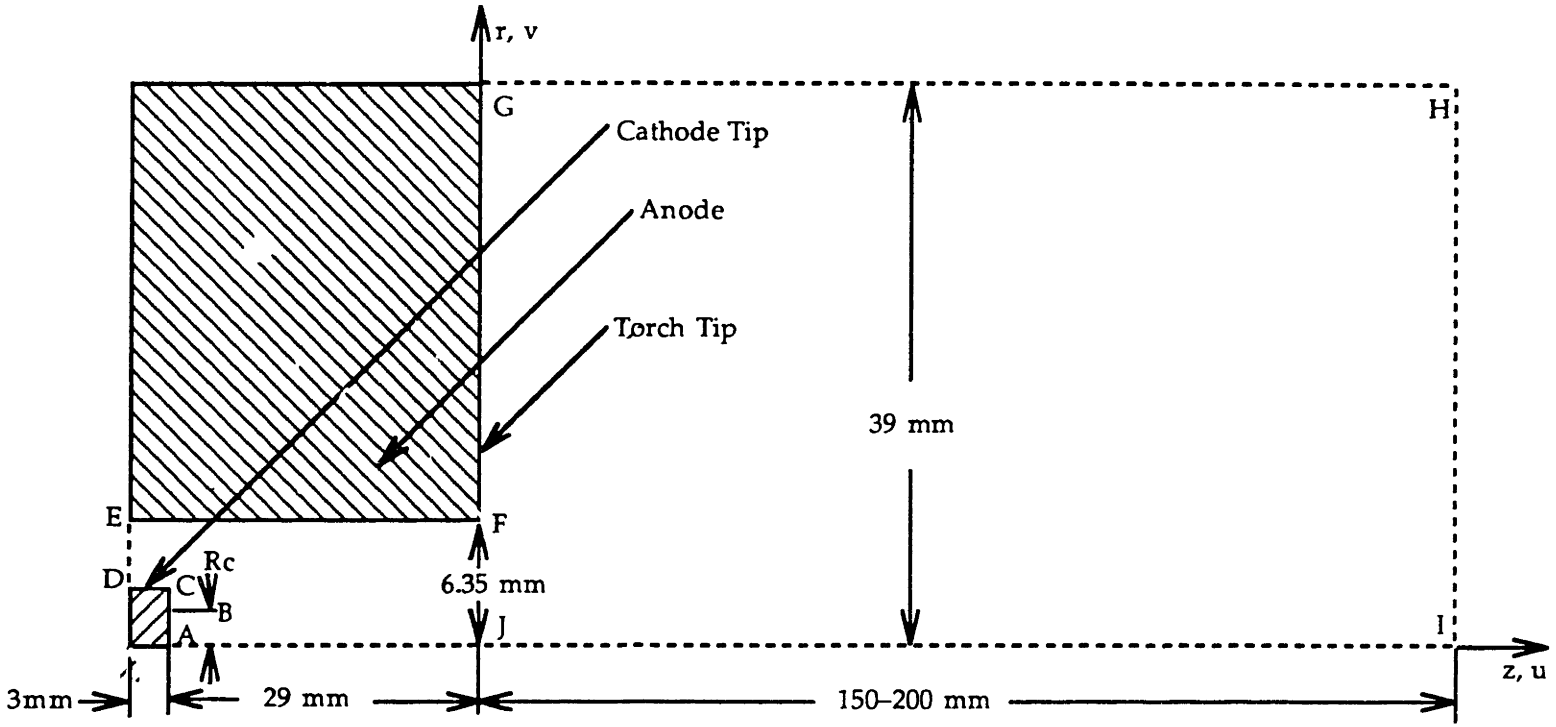

Figure IV.A.3. Computational domain used in this study.

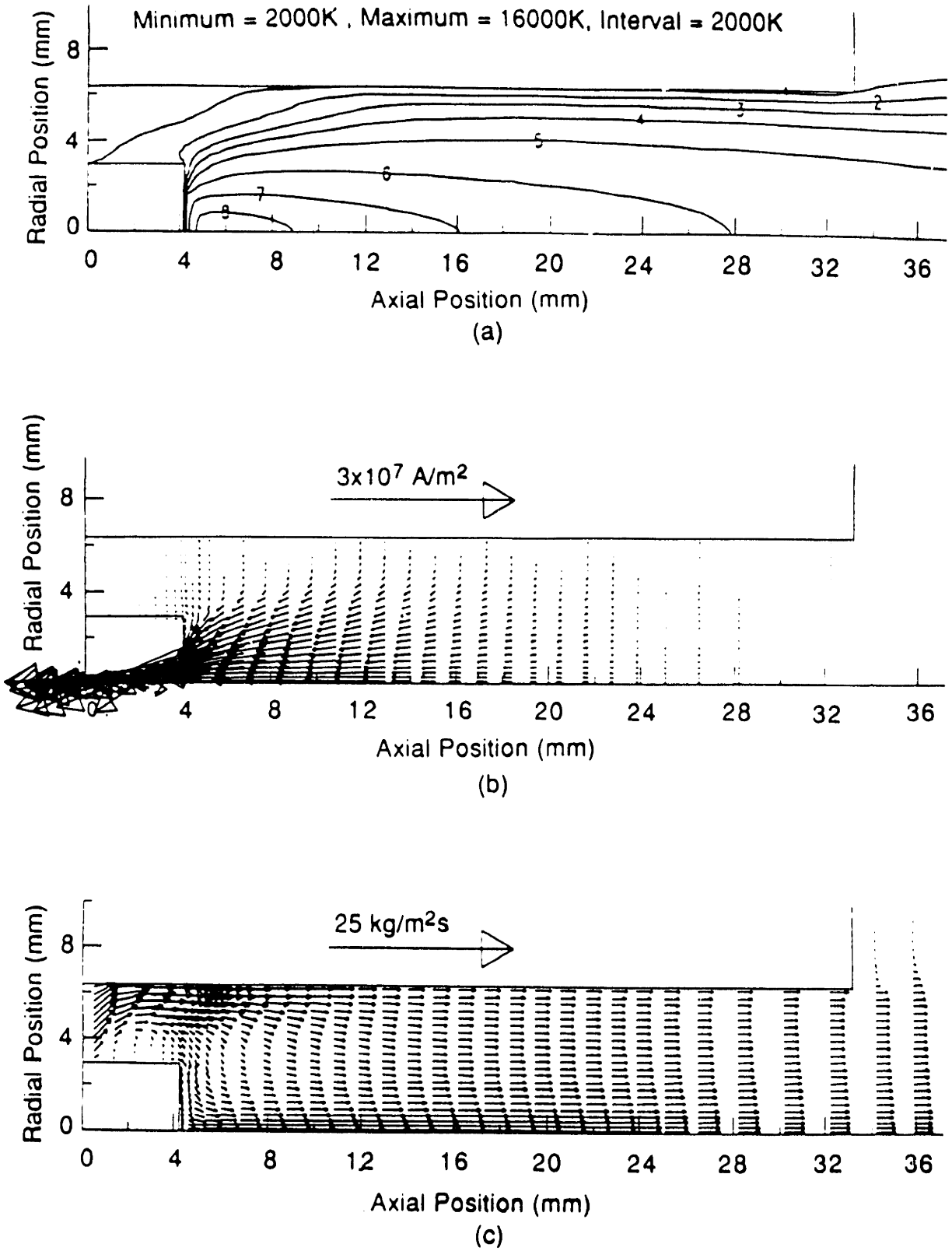

Figure IV.A.4. Isotherms (a) current density vectors (b) and mass flow (ρu product) vectors (c) in the non-transferred plasma torch, (case B23, 250 A, 0.59 scmh of argon, Sw=5.0). Minimum isotherm is 2000K, interval is 2000K, maximum is 16000K.

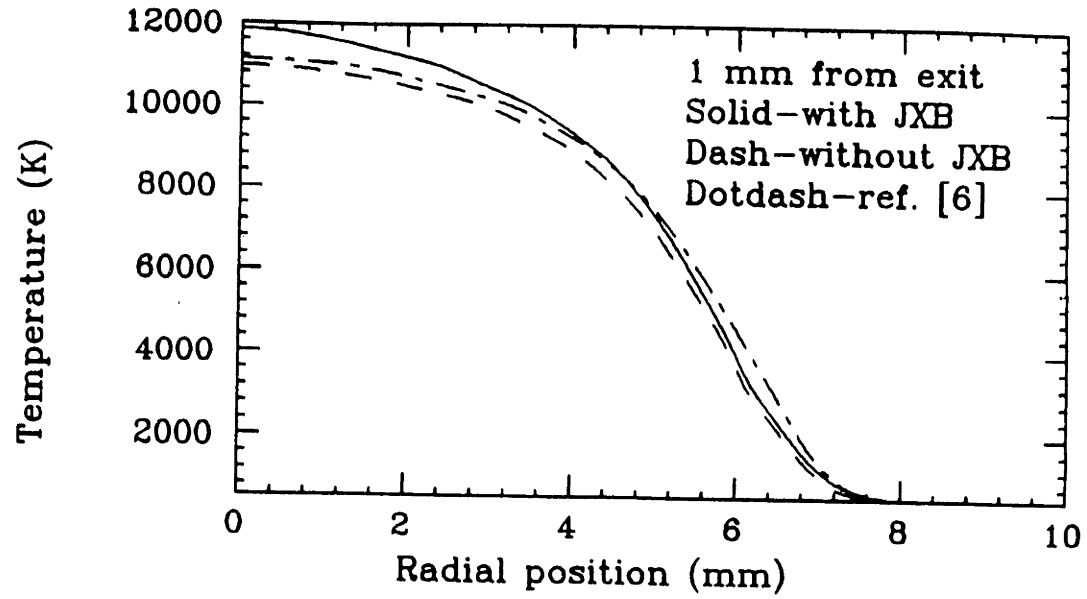

(a)

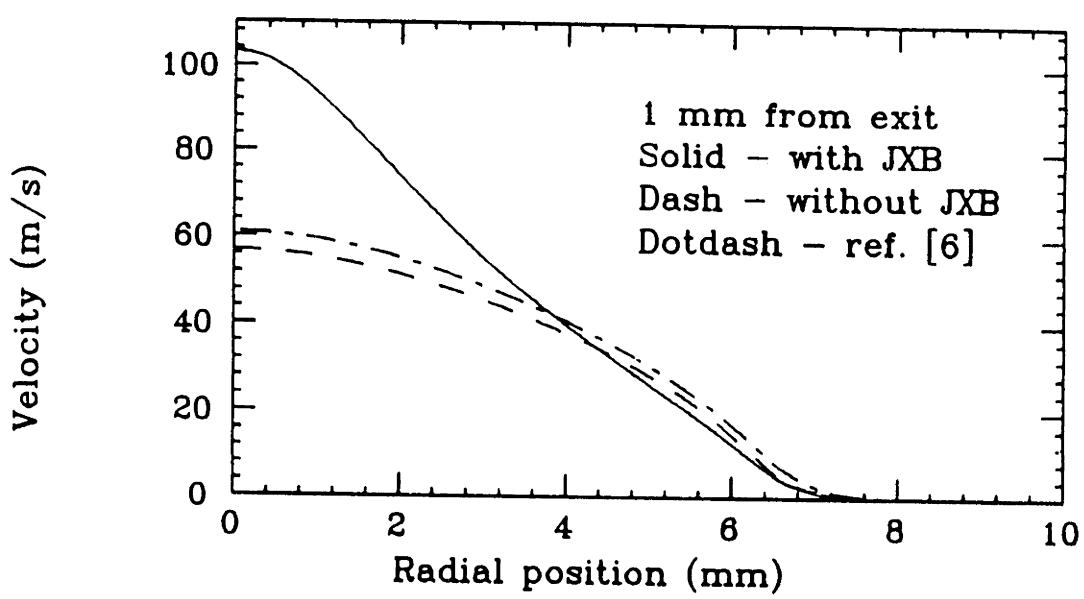

(b)

Figure IV.A.5. Effect of electromagnetic forces on the radial profiles of temperature (a) and velocity (b) at the torch exit, (case B23, 250 A, 0.59 scmh argon, Sw=0.0).

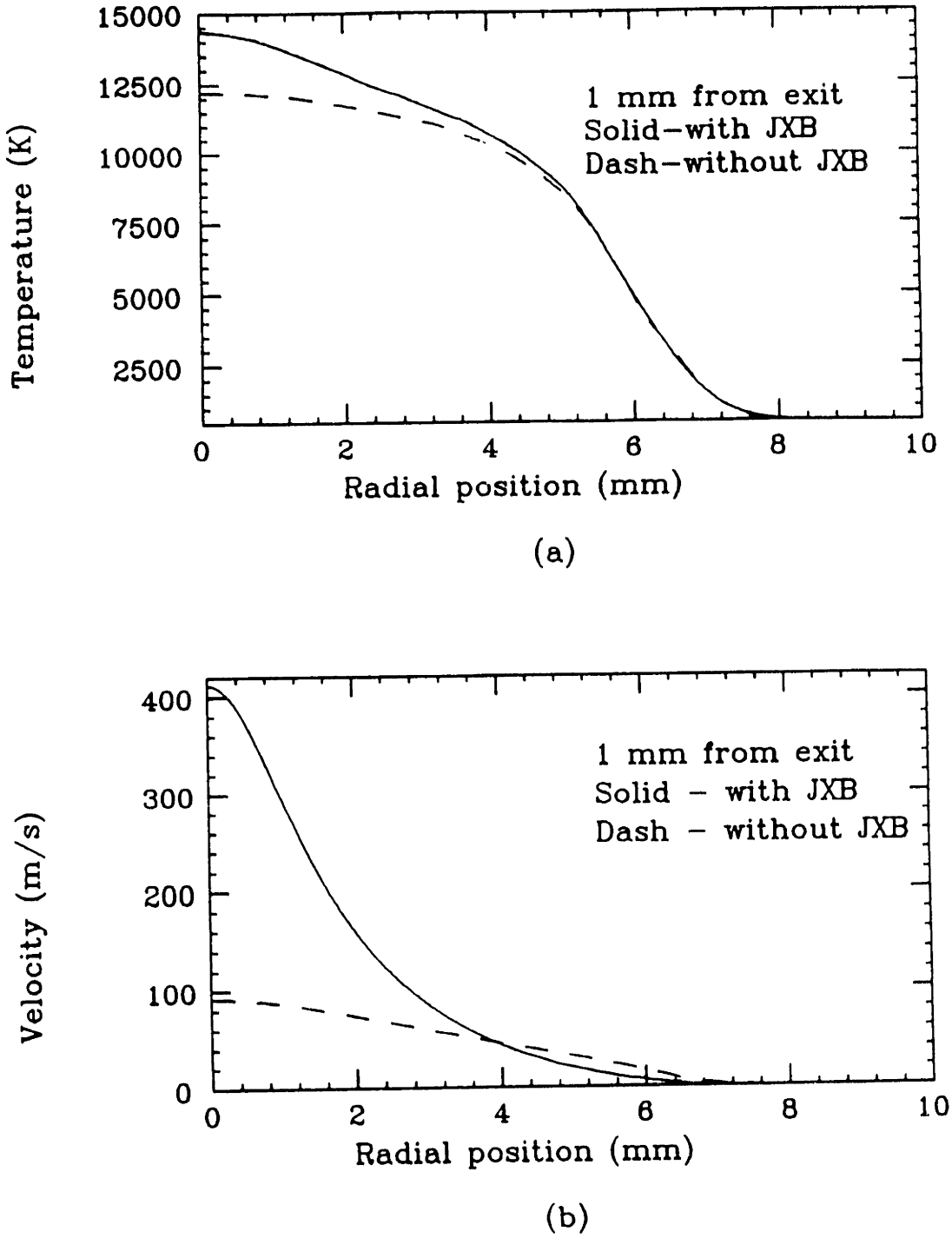

Figure IV.A.6. Effect of electromagnetic forces on the radial profiles of temperature (a) and velocity (b) at the torch exit, (case B31, 750 A, 0.59 scmh argon, Sw=0.0).

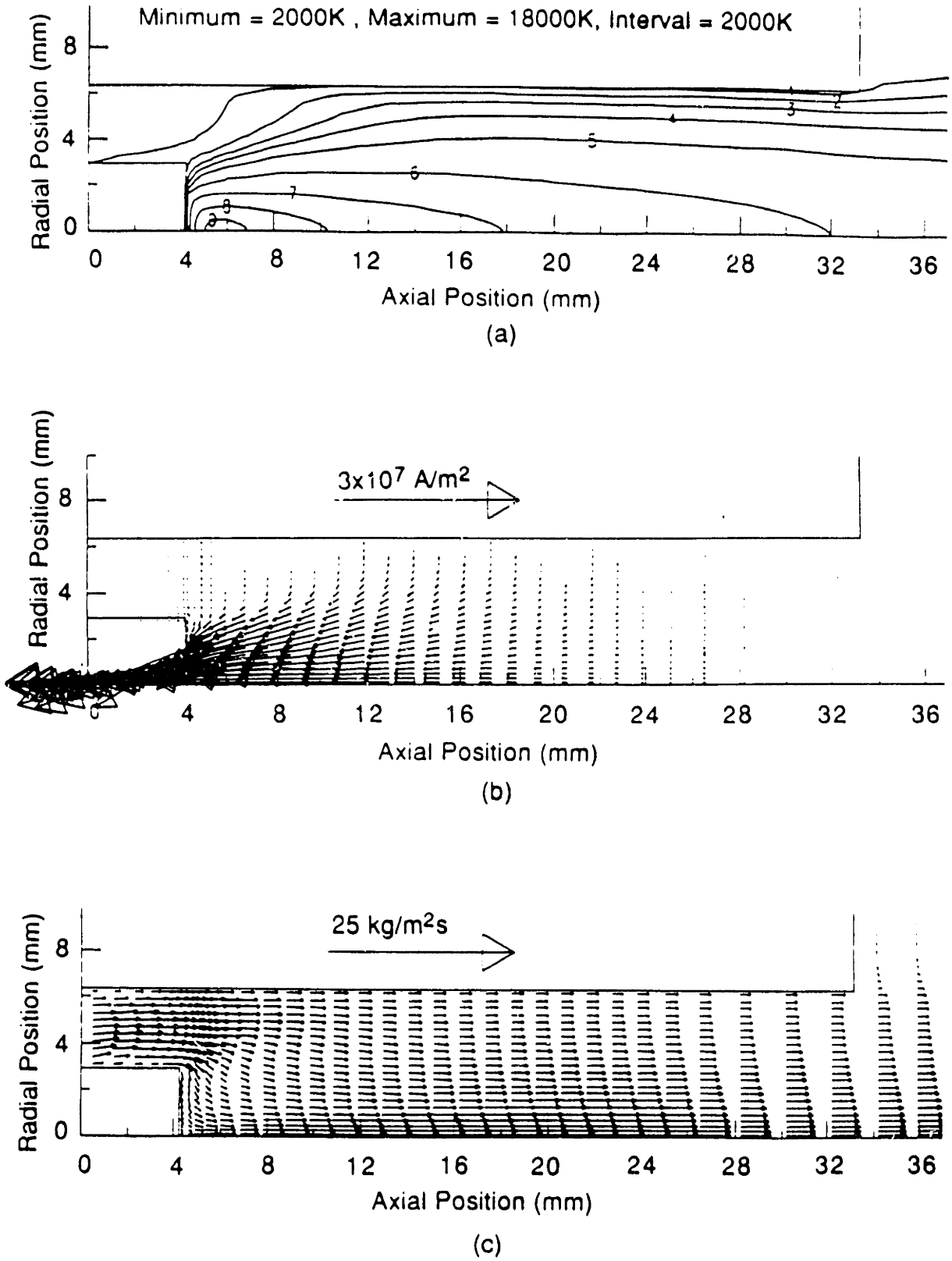

Figure IV.A.7. Isotherms (a) current density vectors (b) and mass flow (ρu product) vectors (c) in the non-transferred plasma torch, (case B23, 250 A, 0.59 scmh of argon, no swirl). Minimum isotherm is 2000K, interval is 2000K, maximum is 18000K.

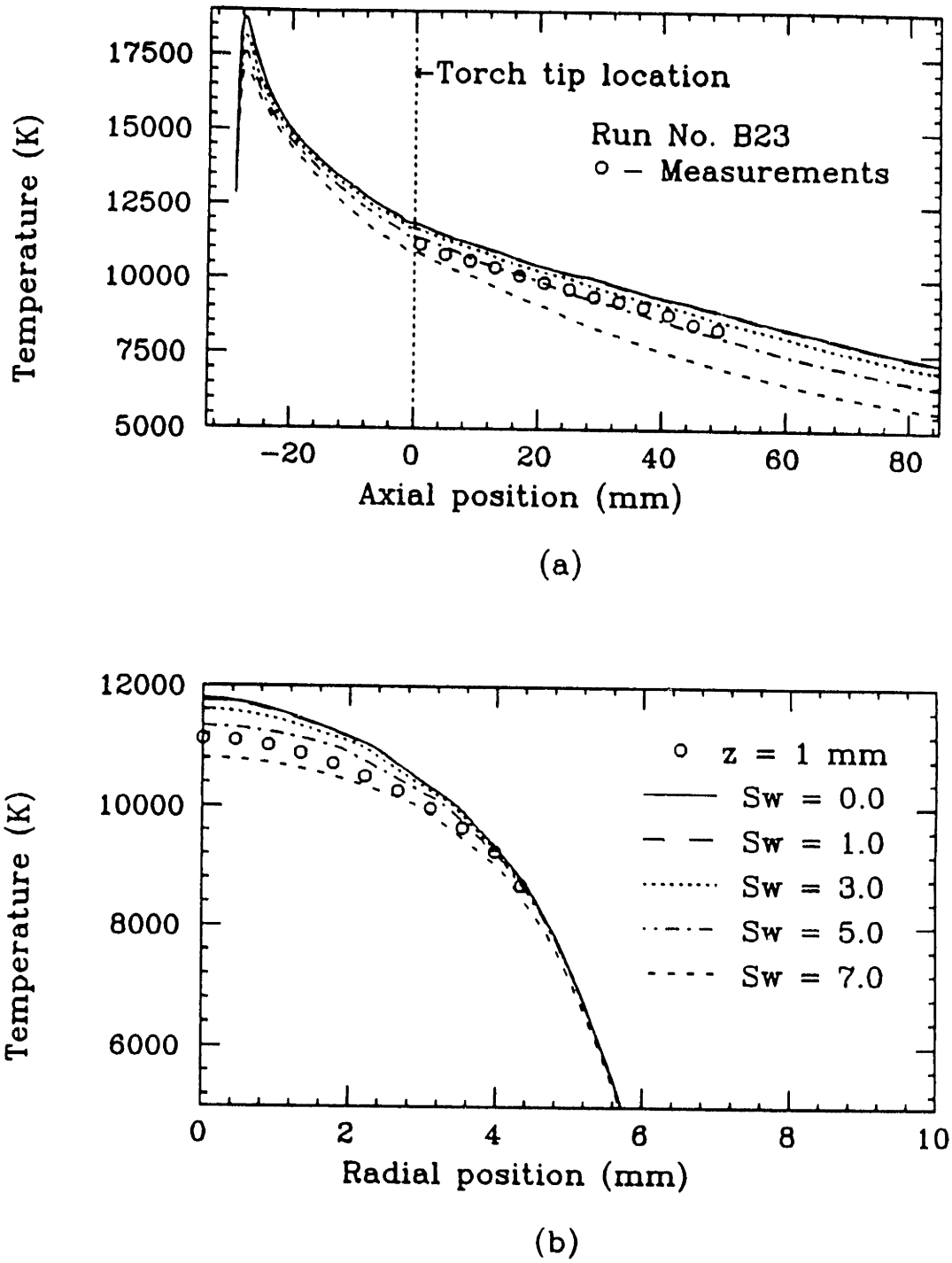

Figure IV.A.8. Effect of swirl on the axial profile (a) and on the radial profile at the torch exit (b). (case B23, 250 A, 0.59 scmh argon).

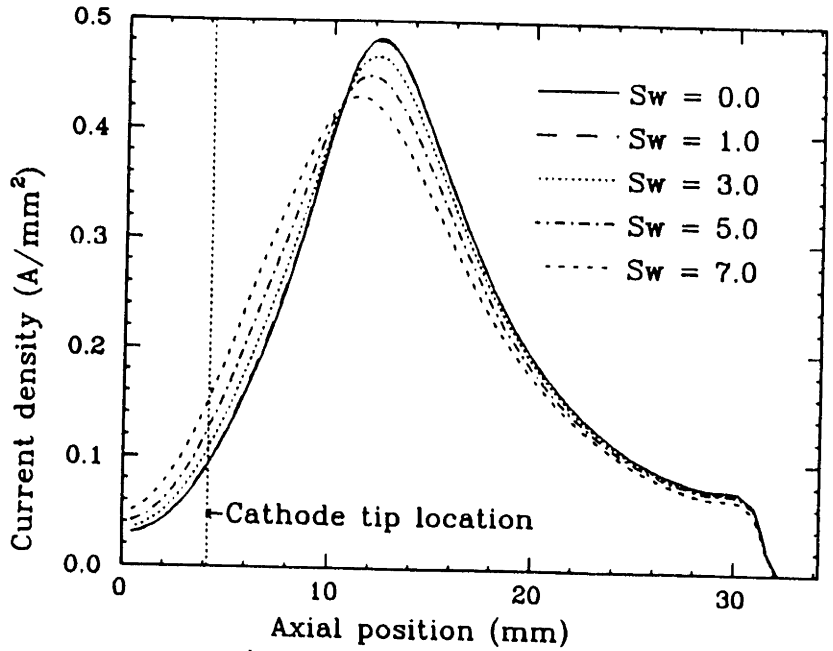

Figure IV.A.9. Effect of swirl on the radial current density at the anode. (case B23, 250 A, 0.59 scmh argon).

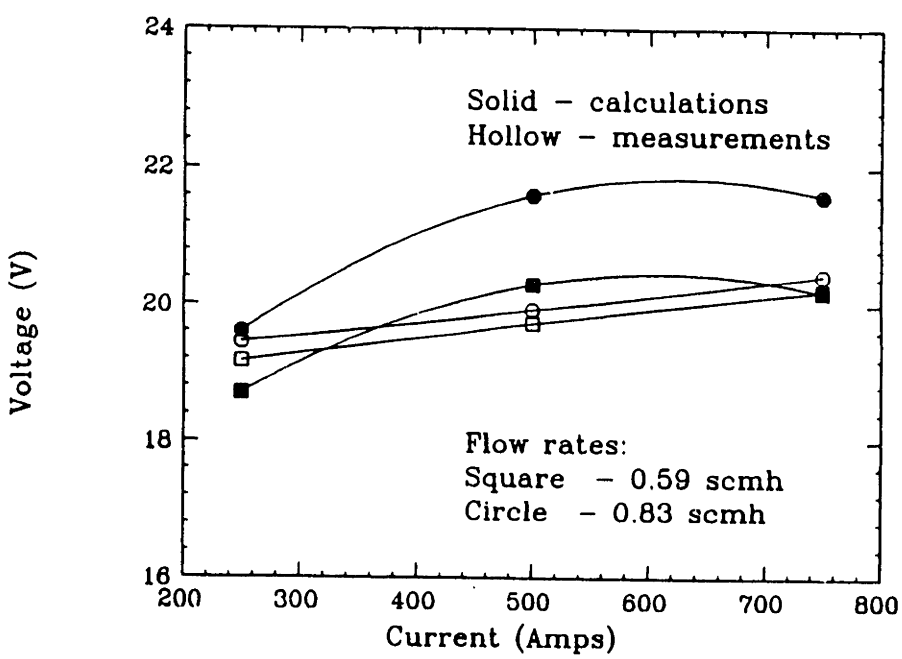

Figure IV.A.10. Calculated and experimental current-voltage characteristics of the plasma torch, calculated (solid symbols) and measured (open symbols).

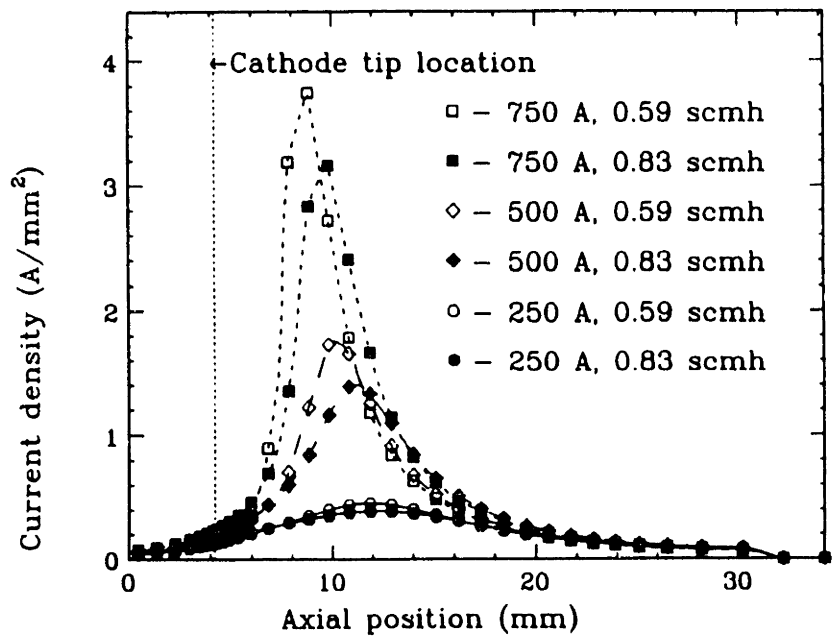

Figure IV.A.11. Effect of current and flow rate on the calculated radial current density at the anode - Runs B23,B24,B27,B28,B31,B32.

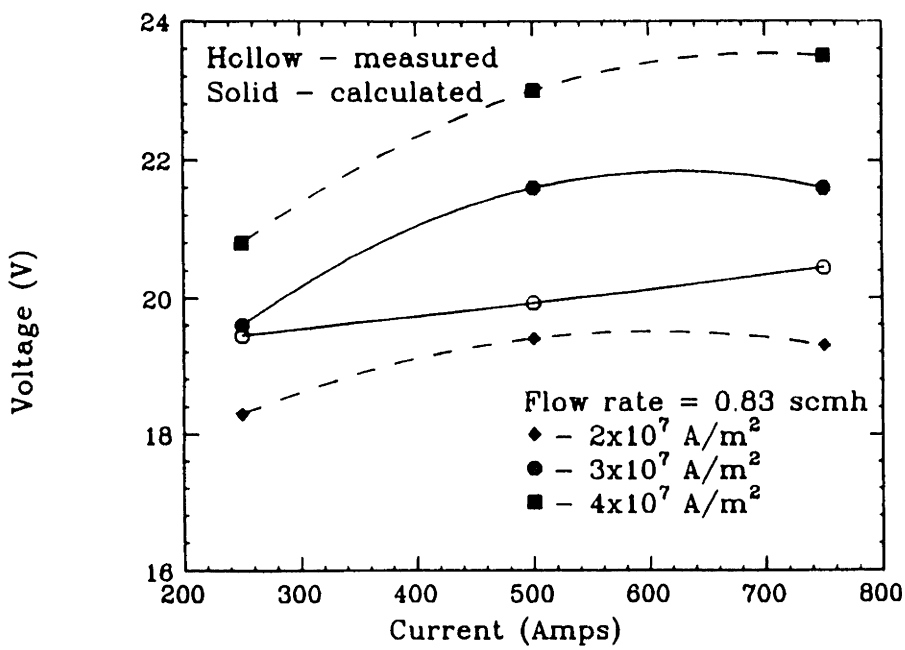

Figure IV.A.12. Dependence of the calculated current-voltage characteristics of the torch on the cathode spot current density.

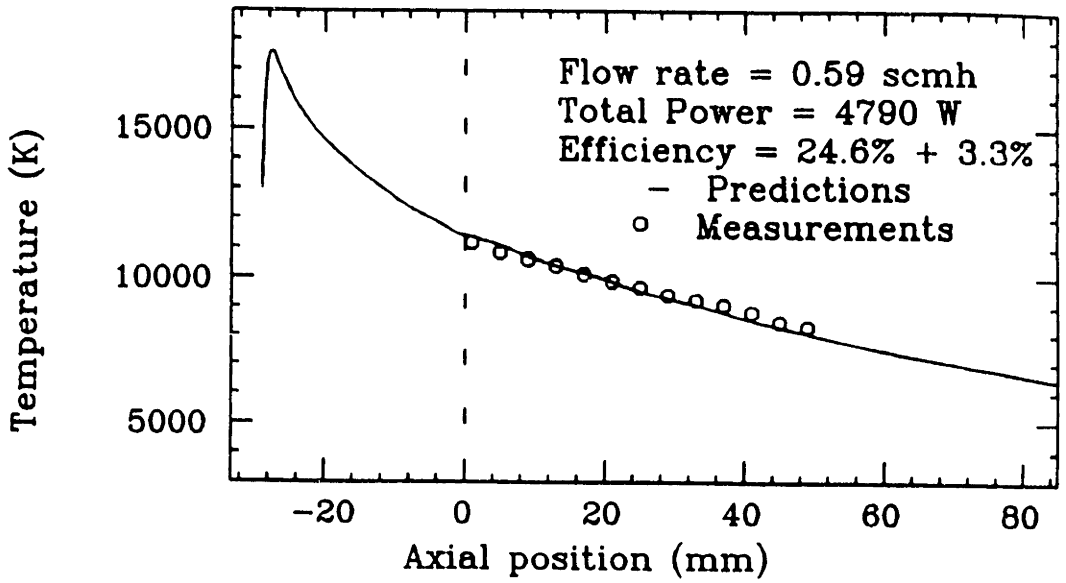

(a)

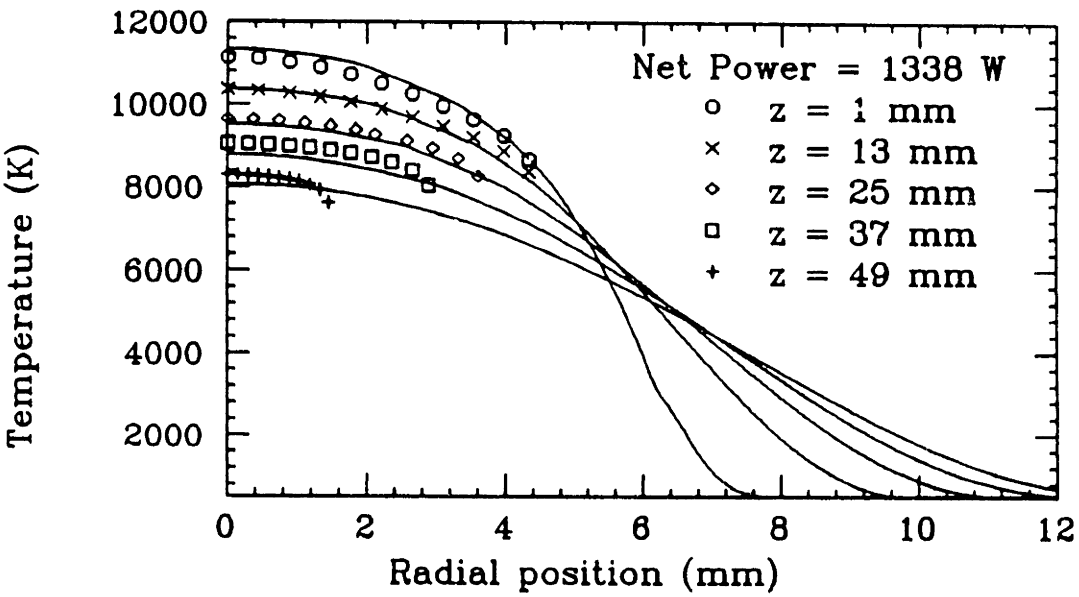

(b)

Figure IV.A.13. Axial (a) and radial (b) profiles of temperature for case B23: 250 A, 0.59 scmh. Discrete figures denote measurements, lines indicate calculations

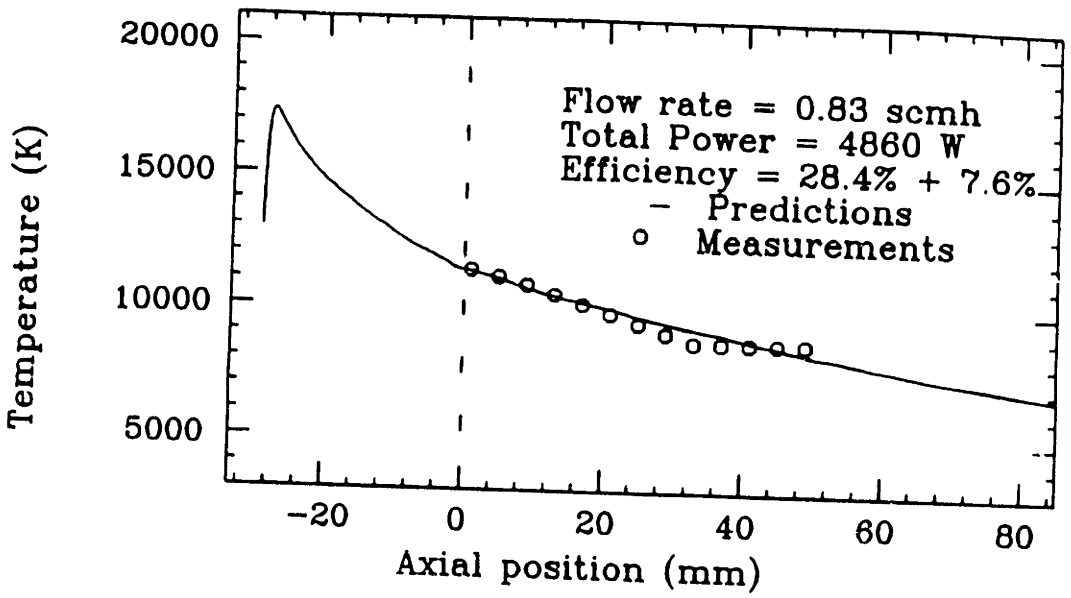

(a)

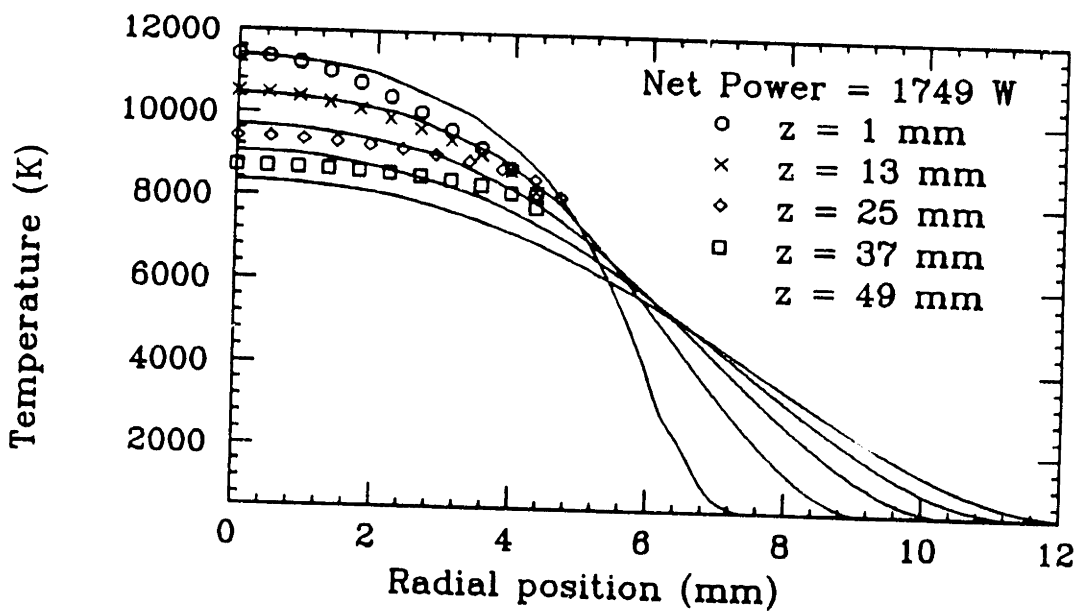

(b)

Figure IV.A.14. Axial (a) and radial (b) profiles of temperature for case B24: 250 A, 0.83 scmh. Discrete figures denote measurements, lines indicate calculations

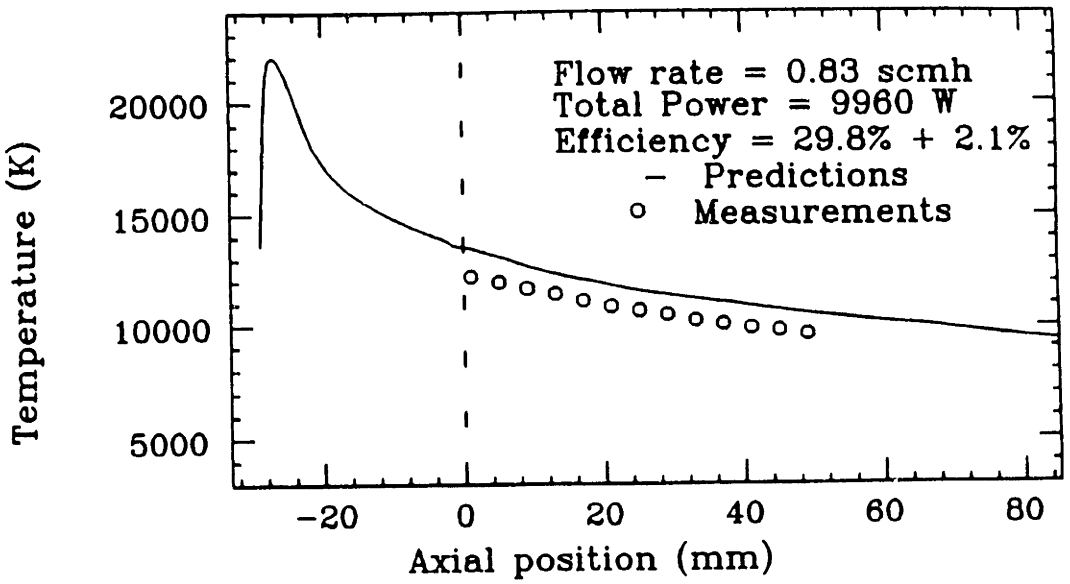

(a)

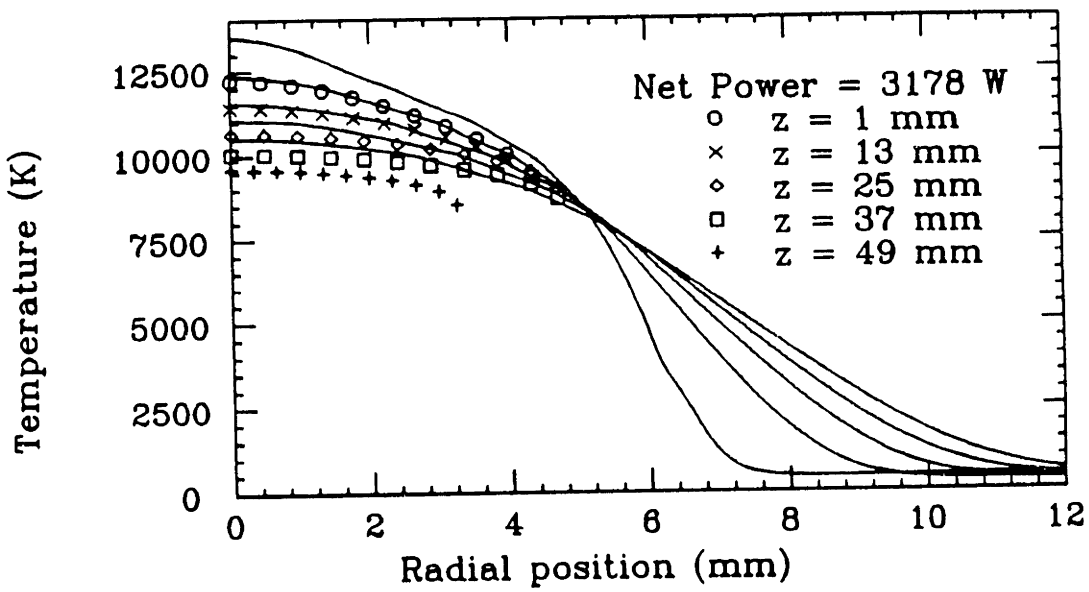

(b)

Figure IV.A.15. Axial (a) and radial (b) profiles of temperature for case B28: 500 A, 0.83 scmh. Discrete figures denote measurements, lines indicate calculations

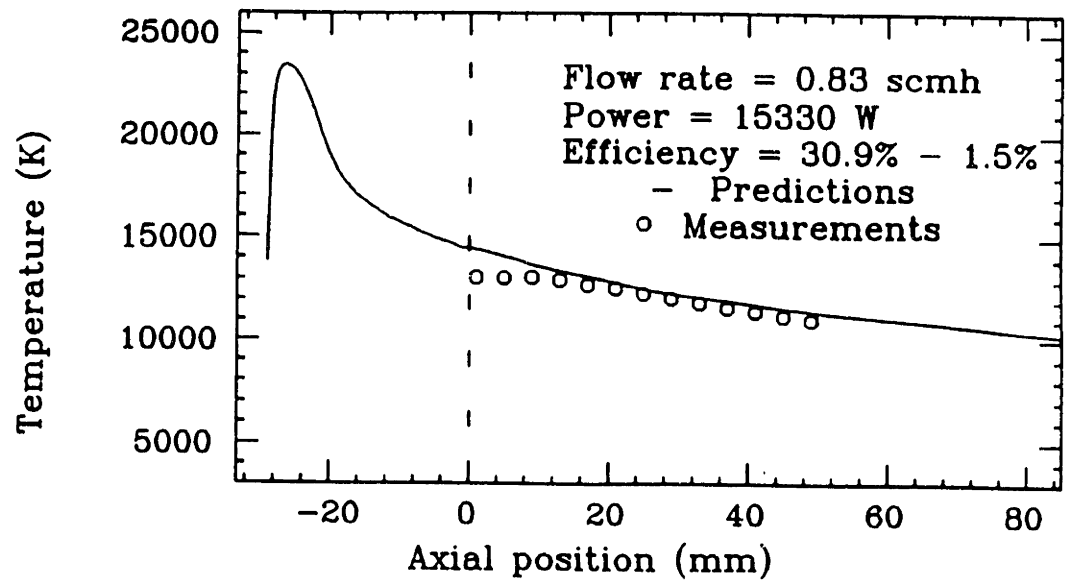

(a)

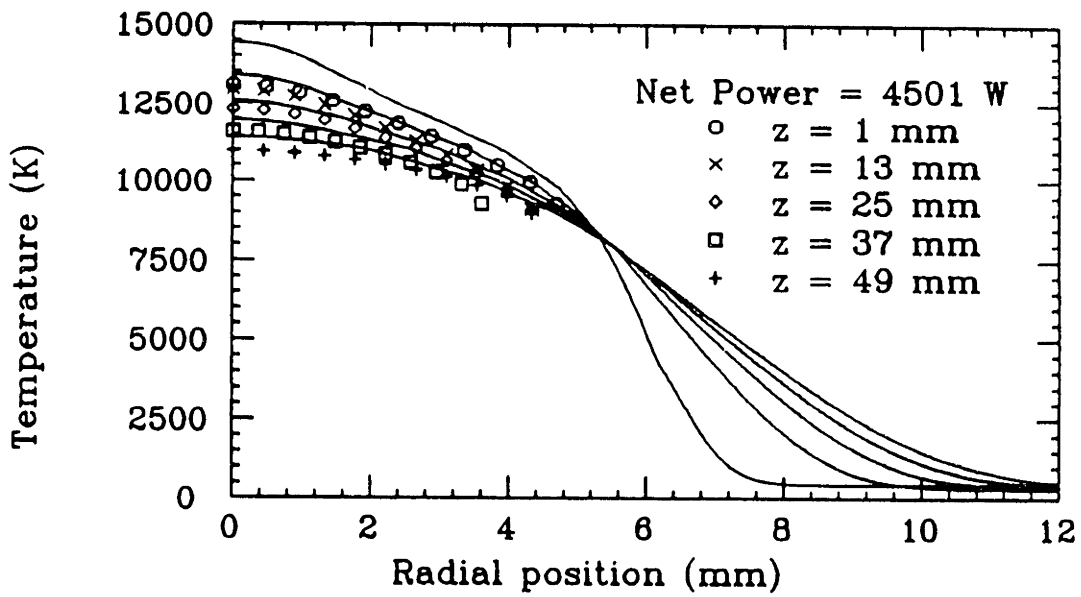

(b)

Figure IV.A.16. Axial (a) and radial (b) profiles of temperature for case B32: 750 A, 0.59 scmh. Discrete figures denote measurements, lines indicate calculations

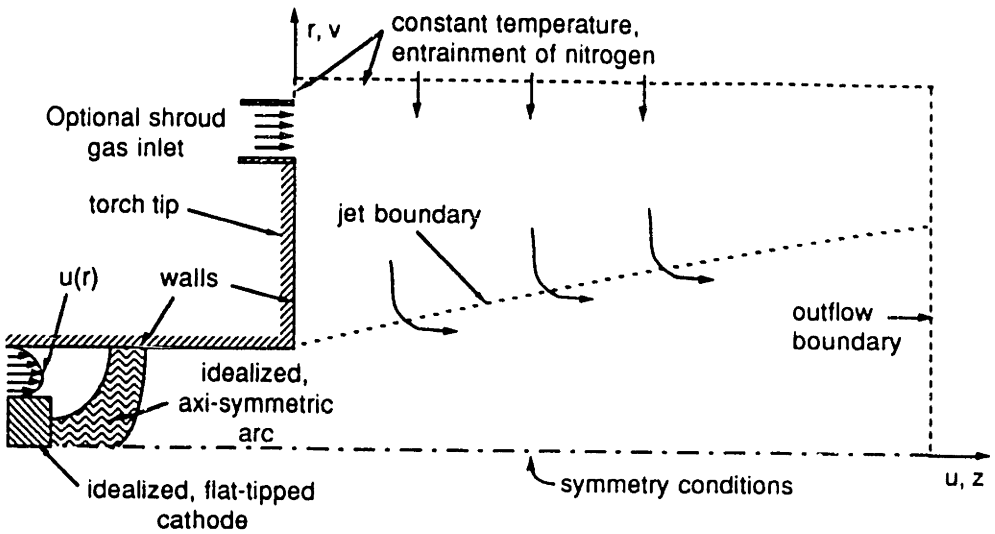

Figure IV.B.1. A schematic sketch of the plasma torch and plume

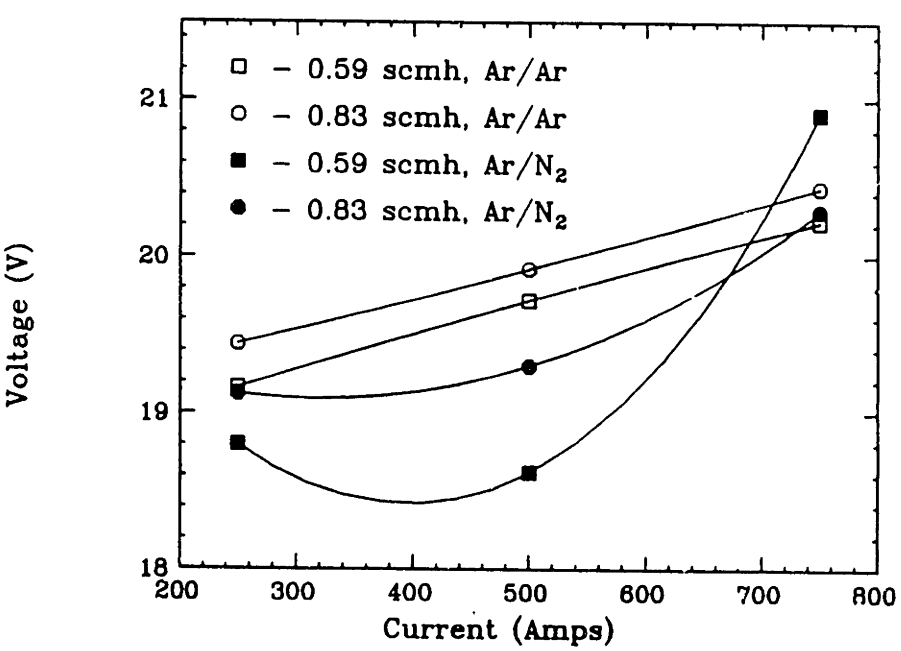

Figure IV.B.2. Current-voltage relationship for the torch used in the BES runs

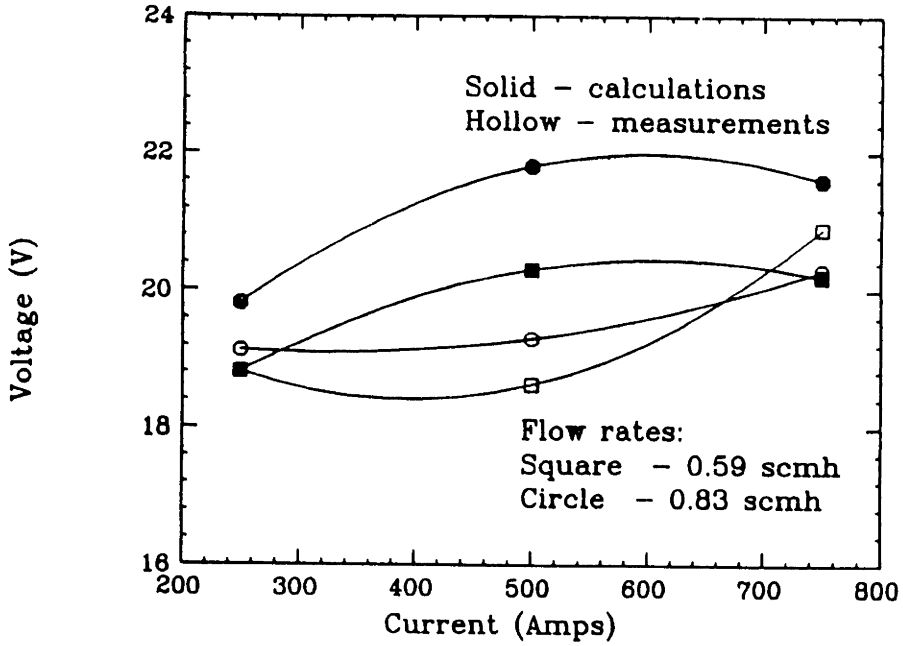

Figure IV.B.3. Calculated and experimental current-voltage relationships for the argon/nitrogen system

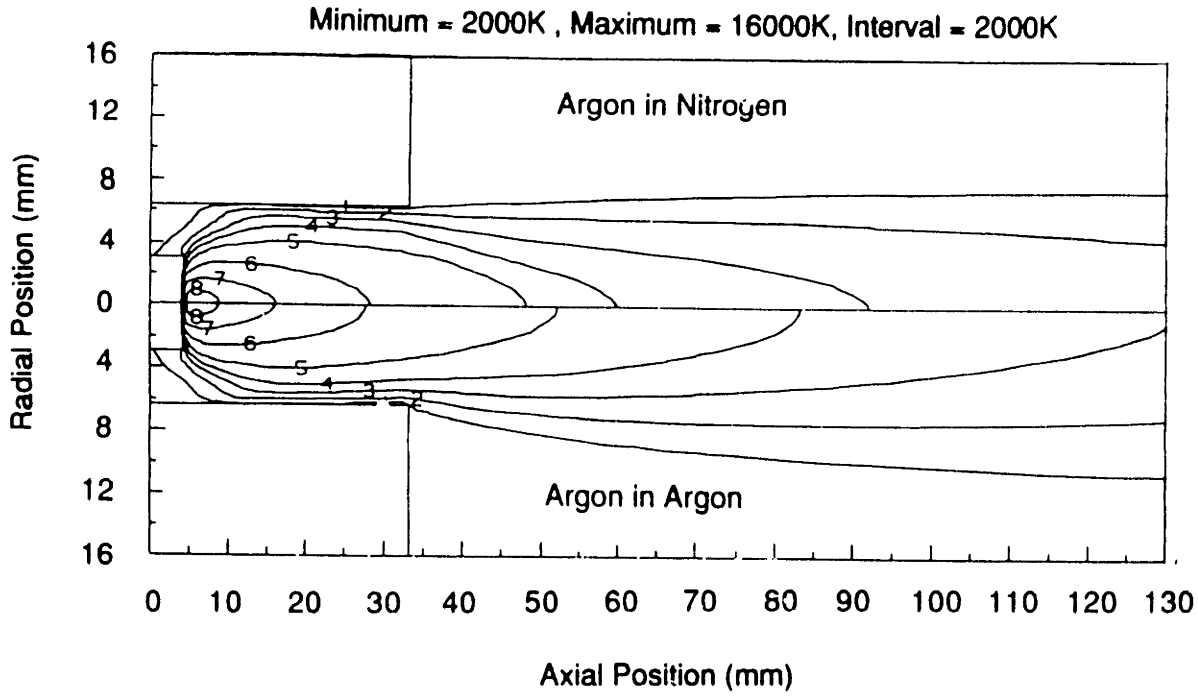

Figure IV.B.4. Calculated temperature contours in the plasma torch and plume for Ar/N_2 and Ar/Ar system (figure is expanded in the radial direction for clarity)

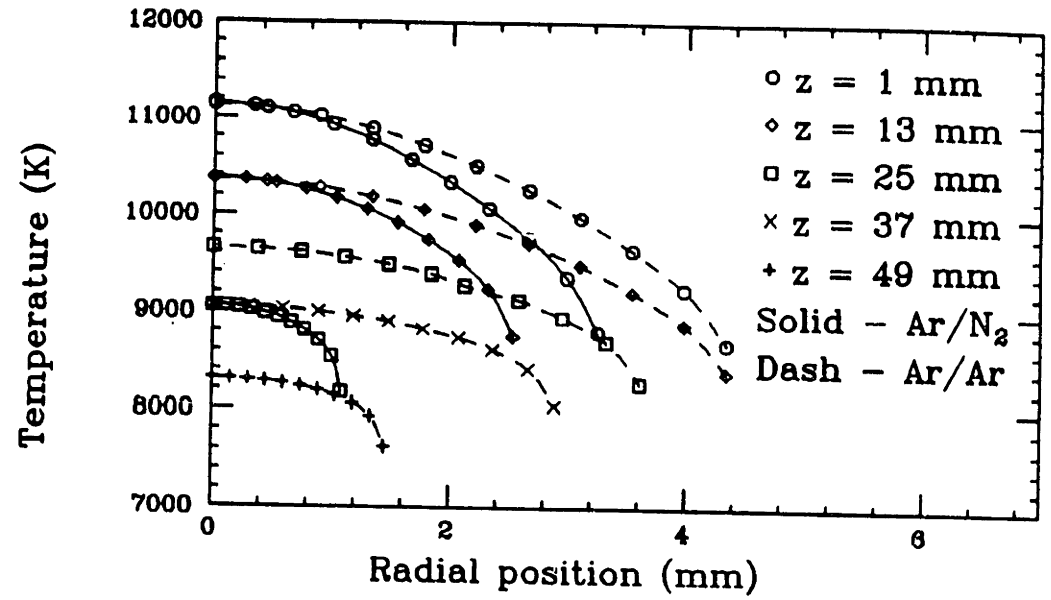

(a)

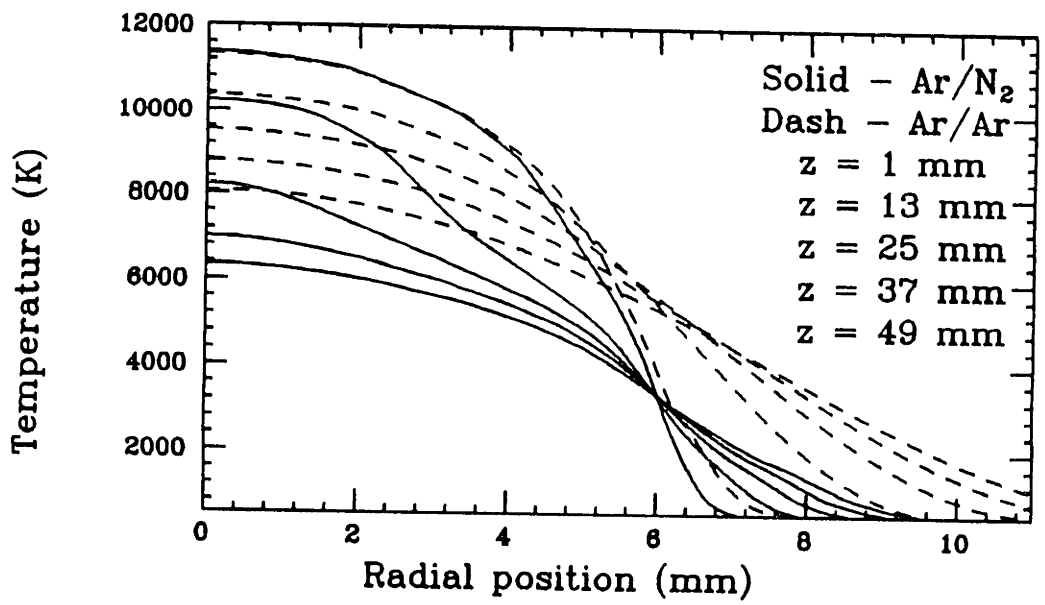

(b)

Figure IV.B.5. Experimentally measured (a) and theoretical radial temperature profiles at five axial positions in the plasma plume (solid - Ar/N_2, dash - Ar/Ar)

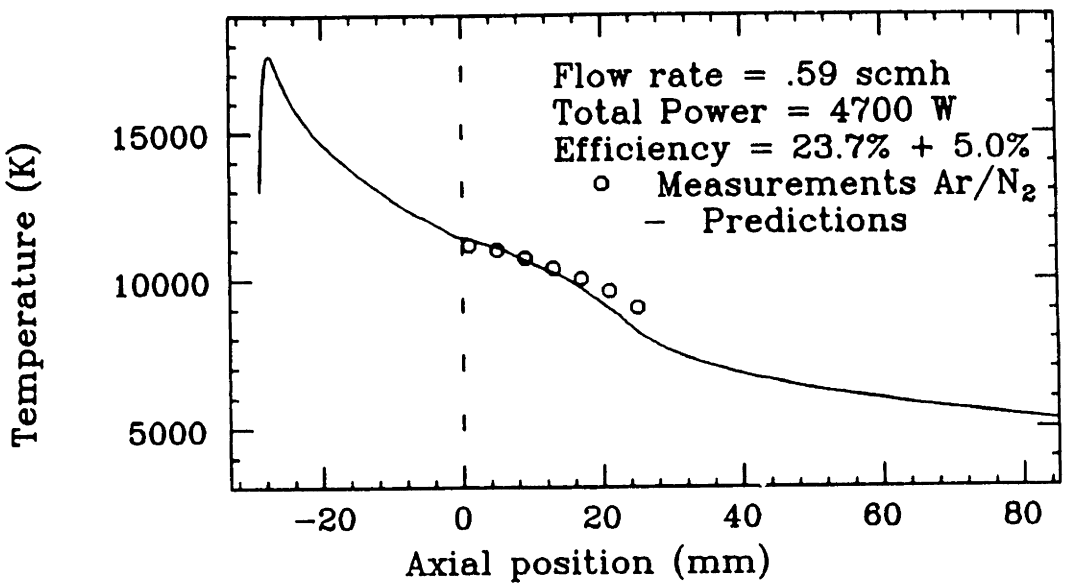

(a)

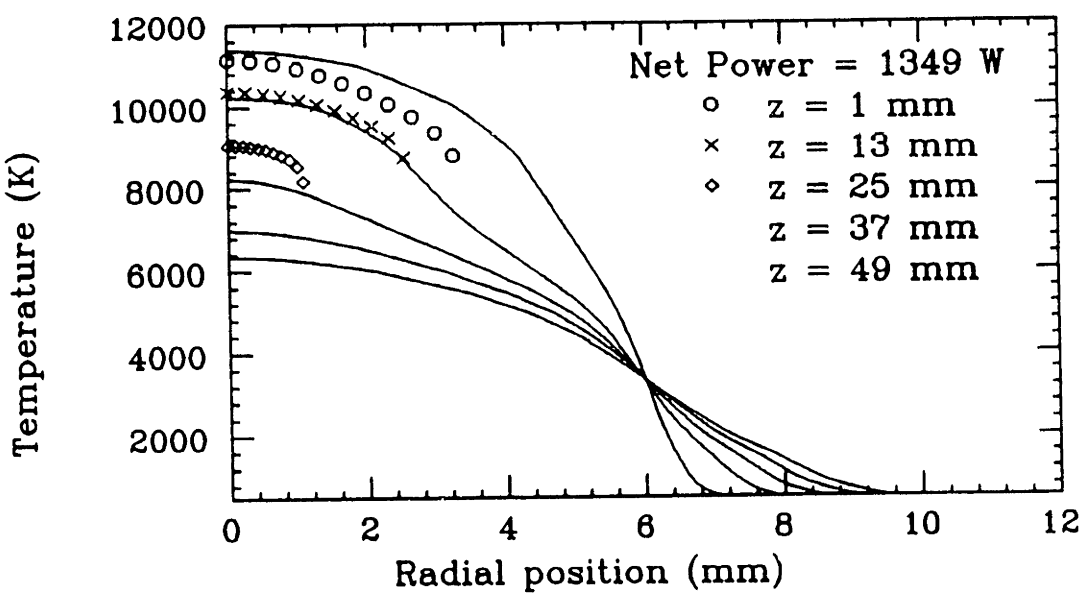

(b)

Figure IV.B.6. Comparison of the experimentally measured and theoretically predicted axial (a) and radial (b) profiles of temperature for run BES25

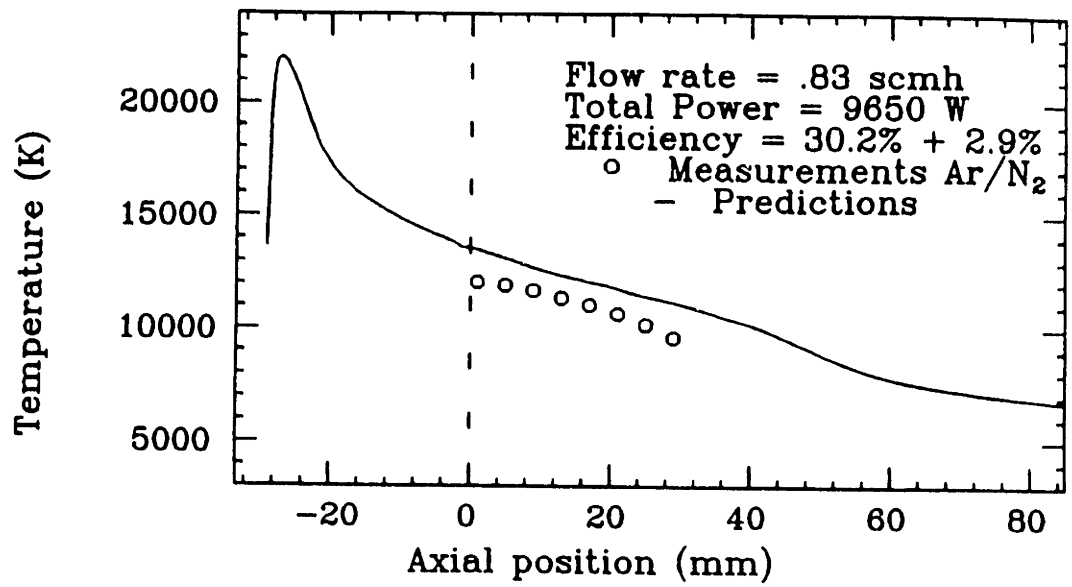

(a)

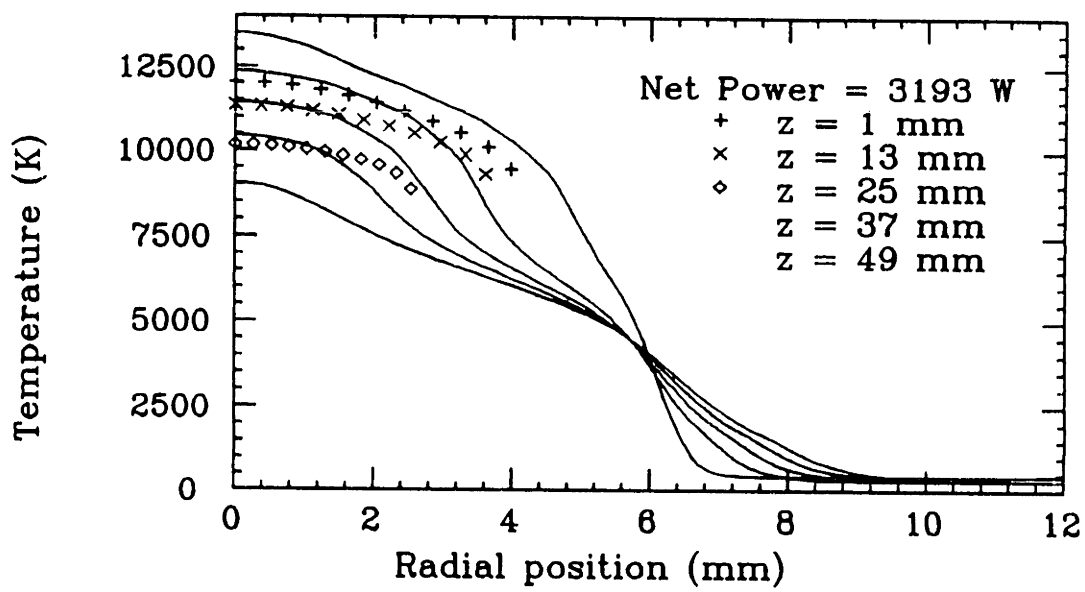

(b)

Figure IV.B.7. Comparison of the experimentally measured and theoretically predicted axial (a) and radial (b) profiles of temperature for run BES30

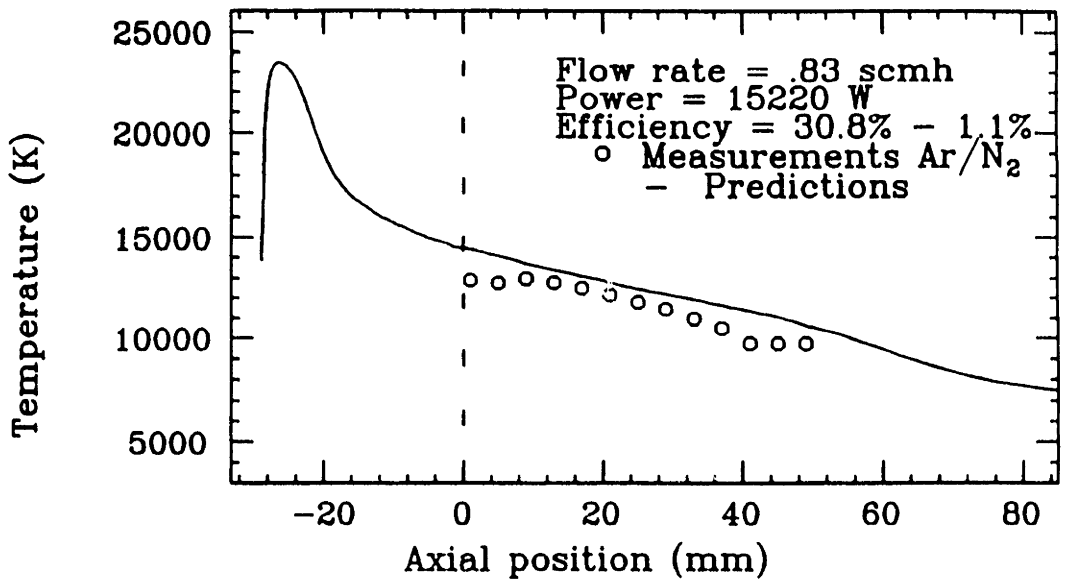

(a)

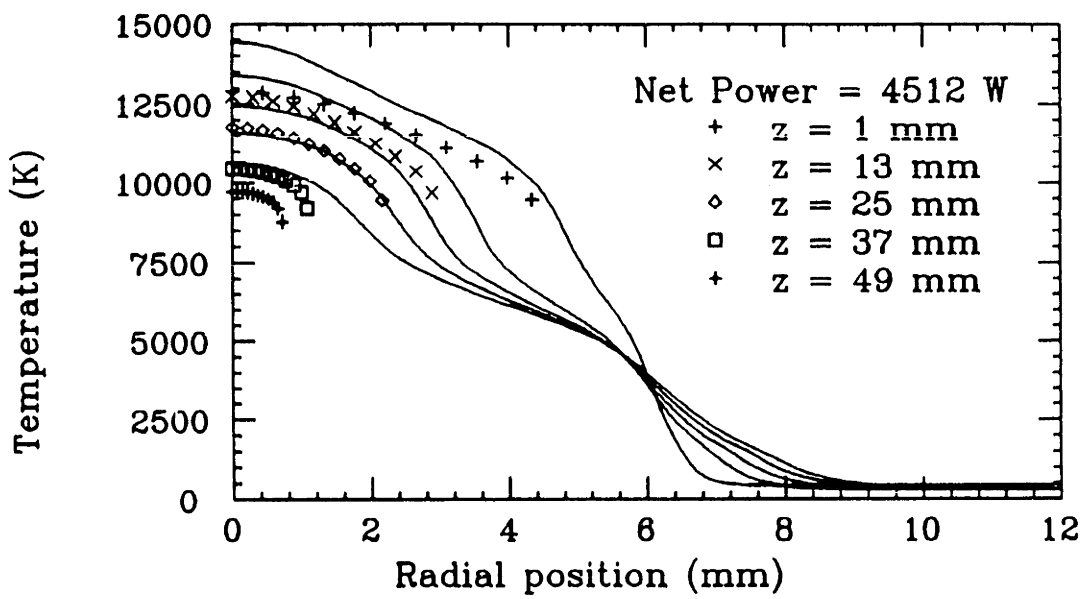

(b)

Figure IV.B.8. Comparison of the experimentally measured and theoretically predicted axial (a) and radial (b) profiles of temperature for run BES34

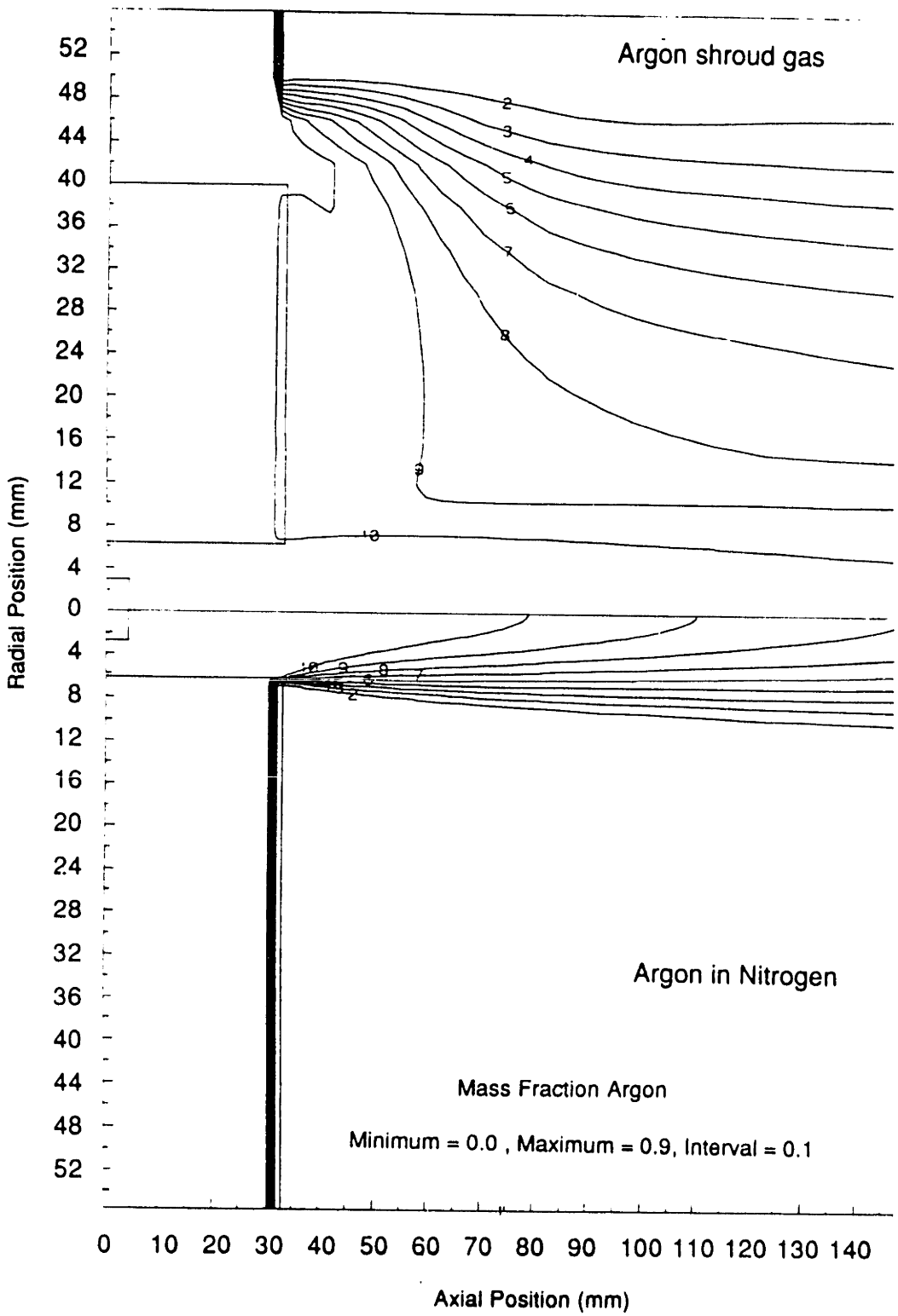

Figure IV.B.9. Comparison of the concentration contours of argon in the plume for the Ar/N_2 system with and without shroud gas.

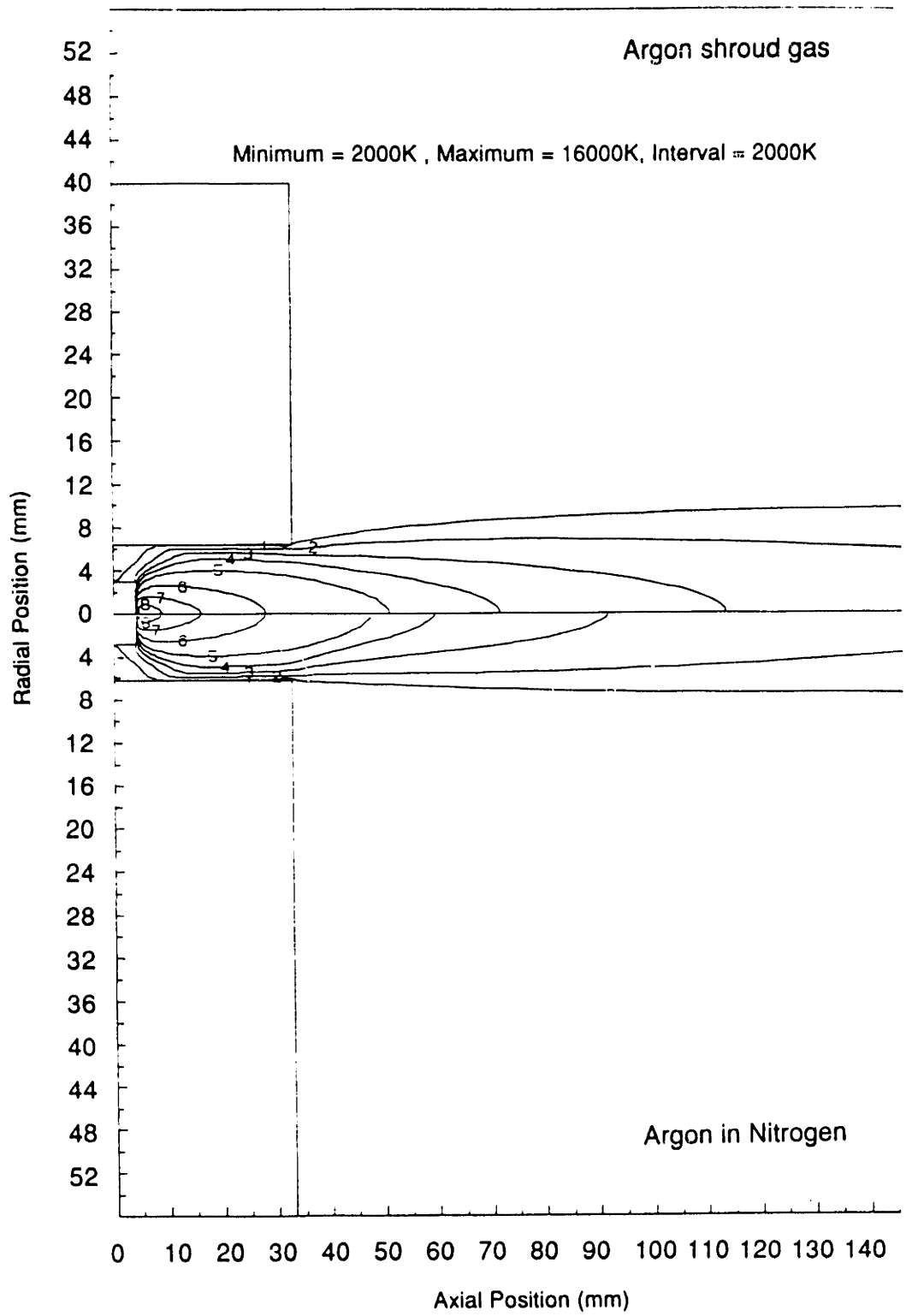

Figure IV.B.10. Comparison of the temperature contours of argon in the plume for the Ar/N_2 system with and without shroud gas.

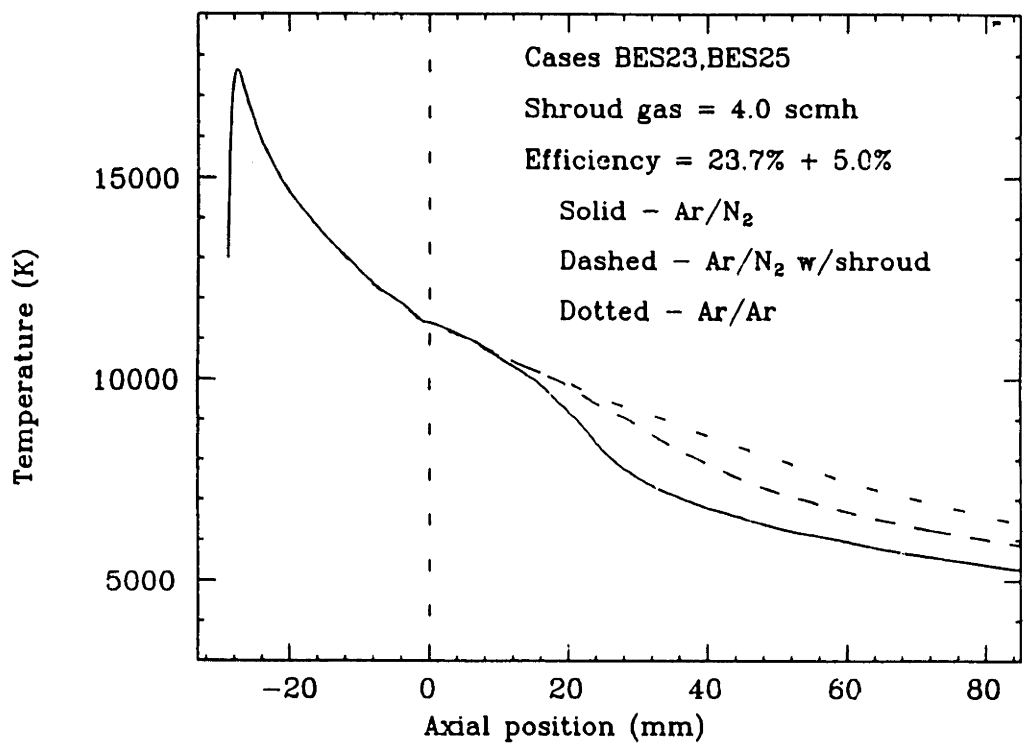

(a)

Figure IV.B.11. Comparison of the axial temperature profile in the plume for the Ar/Ar system and the Ar/N_2 system with and without shroud gas.

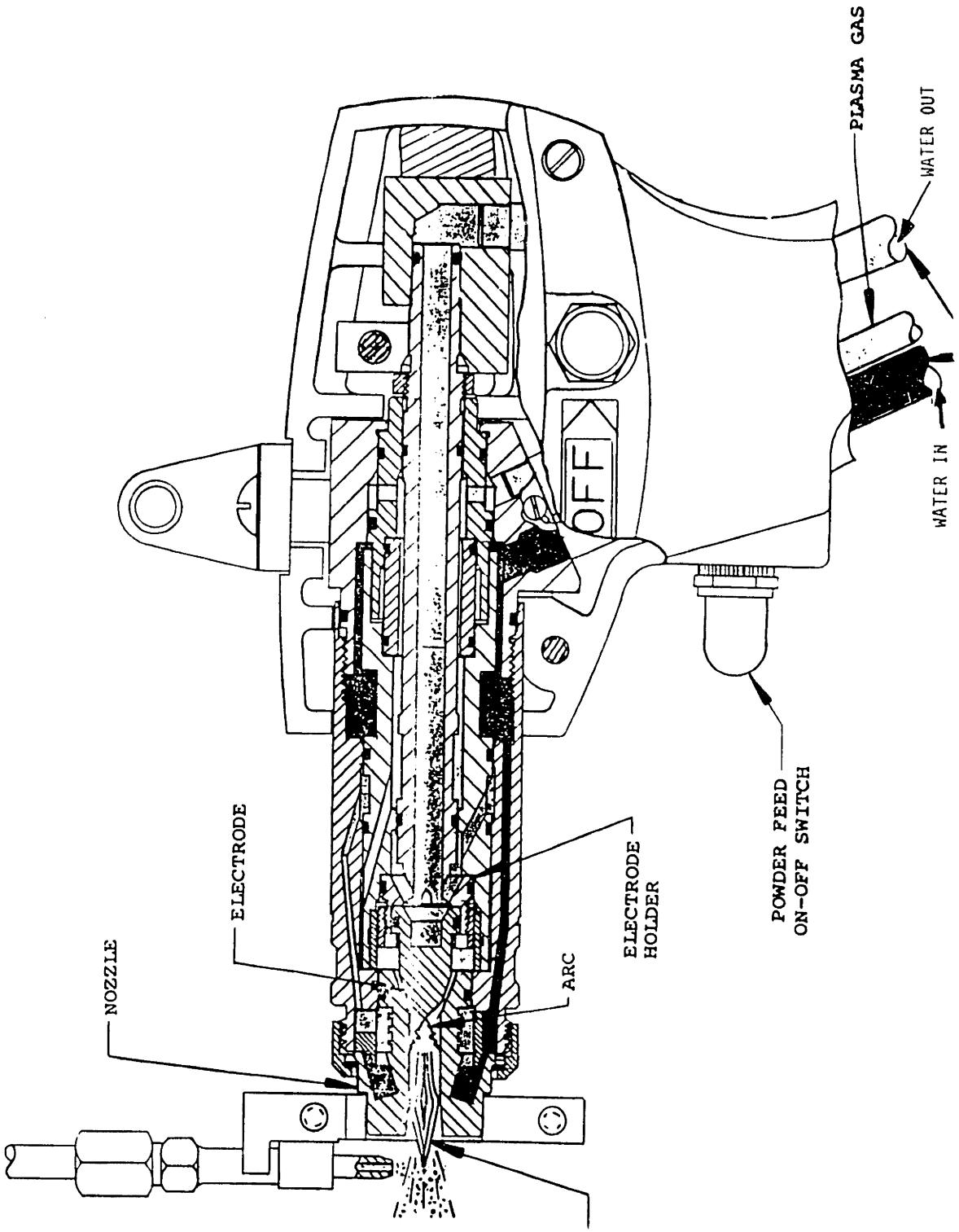

Figure IV.C.1. Cut-away view of the Metco 7mb plasma torch (courtesy Metco Corp., Westbury, NY)

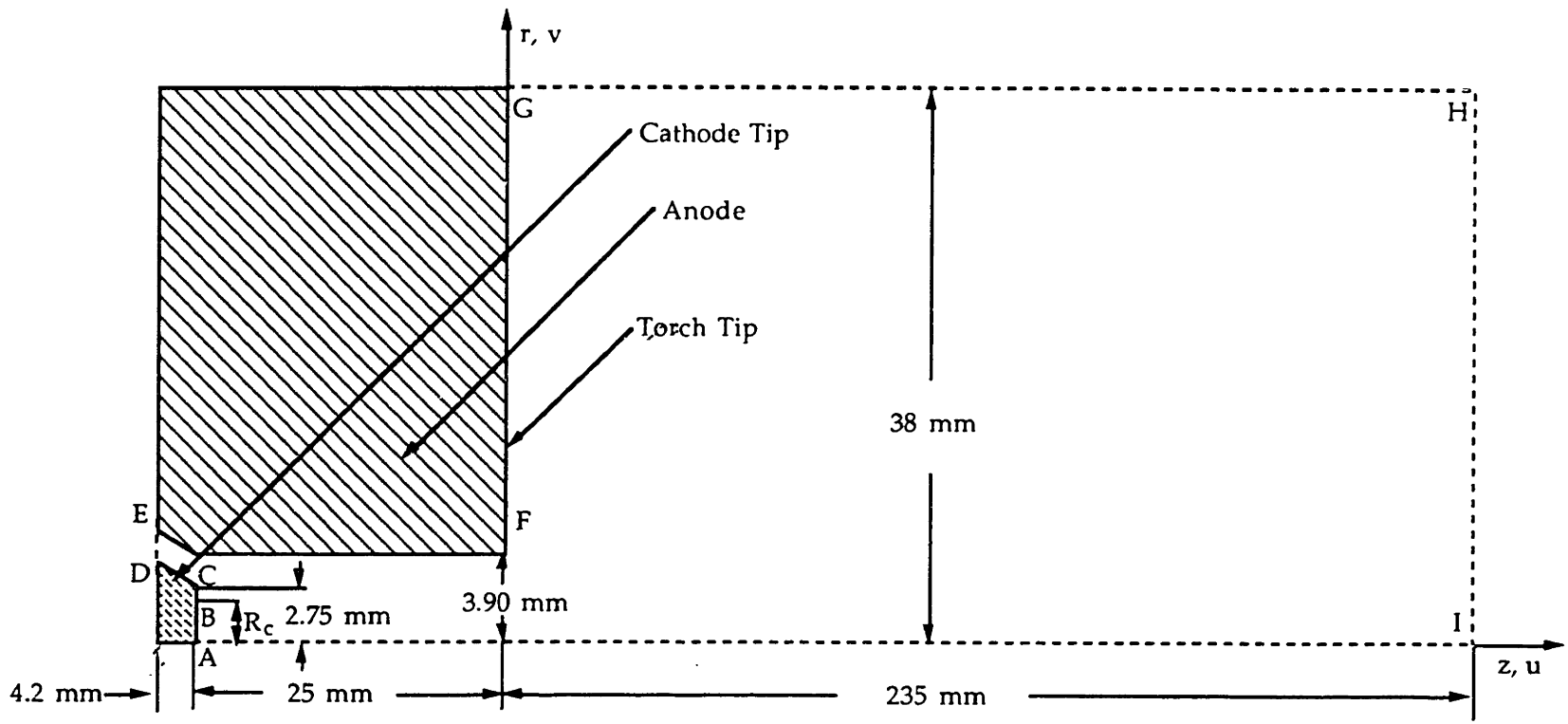

Figure IV.C.2. Computational domain used in the study of the Metco torch.

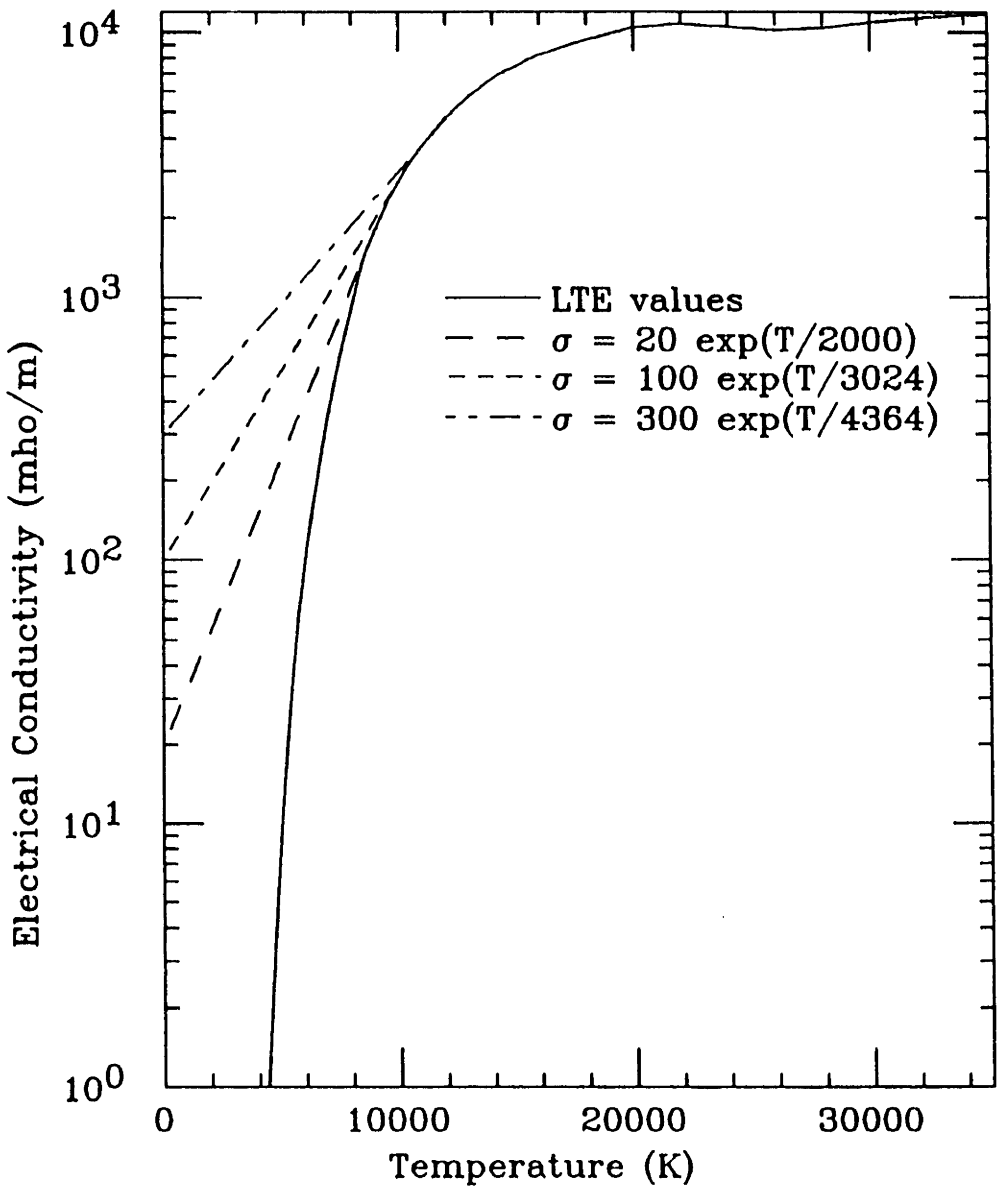

Figure IV.C.3. Temperature dependence of the electrical conductity of argon showing the assumptions used at low temperature and the effect of the constants used in the exponential expression.

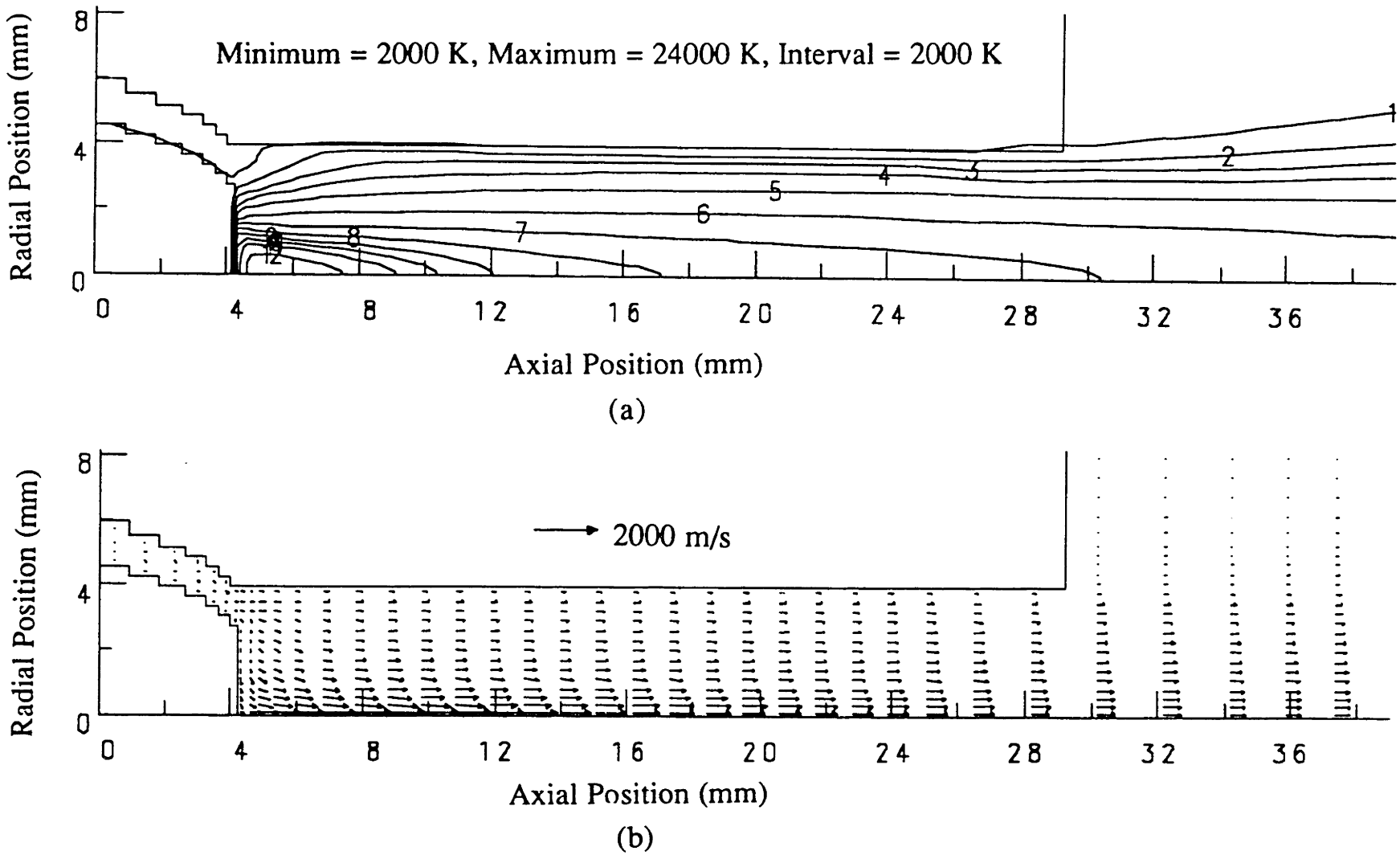

Figure IV.C.4. Isotherms (a) and velocity vectors (b) in the Metco plasma torch, (case 12, 450 A, 23.6 lit./min. of argon, Sw=3.0).

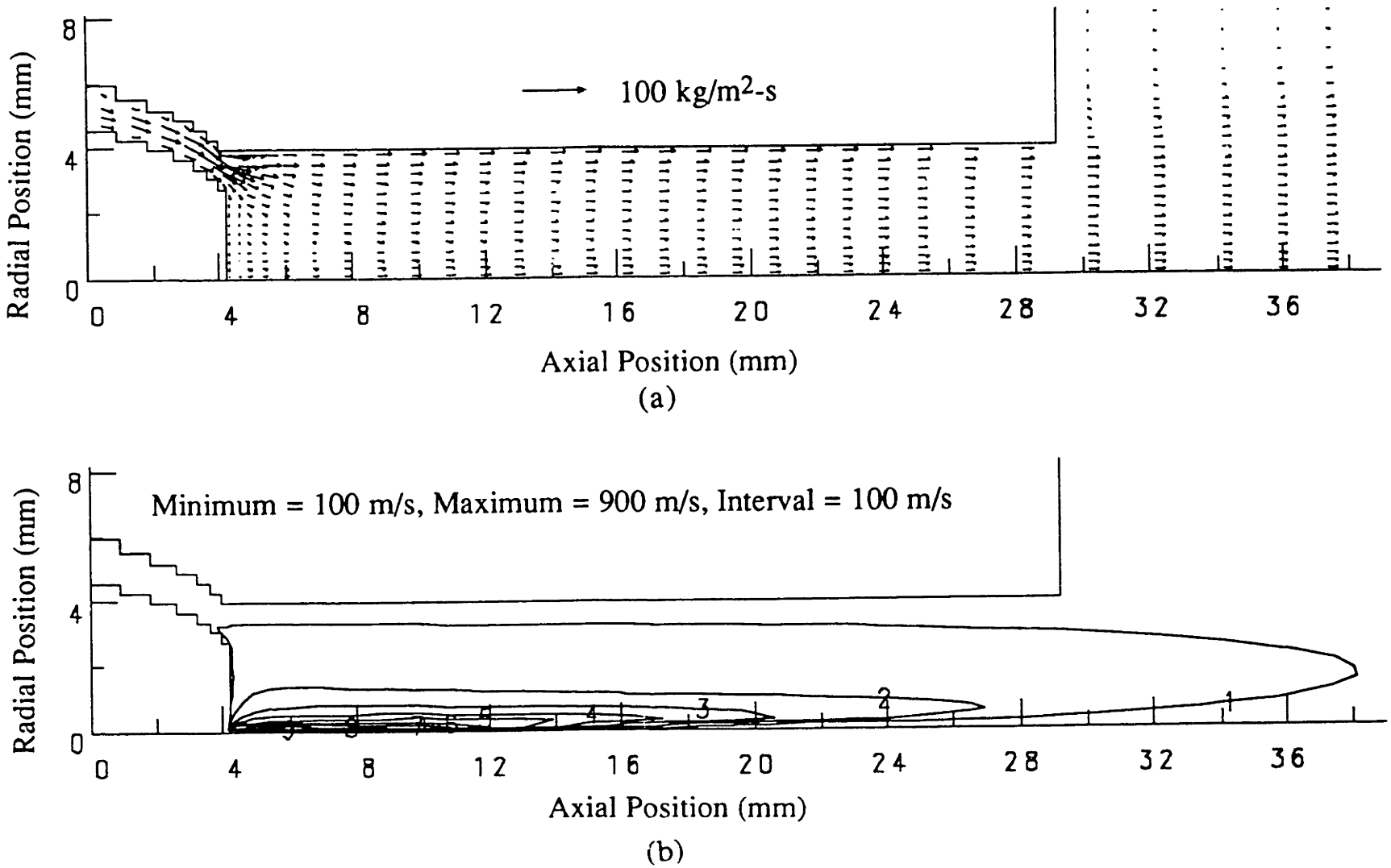

Figure IV.C.5. Mass flow (ρu product) vectors (a) and contours of swirl velocity (b) in the Metco plasma torch, (case 12, 450 A, 23.6 lit./min. of argon, Sw=3.0).

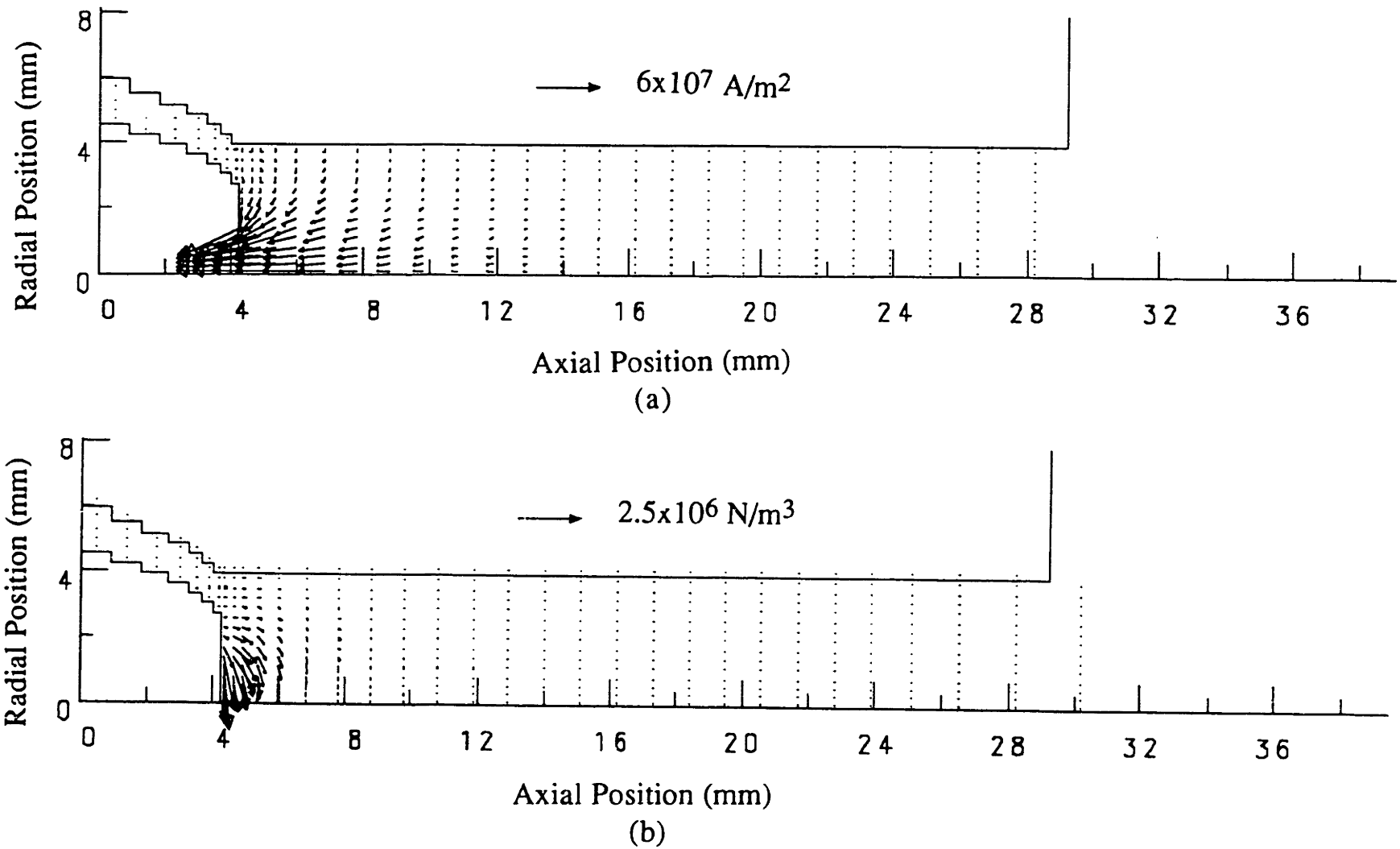

Figure IV.C.6. Current density vectors (a) and body force vectors (b) in the Metco plasma torch, (case 12, 450 A, 23.6 lit./min. of argon, Sw=3.0).

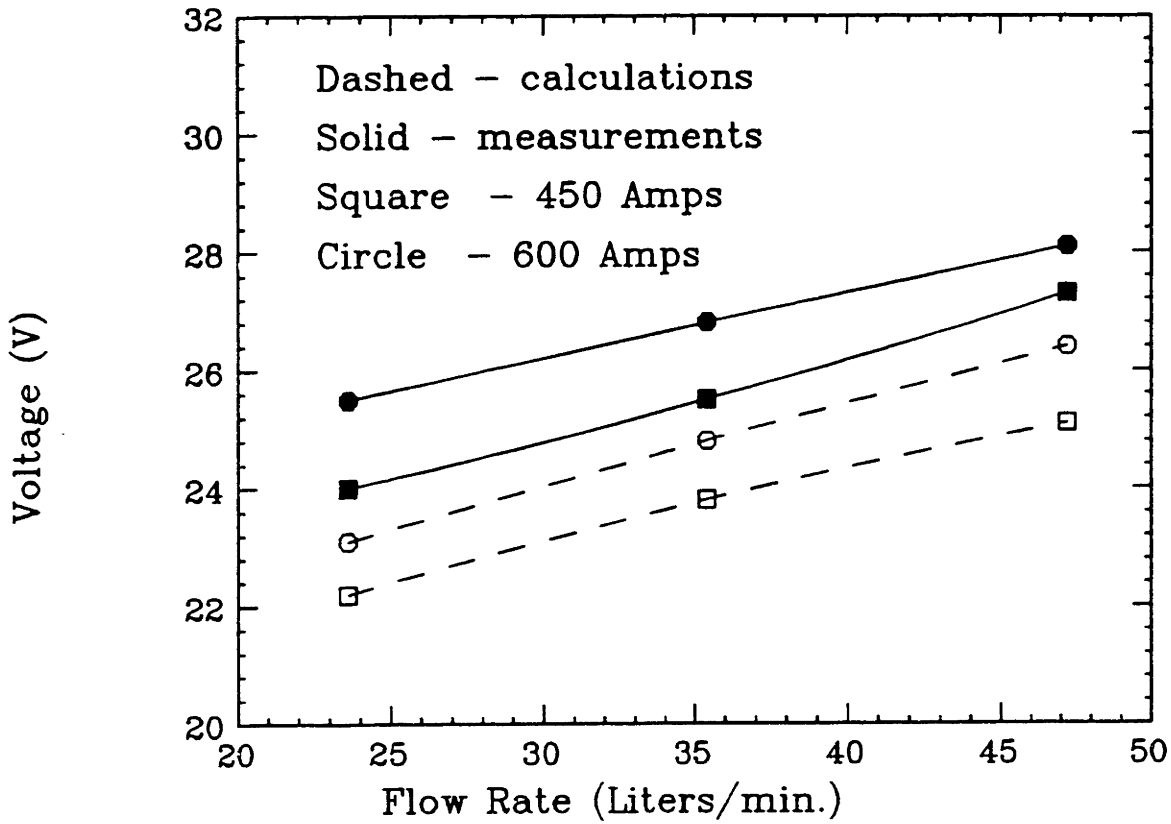

Figure IV.C.7. Calculated and experimentally measured current-voltage characteristics of the plasma torch used by Capetti and Pfender[24], calculated (open symbols) and measured (solid symbols).

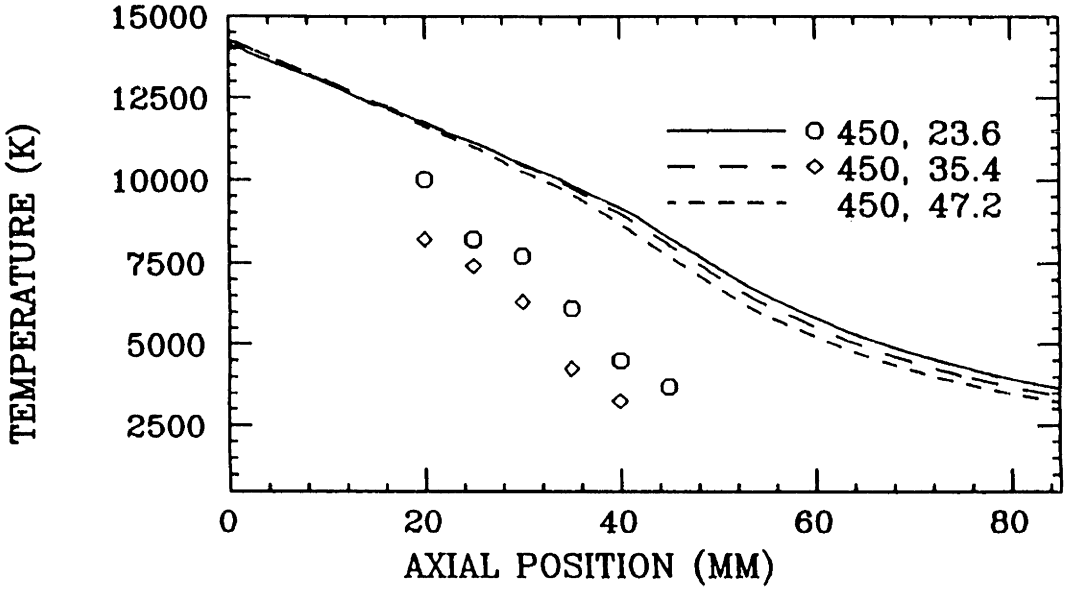

(a)

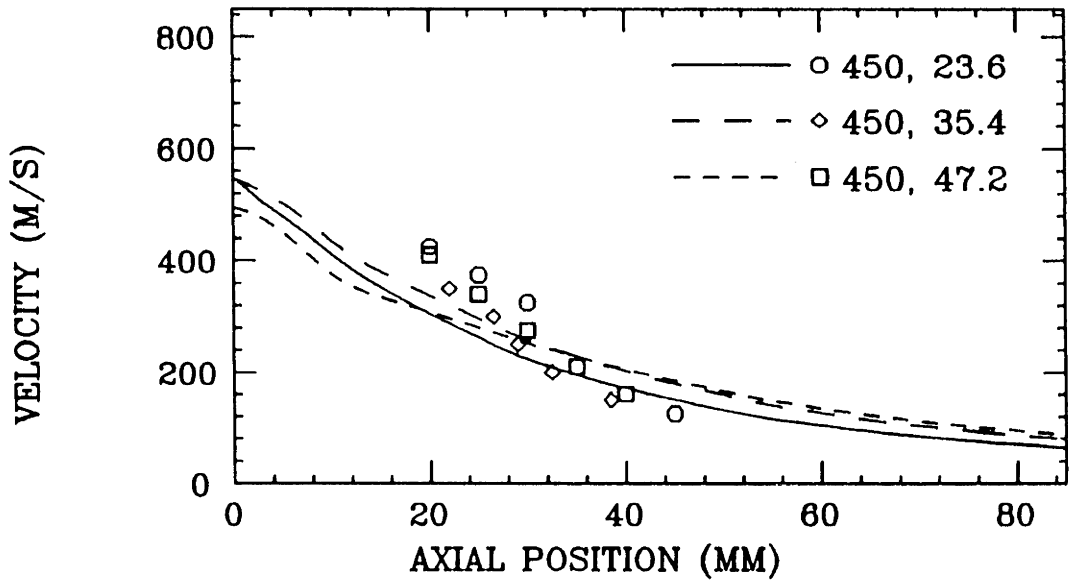

(b)

Figure IV.C.8. Comparison between experimentally measured[24] (symbols) and theoretically predicted (lines) axial profiles of temperature (a) and axial velocity (b) in the plume of the Metco torch for the 450 amp cases.

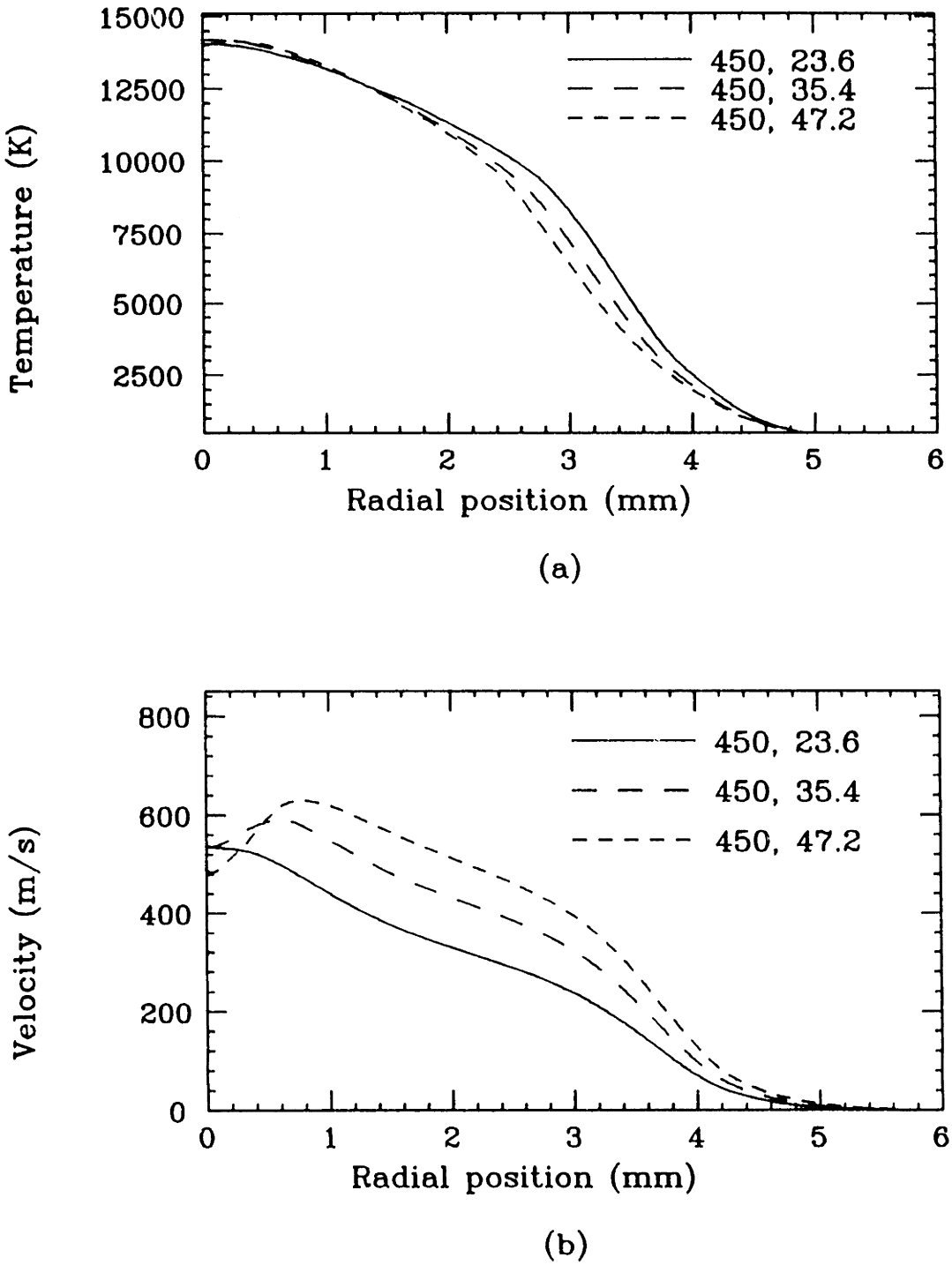

Figure IV.C.9 Theoretically predicted radial profiles of temperature (a) and axial velocity (b) at a position 1 mm from the nozzle exit for the 450 amp cases.

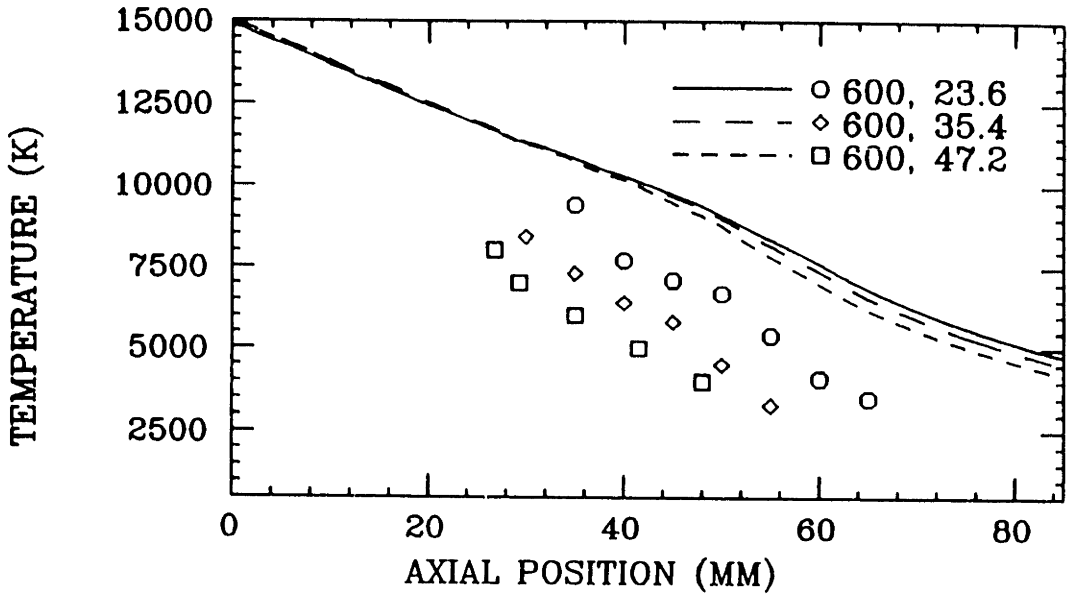

(a)

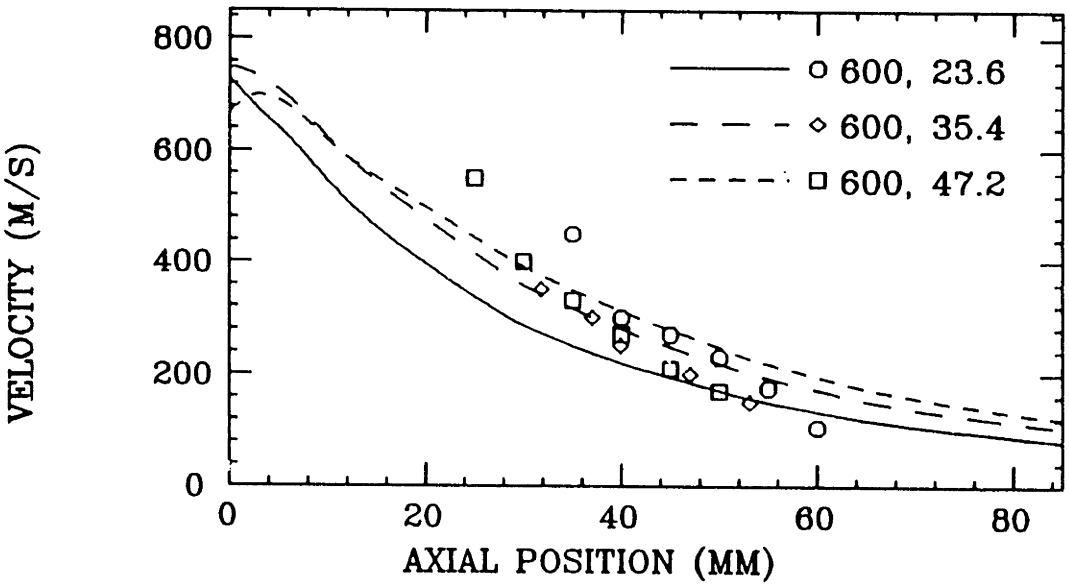

(b)

Figure IV.C.10. Comparison between experimentally measured[24] (symbols) and theoretically predicted (lines) axial profiles of temperature (a) and axial velocity (b) in the plume of the Metco torch for the 600 amp cases.

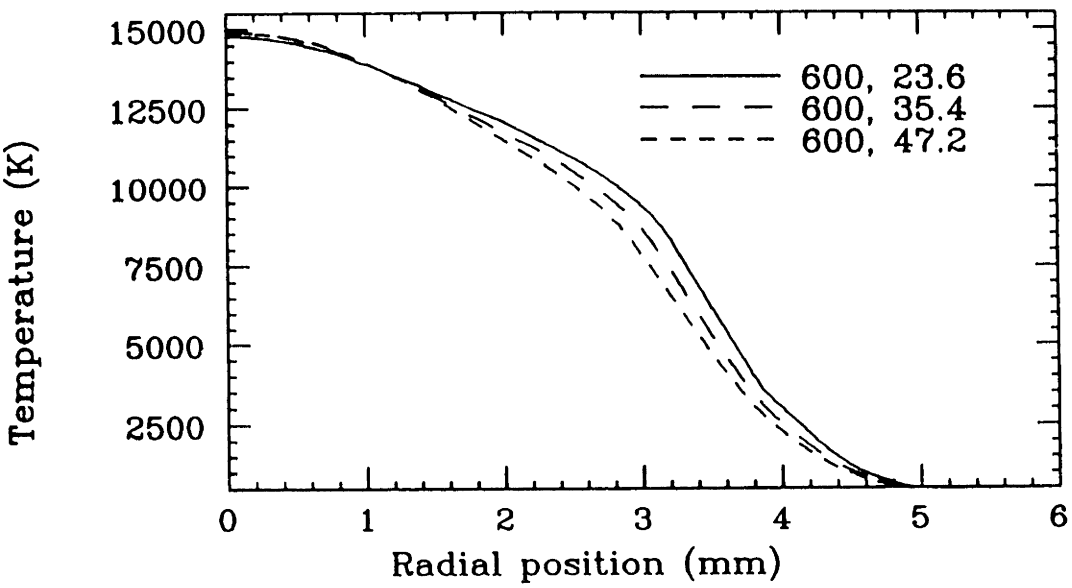

(a)

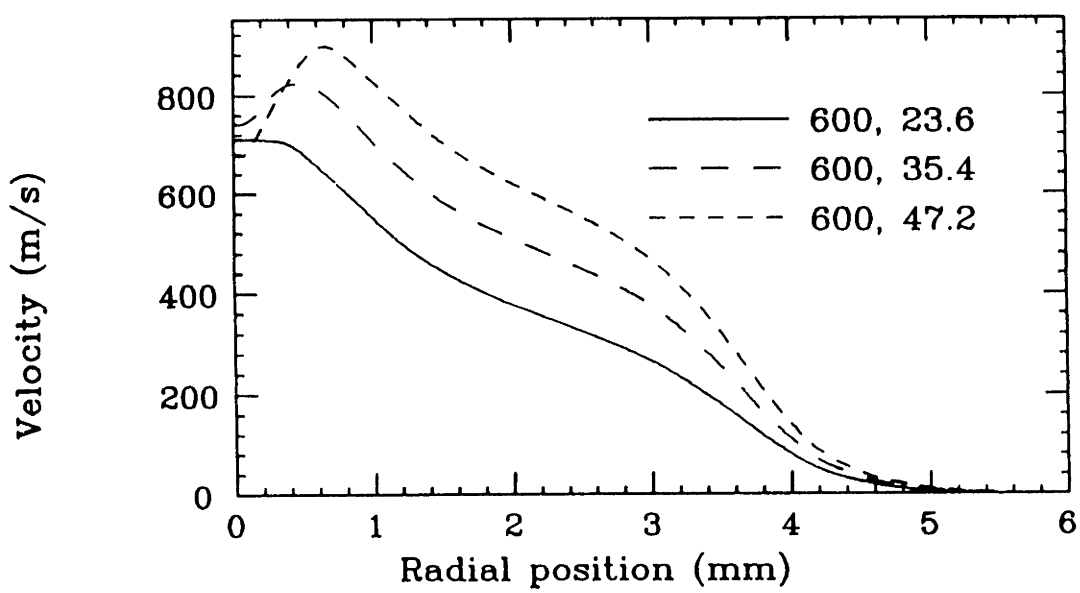

(b)

Figure IV.C.11. Theoretically predicted radial profiles of temperature (a) and axial velocity (b) at a position 1 mm from the nozzle exit for the 600 amp cases.

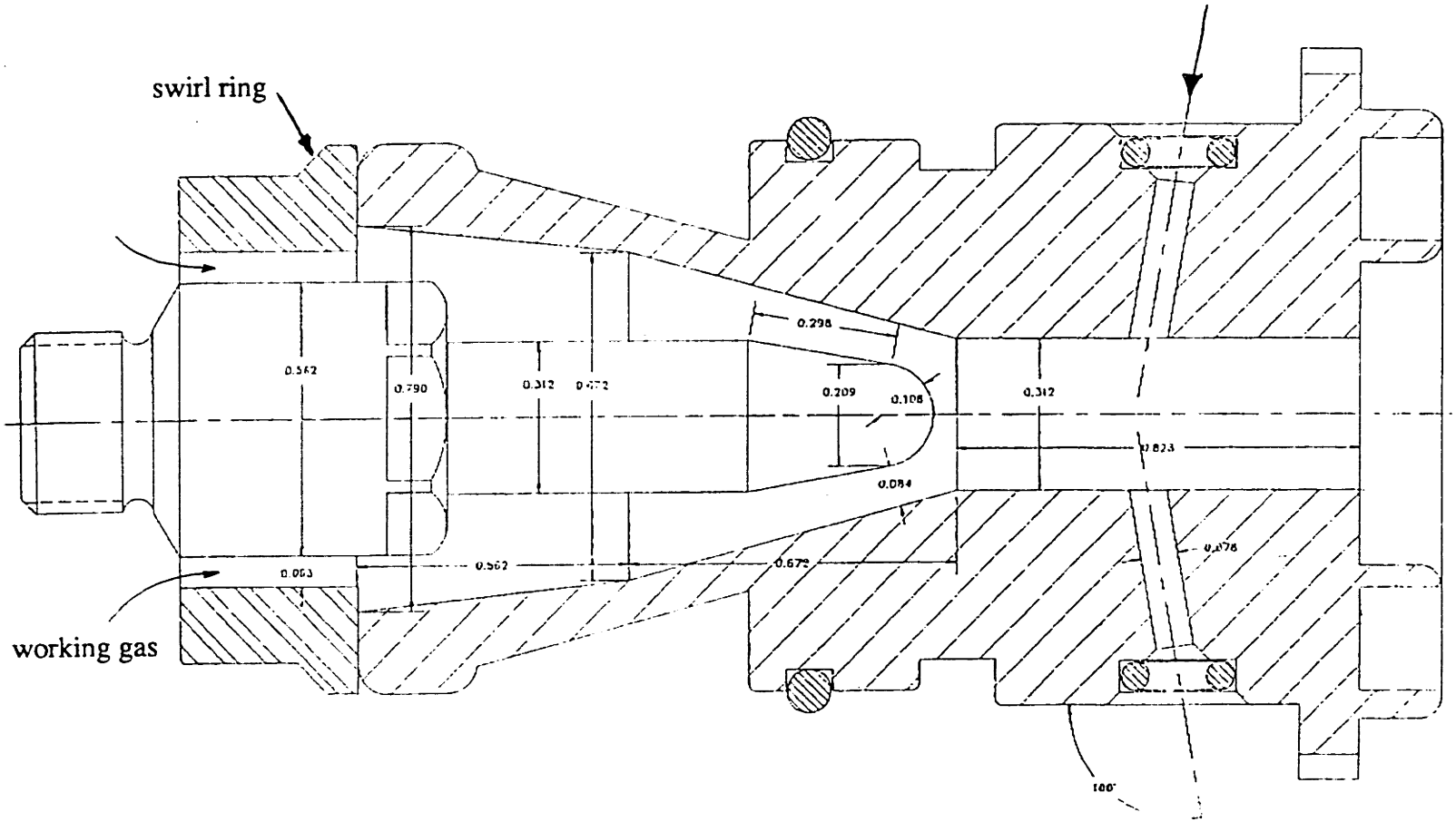

Figure IV.D.1. Cut-away view of the Miller SG-100 plasma torch (courtesy Miller Thermal, Inc. Tustin, CA)

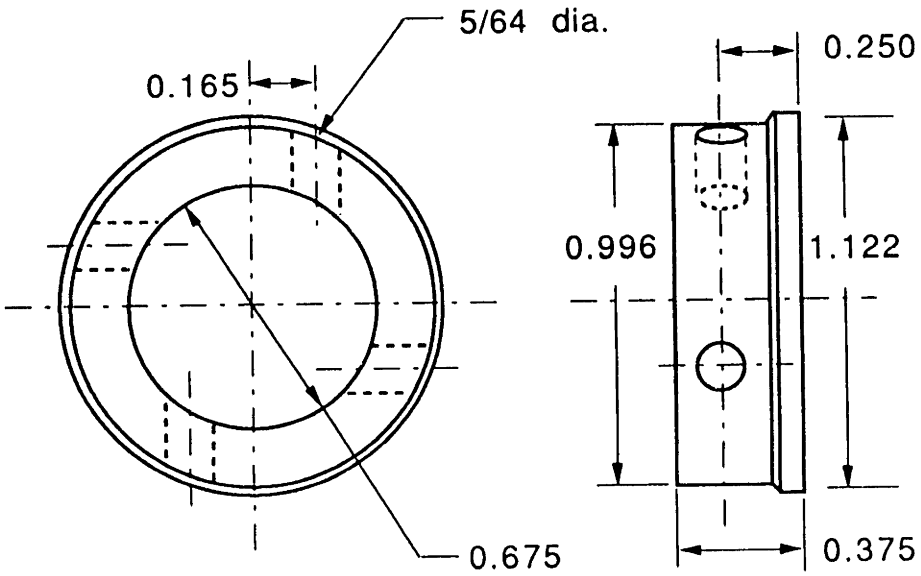

Figure IV.D.2 Illustration of the swirl ring used in the Miller torch for the experiments represented in this section.

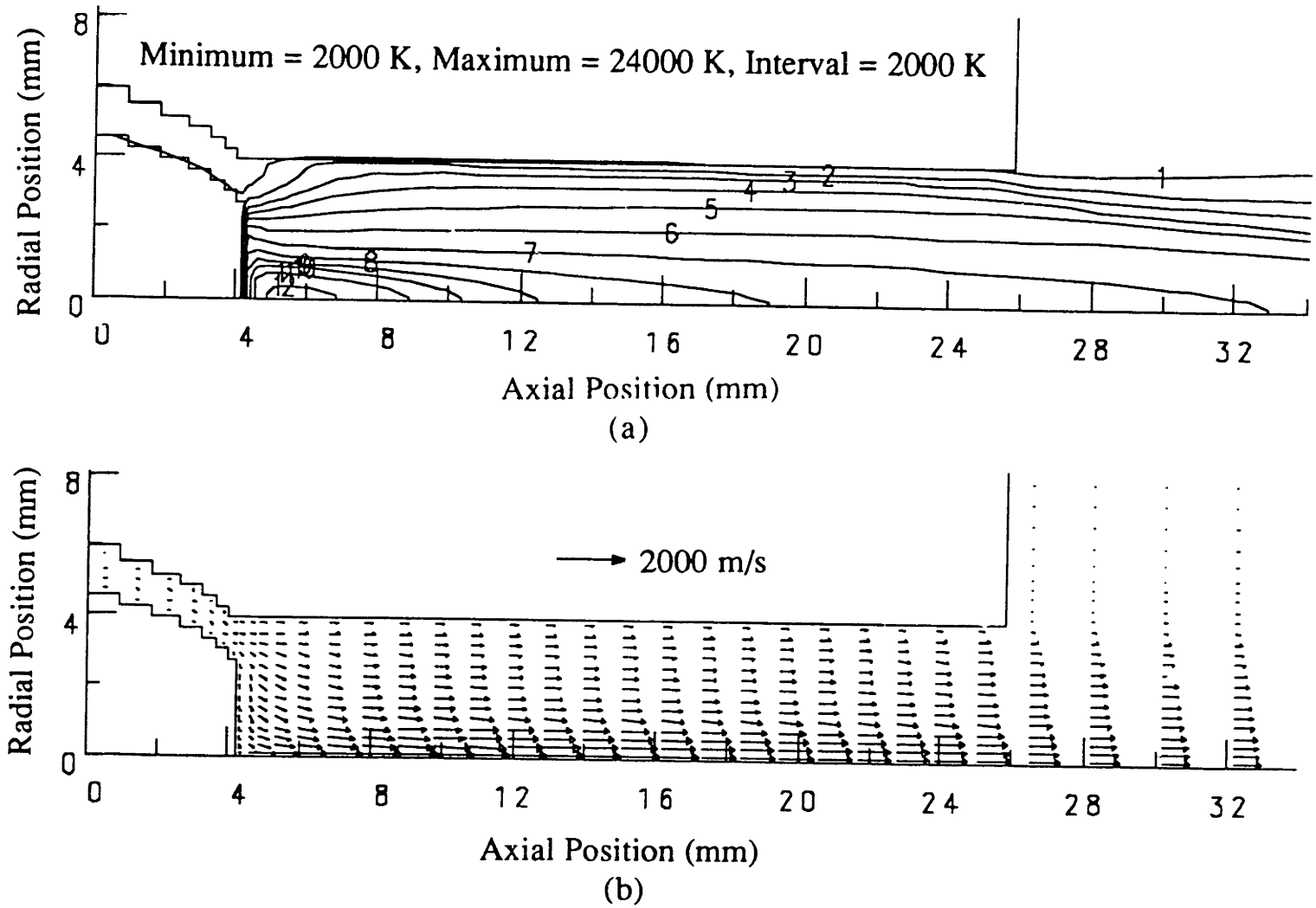

Figure IV.D.3. Isotherms (a) and velocity vectors (b) in the Miller plasma torch, (case 6, 600 A, 75 scfh of argon, Sw=1.22).

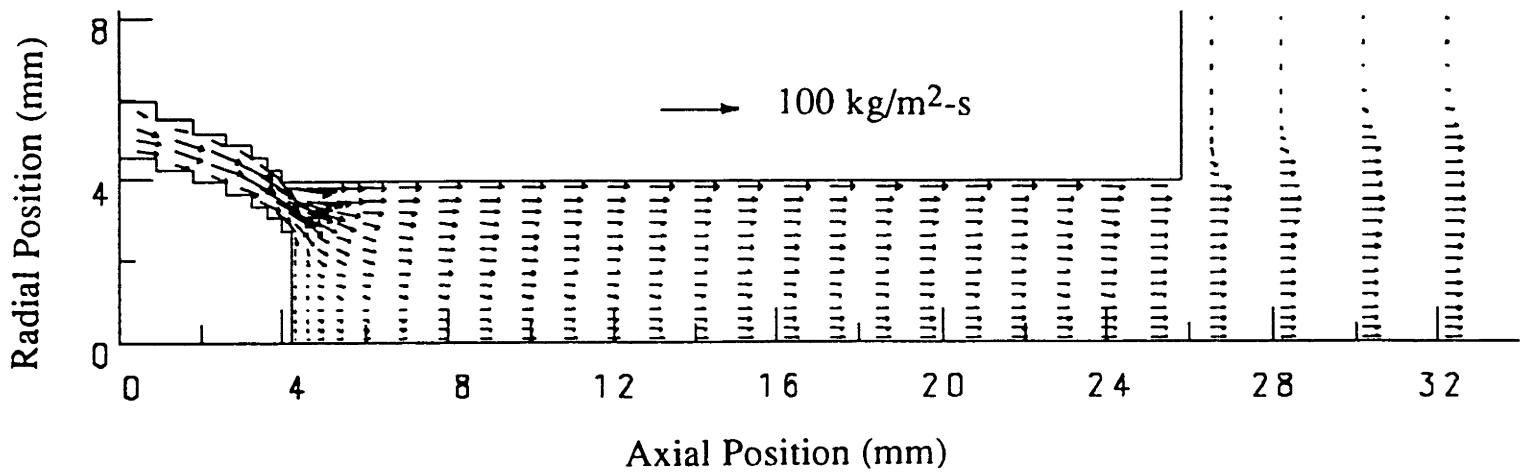

(a)

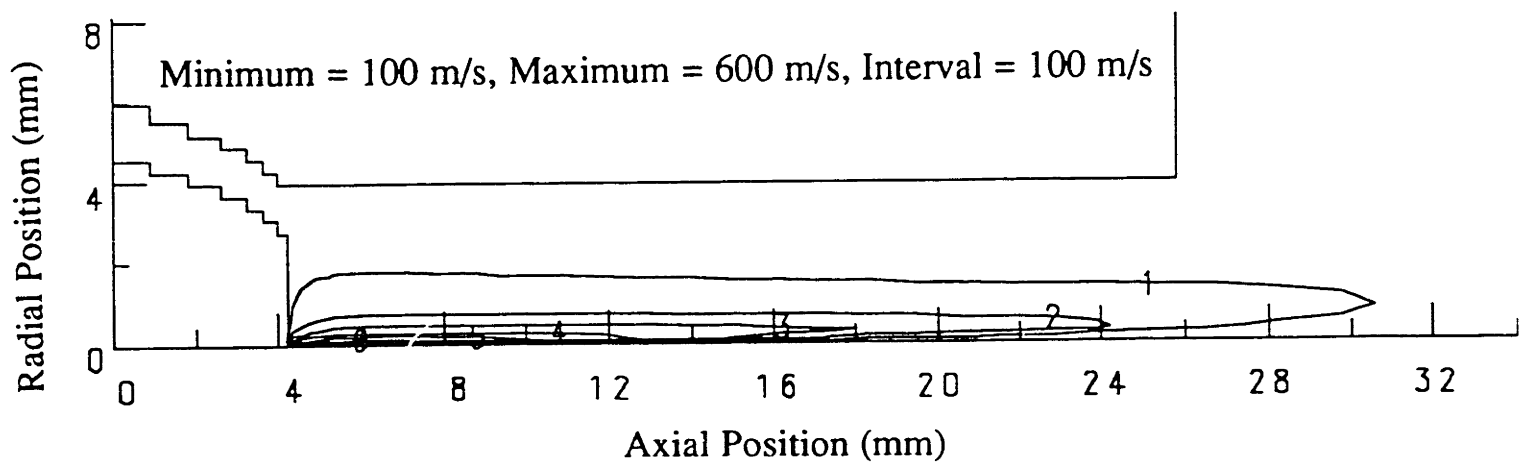

(b)

Figure IV.D.4. Mass flow (ρu product) vectors (a) and contours of swirl velocity (b) in the Miller plasma torch, (case 6, 600 A, 75 scfh of argon, Sw=1.22).

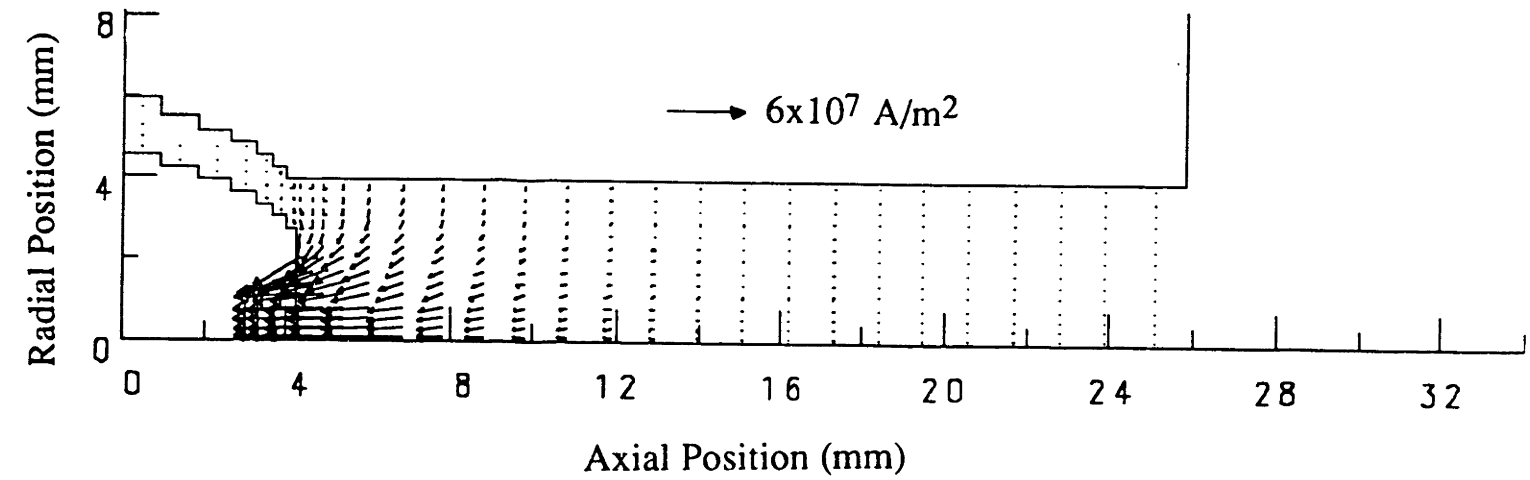

(a)

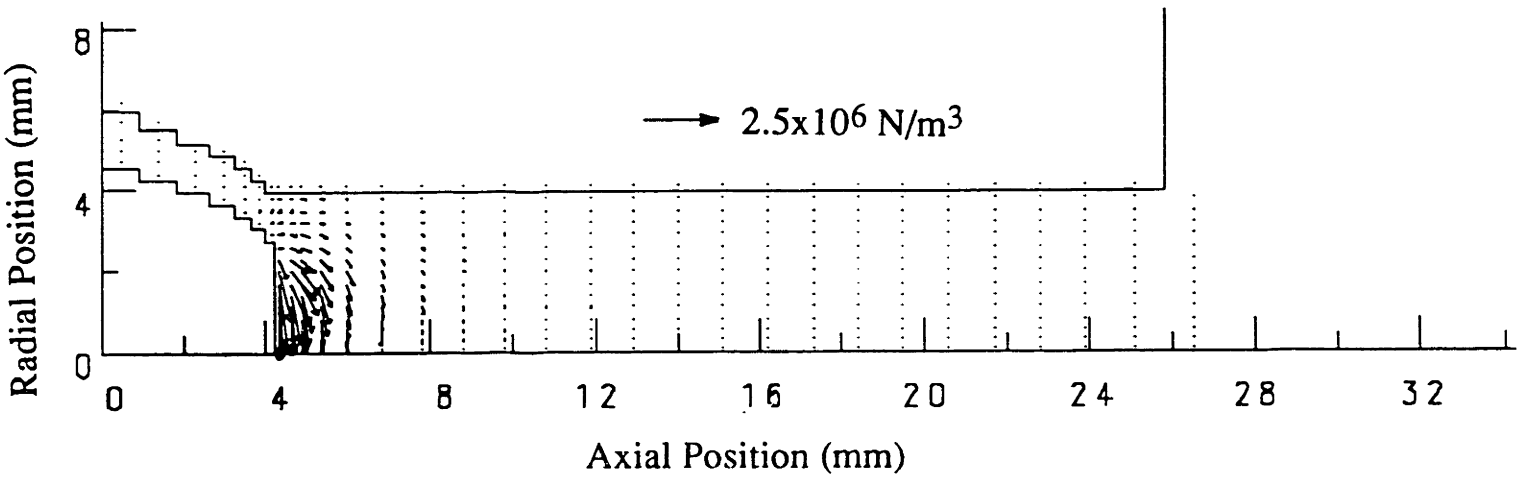

(b)

Figure IV.D.5. Current density vectors (a) and body force vectors (b) in the Miller plasma torch, (case 6, 600 A, 75 scfh of argon, Sw=1.22).

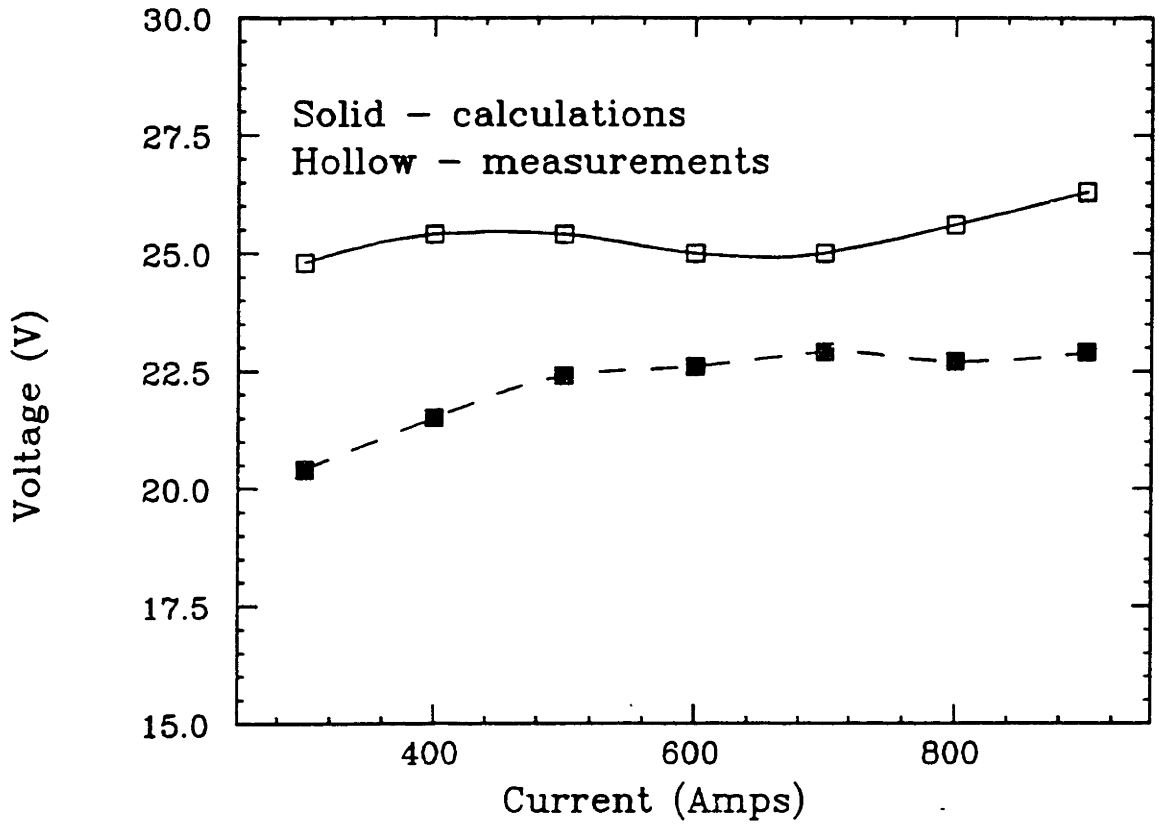

Figure IV.D.6. Calculated and experimental current-voltage characteristics of the Miller SG-100 torch, calculated (solid symbols) and measured (open symbols).

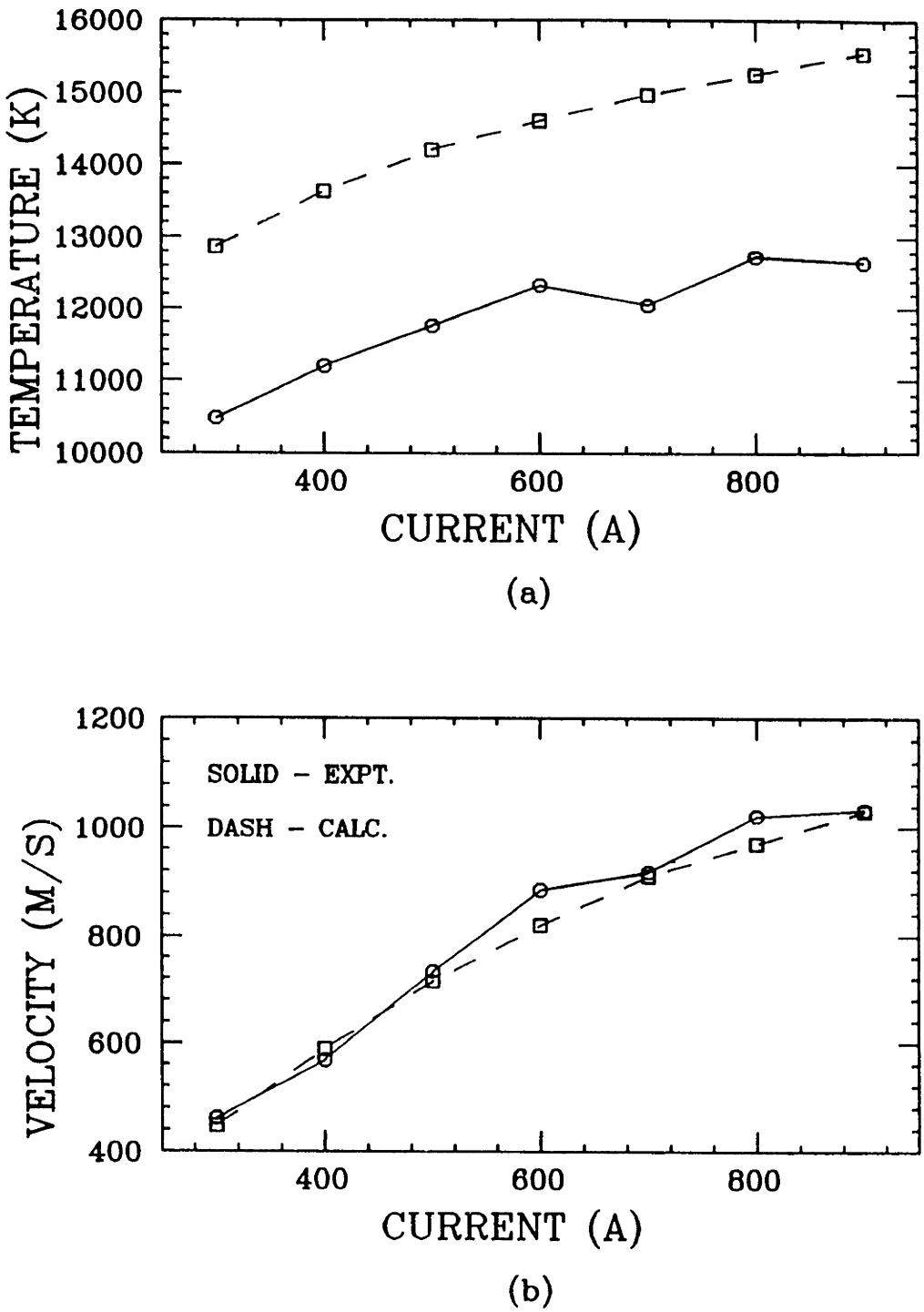

Figure IV.D.7. Comparison of the experimentally measured (circles) and theoretically predicted (squares) center line temperature (a) and velocity (b) at a position 2 mm (case #9, 5 mm) from the exit of the torch nozzle.

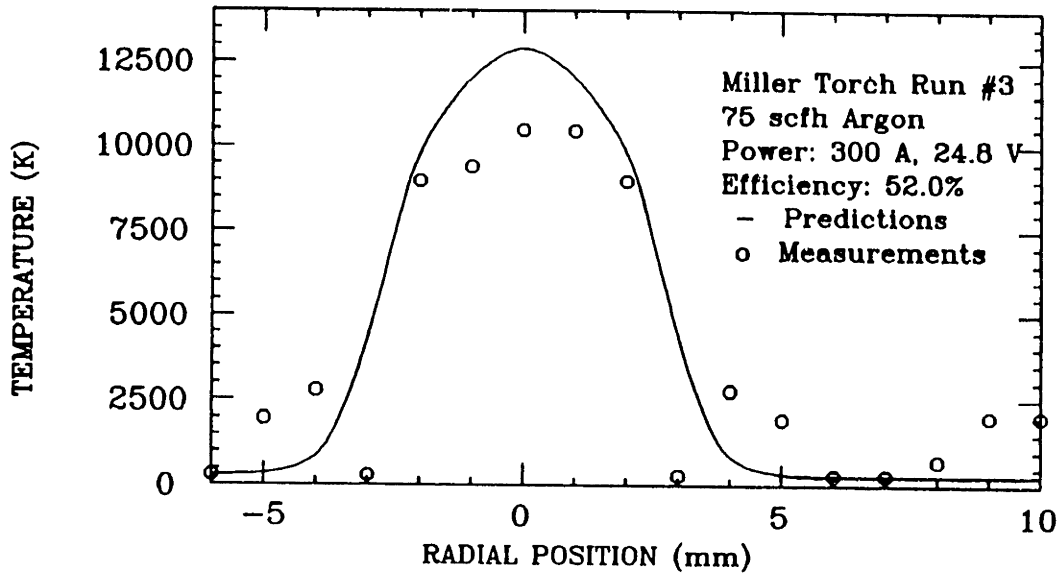

(a)

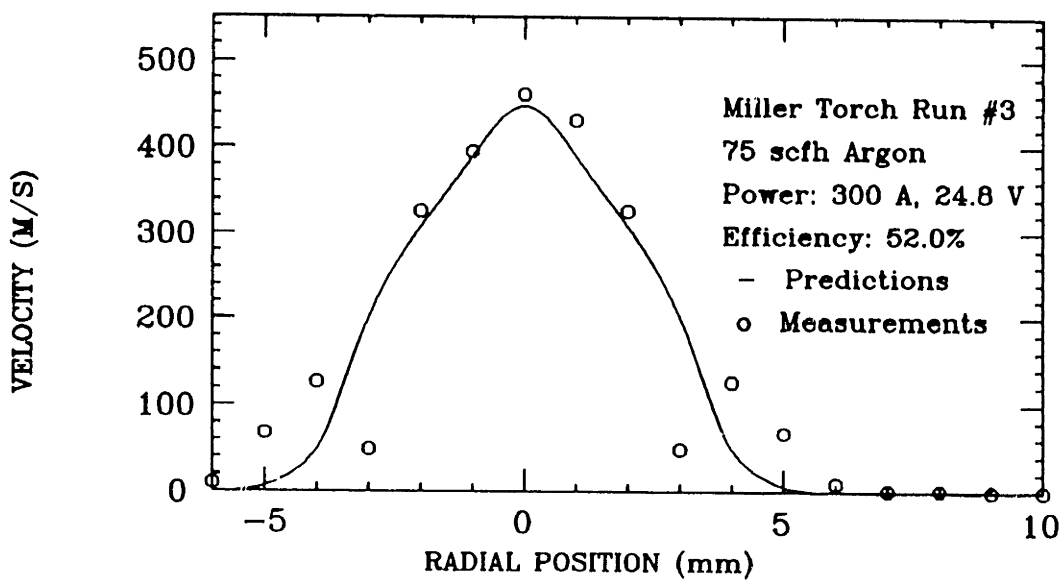

(b)

Figure IV.D.8. Comparison of the experimentally measured and theoretically predicted radial profile of temperature (a) and axial velocity (b) at a position 2 mm from the nozzle exit for the 300 amp case.

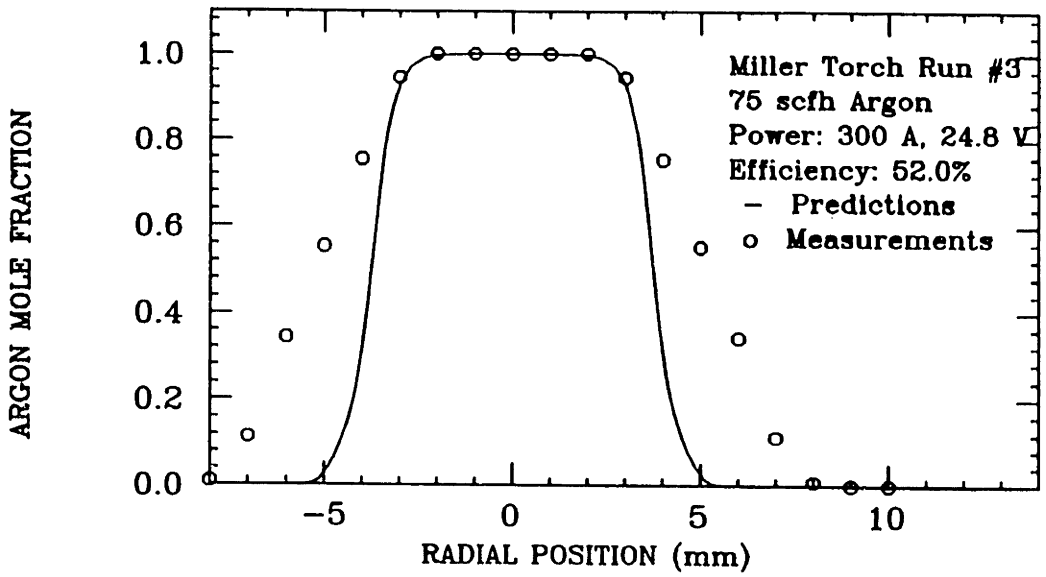

Figure IV.D.9. Comparison of the experimentally measured and theoretically predicted radial profile of argon mole fraction at a position 2 mm from the nozzle exit for the 300 amp case.

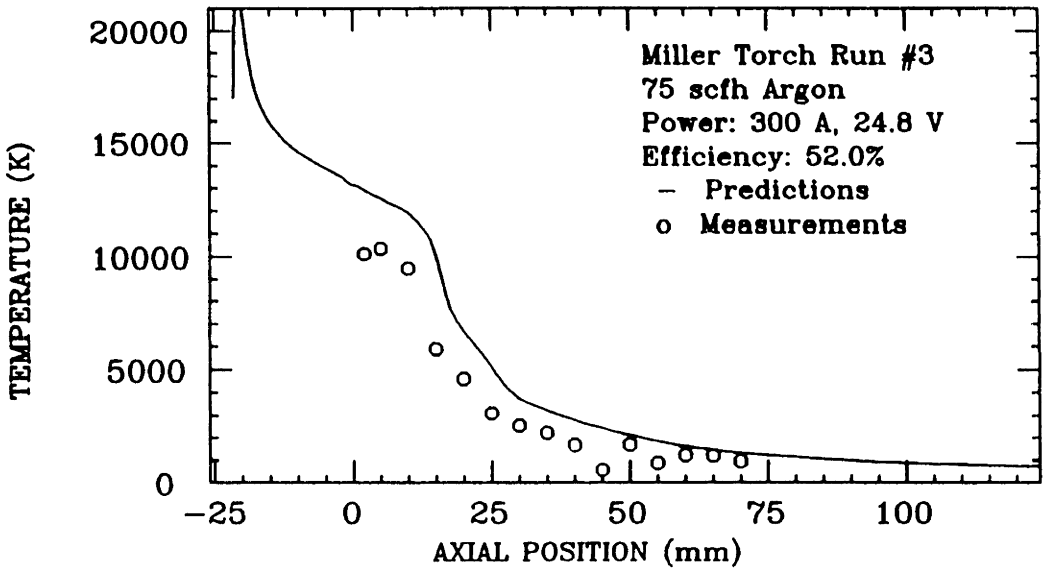

(a)

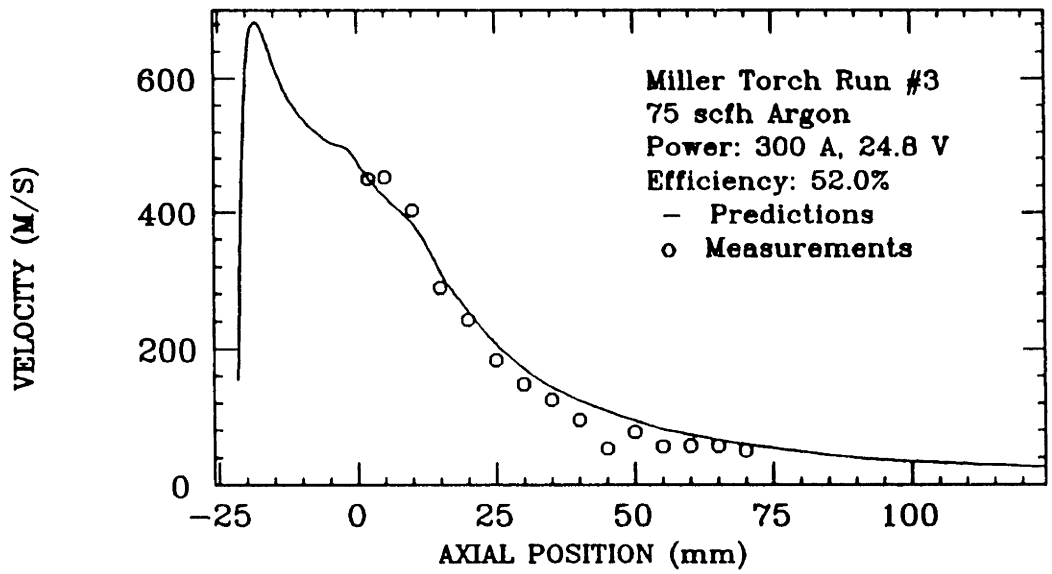

(b)

Figure IV.D.10. Comparison of the experimentally measured and theoretically predicted axial profile of the center line temperature (a) and axial velocity (b) for the 300 amp case.

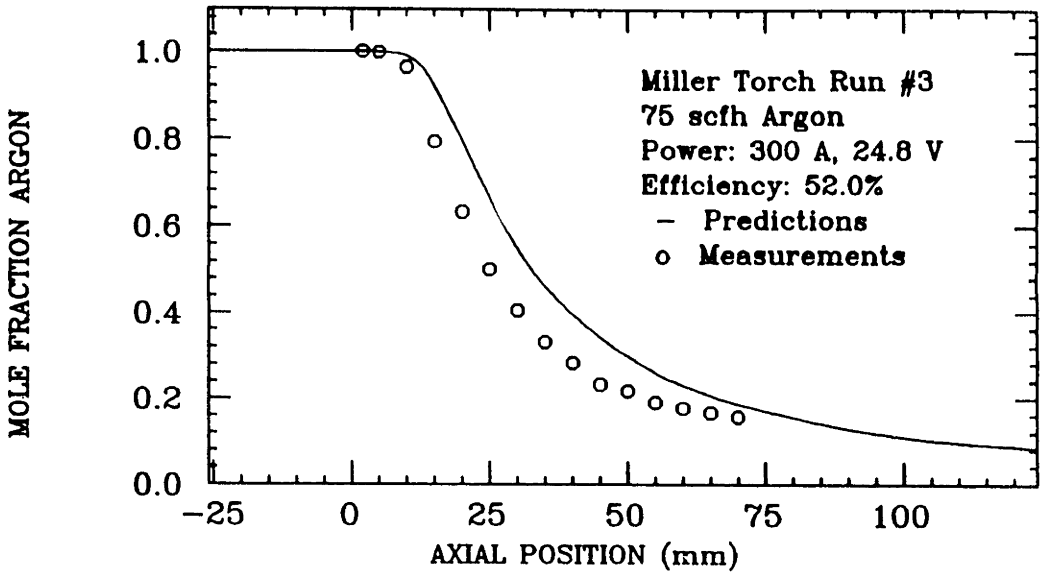

Figure IV.D.11. Comparison of the experimentally measured and theoretically predicted axial profile of the argon mole fraction on the center line for the 300 amp case.

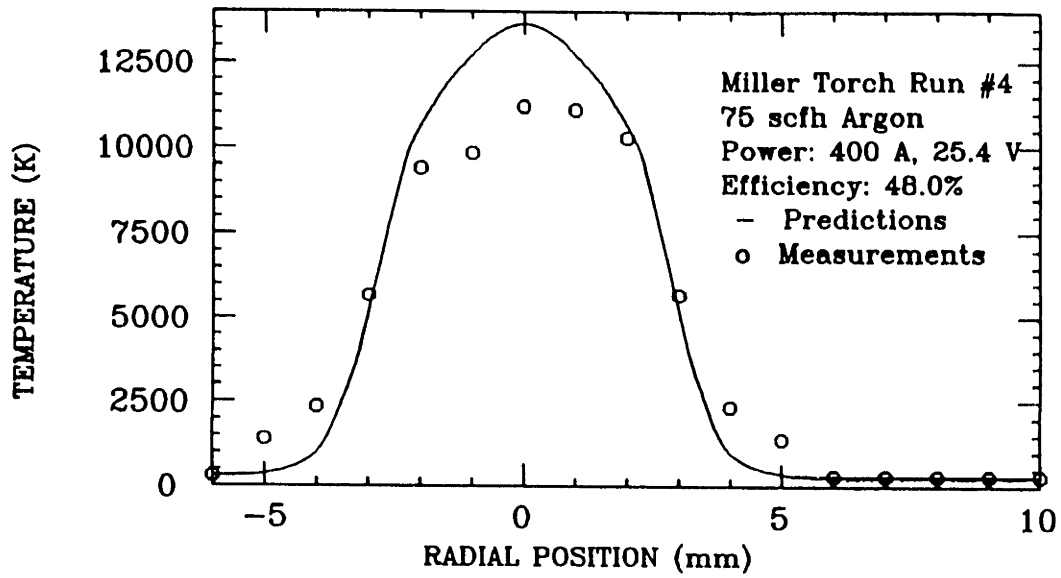

(a)

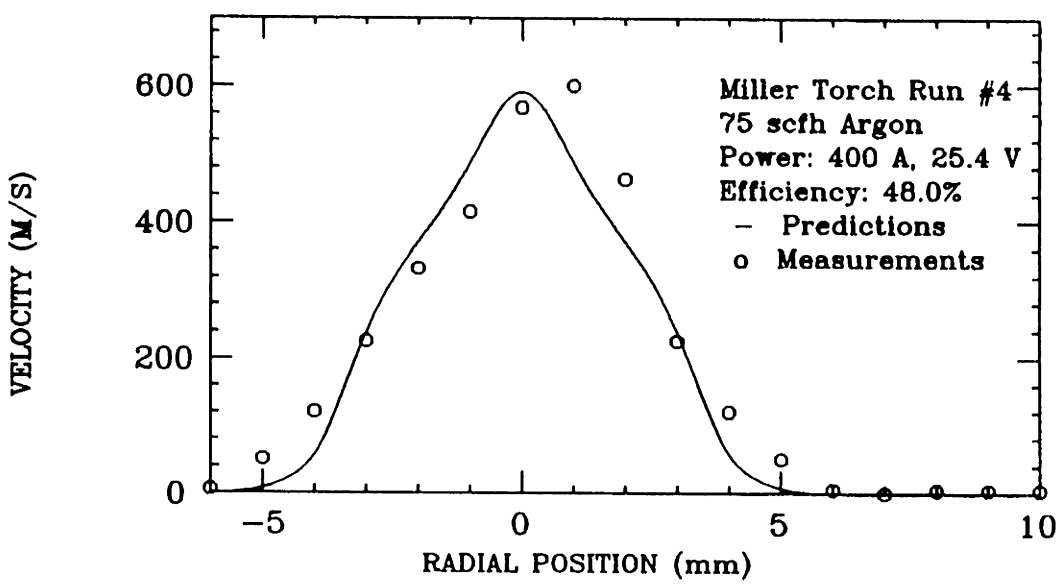

(b)

Figure IV.D.12. Comparison of the experimentally measured and theoretically predicted radial profile of temperature (a) and axial velocity (b) at a position 2 mm from the nozzle exit for the 400 amp case.

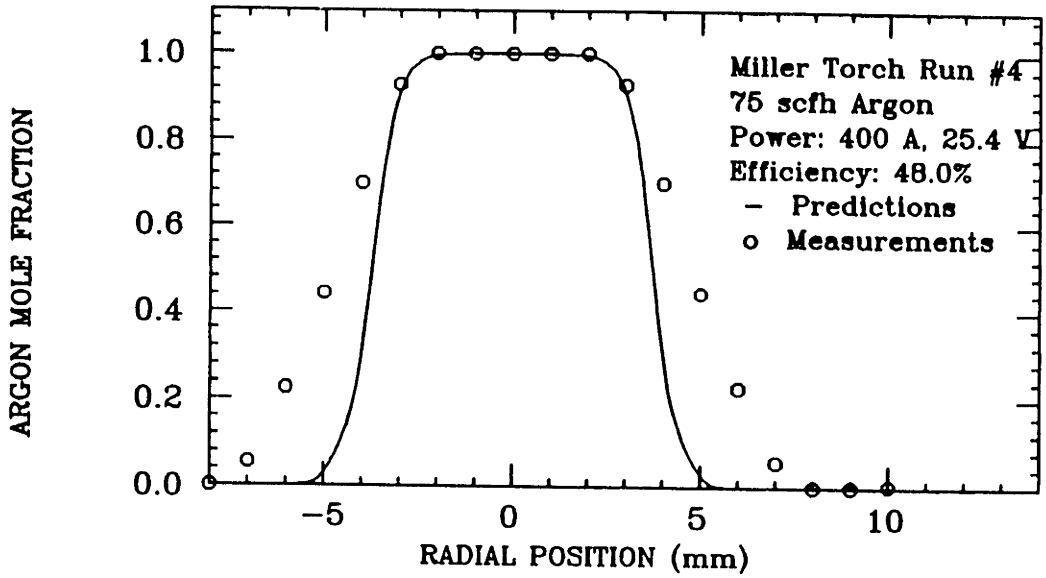

Figure IV.D.13. Comparison of the experimentally measured and theoretically predicted radial profile of argon mole fraction at a position 2 mm from the nozzle exit for the 400 amp case.

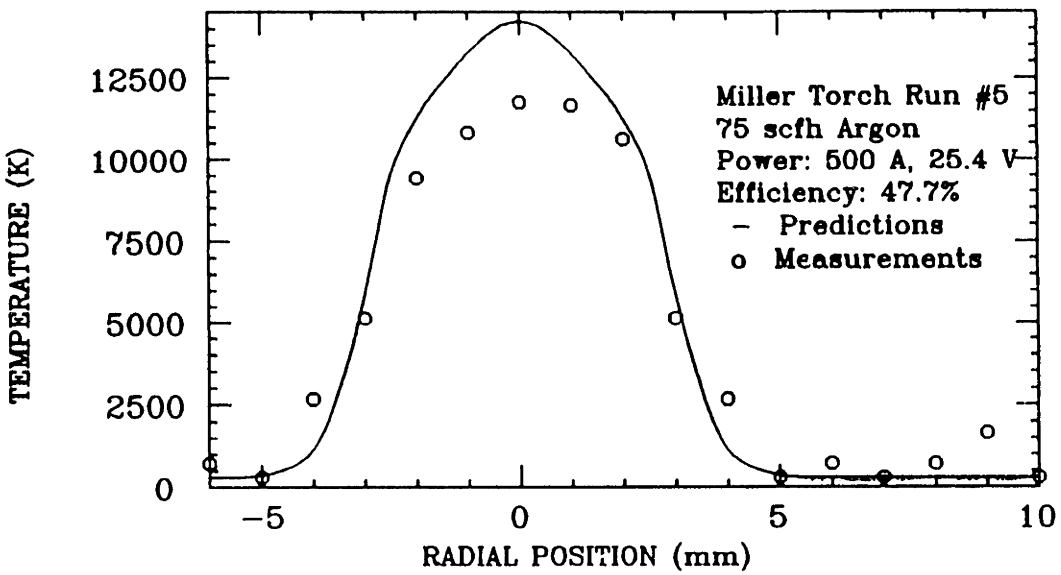

(a)

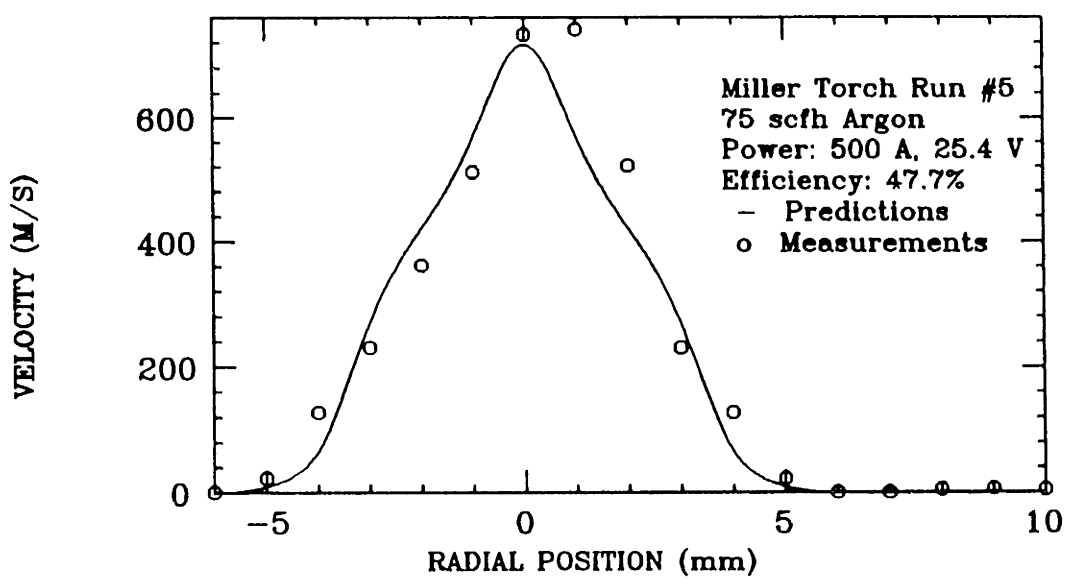

(b)

Figure IV.D.14. Comparison of the experimentally measured and theoretically predicted radial profile of temperature (a) and axial velocity (b) at a position 2 mm from the nozzle exit for the 500 amp case.

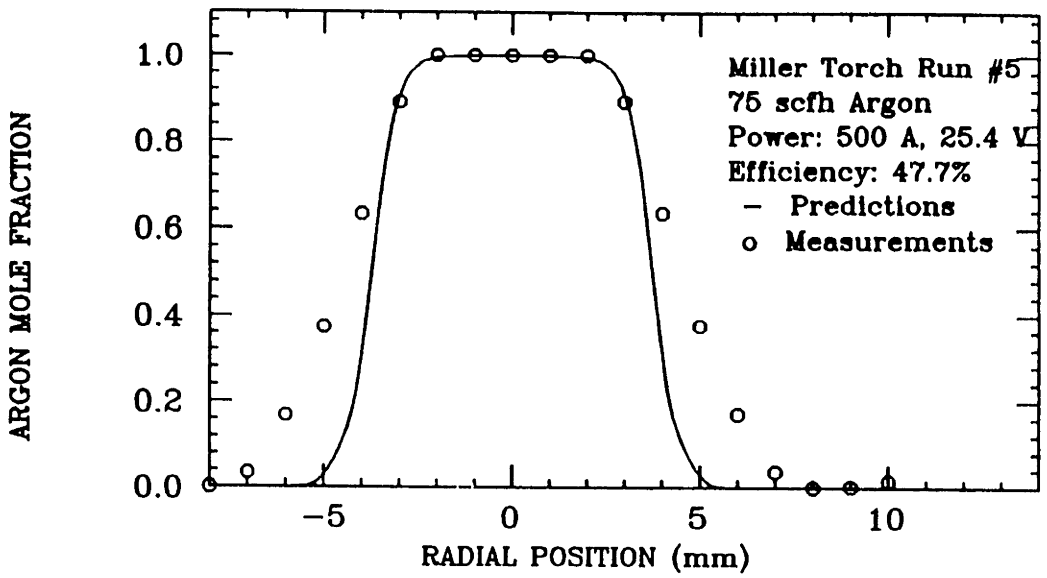

Figure IV.D.15. Comparison of the experimentally measured and theoretically predicted radial profile of argon mole fraction at a position 2 mm from the nozzle exit for the 500 amp case.

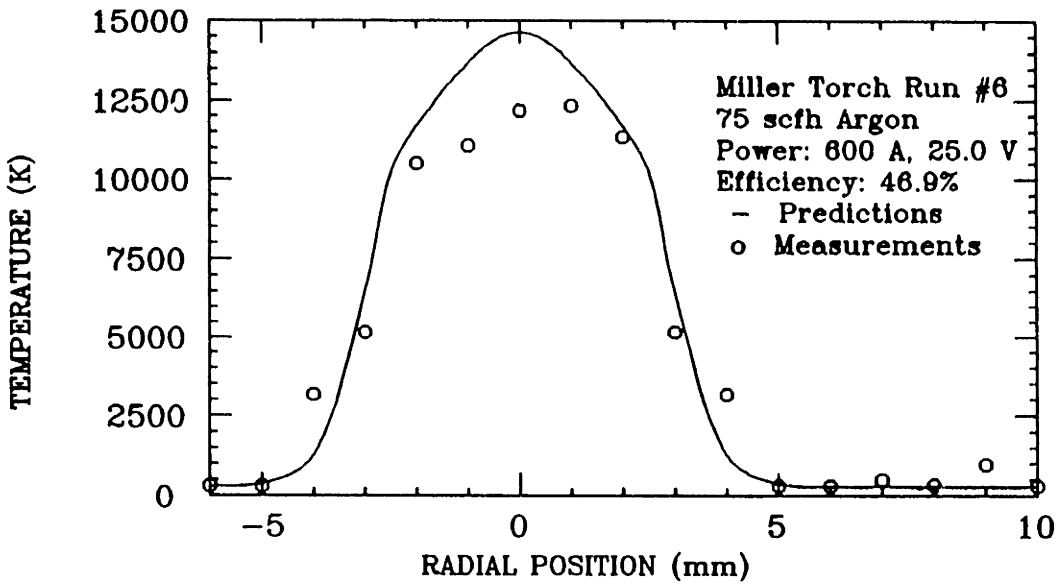

(a)

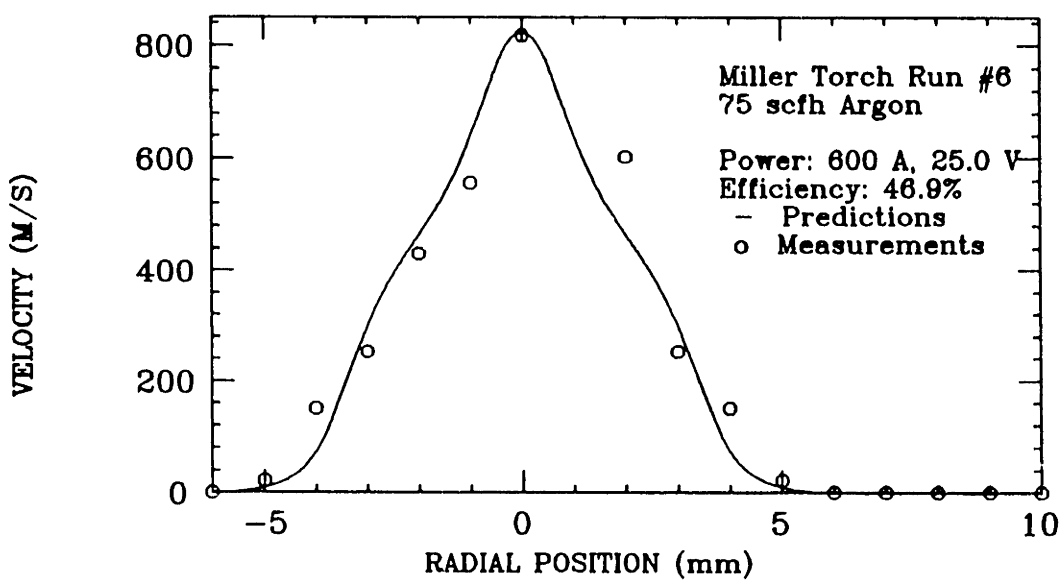

(b)

Figure IV.D.16. Comparison of the experimentally measured and theoretically predicted radial profile of temperature (a) and axial velocity (b) at a position 2 mm from the nozzle exit for the 600 amp case.

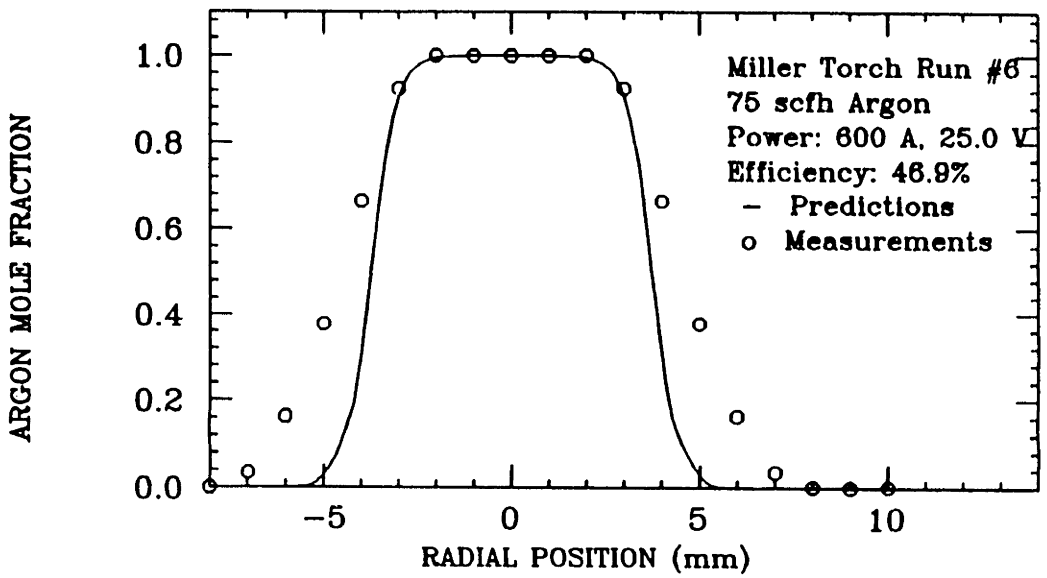

Figure IV.D.17. Comparison of the experimentally measured and theoretically predicted radial profile of argon mole fraction at a position 2 mm from the nozzle exit for the 600 amp case.

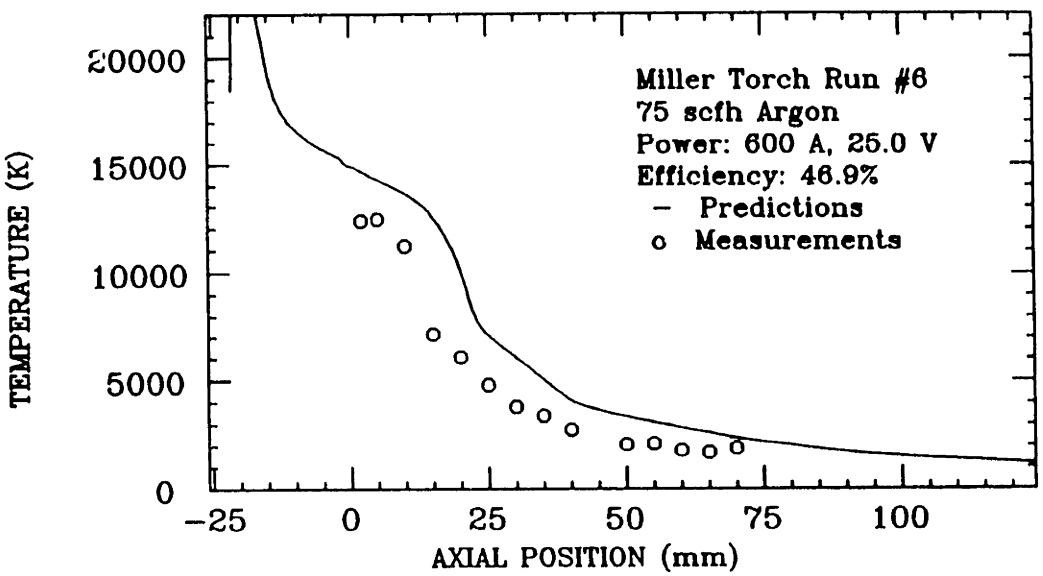

(a)

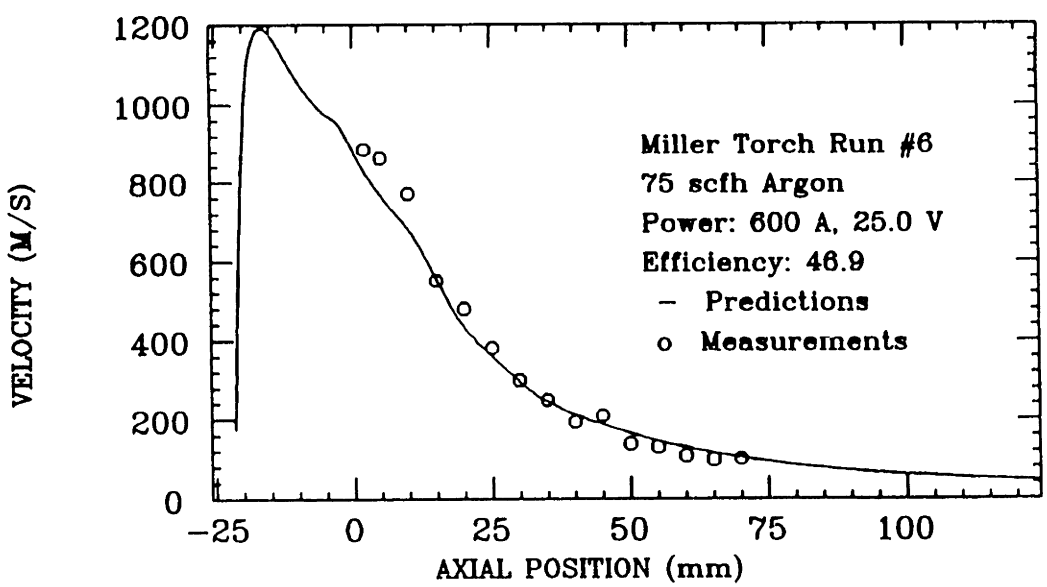

(b)

Figure IV.D.18. Comparison of the experimentally measured and theoretically predicted axial profile of the center line temperature (a) and axial velocity (b) for the 600 amp case.

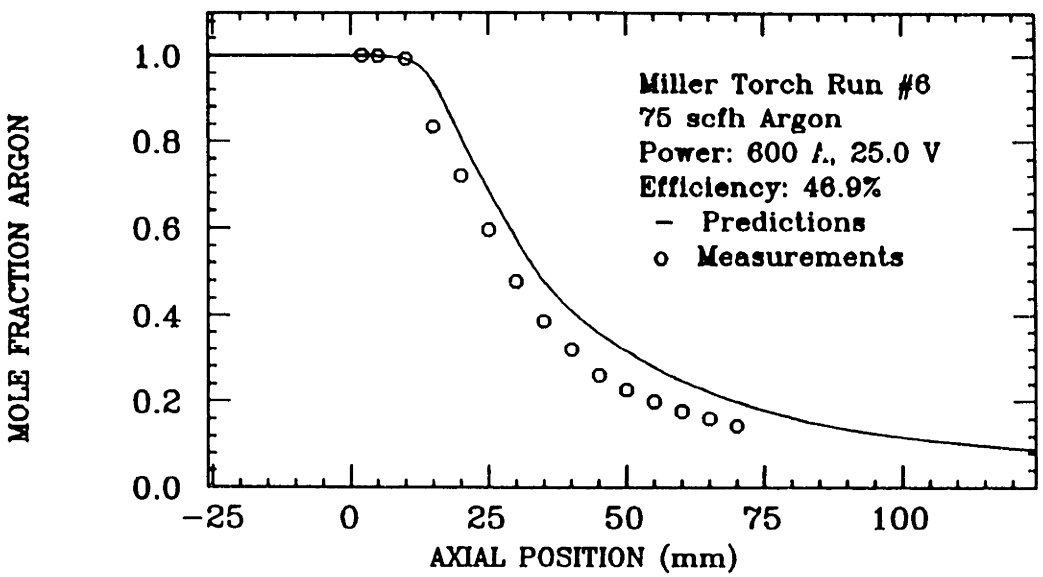

Figure IV.D.19. Comparison of the experimentally measured and theoretically predicted axial profile of the argon mole fraction on the center line for the 600 amp case.

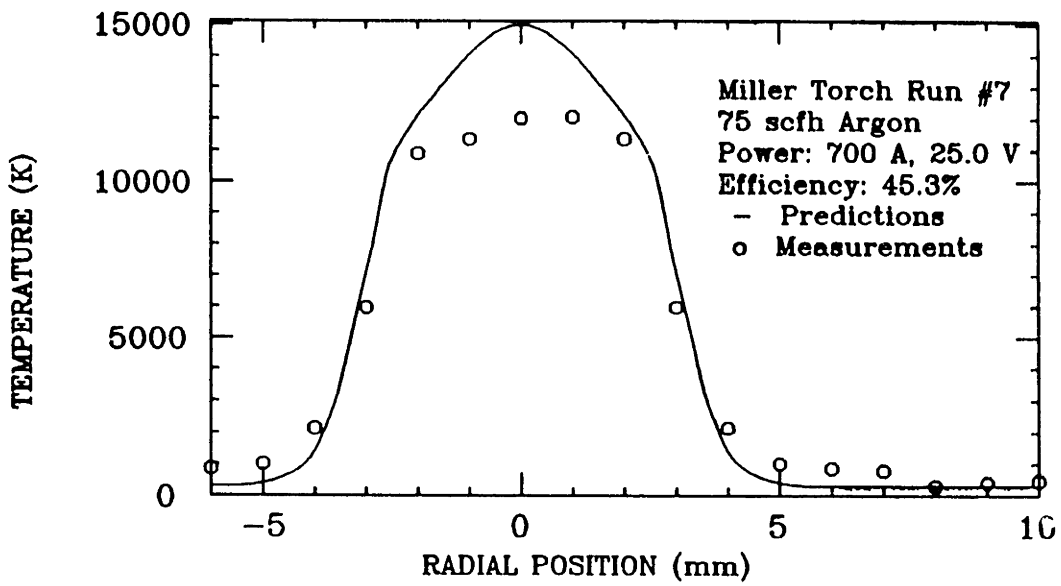

(a)

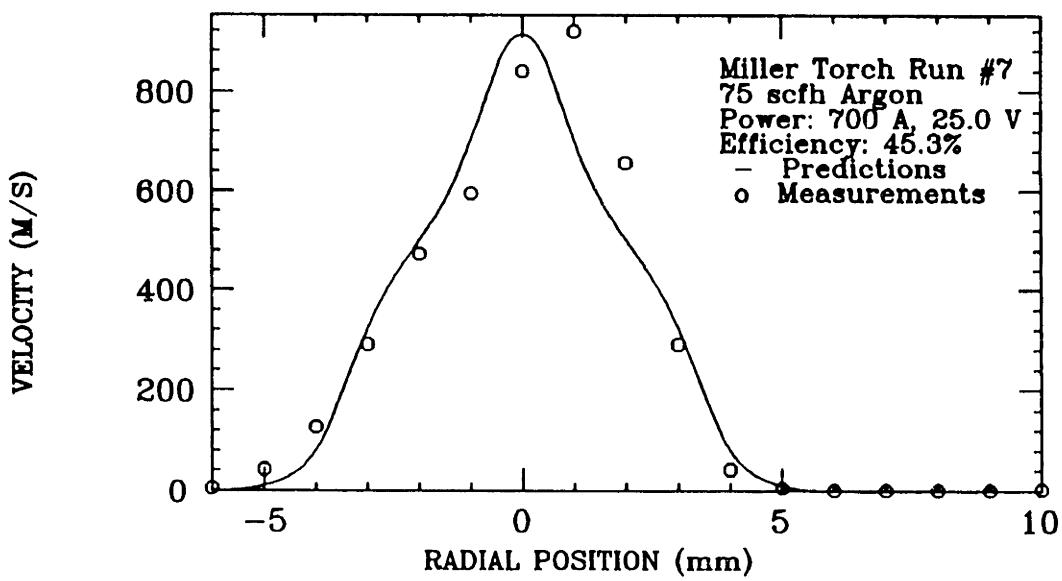

(b)

Figure IV.D.20. Comparison of the experimentally measured and theoretically predicted radial profile of temperature (a) and axial velocity (b) at a position 2 mm from the nozzle exit for the 700 amp case.

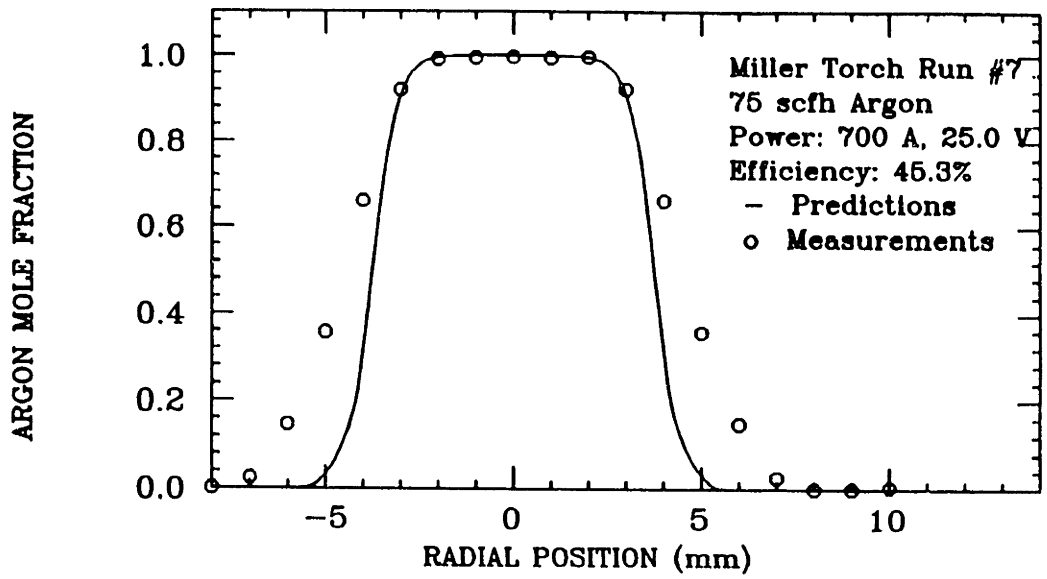

Figure IV.D.21. Comparison of the experimentally measured and theoretically predicted radial profile of argon mole fraction at a position 2 mm from the nozzle exit for the 700 amp case.

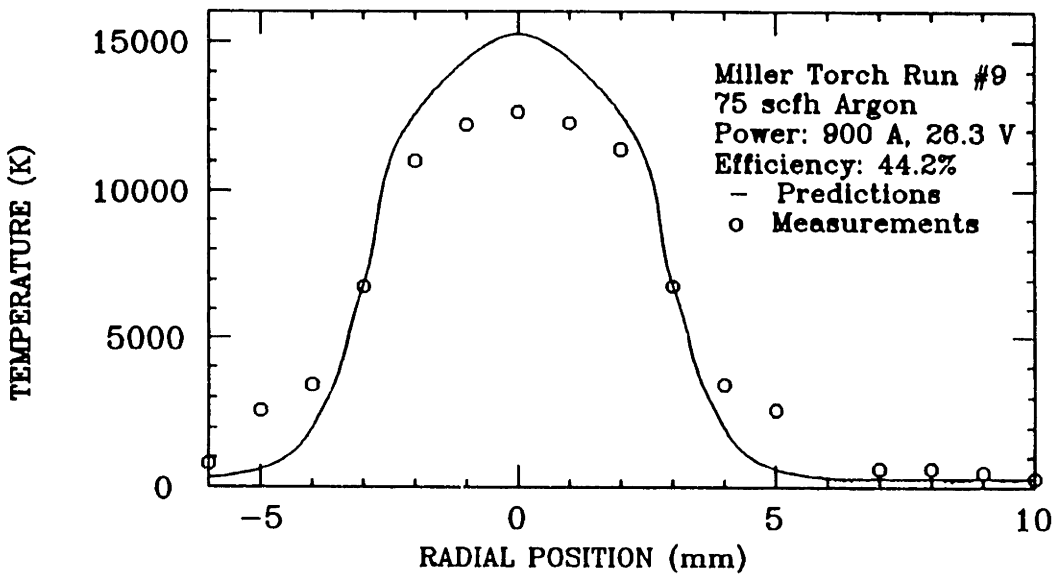

(a)

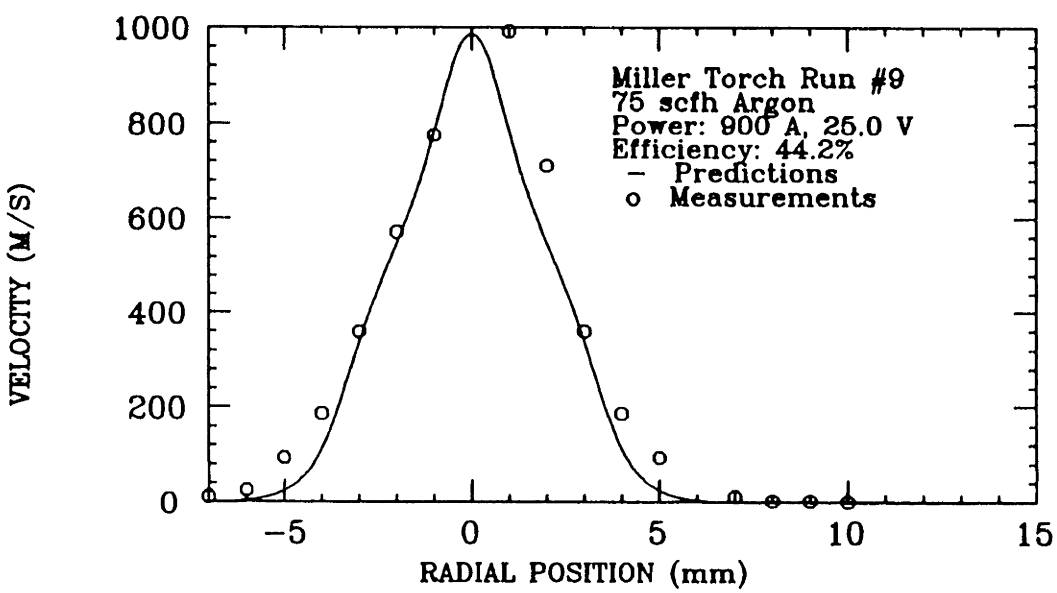

(b)

Figure IV.D.22. Comparison of the experimentally measured and theoretically predicted radial profile of temperature (a) and axial velocity (b) at a position 2 mm from the nozzle exit for the 900 amp case.

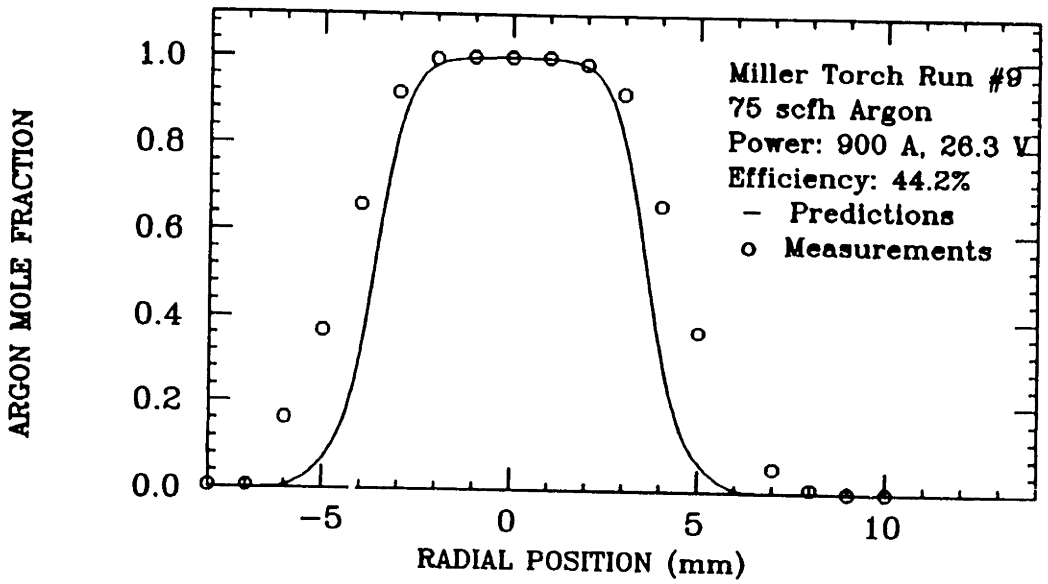

Figure IV.D.23. Comparison of the experimentally measured and theoretically predicted radial profile of argon mole fraction at a position 2 mm from the nozzle exit for the 900 amp case.

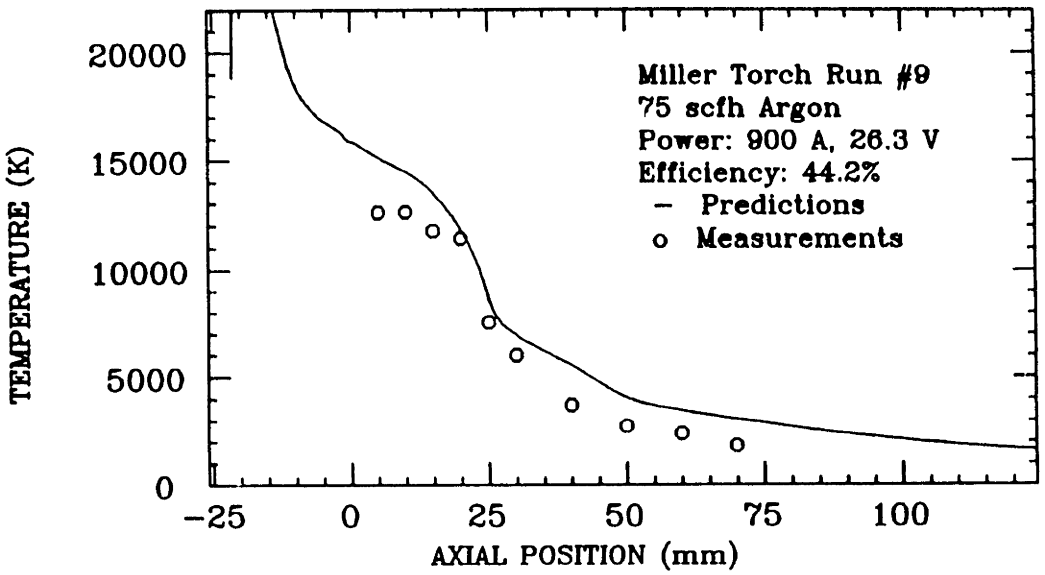

(a)

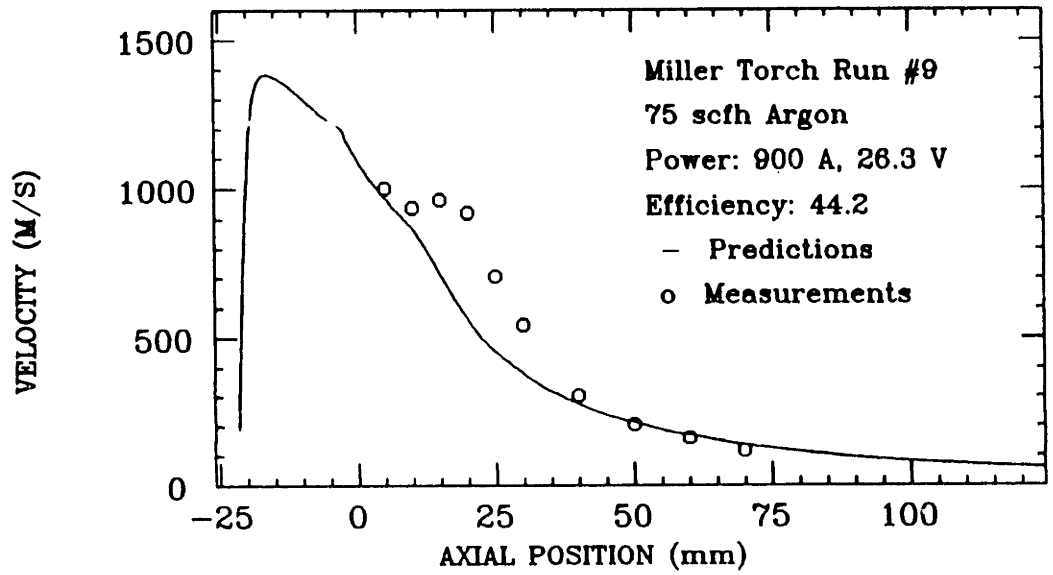

(b)

Figure IV.D.24. Comparison of the experimentally measured and theoretically predicted axial profile of the center line temperature (a) and axial velocity (b) for the 900 amp case.

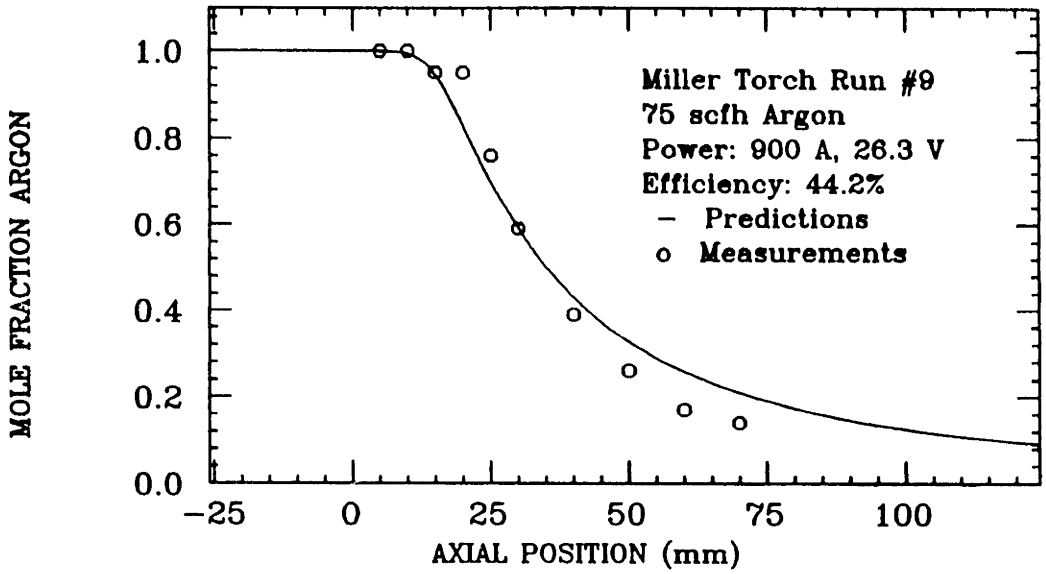

Figure IV.D.25. Comparison of the experimentally measured and theoretically predicted axial profile of the argon mole fraction on the center line for the 900 amp case.

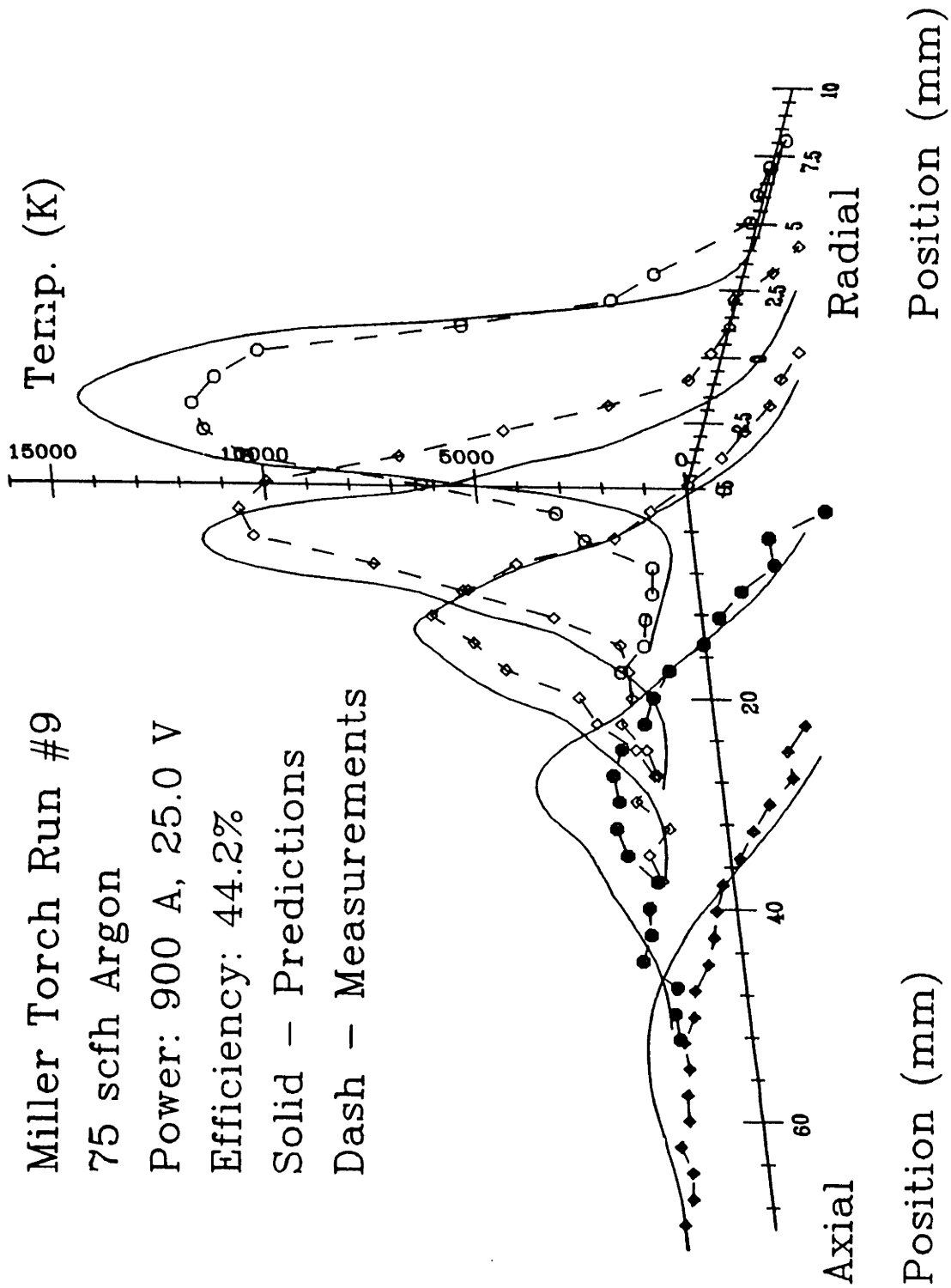

Figure IV.D.26. Comparison of the experimentally measured and theoretically predicted radial profiles of temperature at axial positions of 5, 15, 25, 40, and 60 mm from the nozzle exit for the 900 amp case.

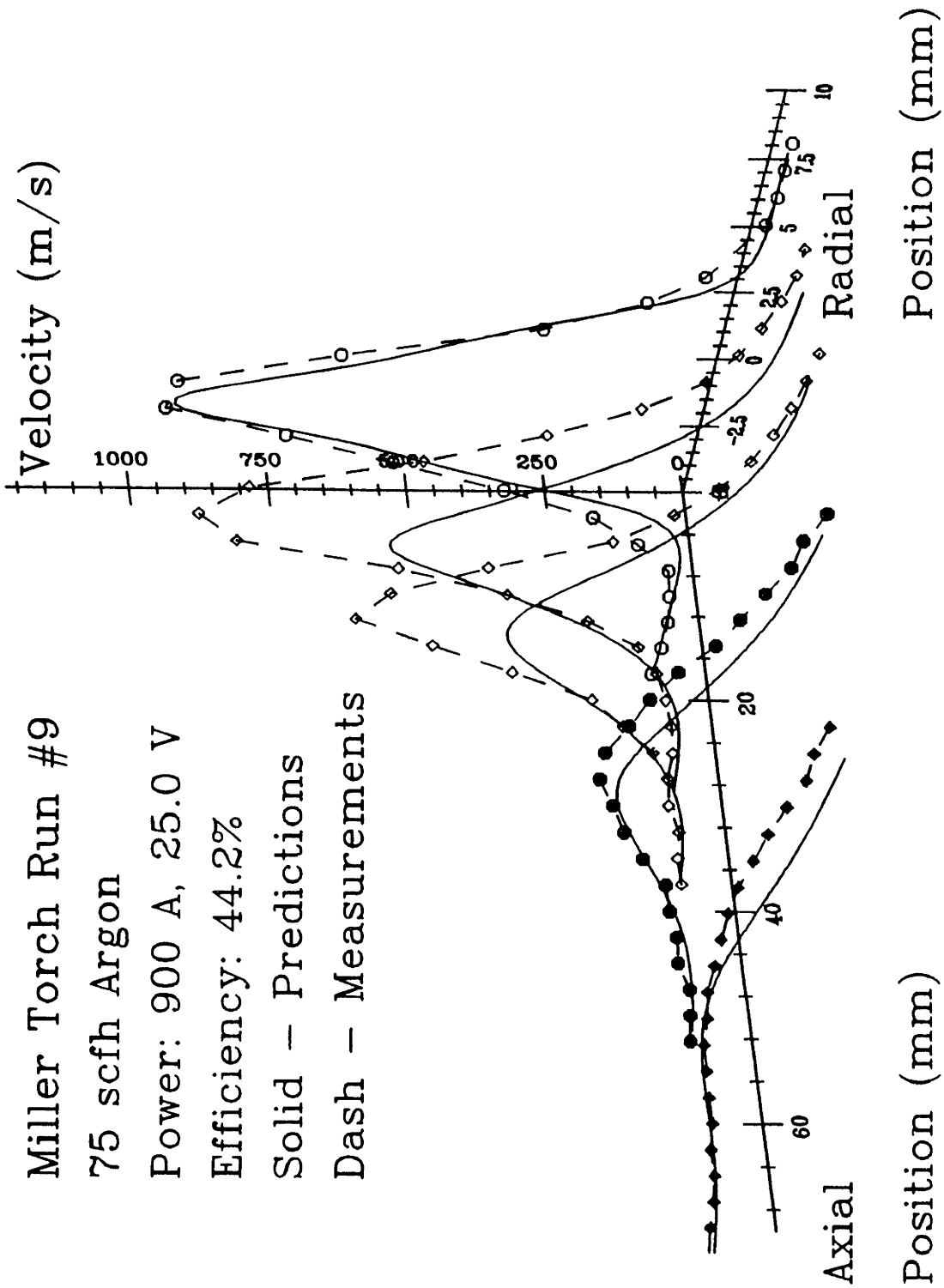

Figure IV.D.27. Comparison of the experimentally measured and theoretically predicted radial profiles of axial velocity at axial positions of 5, 15, 25, 40, and 60 mm from the nozzle exit for the 900 amp case.

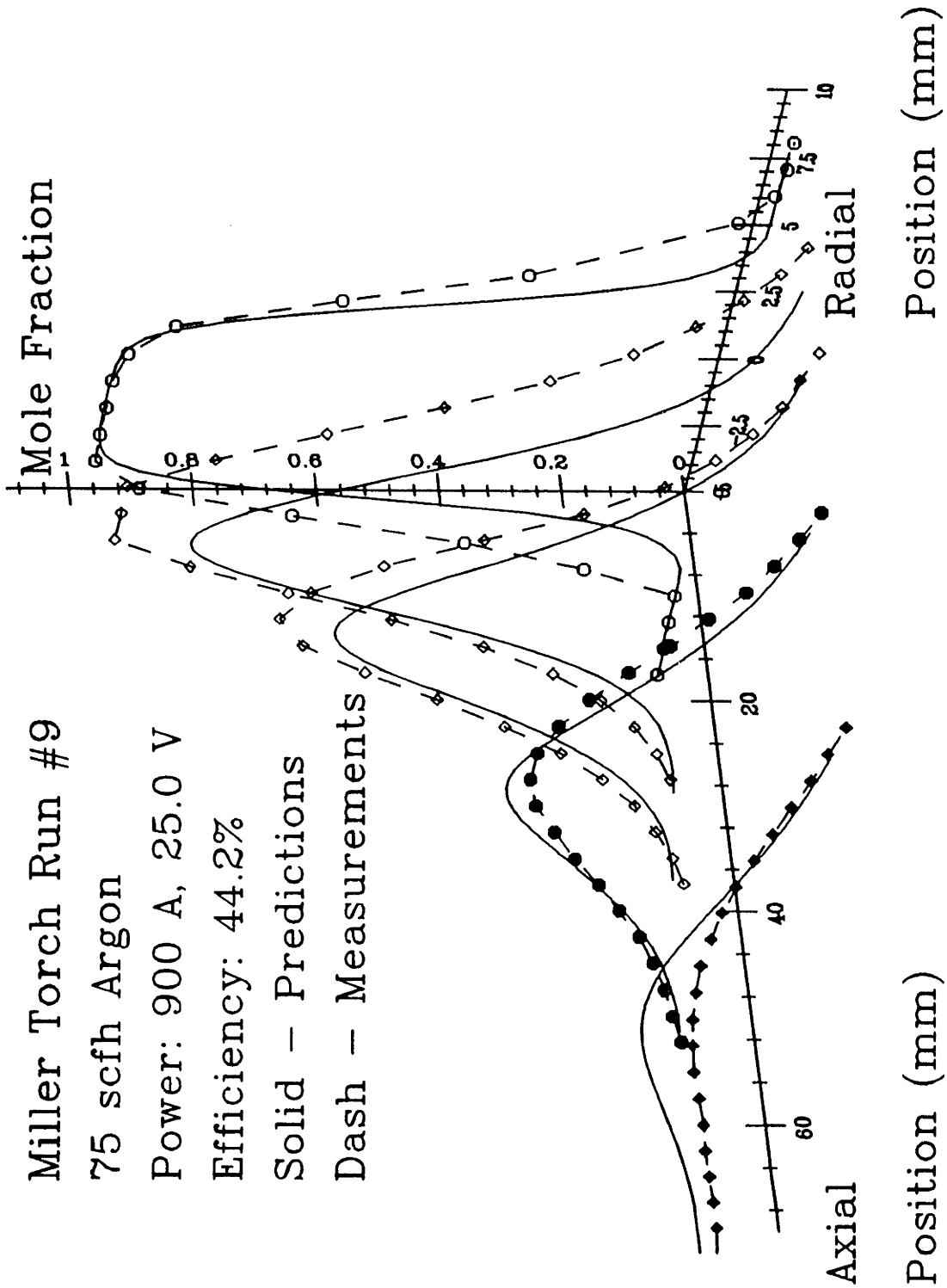

Figure IV.D.28. Comparison of the experimentally measured and theoretically predicted radial profiles of argon mole fraction at axial positions of 5, 15, 25, 40, and 60 mm from the nozzle exit for the 900 amp case.

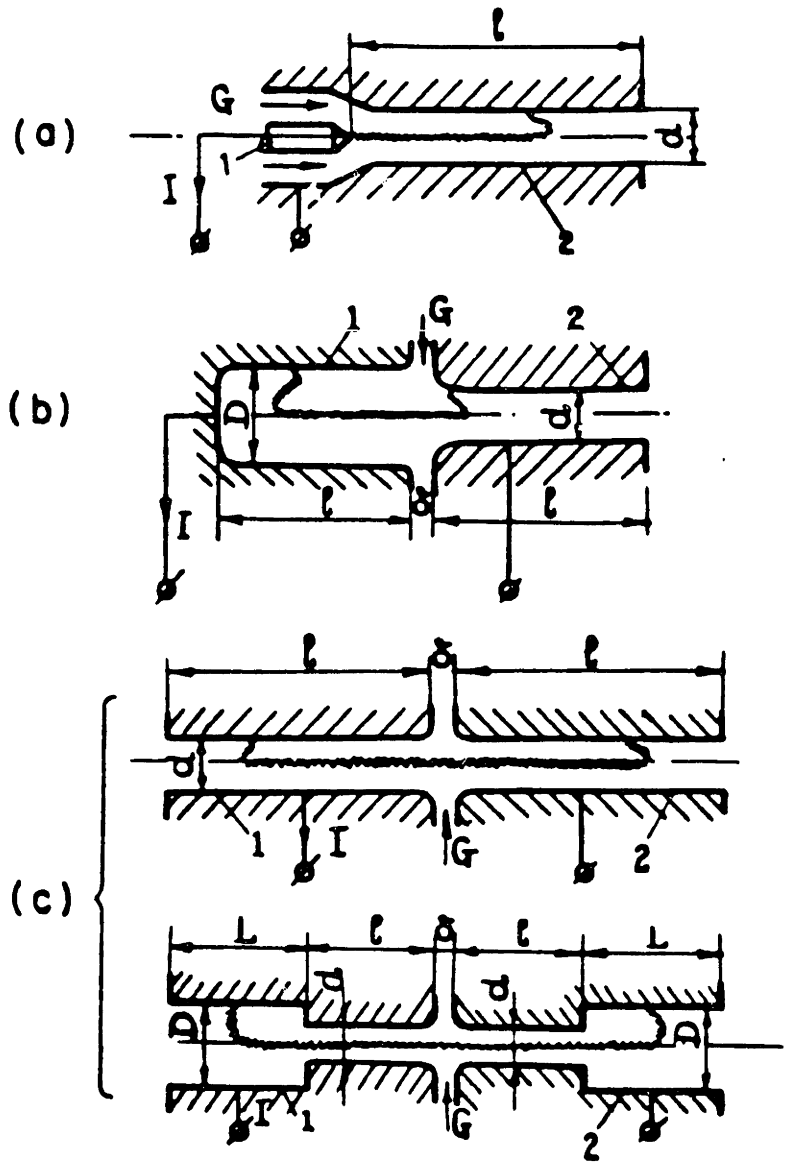

Figure IV.E.1 Schematic illustrations of arc heaters with longitudinal-vortex flow from Shaskov et al.:
(a) one-sided outflow, refractory rod electrode and cooled cylindrical electrode,
(b) one-sided outflow, cooled cylindrical electrodes,
(c) dual outflow, cooled cylindrical electrodes.
(1, 2 denote the electrodes)

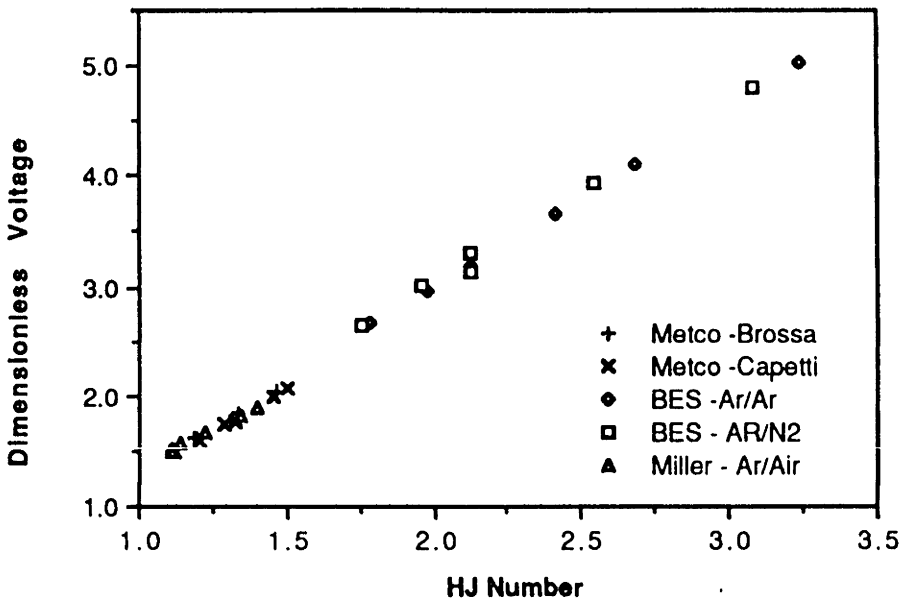

(a)

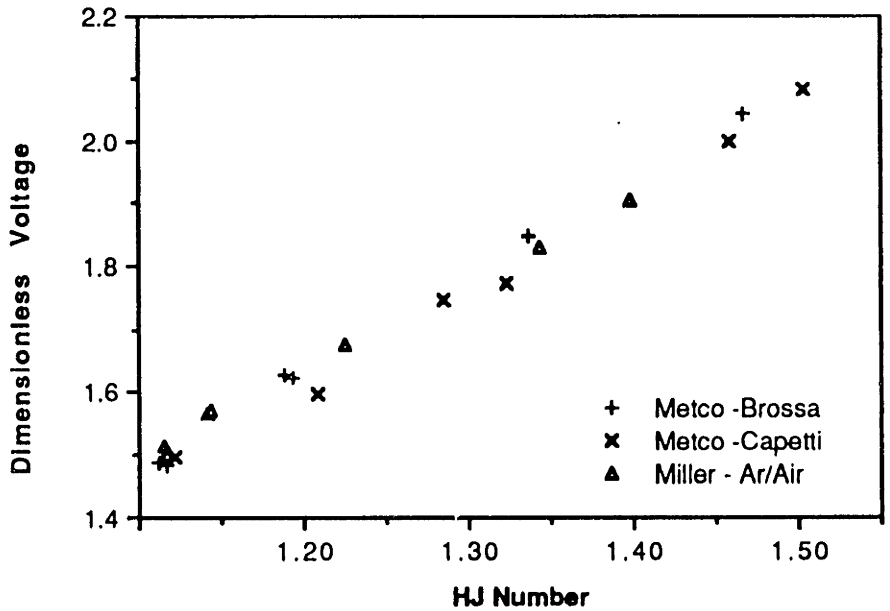

(b)

Figure IV.E.2 Voltage - current characteristics of the torches used in this study correlated using the dimensionless parameters:

Dimensionless Voltage $= \frac{VD\sigma}{I}$, HJ Number $= \frac{\dot{m}D\sigma h}{I^2}$

(a) all cases combined, (b) high gas flow cases.

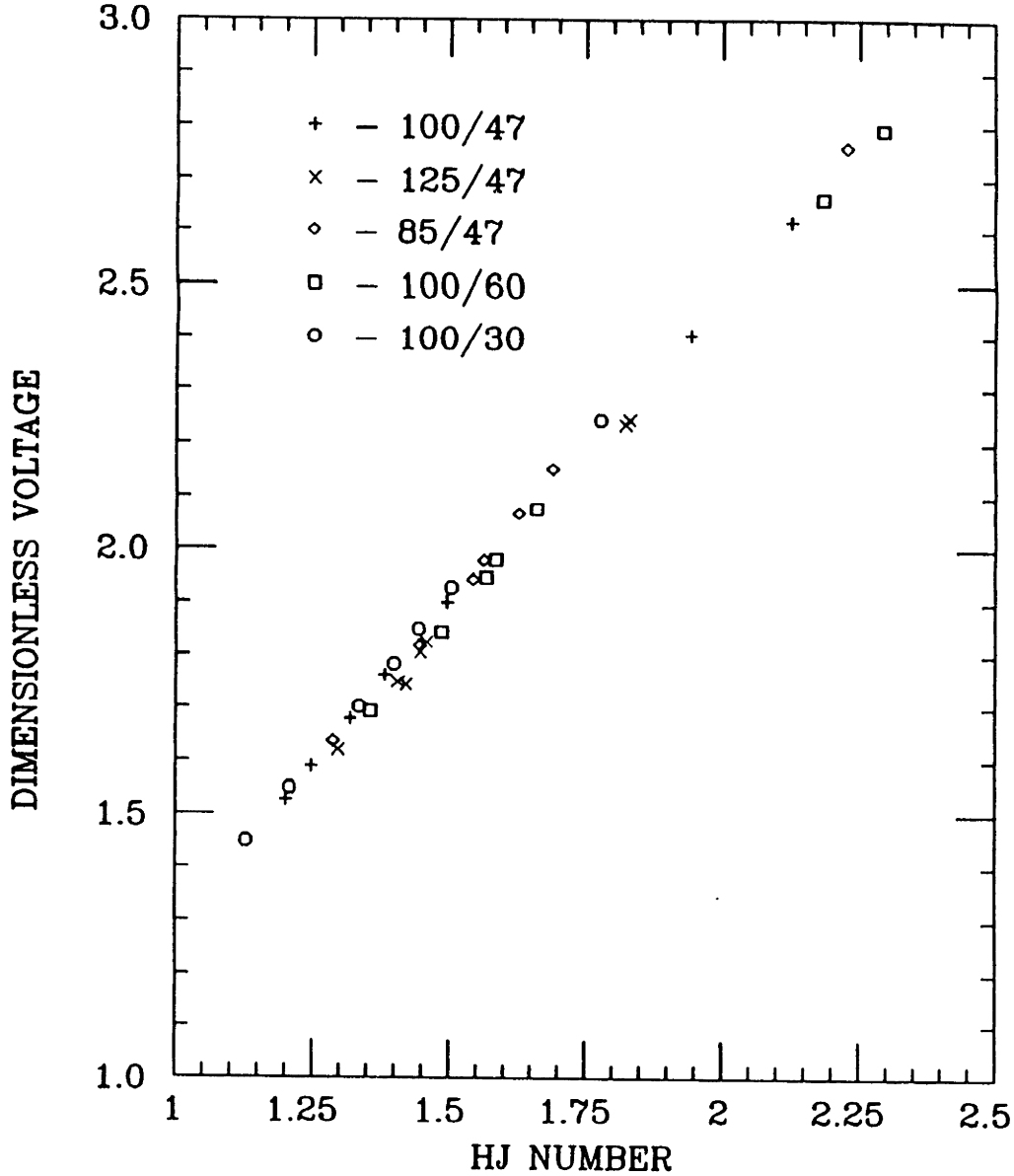

Figure IV.E.2(c) Voltage - current characteristics of the Miller torch operating with mixtures of argon and helium (labels denote the flow of argon/helium respectively in scfh) as the working gas (Table IV.D.V), correlated using the dimensionless parameters:

$$\text{Dimensionless Voltage} = \frac{VD\sigma}{I}, \quad \text{HJ Number} = \frac{\dot{m}D\sigma h}{I^2}$$

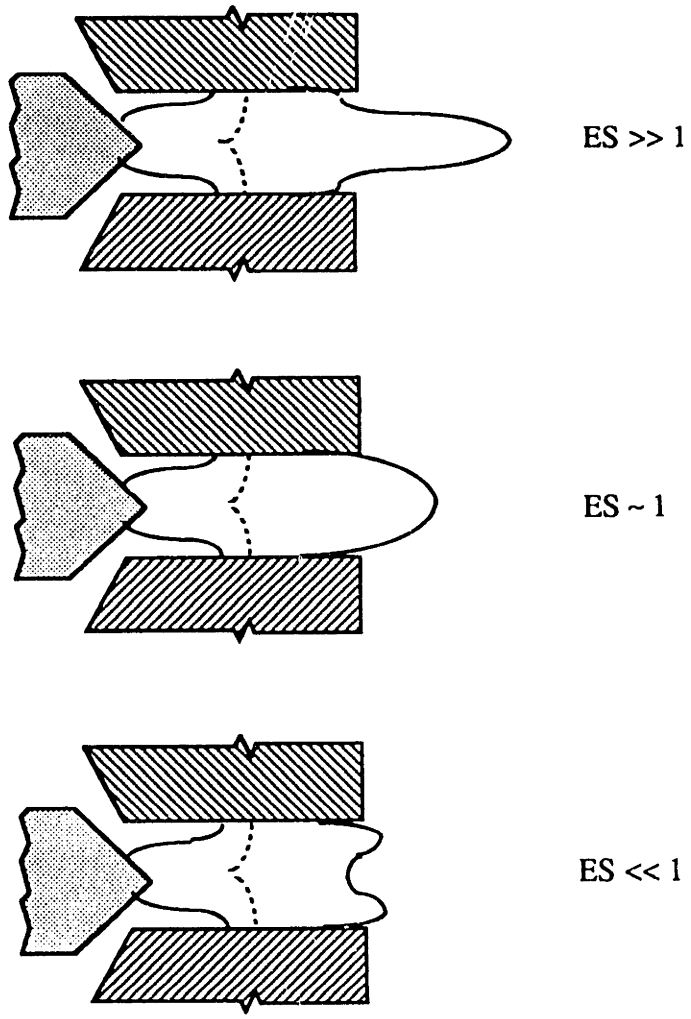

Figure IV.E.3 Schematic illustration of the effect the ratio of electromagnetic forces to the swirl momentum forces (as indicated by the ES number) has on the velocity profiles in the torch.

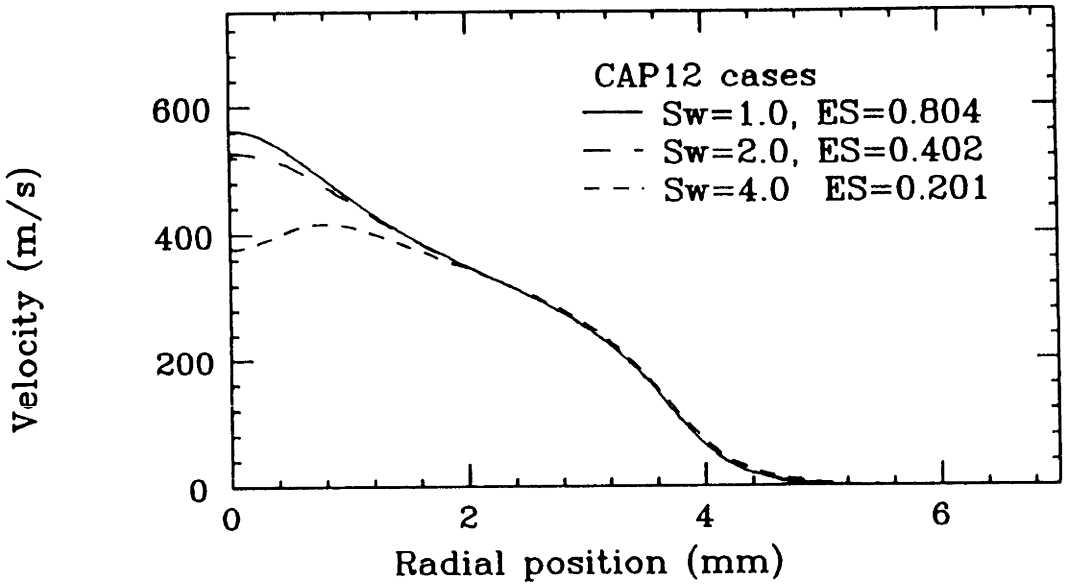

(a)

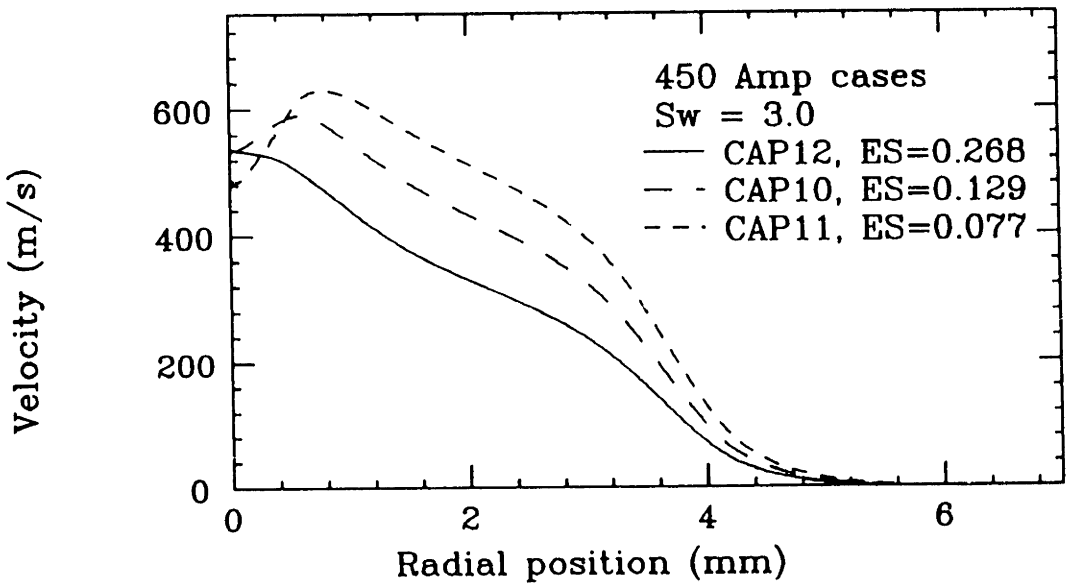

(b)

Figure IV.E.4 Calculated radial profile of the axial velocity taken 1 mm from the torch exit, showing the effect of the ES number for (a) increasing inlet swirl numbers (b) increasing flow rates. (Gas flow: CAP12 - 7.01e-4 kg/sec, CAP10 - 1.05e-3 kg/sec, CAP11 - 1.40e-3 kg/sec)

CHAPTER V. MODELING OF PLASMA SPRAYING

V.A. PARTICLES IN THE SIMPLIFIED TORCH-PLUME MODEL

V.A.1. INTRODUCTION: MATHEMATICAL MODELING OF PLASMA-PARTICLE INTERATIONS

In this first section on plasma spraying the author will present a recently published paper[32] which documents work done in collaboration with Dr. Gerardo Trapaga-Martinez, and Professor Julian Szekley. This work addresses particles injected inside the nozzle of a Miller Plasmadyne torch operating with a mixture of argon and helium, based on the simplified model of the plasma torch as presented in Chapter II. The work presents a brief literature summary, a verification of the particle dynamics model based on previously published experiments regarding particles in a room temperature air jet and then addresses the actual plasma spraying system and the so-called "plasma" effects on particles.

It is is with a great deal of pleasure that I acknowledge the work of Dr. Trapaga on this section, as this work was among the most interesting and enjoyable I participated in during my time at MIT.

A great deal of work has been done on the modelling of plasma-particle interactions in recent years and many significant milestones have been reached. Some examples include the following:

- Calculation of the plasma velocities and temperatures in a plasma plume as a basis for particle models.[1-5]
- Presentation of the particle equations of motion and analysis of the Basset history term.[6-9]
- The effect of variable plasma properties in the particle boundary layer on drag coefficient and heat transfer coefficient.[6-7,10-13]
- Evaporation and vaporization effects on particle momentum and heat transfer.[13-16]
- The effects of deviations from continuum behavior (Knudsen effects).[17-18]
- The effects of internal heat conduction in the particle.[15,19,20]
- Coupling between plasma and particles in dense loading conditions.[21]

Despite these and many other efforts over the past years, a fully unified description of the interaction between injected particles and plasmas has not yet been presented. Experimental information concerning velocities, temperatures, trajectories, and particle sizes is still needed. Modeling efforts in plasma systems make use of parameters derived from empirical correlations which may not be applicable to plasma systems. In addition, vaporization and non-continuum phenomena require more study.

To test the description provided by plasma-particle interaction models a comparison with careful experimental measurements is needed. The work presented in this section includes a single particle model for the calculation of velocities, trajectories, and thermal histories of the particles. This model has incorporated the results from another computer code (developed in this laboratory), which calculates the fluid flow and thermal characteristics of the plasma jet. In this formulation, allowance has been made for non-continuum effects, for particle vaporization, and for temperature gradients within the particle. The theoretical predictions are compared with experimental measurements obtained from two different sources, namely experimental data reported by Lesinski et al.[22] for the injection of alumina particles into a room-temperature turbulent air jet; and simultaneous measurements of the temperature, size, and velocity of alumina particles in a non-transferred plasma jet (with the injection being from inside the torch). This second source consists of work described in earlier publications.[23-24]

V.A.2. MATHEMATICAL MODELING WORK

As the physical phenomena involved in plasma-particle interactions are quite complex, it is useful to briefly describe them and to point out the various mechanisms which may control the momentum, heat and mass transfer. The important phenomena are schematically illustrated in Figure V.A.1, and include those which affect the particle momentum (drag force, boundary layer history, non-continuum effects), thermal history (convection, radiation, evaporation, vaporization, intra-particle conduction, melting, solidification, non-continuum effects) and mass transfer (evaporation, vaporization, transport of vapor across the particle boundary layer).

The mathematical modelling work included in this section describes the following:

- Fluid flow and thermal characteristics of the plasma jet (in the absence of particles)
- Particle velocity and trajectory

- Plasma/particle heat and mass transfer

V.A.2.a Fluid flow and thermal characteristics of the plasma jet

Any calculations of particle behavior in a plasma plume must be based on either experimentally measured or calculated information concerning the conditions present in the plasma plume. Figure V.A.2 is a sketch of the model used to describe the plasma plume, which it may be seen assumes uniform heating in an idealized arc volume within the torch. The heated plasma is forced out of the nozzle, expanding and simultaneously entraining ambient gas from its surroundings.

The description of heat and fluid flow phenomena in the plasma has been extracted from the research in the mathematical modeling of thermal plasmas described in Chapter II which has resulted in a computer code that has been the main tool used in a series of published studies on the behavior of plasma jets.[2-4, 25-26] Applying the results of this code for the plasma jet, a model has been developed to calculate the particle trajectories, heat and mass transfer.

V.A.2.b Particle velocity and trajectories.

The trajectories of single particles can be readily calculated if the flow conditions in the plasma jet are defined and if it is assumed that the presence of the particles does not disturb the plasma flow field. The motion of the particles can be calculated from the Basset-Boussinesq-Ossen equation,[27] which is written in a 2-D form for the case of a non-swirling system, as:

$$\frac{dU_p}{dt} = -\frac{3}{4}\frac{\rho}{\rho_p}\frac{C_D}{D_p}\left(U_p - U\right)U_R - \frac{9}{\rho_p D_p}\sqrt{\frac{\mu\rho}{\pi}}\int\frac{\frac{d}{dt'}\left(U_p - U\right)}{\sqrt{t-t'}}dt' + \sum F_z \qquad [V.A.1]$$

and

$$\frac{dV_p}{dt} = -\frac{3}{4}\frac{\rho}{\rho_p}\frac{C_D}{D_p}(V_p - V)U_R + \sum F_r \qquad [V.A.2]$$

where the subscript p is used to denote the particle, U and V represent the velocity components in the axial and radial directions, ρ is density, μ is viscosity, C_D is the drag coefficient, D_p is the particle diameter, and F_r and F_z represent other forces affecting the particle motion such as gravity. The relative velocity between the particle and its surrounding is given by:

$$U_R = \sqrt{(U - U_p)^2 + (V - V_p)^2} \qquad [V.A.3]$$

In equations [V.A.1] and [V.A.2], the first term on the right-hand side is the drag force acting on the particle. The second term in equation [V.A.1] is the Basset history term representing the time dependent nature of the boundary layer around the particle. This term is presumably needed since, for plasma systems, particle residence times are comparable with boundary layer relaxation times.

In the high velocity flows considered in this paper, the forces of gravity and buoyancy are negligible when compared to the drag force. The steady state drag coefficient or friction factor for constant property, viscous flows is a function of the Reynolds number, Re, based on the relative velocity. A number of semi-empirical relations exist in the literature to determine the value of C_D, most of which give essentially the same result, so a simple expression proposed by White[28] was adopted:

$$C_D = \frac{24}{\mathrm{Re}} + \frac{6}{1 + \mathrm{Re}^{1/2}} + 0.4 \qquad [V.A.4]$$

where Re is the Reynolds number based on the relative gas velocity. The drag coefficient has been corrected to account for non-continuum effects as described in Section V.A.2.c.

The temperature dependence of properties was represented using mean integrated values of the plasma properties across the boundary layer surrounding the particle, evaluated as:

$$\overline{\Phi}_f = \frac{1}{\left(T_f - T_s\right)} \int_{T_s}^{T_f} \Phi dT \qquad [V.A.5]$$

where Φ represents density, viscosity and thermal conductivity, k, and $\overline{\Phi}_f$ is the average property between the bulk fluid temperature, T_f, and the particle surface temperature, T_s.

V.A.2.c Plasma/Particle heat and mass transfer

Heat transfer between the plasma and the particles is quite complex; such effects as heat conduction within the particle, together with the appropriate boundary conditions, and the effects of vaporization, evaporation, and non-continuum effects must be accounted for.

Heat conduction in the particle:

For a spherical particle with symmetric boundary conditions, heat transfer within the particle is described by the conduction equation, i.e.,

$$\frac{\partial H}{\partial t} = \frac{1}{r^2} \frac{\partial}{\partial r}\left(k_p r^2 \frac{\partial T}{\partial r}\right) \qquad [V.A.6]$$

Where r is the radial distance from the center of the particle, and H and k_p are enthalpy and the thermal conductivity of the particle, respectively, and T is the temperature at a given radius. For cases where the rate of heat transfer is not limited by conduction in the particle, the above equation can be simplified using a lumped parameter approximation in which the balance equation becomes,

$$\frac{\partial H}{\partial t} = Q' \qquad [V.A.7]$$

where Q' is the instantaneous rate of heat transfer to the solid. The criteria used to define such conditions is the Biot number, Bi, defined as the ratio of convective heat transfer in the plasma to conductive heat transfer in the particle, which determines the relative importance of heat conduction within a particle. It is usually accepted that for $Bi << 0.1$, internal conduction is relatively fast and temperature variations within the particle can be neglected so that a simplified approach can be used to calculate heat and mass transfer rates.

A more rigorous approach should include the effect of the temperature gradients within the particle. As we shall see, in plasma-particle systems large internal temperature gradients can be generated due to the very high heat fluxes, even at relatively low values of the Biot number. To treat this problem, the Fourier equation must be solved simultaneously with the motion equation, with due allowance for the melting and solidification phenomena and the temperature dependence of properties.

Boundary conditions:

The boundary conditions required to solve the problem need to specify :

- the rate of heat transfer due to convection and radiation,
- particle vaporization and evaporation,
- particle melting and solidification, and
- particle change in size due to vaporization and evaporation.

These contributions can be expressed in terms of a heat balance at the surface of the particle, i.e,

$$Q = k_p\left(\frac{\partial T}{\partial r}\right)_{r=r_o} = h\left(T_f - T_s\right) - \sigma\varepsilon T_s^4 + Q_{vap} \qquad [V.A.8]$$

where k_p is the thermal conductivity, h is the heat transfer coefficient, σ is the Stefan-Boltzman constant, ε is the emissivity, T_S is the particle surface temperature, and T_f, is the surrounding plasma temperature, and Q_{vap} is the particle energy lost by vaporization/evaporation. In addition, we have to include the symmetry condition at the axis of the particle (i.e. $\left(\frac{\partial T}{\partial r}\right)_{r=0}$=0) and the initial boundary condition given by $T_{t=o}$ = T *carrier gas*. The thermal properties of alumina particles were taken to be temperature dependent.(29)

Convection:

The convective heat transfer coefficient may be estimated from semi-empirical Ranz-Marshall type correlations, in terms of the Nusselt number, Nu. As in the case of

particle motion, a number of corrections have been suggested to make this correlation compatible with the plasma environment, e.g Lee et al.[12] for argon and nitrogen plasmas. In this work, however, we proceed in a similar way as for the drag coefficient, where mean integrated values are used to account for the temperature dependence of properties.

Vaporization:

Two steps are considered to account for the rate of mass transfer due to vaporization of the particle (for temperatures below or at the boiling point); these are the evaporation reaction at the surface of the particle (Langmuir evaporation), and mass transfer of species across the boundary layer. In this model, the vaporization of alumina is treated in an approximate way based on the experiments of Brewer and Searcy,[30] where the dominant vapor species was found to be AlO, which is assumed to be produced by the following equilibrium reaction:

$$Al_2O_{3(l)} \rightarrow 2AlO_{(v)} + O_{(g)} \qquad [V.A.9]$$

Thus, the rate of mass loss, $\dot{m}$, can be given in terms of an overall driving force and an overall mass transfer coefficient, K_{MIX}, that combines the two mechanisms mentioned above, i.e.,

$$\dot{m} = K_{MIX}\left(C_s^* - C_f\right) \approx K_{MIX}C_s^* \qquad [V.A.10]$$

where Cf is the concentration of vapor in the bulk fluid (approximately zero), C_s^* is the equilibrium concentration of the evaporating specie (AlO) at the particle surface, given by

$$C_s^* = \frac{MP_v}{RT_s} \qquad [V.A.11]$$

where M is the molecular weight of the vapor, R is the gas constant, and P_v is the equilibrium vapor pressure, which was adapted from the work in reference (30) as:

$$\log(p_v) = 12.879 - \frac{3\times10^4}{T} \qquad [Pa] \qquad [V.A.12]$$

The overall mass transfer coefficient is defined in terms of a mixed control process due to evaporation and mass transfer through the boundary layer, i.e.

$$K_{MIX} = \left(\frac{1}{h_m} + \frac{1}{h_e} \right)^{-1} \qquad [V.A.13]$$

where h_e is the rate coefficient for Langmuir evaporation and is defined as follows:

$$h_e = \alpha \sqrt{\frac{RT}{2\pi M}} \qquad [V.A.14]$$

Here, α is the sticking coefficient. The mass transfer coefficient, h_m, is deduced from another Ranz and Marshall-type correlation, i.e.,

$$h_m = \frac{\mathcal{D}}{D_p}\left(2.0 + 0.6\,\mathrm{Re}^{1/2}\, Sc^{1/3}\right) \qquad [V.A.15]$$

Sc is the Schmidt number, D is the diffusion coefficient and n is the kinematic viscosity. The diffusion coefficient of the evaporating specie in the plasma can be estimated as a function of temperature based on Chapman-Enskog theory.(31)

Thus, the rate of heat transfer due to vaporization may be given by:

$$Q_{vap} = \dot{m}\left\{ L_e + \left(H_{v(T_f)} - H_{v(T_s)} \right) + \left(H_{l(T_s)} - H_{s(T_o)} \right) \right\} \qquad [V.A.16]$$

where L_e is the enthalpy of vaporization and H is the enthalpy of alumina, and the subscripts v, l, and s, denote vapor, liquid and solid states, respectively. The first term in this equation represents the energy involved in the vaporization process itself, the middle term represents the energy required to heat the vapor from the particle surface temperature (T_s) to the film temperature (T_f), and the last term accounts for the loss of particle energy due to mass loss. We note that when the particle surface temperature is near the boiling point (3800K), the evaporation rate is then limited by the rate of heat transfer to the particle. The enthalpy of dissociation is not explicitly accounted for, except insofar as it may be represented in the data for the enthalpy of vaporization, L_e.

Non-continuum effects:

Knudsen or non-continuum effects represent another important aspect that must be considered when dealing with the behavior of fine powders ($D_p < 1$ to 30 μm) under plasma conditions, whether at atmospheric pressure or soft vacuum conditions. These are due to rarification effects in the gas, and are important in the regime ($10^{-2} < Kn < 1$), where the Knudsen number is defined as $Kn = l/D_p$ and l is the mean free path of molecules in the plasma. In essence, under such conditions "slip flow" and "temperature jump" boundary conditions have to be employed in conjunction with the continuum equations for momentum and heat transfer. The correction for the drag coefficient and Nusselt number used in this analysis were applied as prescribed by Chen and Pfender:[17-18]

$$(C_D)_{NC} = (\alpha_{KN})^{0.45} C_D \qquad [V.A.17]$$

on the drag coefficient, and

$$(Nu)_{NC} = \alpha_{KN} Nu \qquad [V.A.18]$$

on the heat transfer coefficient (Nusselt number), where the subscript NC denotes non continuum, and the Knudsen correction factor, α_{KN} is given by

$$\alpha_{KN} = \frac{1}{1 + \left(z^* / r_p\right)} \qquad [V.A.19]$$

where z^* represents a distance, proposed by Chen and Pfender, over which the plasma temperature undergoes a temperature jump. This "temperature jump approach" involves an iterative procedure in which the conduction equation is solved in terms of a heat conduction potential across the particle boundary layer. Typical numerical values of the correction factor for non-continuum effects can vary between 1.0 to 0.4, with an increase of the Knudsen number from 0.01 to 1.0.

V.A.2.c. Solution Method

In the calculation of particle trajectories and temperature histories, it is assumed that the particles do not affect the plasma velocity and temperature fields. This assumption is

reasonable for situations where the rate of injection is relatively low (e.g. 3lb/hr or 0.0004 kg/s, which is the value in the INEL experiments;[23-24] this corresponds to a volume fraction of solids in the plume of about 6×10^{-6}). In such situations, it is possible to decouple the calculation for the plasma from that for the particle dynamics and heat transfer. Thus, for a given plasma temperature and velocity field it is possible to solve the particle governing equations, using the associated boundary conditions described in the previous section. Using the lumped parameter approach, the governing equations for the particle can be solved simultaneously using a fourth order Runge-Kutta algorithm, for both the motion, and the energy equation. To solve the Fourier equation for conduction in the particle the so-called "Enthalpy method"[32-33] has been used, with an adaptive grid to account for the size change of the particle due to mass loss.

V.A.3. Computed results

Computed results will be presented for the analysis of plasma-particle interactions, where the main focus has been on the study of the different effects involved in those interactions, as well as on the comparison of predictions with available experimental information. The study is thus presented for the following two systems:

- Cold flow analysis, in which the model is applied to a previously studied isothermal system to validate the theoretical approach.
- Plasma - Particle interactions in which a rigorous representation and analysis of the problem is presented.

V.A.3.a. Cold flow analysis

In this section we model the injection of alumina particles into a room-temperature turbulent air jet; the predictions are compared with experimental data reported by Lesinski et al.,[22] in which laser doppler anemometry was used to measure jet velocities and particle velocities. A sensitivity analysis is carried out to investigate the effect of the particle size distribution and injection velocity distribution on the particle trajectories in the turbulent jet. Results and comparisons are presented for for the two mean particle sizes reported by Lesinski (i.e. 13.7 and 97 μm). The calculations presented here are based on the experimental setup they used which is illustrated in Figure V.A.3, which also gives the parameters used in this study. In discussing the results with reference to this figure the direction X will be referred to as the radial direction.

The computational domain and the calculated gas velocities for the air jet are given in Figure V.A.4, while Figure V.A.5 shows a comparison between experimentally measured and theoretically predicted radial profiles of axial velocity at six axial positions along the air jet. A comparison between the experimentally measured and theoretically predicted axial velocity profile along the jet centerline is represented in Figure V.A.6. Figures V.A.5 and V.A.6 show that the agreement between the experimental values and the theoretical predictions for the jet is indeed quite good.

Comparisons of the measured mean particle velocities with those predicted numerically are given in Figures V.A.7 and V.A.8 as a function of the radial position at four different axial locations, for mean particle diameters of 97 and 13.7 μm, respectively. The theoretical results shown in these figures involve a range of particle diameters of 6 μm above and below the mean diameter, and a range of particle injection velocities between 2 and 8 m/s. It is seen that while the agreement for the 97 μm particles is excellent, for the small diameter particles it is not so satisfactory, particularly in the region close to the nozzle exit. It is clear that the small particles are confined on the side of injection, while the large particles are more widely dispersed.

A different representation of this phenomena is shown in Figure V.A.9(a) and V.A.9(b) which illustrates the predicted trajectories of the particles in the *Z-X* plane. It is readily apparent that the smaller particles are unable to completely penetrate the jet resulting in a narrow dispersion, while the larger particles pass through the axis of the jet, and are more broadly dispersed.

To study the effect that the radial velocity component of the jet has on the trajectory of the particles, a set of calculations was carried out assuming a radial gas velocity of zero and the corresponding results are presented in Figures V.A.10 and V.A.11, for the two different particle sizes. The main issue here is the relative importance of the radial gas velocity, compared to the initial injection velocity, and the resulting effect on the particle trajectory. It is also interesting that Lesinski et.al. only measured the axial velocity component of the gas and this may result in a significant error in the measured particle velocities which they calculated, especially in the the vicinity of the injection port and at the nozzle exit. As seen in Figure V.A.10, the behavior for the large particles is hardly affected by the radial gas velocity, and the agreement with the experimental data remains quite good. In contrast, it can be seen in Figure V.A.11 that a different behavior is

observed for the smaller particles when the radial velocity components are not included in the calculation. This change in behavior is more marked for the regions close to the nozzle exit and injection port; the difference may be seen by comparing with the previously shown results of Figure V.A.8.

Since the turbulent dispersion of particles due to fluctuating velocity components in the flow was not accounted for in the model, it has been suggested that this may be the cause of the observed disagreement between the measurements and predictions for the small particles seen in Figures V.A.8 and V.A.11. In order to investigate this, and further validate our model, a commercial code, FLUENT, which can calculate the turbulent dispersion of particles using a stochastic model,[34] was used to track the particles in the turbulent air jet. The results of these calculations are essentially the same as those shown in Figure V.A.11, whether turbulent dispersion is included or not.

The reasons for the observed difference between measurements and predictions is not clear. The model includes several simplifications, for example: the k-ε model assumes time averaged isotropic turbulent flow, the model uses empirical correlations which may be questioned for small particles, and the initial conditions of the particles are uncertain. On the other hand, some experimental effects may be responsible for the rather wide dispersion of particles observed experimentally. It is suggested that, as the air jet used in reference[22] was enclosed, that some small particles may have been unintentionally recirculated within the chamber. These particles could have been entrained into the jet , resulting in the wide dispersion observed experimentally.

V.A.3.a. Plasma - particle interaction analysis

In this section, results are presented for the injection of alumina particles into an Ar-He plasma jet. The predictions are compared with experimental measurements obtained at INEL[23,24] for the velocity and temperature of alumina particles of 35 μm mean diameter. The objective here is to analyze the different factors that affect the particle behavior in this particular operation.

The schematic of the commercial non-transferred plasma torch represented in this study is shown in Figure V.A.12, together with the operating conditions. As shown in the figure, alumina powders are injected into the plasma jet from inside the torch. The

particles then travel through the nozzle into a chamber containing air at atmospheric pressure.

Figure V.A.13 compares the experimentally measured and theoretically predicted temperatures along the axis of the turbulent Ar-He plasma jet. The corresponding comparison between the measured and calculated radial temperature profiles at different distances from the torch tip is shown if Figure V.A.14. Here, in contrast to the previous figure, the agreement observed is not very satisfactory, particularly since the experimental profiles remain flat for a given axial location, which is not the behavior represented theoretically. The agreement shown in the comparison, while not completely satisfactory, is reasonable considering the simplifications in the model (e.g. assumptions about the arc, turbulence and the Ar/He mix), as well as the difficulties in making the temperature measurements (e.g. the effect of mixing with air and the assumption of Local Thermodynamic Equilibrium, LTE, as well as the limitations on measurable temperature range).[35] The LTE assumption, in particular, has been questioned in making spectroscopic temperature measurements.

Figure V.A.15 shows a comparison between the measured and calculated velocities and temperatures for the plasma and particles along their trajectories. The plots illustrate a similar behavior for the two particle sizes. It is seen in Figure V.A.15 (a) that the particles are initially accelerated, reaching a maximum velocity of about 350 m/s, and then decelerate at a slow rate. The particle velocities are over predicted by about 30% compared to the experimental data. The corresponding plasma and particle thermal histories (particle surface temperature) are represented in Figure V.A.15 (b) together with the experimental data. A similar trend is shown for the particle thermal histories, with a high initial heating rate, and a maximum particle surface temperature between the melting and boiling temperatures (i.e. ~2900 K). The predicted particle temperatures are only about 19% higher than the experimental values. It was seen that the history term in the equation of motion did not produce a significant effect on the particle trajectory and thermal history, and so could be neglected.

Predicted particle trajectories in the plasma jet are shown in Figure V.A.16 for the two particle sizes. The observed particle displacement in the radial direction is only a few mm (comparable to the diameter of the nozzle), after the particles have travelled an axial distance of 200 mm. It is also interesting to note that the particles cross the axis of the jet, at an axial distance from the injection position of about 100 mm.

Also important in the prediction of particle temperatures in a plasma system is the internal temperature gradient within the particles. A common approach is to neglect those gradients and to calculate temperature histories based on a lumped parameter model, since the typical Biot number is usually quite small in such plasma-particle systems (Bi ~.01 - .06). Figure V.A.17 compares results of particle temperature histories calculated using a lumped parameter model, with those obtained by the enthalpy method in which internal particle temperatures are calculated. It is seen that very large temperature differences between the particle center and surface are obtained by the enthalpy approach, although the mean temperature is quite close to the one obtained by the lumped parameter model. The maximum temperature differences are as high as 770 K for 35 μm particles and 625 K for 27 μm particles. The important implication is that higher temperatures will be reached at the particle surface than can be predicted by a lumped parameter model. This may lead to unrealistic predictions of the effects of particle vaporization by the lumped parameter model, resulting in poor comparison with experiments.

Further analysis determined the limiting factors controlling evaporation phenomena in plasma-particle systems. Figure V.A.18(a) shows the mass transfer coefficients due to Langmuir vaporization, diffusion mass transfer, and the two combined (overall); the vaporization process in this system is controlled by both mechanisms during the particle heating period, and then is governed by mass transfer across the boundary layer once the plasma temperature drops. Figure V.A.18 (b) shows the calculated evaporation rates and change in particle diameters, corresponding to this analysis.

In a different set of calculations the effect of vaporization and non-continuum effects on particle velocities and temperatures were investigated for a particle 27 μm in diameter. Figures V.A.19 (a) and V.A.19(b), illustrate such effects by comparing four different conditions:

- A limiting case in which non-continuum effects were neglected, as was the heat flux contribution due to particle vaporization. This hypothetical case establishes the maximum surface temperature of the particle along the plasma jet, for the purpose of comparison with the other cases.

- A situation in which the heat flux from vaporization was neglected in the calculation.

- A situation in which non-continuum effects were neglected in the calculation.

- A rigorous calculation in which both effects (vaporization and non-continuum effects) were taken into account.

A comparison of Figures V.A.19(a) and V.A.19(b) shows that vaporization and non-continuum effects have a stronger effect on the particle surface temperature than on its velocity (i.e. the heat transfer coefficient is more sensitive to these effects, than the drag coefficient). Moreover, the correction factors due to non-continuum effects represent the dominant effect.

V.A.4. Discussion and Conclusions

A complete mathematical representation has been presented for the interaction of a non-transferred plasma jet with particles injected inside the torch. This is the first work (to our knowledge) that has modelled the particles from inside the torch. As particle injection is often done in this way the knowledge of phenomena in the nozzle is very important. In the formulation, allowance was made for non-continuum effects, particle vaporization, and temperature gradients within the particles.

Particular attention was given to validating the theoretical model by comparing the predictions with experimental measurements available for two specific systems:

- A system for alumina particles injected into a turbulent, room temperature air jet.
- Alumina particles injected into an Ar-He plasma jet.

For the air jet it was found that:

- For small particles, the radial component of the gas velocity is important in determining the particle trajectory.
- The agreement between the model and the measurements was quite good for the larger particles, but not as satisfactory for the smaller ones.
- Turbulent dispersion of the particles due to fluctuating velocity components did not significantly affect the axial velocity distributions of the particles.

For injection of alumina particles into an argon/helium plasma jet in an air atmosphere:

- Particle velocities were overestimated by a maximum of 37%.
- Particle temperatures were overestimated by a maximum of 20%.
- Vaporization effects can be significant for small (25 μm) particles
- Temperature differences within a particle can be quite large (~ 750 K)

In addition, the importance of a number of issues has been emphasized by this work. These include the following:

- Further refinement of the plasma torch and plume model is needed.
- A better representation for the enthalpy of alumina vapor at plasma temperatures is needed.
- An allowance needs to be included for the effect of vaporization/evaporation on the drag coefficient.
- Investigations into non-equilibrium effects in the boundary layer surrounding the particle are needed.
- More experimental data is needed on the temperatures and velocities of both the plume and the particles.
- Injection is critical in determining both temperature and velocity of the particle- this needs to be studied more.
- The knowledge of the radial velocities in the plume may be very important in determining the particle trajectories. This emphasizes the importance of knowing both the axial and radial components of velocity.

V.C. REFERENCES

1. J. McKelliget, J. Szekely, M. Vardelle and P. Fauchis, Plasma Chem. Plasma Proc., **2**, 317, (1982).
2. N. El-Kaddah, J. McKelliget and J. Szekely, Met. Trans. **15B**, 59, (1984).
3. A.H. Dilawari and J. Szekely, Plasma Chem. Plasma Proc., **7**, (3), 317, (1987).
4. A. Dilawari and J. Szekely, Int. J. Heat Mass Transfer, **30**, (11), 2357, (1987).
5. Y.P. Chyou and E. Pfender, Plasma Chem. Plasma Proc., **9**,(2), 291-328, (1989).
6. J.A. Lewis and W.H. Gauvin, A.I.Ch.E. J. **19**, (5), 982, (1973).
7. M. Vardelle, A. Vardelle, P. Fauchis and M. Boulos, AIChEJ, **29**, 236, (1983).
8. E. Pfender and C. Lee, Plasma Chem. Plasma Proces., **5**, (3), 211-237, (1985).
9. D. Bhattacharya and W. Gauvin, AIChEJ, **21**, 879, (1975).
10. N. Sayegh and W. Gauvin, AIChE J , **25**, (3), 523-534, (1979).
11. J. Fiszdon, Int. J. Heat Mass Transfer, **22**, 749-761, (1979).
12. C. Lee, C. Hsu and E. Pfender, 5th Int. Symp. on Plasma Chem., Edinburgh, Scotland, **2**, (1981).
13. R.M. Young and E. Pfender, Plasma Chem. Plasma Proc., **7**, (2), 211-229,(1987)
14. X. Chen and E. Pfender, Plasma Chem. Plasma Proc., **2**, (2), 185, (1982).
15. P. Fauchais, M. Vardelle, A. Vardelle, and J.F. Coudert, Met. Trans. B, 20B, 1989, pp. 263-276.
16. Y.P. Chyou and E. Pfender, Plasma Chem. Plasma Proc. **9**, (1), 45-71, (1989).
17. X. Chen and E. Pfender, Plasma Chem. Plasma Proc., **3**, (1), 97, (1983).
18. X. Chen and E. Pfender, Plasma Chem. Plasma Proc., **3**, (3), 351, (1983).
19. X. Chen and E. Pfender, Plasma Chem. Plasma Proc., **2**, (3), 293, 1982.
20. E. Bourdin, P. Fauchis, and M. Boulos, Int. J. H. & M. Transfer, **26**, 567, 1983.
21. C. Lee and E. Pfender, Plasma Chem. Plasma Proc., **7**, (1), 1-27, (1987).
22. J. Lesinski, B. Mizera-Lesinska, J. C. Fanton, and M.I. Boulos, J. AIChE, **27**, (3), 358-364, (1981).
23. G. Trapaga, R. Westhoff, J. Szekely, J. Fincke, and W.D. Swank, Plasma Processing and Synthesis of Material III, Eds. D. Apelian and J. Szekely, **190**, 191-199, (1991).
24. J.R. Fincke, and W.D. Swank, Plasma Processing and Synthesis of Material III, Eds. D. Apelian and J. Szekely, **190**, 207-212, (1991).
25. A.H. Dilawari, J. Szekely and R. Westhoff, ISIJ International, **30**, (5), (1990)

26. R. Westhoff, J.Szekely and A.H. Dilawari, Plasma Processing and Synthesis of Materials III, Eds. D. Apelian and J. Szekely, **190**, 213-219, (1991).
27. G. Rudinger , Fundamentals of Gas-Particle Flow, Elsevier Scientific Publishing Company (1980).
28. F.M. White, Viscous fluid flow, McGraw-Hill, New York, 1974.
29. G. Trapaga, Sc.D. Thesis, M.I.T. (1990)
30. L. Brewer and A.W. Searcy, J. Am. Chem. Soc. **73**, 5308-5314, (1951).
31. R. Bird, W. Stewart, and E. Lightfoot, Transport Phenomena, J. Wiley & Sons, New York, p. 511, (1960).
32. J. Crank, Free and Moving Boundary Problems, Clarendon Press, Oxford, 1984.
33. V. Voller and M. Cross, J. Heat Mass Transfer, **24**, 545-556, (1981)
34. Creare Incorporated, FLUENT Manual, Technical Note, Hanover N.H. p. 4-8, (1987).
35. A.H. Dilawari, J. Szekely, J. Batdorf, R. Detering, and C.B. Shaw, Plasma Chem. Plasma Proc., **10**, (2), 321-337, 1990.
36. R. Westhoff, G. Trapaga, and J. Szekely, "Plasma-Particle Interactions in Plasma Spraying" Met. Trans B, in press. (1992).

- Particle diameter (μm):	D_p = 27 - 35
- Emissivity :	ε = 0.3
- Heat of fusion (J/Kg):	H_{fus} = 1 x 10^6
- Heat of vaporization (J/Kg):	H_v = 2.467 x 10^7
- Thermal conductivity (W/m K):	k = 30
- Melting temperature (C):	T_m = 2050
- Boiling temperature (C):	T_b = 3527
- Density (Kg/m3):	ρ = 3900
- Specific heat (J/Kg):	Cp = 1700

Table V.A.I. Input data (Alumina particles in a Ar/He plasma)

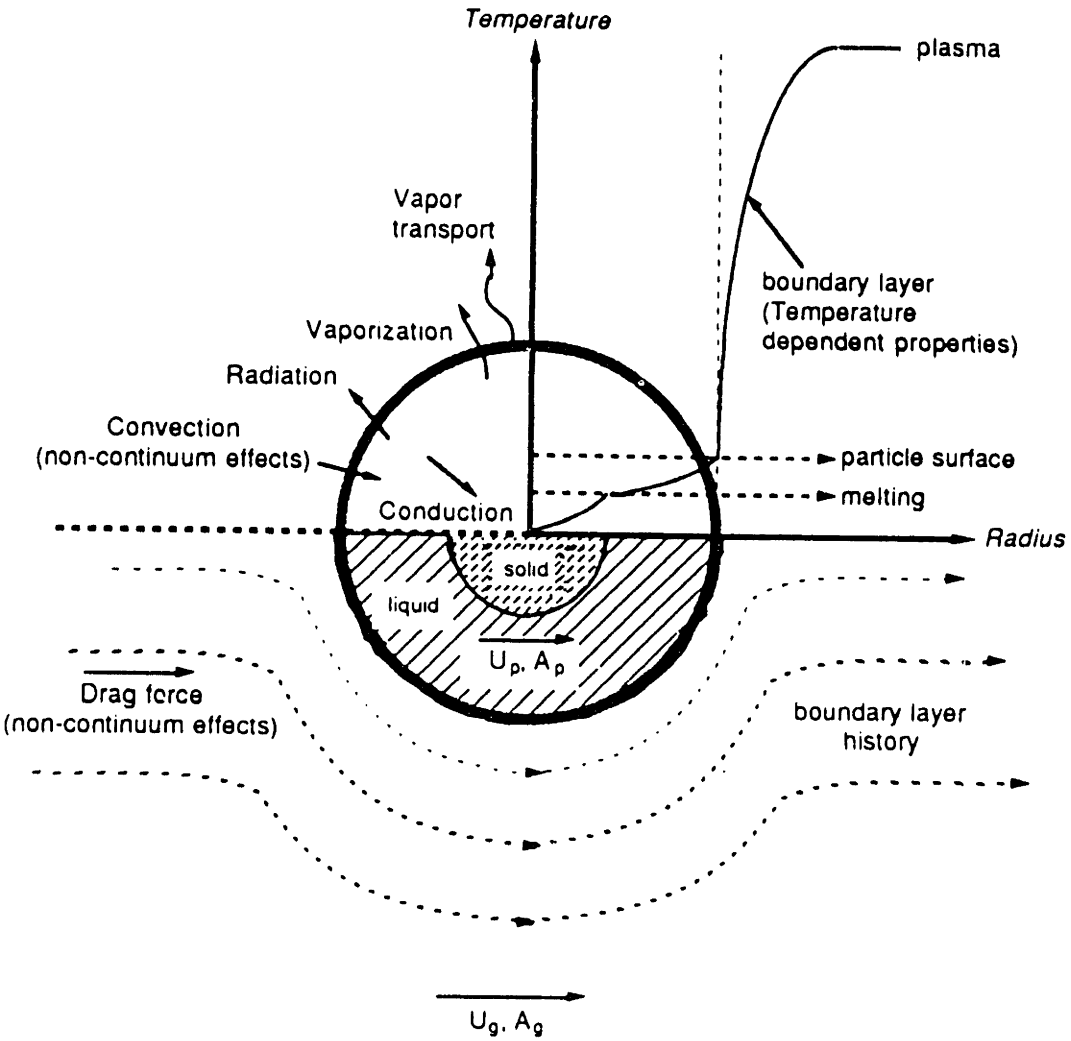

Figure V.A.1 Schematic illustration of particle heat, mass, and momentum transfer phenomena.

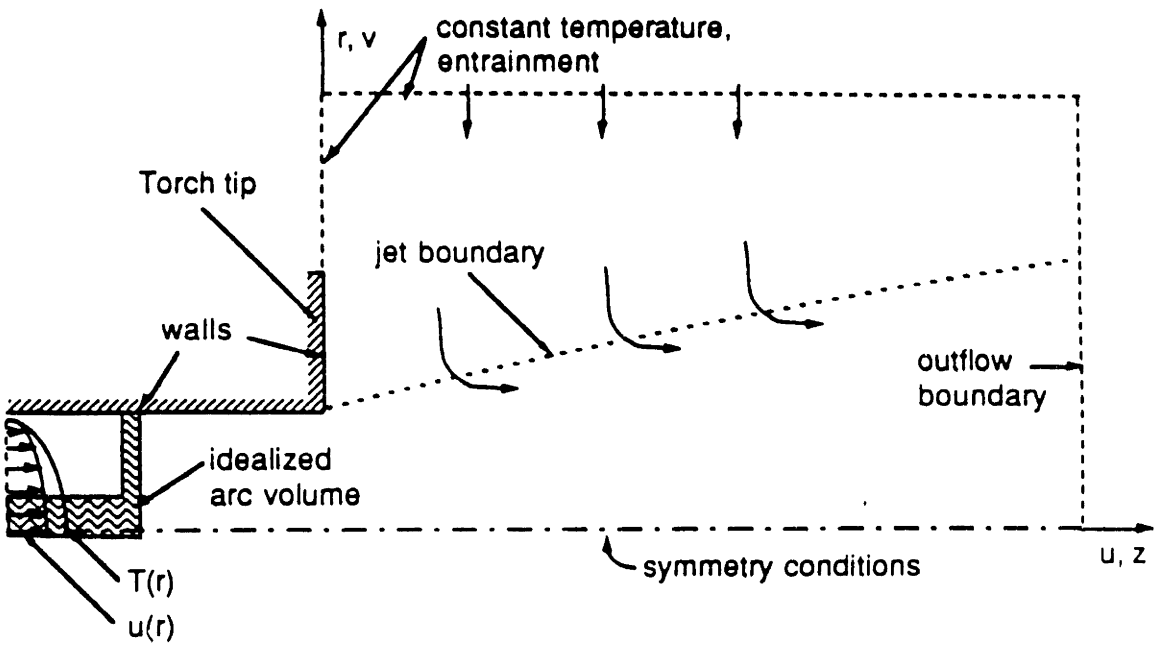

Figure V.A.2 Schematic sketch of the model used to describe the plasma plume.

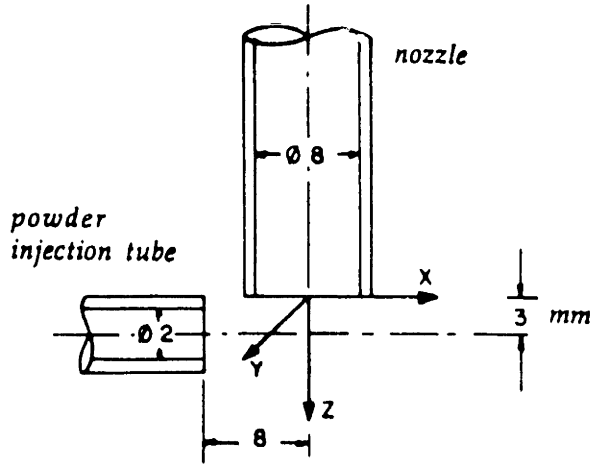

- Powder material: glass
- Density: 2.5 gr/cm^3
- Particle diameter:
  - *Powder A:* 97 ± 10 μm
  - *Powder B:* 13.7 ± 5 μm
- Powder feed rate:
  - *Powder A:* 0.05 *gr / s*
  - *Powder B:* 0.04 *gr / s*
- Injection velocity: 5.0 ± 0.7 m/s
- Reynolds number: 4.85 x 10^4
  (principal jet)

Figure V.A.3 Experimental setup and parameters used in studying the motion of alumina particles in a room-temperature air jet by Lesinski et al.

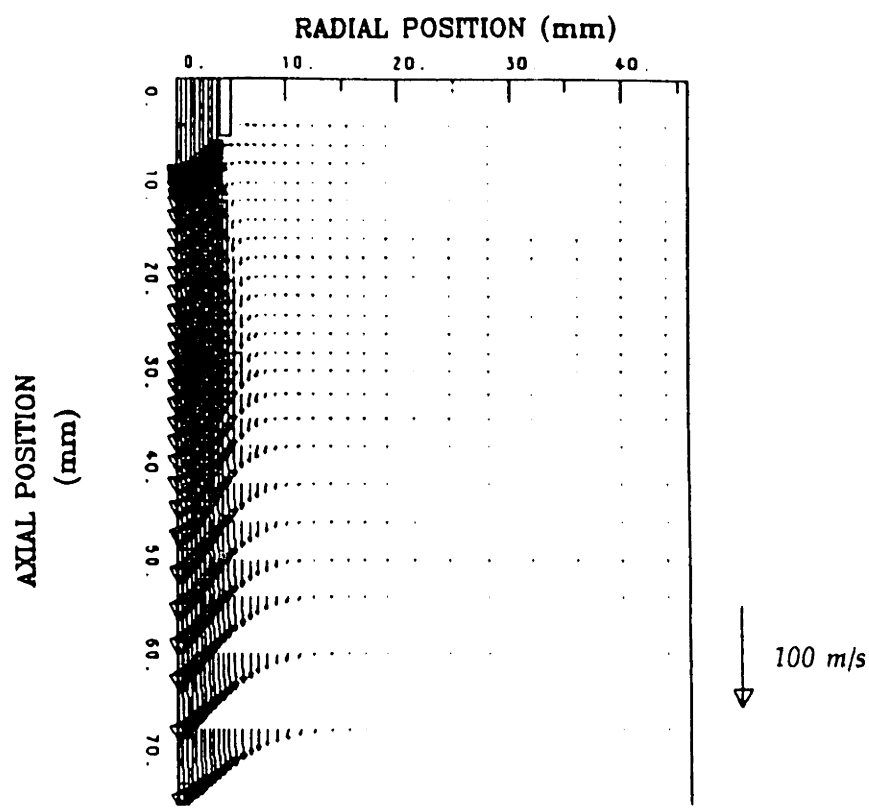

Figure V.A.4 Computational domain and calculated gas velocity vectors in the air jet.

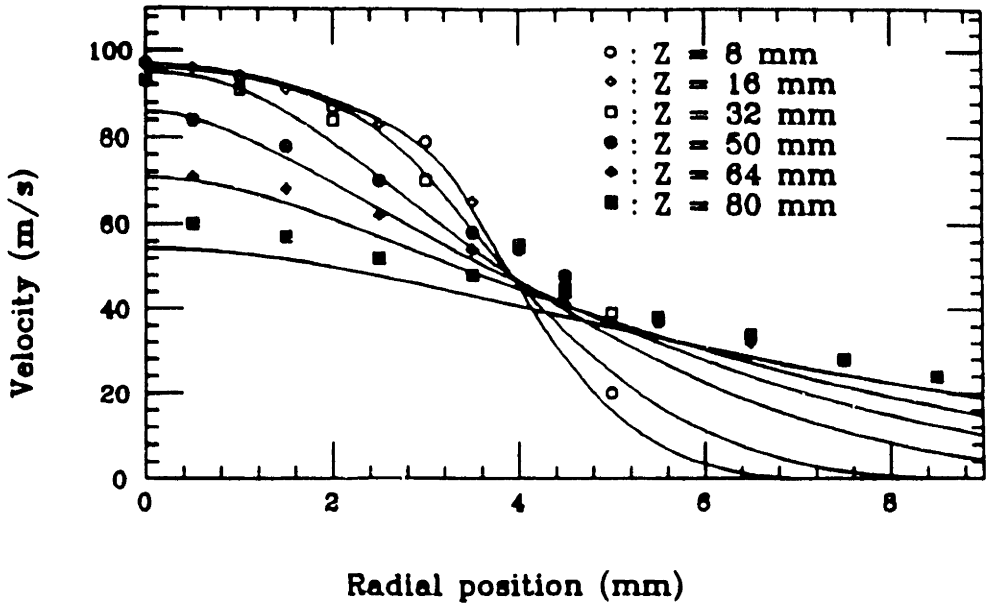

Figure V.A.5 Comparison of radial profiles of the calculated axial velocity with the experimentally measured axial velocity of Lesinski et. al.

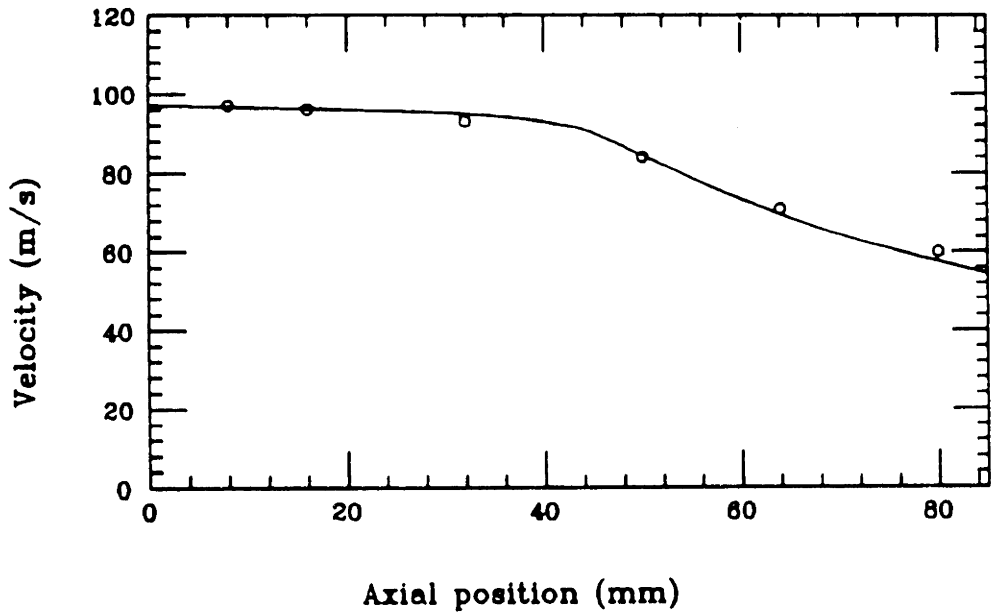

Figure V.A.6 Comparison of the calculated axial velocity profile on the jet axis with measurements.

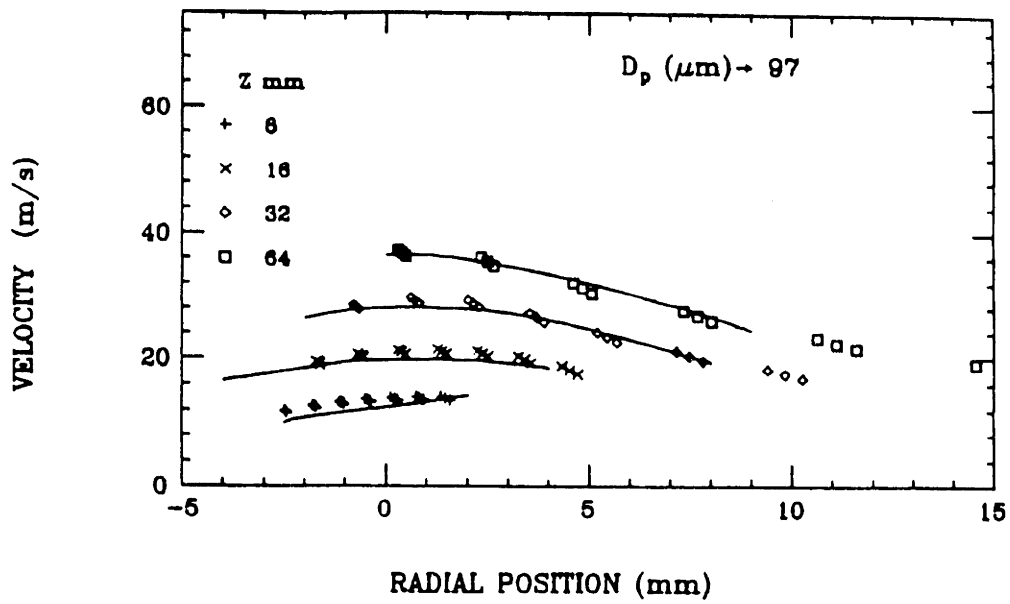

Figure V.A.7 Comparison of the measured mean particle velocities (shown by the solid lines) with those calculated with the particle model (discrete points) for particles with a mean diameter of 97 microns.

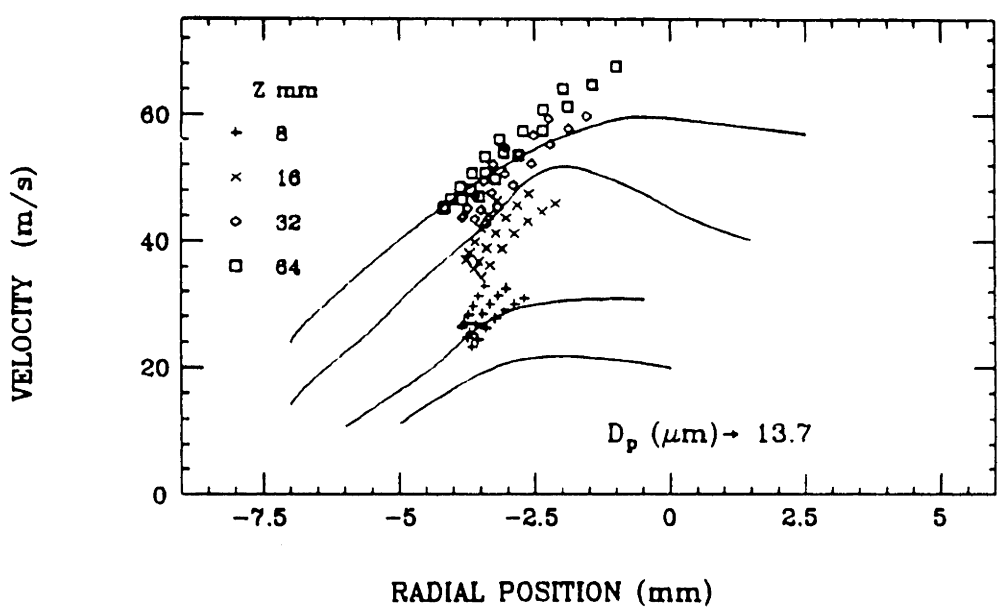

Figure V.A.8 Comparison of the measured mean particle velocities (shown by the solid lines) with those calculated with the particle model (discrete points) for particles with a mean diameter of 13.7 microns.

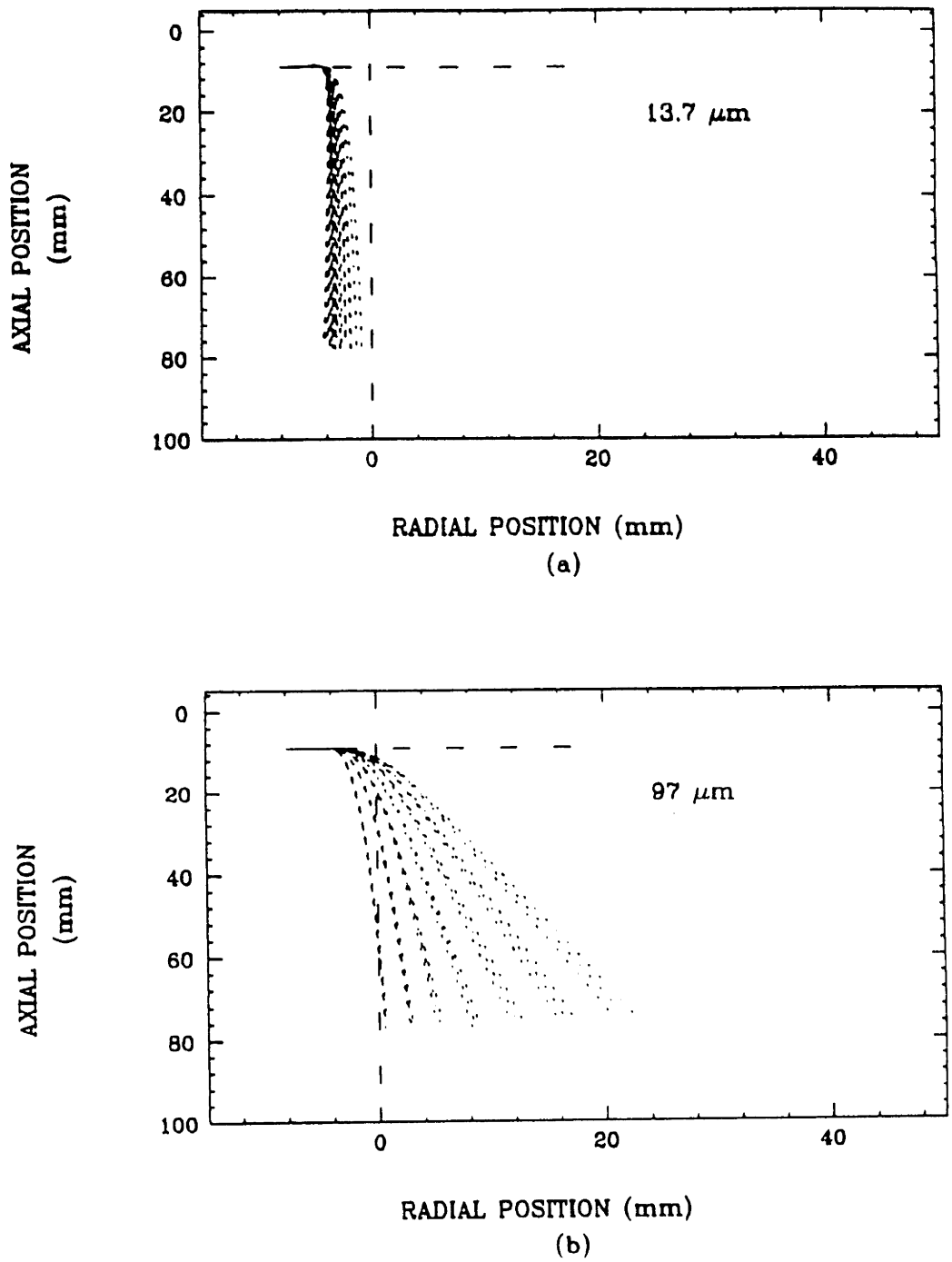

Figure V.A.9 Calculated trajectories for particles with a mean diameter of 97 microns and a mean injection velocity of 5.0 m/s.

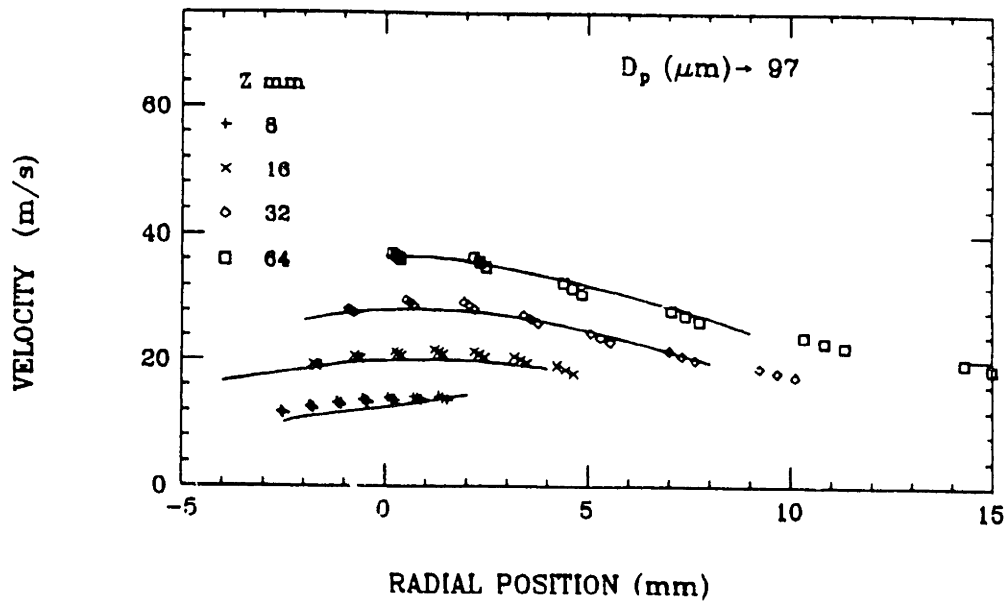

Figure V.A.10 Comparison of the measured mean particle velocities (shown by the solid lines) with those calculated with the particle model (discrete points) for particles with a mean diameter of 97 microns (assuming radial gas velocity is zero).

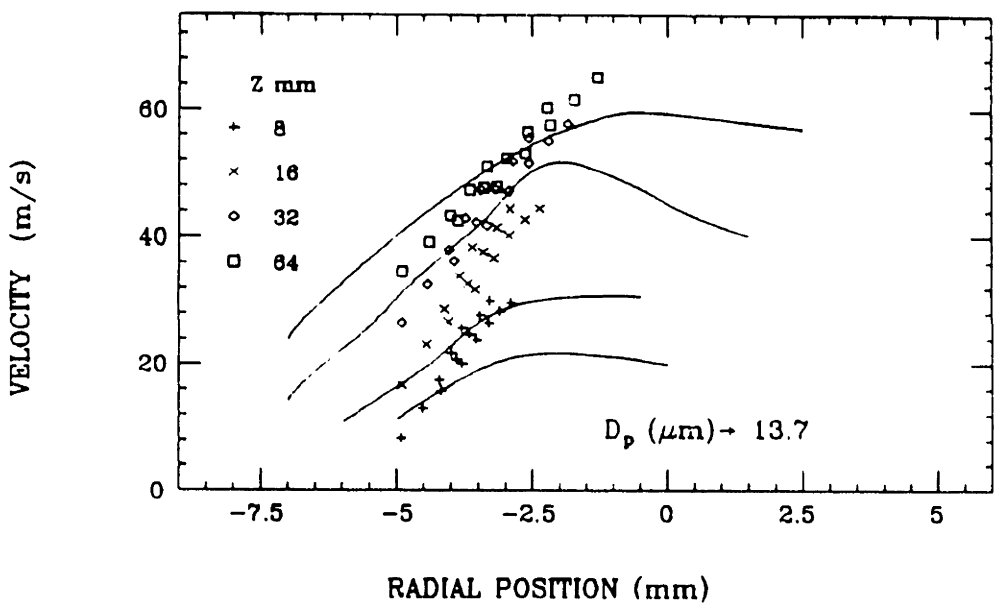

Figure V.A.11 Comparison of the measured mean particle velocities (shown by the solid lines) with those calculated with the particle model (discrete points) for particles with a mean diameter of 13.7 microns (assuming radial gas velocity is zero).

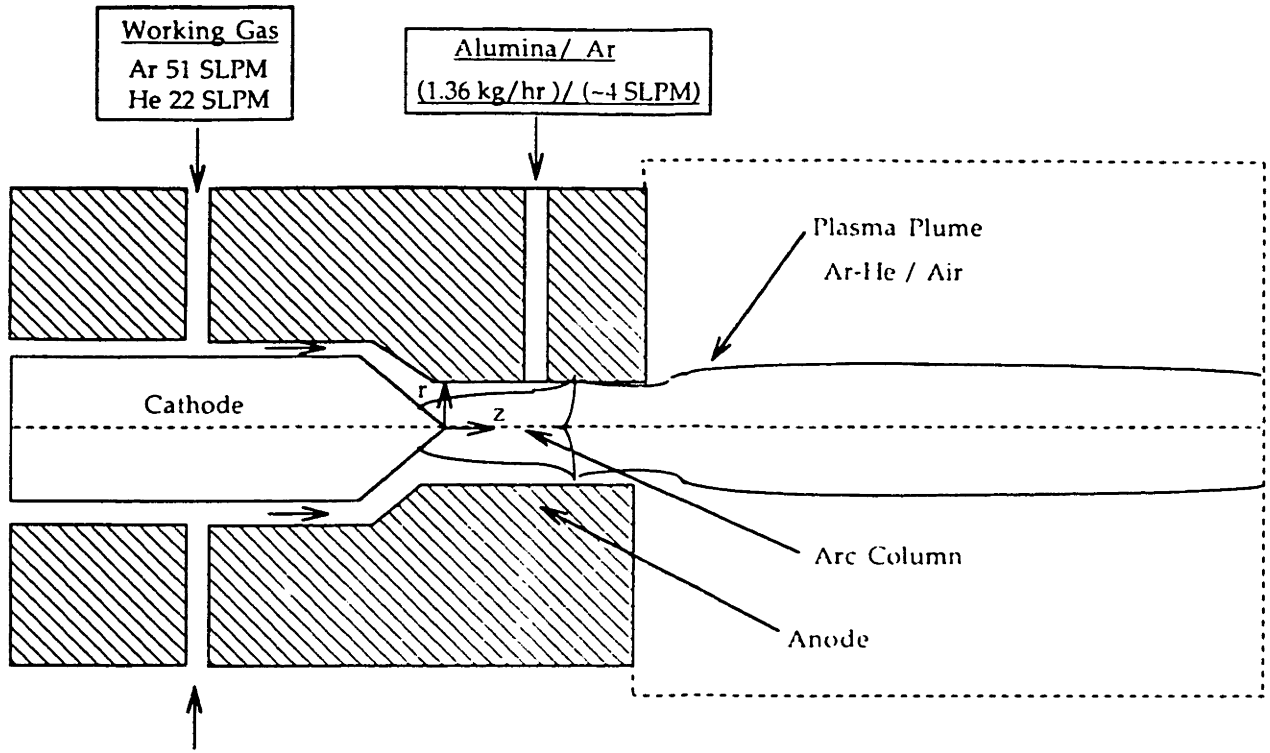

Figure V.A.12 Schematic of the Miller plasma torch and operating conditions for the spraying of alumina particles (Power: 900 A, 35.4 V @ Efficiency = 69%).

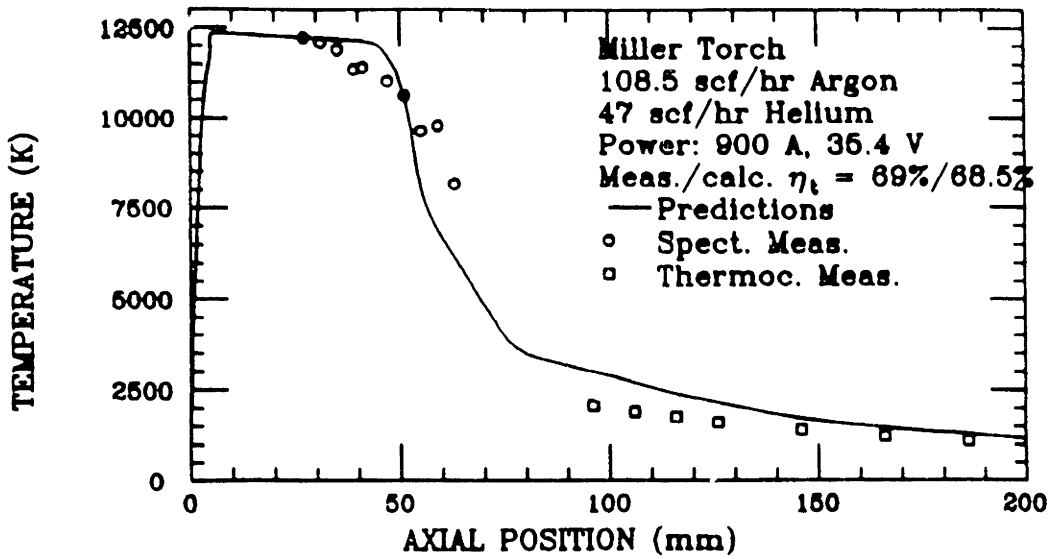

Figure V.A.13 Comparison of measured and calculated axial temperature profiles in the turbulent plasma jet issuing from a plasma torch.

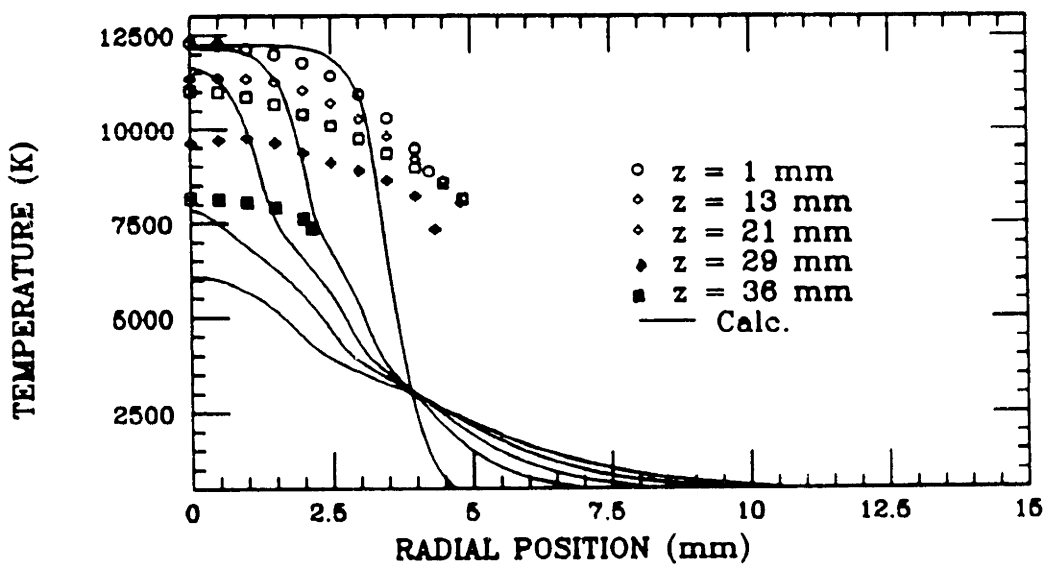

Figure V.A.14 Comparison of measured and calculated radial temperature profiles in a turbulent plasma jet.

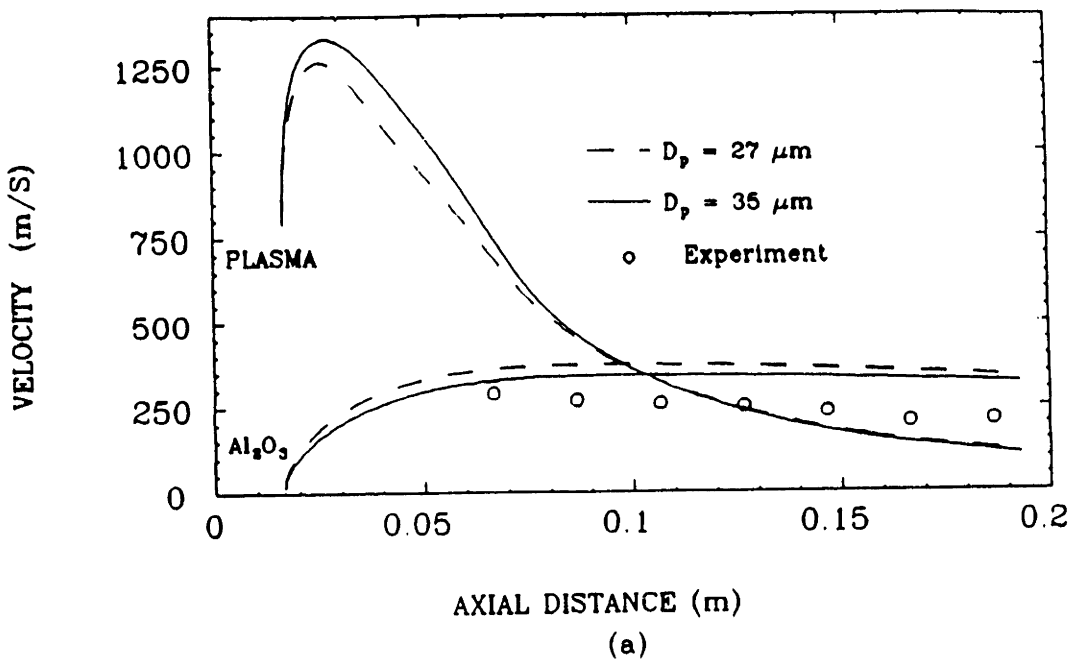

(a)

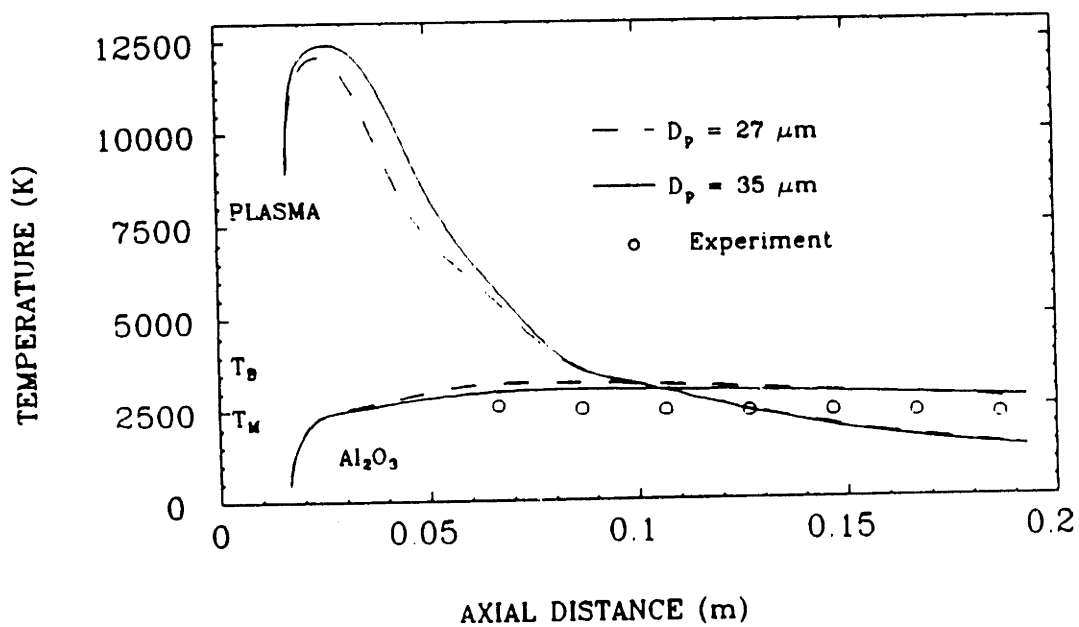

(b)

Figure V.A.15 Comparison of measured (at the center line) and calculated particle velocities (a) and particle surface temperatures (b) for two different particle sizes and for an injection velocity of 13 m/s.

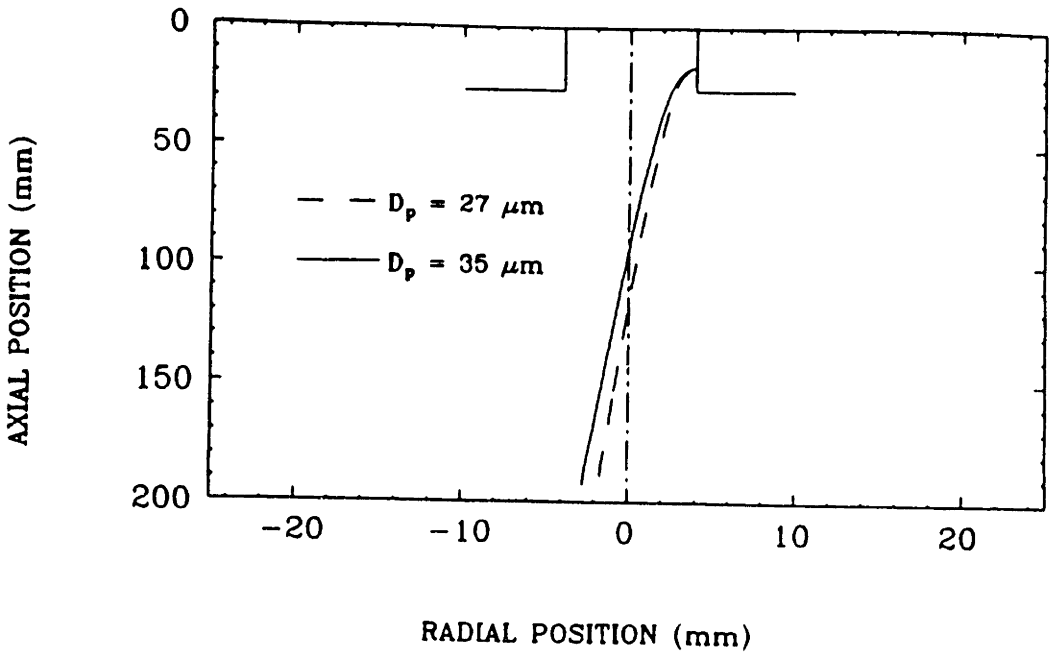

Figure V.A.16 Calculated particle trajectories in the plasma jet for 27 and 35 μm particles with injection velocities of 13 m/s. The injection point is located 10 mm inside the torch.

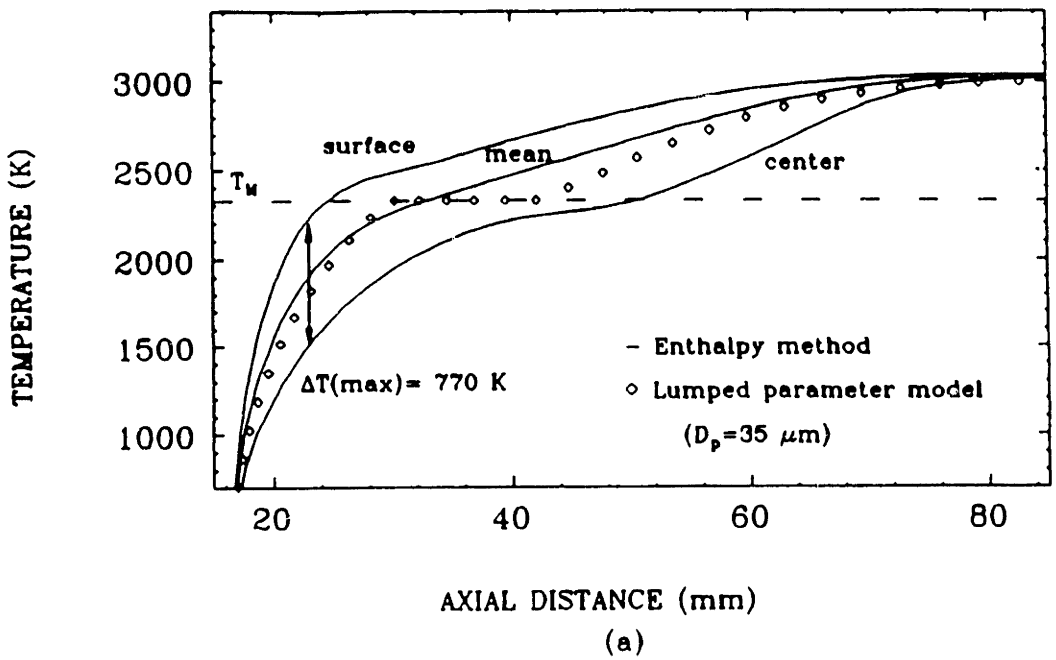

(a)

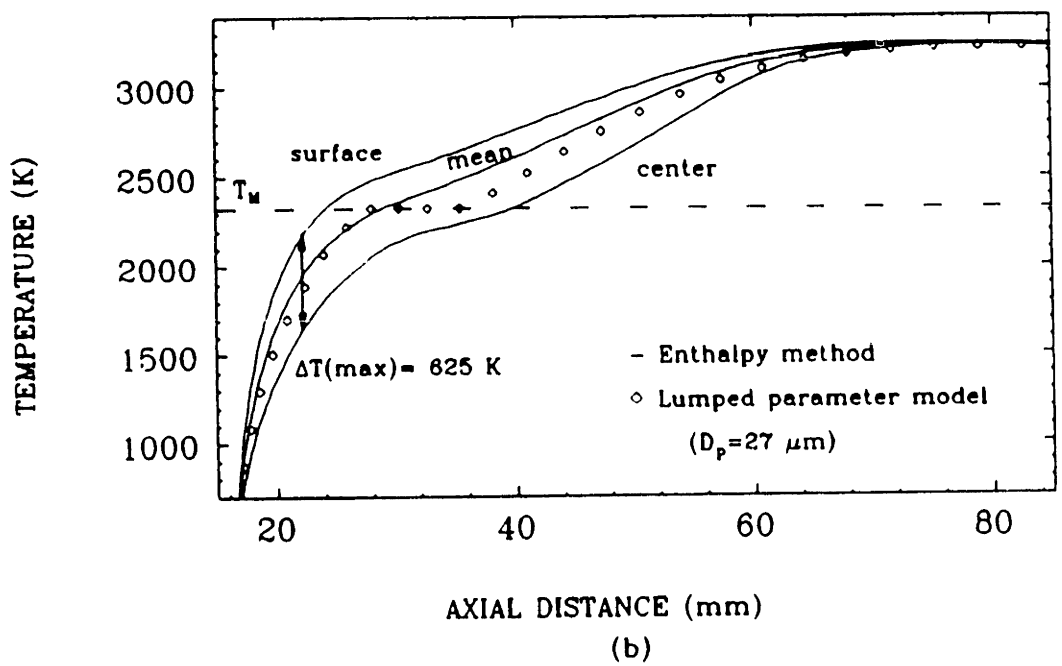

(b)

Figure V.A.17 Comparison of predictions for particle temperature histories calculated by a lumped parameter model and by the enthalpy method.
(a) 35 μm, and (b) 27 μm.

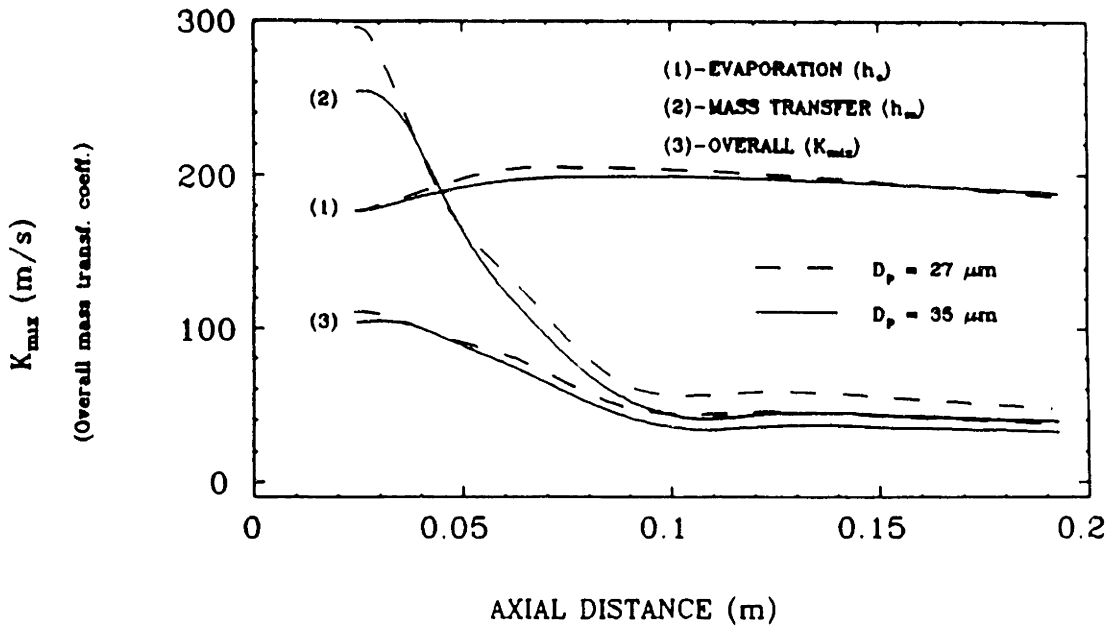

(a)

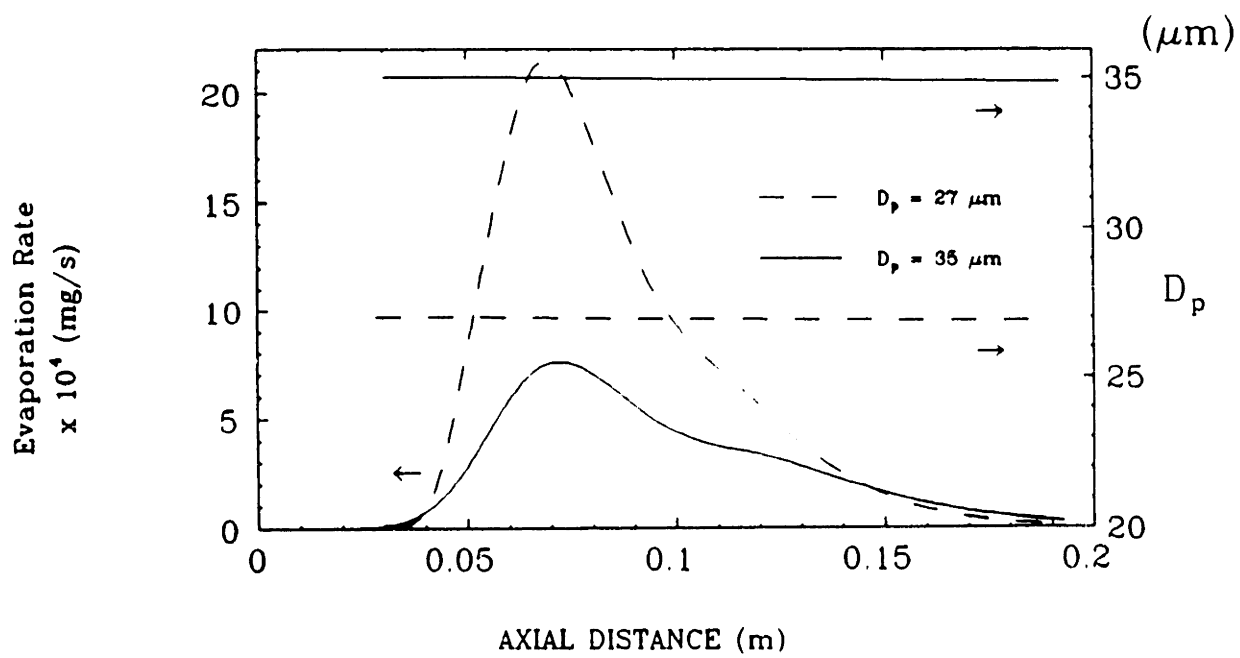

(b)

Figure V.A.18 (a) Calculated mass transfer coefficients due to Langmuir vaporization, diffusion mass transfer and overall (mixed control).
(b) Calculated evaporation rate and particle diameter for 27 and 35 μm particles with injection velocity of 13 m/s.

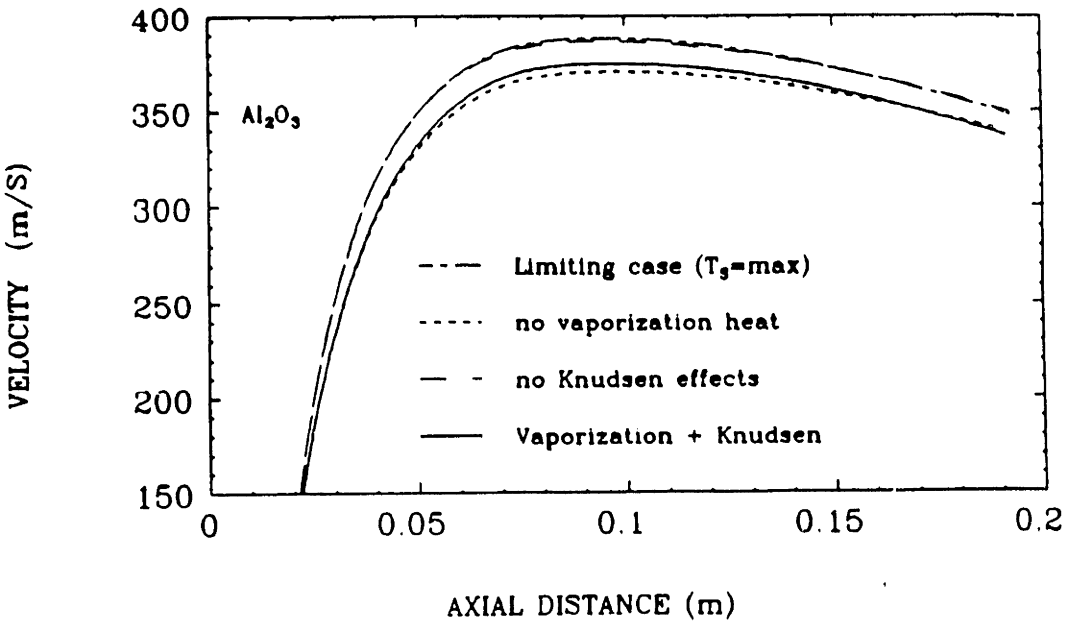

(a)

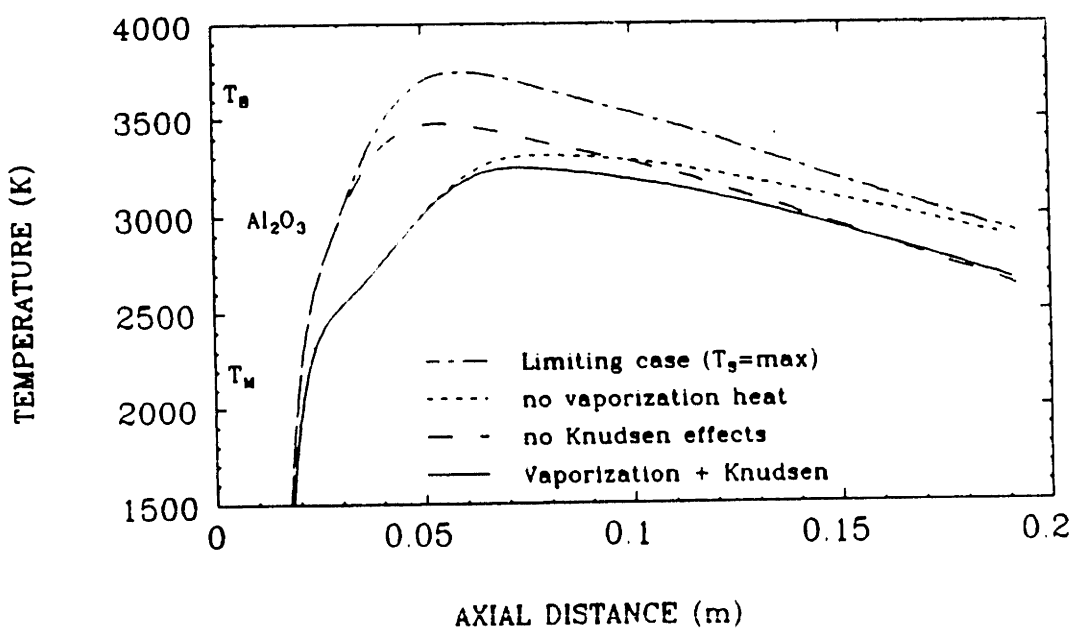

(b)

Figure V.A.19 Effect of vaporization and non-continuum (Knudsen) behavior on the prediction of particle velocities (a), and particle temperatures (b), for alumina particles with a mean diameter of 27 μm in an Ar-He plasma jet. For the limiting case, Knudsen effects are neglected in the calculation, as well as the heat flux terms due to vaporization of the particle.

CHAPTER VI: CONCLUSION

VI.A DISCUSSION

This thesis has presented three aspects of the modeling of plasma processing, namely plasma plumes, torches and particles in a plasma. Together these form a significant investigation into the modeling of thermal plasma systems.

The important contributions and findings of the work presented in this thesis will now be summarized:

The plasma plume work has illustrated that such a model is able to provide useful insight into plasma plumes, and can provide quantitative results which compare well with experiments. This is especially true for laminar plumes but is also true for turbulent cases to a lesser extent.

The model is also able to account for the intermixing of dissimilar gases into the plume, which in the case of air or nitrogen in a plume of argon, will quench the plume temperature rather quickly. While in some situations such as plasma spraying this may be a disadvantage, in others, such as plasma synthesis it might be exploited to quench-in high temperature species or phases.

The model has shown some difficulty in representing turbulent or transitional plasma plumes as it is based on a high Reynolds number turbulence model. This would be a potentially fruitful area of future work.

The work inside the plasma torch has generated a great deal of new insight into the operation of plasma torches.

The earlier work based on a simplified model showed the effect of the size (length and radius) of a postulated arc. The results show how long arcs tend to give higher efficiencies than shorter ones due to lower heat losses. In addition the effect of arc radius indicates that for wide arcs the conductive losses to the wall may dominate, while for very narrow arcs the radiative losses become important enough to lower the efficiency. In between is a relative maximum efficiency. In fact, the calculations indicated that the arc

shape had a subtle rather than an overwhelming effect on the temperature and velocity profiles at the torch exit.

The simplified model shows, and the more complete model concurs that the swirl which is introduced upstream of the arc is overwhelmed by the large increase in axial momentum caused by the heating and expansion. The result is that at the torch exit, the actual swirl numbers are relatively small, and so it will be difficult to produce significant swirl in the plume. This is important, as it may be desirable to introduce swirl in synthesis applications in order to promote mixing. If this needs to be done, the model indicates that some special measures may be required to produce highly swirling flows at the torch exit.

Finally, the simplified model suffered from a couple of shortcomings, one of which is the inability to predict arc voltage or overall power level. Because of this it remained strongly dependent on experimental measurements of torch voltage. In addition, a critical problem was shown to be the neglect of the electromagnetic forces in the problem formulation. It was shown that these may indeed have a significant effect on the shape of the velocity profile at the torch exit, though they have a lesser effect on the temperature profile. In fact, the agreement between the experimental results and the simplified theory (shown in the laminar cases) may have been due to a fortuitous combination of neglecting the E/M forces and the swirl at the same time, as they have opposite tendencies in shaping the velocity profile. Specifically, the E/M forces tend to "pinch" flow into the center line, while swirl tends to push it outward, due to the centrifugal force.

In the turbulent cases this became more clear, as the comparison was made with both temperature and velocity profiles from experiments. This showed that the simplified model gave much lower velocities in all the cases calculated. The indication then, was that the electromagnetic forces were indeed important, and this was backed up by an order of magnitude analysis.

The more complete model of the plasma torch offered additional insights into the behavior of plasma torches by calculating the current path and heat generation pattern within the torch. In this way the torch voltage could be approximated, as well as the temperatures and velocities in the torch and plume regions. The importance of the electromagnetic forces was shown explicitly by studying the effect they had on the velocity and temperature profiles, which was quite significant.

This work includes a study of swirl in the plasma torch and provided a helpful method of quantifying swirl, based on a macroscopic momentum balance on the gas injection region. The calculations threw new light onto the effect of swirl in the plasma torch, showing how swirl "spreads out" the arc root on the anode. Such an effect is consistent with the experimental observation that swirl extends the electrode life. Another effect shown was that, for the torch studied, the increase of swirl tended to decrease the torch voltage, which has not directly been verified experimentally. Discussions with experimentalists indicate that the trend usually observed is the opposite of this,(1) but that the result may depend on other torch conditions. In fact, for a large nozzle diameter and reasonably low currents, it was mentioned(2) that a decrease in arc voltage with increasing swirl could possibly occur. In addition, it should be noted that in general, the swirl in the torch has been rather poorly quantified until now, so the means used to "increase the swirl" need to be clearly understood before drawing final conclusions.

The model also showed that a complex interaction exists between the electromagnetic forces and swirl regarding the role they play in determining the temperature and more importantly, the velocity profiles. In addition, the model gave predictions about the swirl at the exit which tended to increase with increasing flow rate (because the incremental increase in axial momentum is relatively less). The swirl at the exit also tended to decrease with increasing current, because of the larger increase in axial momentum from both the gas expansion and JXB forces.

The complete model gave good agreement with experiments, especially when the calculated heat balance was in agreement with that found experimentally. In some cases the disagreement was due to the over predictions by the model of torch voltage resulting in high temperatures. Such integral errors stem from the lack of "adjustable parameters" in the model which would allow us to "tune" the results.

The model showed good results for laminar, argon in nitrogen systems, illustrating the effect of mixing. The different current-voltage behavior of the torch observed in this system was not well represented. This indicates that the differences observed may be due to local composition changes in the anode or cathode when the torch is operated in nitrogen, rather than by fluid flow effects such as increased turbulence, etc.

The model illustrated the effectiveness that a shroud gas of argon can have in isolating the jet from an ambient air atmosphere. Such a shroud gas could be useful in preventing the quick quench caused by the diatomic atmospheric gas, increasing the length of the hot zone. It may also be used to prevent such effects as oxidation by the entrained air. This model could be used for optimization of the strength and position of a shroud gas.

Dimensional analysis was used to get an overall picture of which phenomena may be important in determining the behavior of plasma torches. It was found that one number in particular could give an indication of the exit velocity profile, namely, the ES number, which is the ratio of electromagnetic forces to the swirl forces. For ES numbers much greater than one the velocity profile could become very peaked in the center, while for small values of the ratio a bi-modal profile could be obtained. In between, it appears, is the regime in which most torches seem to be operated, at least in argon systems, giving a profile which is moderately peaked on the axis.

The study of particle behavior in gas flows was done in two sections: First, the momentum transport section of the model was tested for a room temperature cases, illustrating that the model worked well for larger particles. Some significant discrepancies, however, were observed with smaller particles, which casts some doubt on the ability to model the behavior of very small particles Some questions may be raised about the (previously published) experimental results as well.

Finally, the case study on plasma spraying showed some important results regarding plasma-particle interactions. The most important of these was that the "plasma" effects such as variable properties, and non-continuum effects did indeed improve the comparison with experimental measurements, by decreasing the heat flux and momentum transfer compared with standard models. In addition, the vaporization effects were significant for the smaller particles. The resulting particle temperatures and velocities were in reasonably good agreements with those measured. Also the temperature differences between the center and edge of the particles could become quite large due to the high heat fluxes in the system.

VI.B SUGGESTED FUTURE WORK

The work presented in this thesis points to a number of new exciting areas that should be explored. These would offer new insight into plasma processing and improve the ability of models to predict the behavior of plasma systems operating with plasma torches.

Plasma plumes

The model of the plasma plume for turbulent cases should be updated using a better model of turbulence, which could represent the time-dependent nature of the turbulent fluctuations in the plume. Indeed, it has been indicated that the plume actually entrains "chunks" of ambient gas which can retain their identity for some time. One type of model that might be explored is the two-fluid model of turbulence, which is able to represent such phenomena in combustion, where it has been referred to as inherent "unmixedness."(3)

The effect of gas mixtures should be taken into account more rigorously based on an equilibrium description of the mixture. This is a difficult task however, requiring the solution of the equilibrium problem and subsequent evaluation of the properties either for each control volume in the domain, or for a range of concentrations which could then be used for interpolations within the domain. Much more work needs to be done regarding the calculation of plasma properties in general.

Plasma torches

While valuable new work has been done on the transport phenomena in plasma torches, a number of issues remain to be studied in this area:

The representation of plasma torches in which the flow inside the torch is turbulent needs more attention, especially regarding the electromagnetic forces. Torch modeling would also benefit from a better model of the laminar-turbulent transition which can occur in the plasma plume.

A complex interplay between swirl and electromagnetic forces has been shown to occur in the plasma torch, and these phenomena have been examined using dimensional analysis, but further study is needed in this area.

The cathode boundary condition for both heat and current flow, needs to be quantified more precisely, as well as relaxing some of the assumptions about the cathode geometry. This, in fact is a reasonably complex undertaking which could involve body fitted coordinates in the cathode region, as well as a complete model of the heat transfer in the cathode itself. The Richardson-Dushman equation then could be used to derive the current density from the cathode, based on its surface temperature.

The assumption of axial symmetry leads to difficulties in modeling the arc. While these difficulties may be circumvented by making assumptions about the electrical conductivity at low temperatures or about the specific point of arc attachment, these are not completely satisfactory, and may limit the usefulness of the model. The modeling of the fully three-dimensional, transient arc phenomena, while quite complex, may be the ultimate answer to this difficulty

The assumption of LTE, which has been called into question in the plasma plume, may be even more unrealistic in the nozzle of the plasma torch. This assumption should be relaxed, by postulating at least a two temperature model for the heat flow, which accounts for the temperature of electrons and heavy particles individually. Such an approach would require a reliable data base for the temperature dependence of two-temperature plasma properties, which is not readily available at present.

The anode heat losses may not be reliably represented by the model. Some improvement may be provided by a non equilibrium plasma model. In fact, the model could be extended to include a specific allowance for water cooling of the anode, which would allow one to calculate the anode surface temperature, which may affect the arc length. Such a change, to include the effects of conjugate heat transfer is a complex modification of the present model, which might be more easily included by moving the analysis to a commercial code such as PHOENICS or FLUENT.

Plasma-Particle Interactions

While a great deal of recent progress has been made, a number of issues remain unresolved or have not been adequately addressed. These include the following:

Vaporization and dissociation phenomena need to be better understood, for example, the vaporization of alumina has been based on experimental information on AlO vapor, while the actual equilibrium problem may contain more species. In addition, the heat capacity and enthalpy of alumina vapor needs to be known more reliably. Furthermore a number of complex issues pertaining to mass transfer of vapor in the boundary layer need to be more fully explored.

Some additional phenomena of potential relevance to plasma systems, such as non-continuum effects, the strong temperature dependence of property values, and particle charging effects are still not fully verified at this point; until a comprehensive comparison is made with appropriate experiments questions may arise about the absolute accuracy of the model predictions.

For a large number of the plasma-particle interaction studies, the effect which the particles have on the plasma (two-way interaction) has been neglected; in part this is due to the necessarily three-dimensional nature of the problem considered for any non-axi-symmetric injection scheme. The two way interaction between the plasma gas and the injected particles may be able to explain the over-predicted particle velocities and temperatures in some systems.

In plasma spray applications, plasma-particle interactions may be of equal importance to the study of the phenomena associated with the impact of the molten droplets onto the solid surface. While useful progress has been made in this area,(4) a great deal of further work would be desirable.

VI.C. REFERENCES

1. Private communication, Dr. Merle L. Thorpe, President, Hobart TAFA, Inc. 146 Pembroke Road, Concord, NH, 03301-5706.
2. Private communication, Prof. Pierre Fauchais, Universite de Limoges, 123 Avenue Albert-Thomas, 87060 Limoges Cedex, France.
3. Prof. Brian Spalding, in the 1991 Hottel lecture at MIT.
4. G. Trapaga, Ph.D. Thesis, Department of Materials Science and Engineering, Massachusetts Institute of Technology, (1990).

APPENDIX I. PLASMA PROPERTIES

AI.A EQUILIBRIUM COMPOSITION

The thermodynamic and transport properties of a plasma gas are a required element of any thermal plasma modelling effort. For the most part, the required properties for LTE properties are available in the literature.(1-9) These properties are nearly all based on a solution of the equilibrium composition of the plasma. A noted exception is the radiation data of Evans and Tankin.(9) Once the equilibrium problem is solved, the thermodynamic and transport properties can be derived.

One way of approaching the equilibrium problem which allows for the possibility of thermal non-equilibrium (i.e. different temperatures of heavy particles and electrons) has been outlined by Hsu and Pfender,(10) and is presented here, as the method used to generate Figure I.A.1 of this thesis. This work was originally pursued to explore the possibility of including non-equilibrium effects within the torch, but was not fully completed due to time and funding limitations. It is presented here for the sake of completeness.

The equilibrium problem can be posed by stating a two temperature Saha equation, which is actually an equation describing chemical equilibrium, for the number density of the species of interest, namely electrons, n_e, neutral atoms, n_0,and singly, doubly and triply ionized atoms, n_1, n_2, n_3 respectively. These are written as follows:

$$n_e\left[\frac{n_1}{n_0}\right]^{\frac{T_h}{T_e}} = \frac{2Z_1(T_e)}{Z_0(T_e)}\left[\frac{2\pi m_e k_b T_e}{h^2}\right]^{\frac{3}{2}}\exp\left[-\left(\frac{E_1-\Delta E_1}{k_b T_e}\right)\right] \qquad [AI.A.1]$$

$$n_e\left[\frac{n_2}{n_1}\right]^{\frac{T_h}{T_e}} = \frac{2Z_2(T_e)}{Z_1(T_e)}\left[\frac{2\pi m_e k_b T_e}{h^2}\right]^{\frac{3}{2}}\exp\left[-\left(\frac{E_2-\Delta E_2}{k_b T_e}\right)\right] \qquad [AI.A.2]$$

$$n_e\left[\frac{n_3}{n_2}\right]^{\frac{T_h}{T_e}} = \frac{2Z_3(T_e)}{Z_2(T_e)}\left[\frac{2\pi m_e k_b T_e}{h^2}\right]^{\frac{3}{2}}\exp\left[-\left(\frac{E_3-\Delta E_3}{k_b T_e}\right)\right] \qquad [AI.A.3]$$

where Z_0, Z_1, Z_2, and Z_3 are the partition functions for excitation of the neutral and ionized atoms (which are a function of the electron temperature. Also, m_e is the mass of an electron, k_b is Boltzmann's constant, T_e and T_h are the electron and heavy particle temperatures, and h is Planck's constant. E_1, E_2 and E_3 are the respective ionization energies of ions and ΔE_1, ΔE_2 and ΔE_3, are the quantities by which the ionization potential is lowered due to coulomb interactions. These are calculated following Hsu and Pfender(10) as

$$\Delta E_{r+1} = \frac{(r+1)e^2}{4\pi\varepsilon_o\lambda_D} \qquad [AI.A.4]$$

Here, ε_0 is the dielectric constant and e is the electronic charge. The Debye shielding distance, λ_D is given by

$$\lambda_D = \left[\frac{\varepsilon_0 k_b T_e}{e^2 n_e\left(1+\frac{T_e}{T_h}\right)}\right]^{\frac{1}{2}} \qquad [AI.A.5]$$

Dalton's law for the gas pressure is given by

$$p = n_e k_b T_e + (n_0 + n_1 + n_2 + n_3)k_b T_h \qquad [AI.A.6]$$

where p is the total operating pressure. The condition of quasi-neutrality requires that

$$n_e = n_1 + 2n_2 + 3n_3 \qquad [AI.A.7]$$

Together these comprise a set of five equations [AI.A.1-3,6-7] for five unknowns, n_e, n_0, n_1, n_2, n_3. It may be solved iteratively so long as care is taken to prevent divergence of the equations. This can be done by first solving in the order presented, solving [AI.A.1] for n_1, [AI.A.2] for n_2, [AI.A.3] for n_3, [AI.A.6] for n_0, and [AI.A.7] for n_e, until $n_1 < n_2$, (at about 25,000K). At this point, equations [AI.A.1], and [AI.A.6], must be recast to solve for n_0 and n_1 respectively. This prevents divergence and the solution can be completed.

The internal partition functions are given by summing the following expression over all the possible energy levels of the particle:

$$Z = \sum_{i=0}^{\infty} w_i e^{-\varepsilon_i / k_b T} \qquad [AI.A.8]$$

where w_i is the statistical weight due to the degeneracy of the particle at the e_i energy level. The energy levels were taken from the tables of Moore(11) and the later tables of Bashkin and Stoner.(12) The method used for terminating the infinite series was that of Drellishak, et al.(13) In this way the equilibrium composition of an argon plasma could be calculated versus temperature.

The methods of calculating the thermodynamic and transport coefficients from the equilibrium composition is given by other authors, and in fact has been done for several different plasmas. The resulting plasma properties are highly non-linear with temperature. This is illustrated in Figures AI.A.1-AI.A.4 which shows the thermodynamic and transport coefficients for argon, nitrogen, air and helium.

Figures (a) of AI.A.1-AI.A.4 illustrate the temperature dependence of the density which is reasonably like an ideal gas. Figures (b) show the heat capacity which illustrates the narrow peaks for ionization (e.g argon at 15000K) and for dissociation (e.g. nitrogen at 7000K). Figures (c) illustrate the behavior of the viscosity, which obeys classical kinetic theory (i.e. the viscosity increases with temperature) until ionization becomes significant. When this happens (e.g. for argon above 10000K) the long range coulomb collisions begin to dominate, making the plasma less collisional, and hence the viscosity decreases. Figures (d) illustrate the thermal conductivity of plasma which is also highly non-linear due to the combination of the translational and the reactive conductivity. Figures (e) show the radiative loss coefficient of the plasma, which is usually determined experimentally. Finally, the electrical conductivity is shown in Figures (f) which is quite low (~0) below about 5000K for most gases. Note that Figure AI.A.1 shows both the LTE values of the electrical conductivity and the conductivity *which is assumed* at low temperatures to allow the axi-symmetric model of the arc to converge in an acceptable manner, as was mentioned in Section IV.A.2.

REFERENCES

1. C. H. Liu, Ph.D. Thesis, Department of Mechanical Engineering, Univ. Of Minnesota, Minneapolis, Minnesota (1977).
2. R.S. DeVoto, Phys. Fluids, **16**, No. 5, 616, (1973).
3. J. C. Morris, G. R. Bach, and J. M. Yos, Rep. No. ARL-64-180, Aerospace Research Laboratories (1964).
4. J. M. Yos, Technical Memorandum RAD-TM-63-7, Research and Advanced Development Division, AVCO Corporation, Wilmington, Massachusetts (1983).
5. W.J. Lick, and E.W. Emmons, Thermodynamic Properties of Helium to 50000K, Harvard Univ. Press, Cambridge, MA., (1962).
6. W.J. Lick, and E.W. Emmons, Transport Properties of Helium from 200 to 50000K, Harvard Univ. Press, Cambridge, MA., (1965).
7. P. Fauchais, M. Boulos and E. Pfender, *Physical and Thermodynamic Properties of Thermal Plasmas*, in Plasma Technology in Metallurgical Processing, 11-26 (1987).
8. International Union of Pure and Applied Chemistry, "Thermodynamic and Transport Properties of Pure and Mixed Thermal Plasmas at Local Thermodynamic Equilibrium (LTE)", Pure and Appl. Chem., **54**, (6), 1221-1238, (1982).
9. D. C. Evans and R. S. Tankin, *Phys. Fluids* **10**, 1137 (1967).
10. K.C. Hsu and E. Pfender, "Calculation of Thermodynamic and Transport Properties of a Two-Temperature Argon Plasma", 5th International Symposium on Plasma Chemistry, Edinburgh, Scotland, **1**, 144-153, (1981).
11. C.E. Moore, Atomic Energy Levels, NSRDS-NBS, 35, NBS, Wash. D.C. Vols. 1-3, (1971).
12. S. Bashkin, and S.O. Stoner, Atomic Energy Level and Grotrian Diagrams, Vol II, (1978).
13. K.S. Drellishak, C.F. Knopf, and A.B. Cambel, "Partition Functions and Thermodynamic Properties of an Argon Plasma", Phys. Fluids, **6**, (9), 1280-1288, (1963).

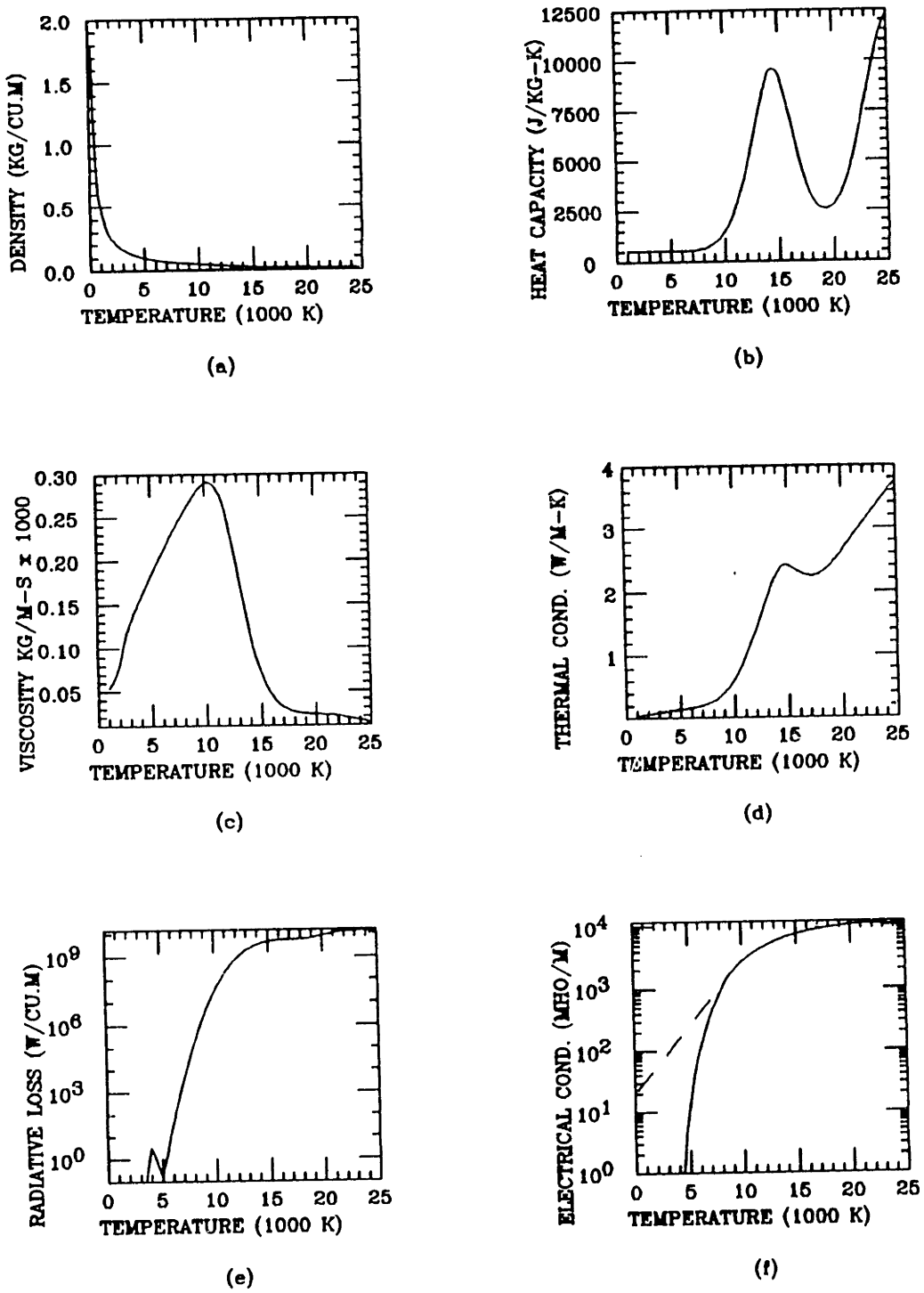

Figure AI.A.1 Thermodynamic and transport properties of a LTE argon plasma versus temperature (a) density, (b) heat capacity, (c) viscosity, (d) thermal conductivity, (e) radiative loss, and (f) electrical conductivity.

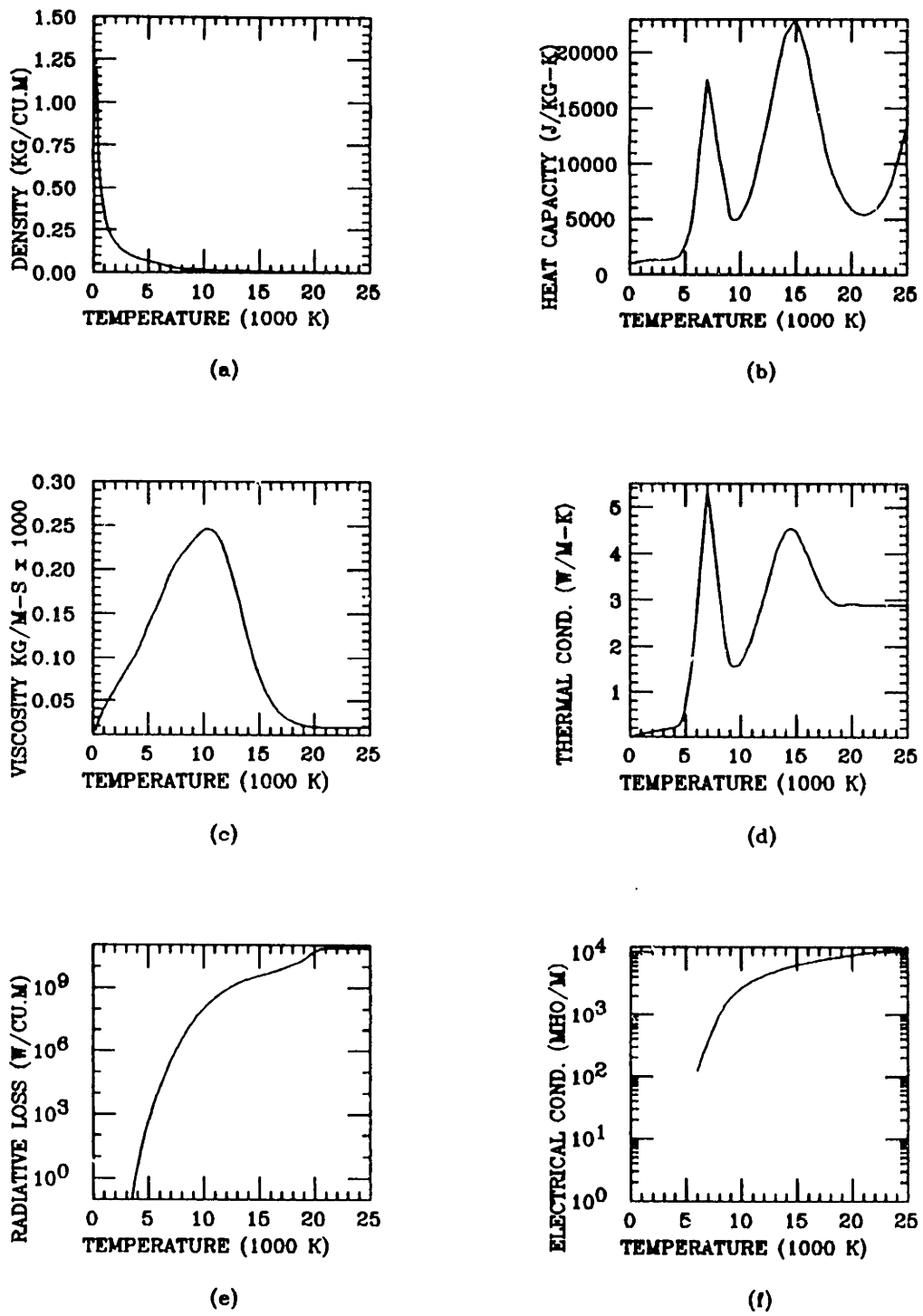

Figure AI.A.2 Thermodynamic and transport properties of a LTE nitrogen plasma versus temperature (a) density, (b) heat capacity, (c) viscosity, (d) thermal conductivity, (e) radiative loss, and (f) electrical conductivity.

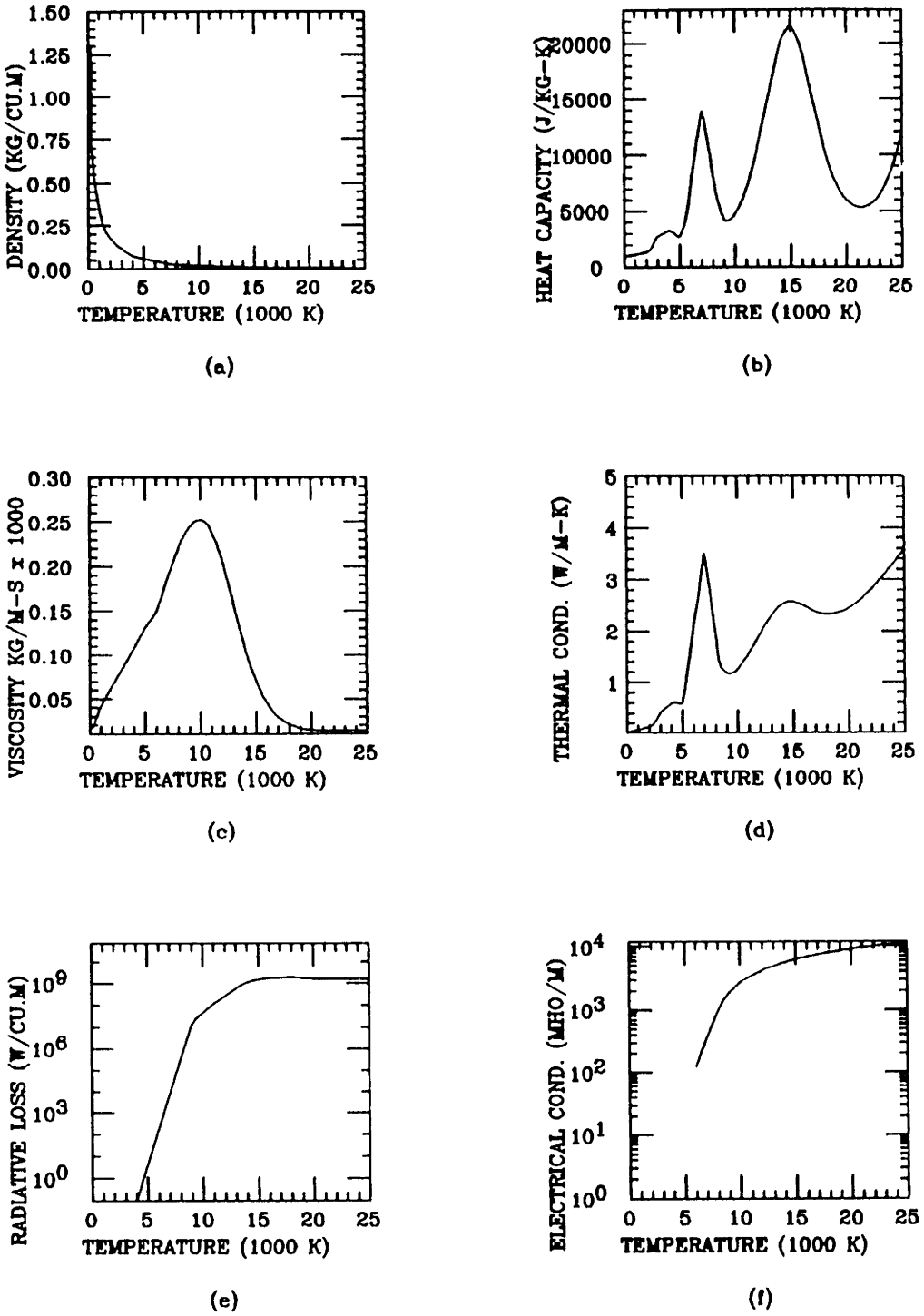

Figure AI.A.3 Thermodynamic and transport properties of a LTE air plasma versus temperature (a) density, (b) heat capacity, (c) viscosity, (d) thermal conductivity, (e) radiative loss, and (f) electrical conductivity.

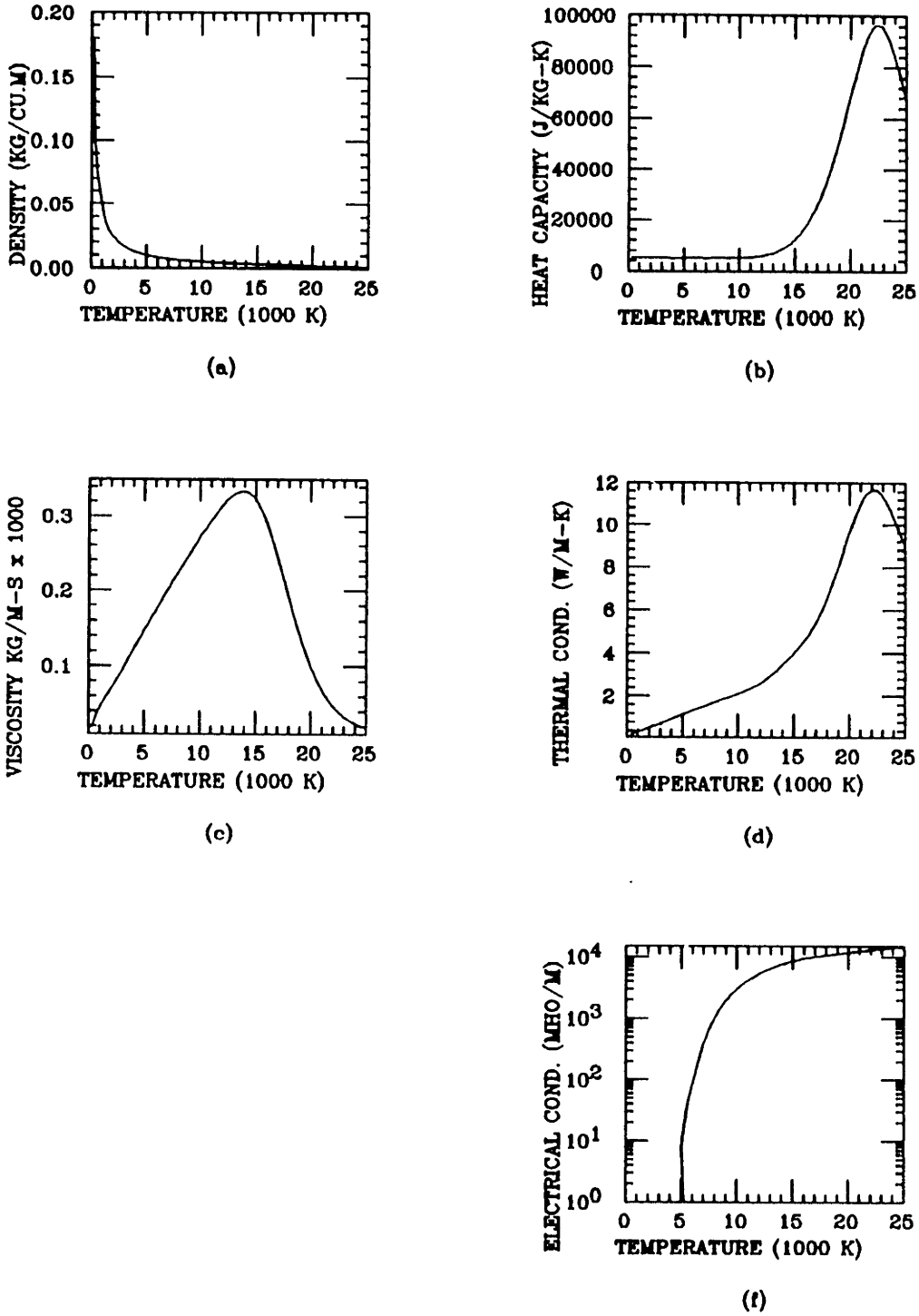

Figure AI.A.4 Thermodynamic and transport properties of a LTE helium plasma versus temperature (a) density, (b) heat capacity, (c) viscosity, (d) thermal conductivity, (e) radiative loss, and (f) electrical conductivity.

APPENDIX II. CURRENT - VOLTAGE CORRELATION PROGRAM

The following program correlates the current voltage characteristics of torches operating with mixtures of argon and helium as described in Section IV.E.2

```
        PROGRAM CORREL
C
C------THIS ROUTINE TAKES TWO PROPERTY SUBROUTINES, AND RETURNS THE
C      THERMODYNAMIC PROPERTIES,TRANSPORT PROPERTIES,AND RADIATION
C      LOSS PER UNIT VOLUME IN M.K.S. UINTS FOR A MIXTURE OF THE TWO
C      GASES.  USING THESE PROPERTIES IT CAN CORRELATE THE CURRENT -
C      VOLTAGE CHARACTERISTIC OF PLASMA TORCHES USING THE HJ NUMBER
C      AND THE DIMENSIONLESS VOLTAGE.
C
C      1=DENSITY , 2=VISCOSITY , 3=THERMAL CONDUCTIVITY ,
C      4=SPECIFIC HEAT , 5=RADIATION LOSS , 6=ELECTRICAL CONDCTIVITY ,
C      7=PRANDTL #
C
C      TEMPERATURE IS IN KELVIN AND RADITION IN WATTS/CUBIC METRE
C

         WTONE=39.95        !  Molecular weight of Argon
         WTTWO=4.003        !  Molecular weight of Helium
         VW=4.0             !  Work function of copper
         PSTD=101325        !  Standard Pressure (N/m**2)
         TSTD=300           !  Standard temperature (K)
         CONV=7.866E-6      !  Conversion factor to change volume flow
C                              rate
C                              to Std.Cu.Meters/Sec.
         GAMMA=1.2          !  Ratio of specific heats for the mix (argon
C                              and helium)
         EMUNOT=4*3.14159*1.0E-7
         RSQRTE=1./SQRT(8.)
         RMWT=WTONE/WTTWO
         VATERM=SQRT(1.+RMWT)
         VBTERM=(WTTWO/WTONE)**0.25
C--------Read the data file type
C          1 = Case No., Current, Voltage, Mass flow (Primary), Mass
C           Fraction
C          2 = Case No., Current, Power, Volume Flow (primary), Mole
C           Fraction
C
         READ(5,*) MODE,DN,SW    ! Mode number, Nozzle diameter, Swirl
            Number
         AREA=3.14159*DN**2/4.   ! Nozzle area
        WRITE(7,890)
 890    FORMAT('(  Case    V     I       Hbar     Tbar      Mubar     Rhobar'
     1   '     Conbar    Sigbar )')
        WRITE(7,910)
 910    FORMAT('( Case    Re     Ma      CJ      EM       HJ     '
     1   ' Vdim     ES )')
100      IF(MODE.EQ.1)THEN
          READ(5,*) KASE,CUR,VOLT,GM,G
```

```
          IF(KASE.LT.0)GO TO 1000
          POW=CUR*VOLT          ! Power level
          GONE=G/WTONE
          GTWO=(1.-G)/WTTWO
          GTOT=GONE+GTWO
          GMF=GONE/GTOT
         ENDIF
         IF(MODE.EQ.2)THEN
          READ(5,*) KASE,CUR,POW,QF,GMF
          IF(KASE.LT.0)GO TO 1000
C--------Calculate the mass fraction, Voltage and Mass flow
          GONE=GMF*WTONE
          GTWO=(1.-GMF)*WTTWO
          GTOT=GONE+GTWO
          G=GONE/GTOT
          VOLT=POW/CUR          ! Voltage
          DENSTD=(PSTD*WTONE)/(8314*TSTD)  !  Standard density, ideal
            gas
          GM=QF*CONV*DENSTD
         ENDIF
C--------Calculate the Joule heat and the average Enthalpy
          ANOHT=CUR*(2.76+VW)  !  Anode heat
          HTJOUL=POW-ANOHT     !  Joule heating
          HBAR=HTJOUL/GM
C-------Look up the temperature and properties
        CALL TEMPHE(1,G,HBAR,TBAR)
        CALL ONERHO(1,TBAR,RHOONE,JTOP,JBOT)
        CALL ONEEMU(0,TBAR,EMUONE,JTOP,JBOT)
        CALL ONETHK(0,TBAR,CONONE,JTOP,JBOT)
        CALL ONESIG(0,TBAR,SIGONE,JTOP,JBOT)
        CALL HELRHO(1,TBAR,RHOTWO,JTOP,JBOT)
        CALL HELEMU(0,TBAR,EMUTWO,JTOP,JBOT)
        CALL HELTHK(0,TBAR,CONTWO,JTOP,JBOT)
        CALL HELSIG(0,TBAR,SIGTWO,JTOP,JBOT)
C
C-------Calculate the mixture properties
C
        RHOBAR=RHOONE*GMF+(1.-GMF)*RHOTWO    ! Density
C
C-------Wilke mixing formula
C
        RVIS=EMUONE/EMUTWO
        PHI12=(1.+SQRT(RVIS)*VBTERM)**2
        PHI12=PHI12*RSQRTE/VATERM
        PHI21=PHI12*RMWT/RVIS
        GMF2=1.-GMF
        GPHI12=GMF+GMF2*PHI12
        GPHI21=GMF*PHI21+GMF2
C
C-------Wilke mixed properties
C
        EMUBAR=GMF*EMUONE/GPHI12+GMF2*EMUTWO/GPHI21
        CONBAR=GMF*CONONE/GPHI12+GMF2*CONTWO/GPHI21
        SIGBAR=GMF*SIGONE/GPHI12+GMF2*SIGTWO/GPHI21
C
C-------Calculate the needed Values
C
        UBAR=GM/RHOBAR/AREA         ! Average velocity
```

```
      RE=RHOBAR*UBAR*DN/EMUBAR     ! Reynolds number (Average)
      VS=SQRT(GAMMA*8314*TBAR/WTONE)    ! Speed of sound
      TMACH=UBAR/VS                     ! Mach number
      CJNUM=SIGBAR*CONBAR*TBAR*DN**2/CUR**2          ! CJ number
      EMNUM=EMUNOT*CUR**2/(RHOBAR*UBAR**2*DN**2)     ! EM number
      HJNUM=SIGBAR*HBAR*GM*DN/CUR**2                 ! HJ number
      VDIM=VOLT*DN*SIGBAR/CUR                        ! Dimensionless
          Voltage
      ESNUM=EMNUM/SW                                 ! ES number
C
C-------WRITE OUT TABLES
 900  WRITE(7,902)KASE,VOLT,CUR,HBAR,TBAR,EMUBAR,RHOBAR,CONBAR,SIGBAR
 902  FORMAT(1X,'(',I4,1X,F5.1,1X,F5.0,1X,1PE10.3,1X,0PF7.0,1X,
     1 1PE10.3,1X,0PF7.4,1X,F7.4,1X,F8.3,')')
 950  WRITE(7,952)KASE,RE,TMACH,CJNUM,EMNUM,HJNUM,VDIM,ESNUM
 952  FORMAT(1X,I4,1X,F5.0,1X,F5.3,1X,F7.3,1X,F7.3,1X,F7.3,1X,F7.3,
     1  1X,F7.3)
      GO TO 100
 1000 CONTINUE
      STOP
      END


      SUBROUTINE ARGON
C------THIS ROUTINE TAKES TEMPERATURE,TT,AND RETURNS THE THERMODYNAMIC
C     PROPERTIES,TRANSPORT PROPERTIES,AND RADIATION LOSS PER UNIT
C     VOLUME IN M.K.S. UINTS FOR IONIZED ARGON GAS AT 1 ATM.
C
C     THE VALUES ASSIGNED TO I ARE:
C     1=DENSITY , 2=VISCOSITY , 3=THERMAL CONDUCTIVITY ,
C     4=SPECIFIC HEAT , 5=RADIATION LOSS , 6=ELECTRICAL CONDCTIVITY ,
C     7=PRANDTL #
C
C     TEMPERATURE IS IN KELVIN AND RADITION IN WATTS/CUBIC METRE
C

      DIMENSION RHOTAB(28),EMUTAB(28),THKTAB(28)
      DIMENSION CPTAB(28),RADTAB(28),SIGTAB(28),PRTAB(28)
C
C------------DENSITY
      DATA RHOTAB
     1 /1.783,    1.783,    .487,     .243,     .162,     .122,     .0976,
     1 .0814,     .0697,    .0609,    .0539,    .0478,    .0421,    .0363,
     1 .0303,     .0248,    .0203,    .0173,    .0154,    .0141,    .0131,
     1 .0123,     .0115,    .0107,    .00992,   .00906,   .00823,   .00823/
C------------VISCOSITY
      DATA EMUTAB
     2 /2.1E-5,   2.1E-5,   5.35E-5, 8.07E-5, 1.13E-4, 1.46E-4, 1.82E-4,
     2 2.06E-4,   2.29E-4,  2.51E-4, 2.69E-4, 2.80E-4, 2.71E-4, 2.31E-4,
     2 1.69E-4,   1.09E-4,  6.66E-5, 4.07E-5, 2.97E-5, 2.51E-5, 2.36E-5,
     2 2.33E-5,   2.31E-5,  2.21E-5, 2.00E-5, 1.71E-5, 1.43E-5, 1.43E-5/
C------------THERMAL CONDUCTIVITY
      DATA THKTAB
     3 /1.64E-2,  1.64E-2,  .0427,   .0692,   .0938,   .118,    .143,
     3 .165,      .197,     .258,    .383,    .588,    .913,    1.48,
     3 1.72,      2.08,     2.20,    2.12,    2.06,    2.11,    2.25,
     3 2.44,      2.67,     2.93,    3.19,    3.46,    3.72,    3.72/
```

```
C------------SPECIFIC HEAT
      DATA CPTAB
     4 /520.,     520.,     520.,     520.,     520.,     520.,     520.,
     4 521.,      542.,     633.,     902.,     1530.,    2730.,    4690.,
     4 7230.,     9390.,    9310.,    7070.,    4630.,    3110.,    2550.,
     4 2780.,     3830.,    5790.,    8350.,    10800.,   12300.,  12300./
C------------RADIATION LOSS
      DATA RADTAB
     5 /7*0.0,
     5 0.0,       0.0,      0.0,      4.00E6,   3.53E7,   1.12E8,  3.31E8,
     5 7.86E8,    1.37E9,   1.92E9,   2.27E9,   2.26E9,   2.26E9,  2.63E9,
     5 3.11E9,    3.89E9,   4.74E9,   5.71E9,   6.32E9,   6.70E9,  6.70E9/
C------------ELECTRICAL CONDUCTIVITY
      DATA SIGTAB
     6 /6*0.0,     8.1,
     6 86.6,      377.,     1010.,    1920.,    2980.,    4150.,   5320.,
     6 6450.,     7580.,    8430.,    9290.,    9940.,   10600.,   11200.,
     6 11800.,   12300.,   12900.,   13500.,   14100.,   14700.,   14700./
C------------PRANDTL NUMBER
      DATA PRTAB
     7 /.667,     .667,     .652,     .606,     .626,     .643,     .662,
     7 .65,       .63,      .615,     .634,     .729,     .81,      .732,
     7 .71,       .49,      .282,     .136,     .067,     .037,     .027,
     7 .0265,     .033,     .044,     .0524,    .053,     .047,     .047/
C
      ENTRY ONERHO(LOOK,TT,RHOONE,JTOP,JBOT)
      TTT=TT
      IF(LOOK.EQ.1)THEN
      CALL LOOKONE(TTT,RHOONE,RHOTAB,JTOP,JBOT)
      ELSE
      CALL INTONE(TTT,RHOONE,RHOTAB,JTOP,JBOT)
      ENDIF
      RETURN
C------------VISCOSITY
      ENTRY ONEEMU(LOOK,TT,EMUONE,JTOP,JBOT)
      TTT=TT
      IF(LOOK.EQ.1)THEN
      CALL LOOKONE(TTT,EMUONE,EMUTAB,JTOP,JBOT)
      ELSE
      CALL INTONE(TTT,EMUONE,EMUTAB,JTOP,JBOT)
      ENDIF
      RETURN
C------------THERMAL CONDUCTIVITY
      ENTRY ONETHK(LOOK,TT,THKONE,JTOP,JBOT)
      TTT=TT
      IF(LOOK.EQ.1)THEN
      CALL LOOKONE(TTT,THKONE,THKTAB,JTOP,JBOT)
      ELSE
      CALL INTONE(TTT,THKONE,THKTAB,JTOP,JBOT)
      ENDIF
      RETURN
C------------SPECIFIC HEAT
      ENTRY ONECP(LOOK,TT,CPONE,JTOP,JBOT)
      TTT=TT
      IF(LOOK.EQ.1)THEN
      CALL LOOKONE(TTT,CPONE,CPTAB,JTOP,JBOT)
      ELSE
      CALL INTONE(TTT,CPONE,CPTAB,JTOP,JBOT)
```

```
      ENDIF
      RETURN
C------------RADIATION LOSS
      ENTRY ONERAD(LOOK,TT,RADONE,JTOP,JBOT)
      TTT=TT
      IF(LOOK.EQ.1)THEN
      CALL LOOKONE(TTT,RADONE,RADTAB,JTOP,JBOT)
      ELSE
      CALL INTONE(TTT,RADONE,RADTAB,JTOP,JBOT)
      ENDIF
      RETURN
C------------ELECTRICAL CONDUCTIVITY
      ENTRY ONESIG(LOOK,TT,SIGONE,JTOP,JBOT)
      TTT=TT
      IF(LOOK.EQ.1)THEN
      CALL LOOKONE(TTT,SIGONE,SIGTAB,JTOP,JBOT)
      ELSE
      CALL INTONE(TTT,SIGONE,SIGTAB,JTOP,JBOT)
      ENDIF
      RETURN
C------------PRANDTL NUMBER
      ENTRY ONEPRH(LOOK,TT,PRONE,JTOP,JBOT)
      TTT=TT
      IF(LOOK.EQ.1)THEN
      CALL LOOKONE(TTT,PRONE,PRTAB,JTOP,JBOT)
      ELSE
      CALL INTONE(TTT,PRONE,PRTAB,JTOP,JBOT)
      ENDIF
      RETURN
      END
C
      SUBROUTINE LOOKONE(TTT,VALUE,YTAB,JTOP,JBOT)
      DIMENSION YTAB(28),TTAB(28)
C------------TEMPERATURE
      DATA TTAB
     T /1.E-20,  275.,    1000.,   2000.,   3000.,    4000.,  5000.,
     T 6000.,    7000.,   8000.,   9000.,  10000.,   11000., 12000.,
     T 13000.,  14000.,   15000., 16000.,  17000.,   18000., 19000.,
     T 20000.,  21000.,   22000., 23000.,  24000.,   25000., 1.E20/
C------------BEGIN SEARCH
      JTOP=28
      JBOT=1
C------------START AT MIDDLE
 10   J=(JTOP+JBOT)/2
      IF(TTT.LT.TTAB(J))THEN
      JTOP=J
      ELSE
      JBOT=J
      ENDIF
      IF(JTOP-JBOT .NE. 1)GO TO 10
C------------ENTRY POINT IF JTOP AND JBOT KNOWN
      ENTRY INTONE(TTT,VALUE,YTAB,JTOP,JBOT)
      VALUE=YTAB(JBOT)+(YTAB(JTOP)-YTAB(JBOT))*(TTT-TTAB(JBOT))/
     1 (TTAB(JTOP)-TTAB(JBOT))
      RETURN
C
      END
```

```
      SUBROUTINE HELIUM
C------THIS ROUTINE TAKES TEMPERATURE,TT,AND RETURNS THE THERMODYNAMIC
C     PROPERTIES,TRANSPORT PROPERTIES,AND RADIATION LOSS PER UNIT
C     VOLUME IN M.K.S. UINTS FOR IONIZED HELIUM GAS AT 1 ATM.
C
C     THE VALUES ASSIGNED TO I ARE:
C     1=DENSITY , 2=VISCOSITY , 3=THERMAL CONDUCTIVITY ,
C     4=SPECIFIC HEAT , 5=RADIATION LOSS , 6=ELECTRICAL CONDCTIVITY ,
C     7=PRANDTL #
C
C     TEMPERATURE IS IN KELVIN AND RADITION IN WATTS/CUBIC METRE
C

      DIMENSION RHOTAB(28),EMUTAB(28),THKTAB(28)
      DIMENSION CPTAB(28),RADTAB(28),SIGTAB(28),PRTAB(28)
C
C------------DENSITY
      DATA RHOTAB
    1 /.177402, .177402,  .048786, .024393, .016262, .012196, .009757,
    1 .008131,  .006969,  .006098, .005421, .004877, .004434, .004061,
    1 .003741,  .003461,  .003206, .002963, .002723, .002481, .002234,
    1 .001982,  .001743,  .001524,  .001341, .001197,.001089, .001089/
C------------VISCOSITY
      DATA EMUTAB
    2 /1.88E-5, 1.88E-5,  4.41E-5, 6.96E-5, 9.41E-5, 1.21E-4, 1.47E-4,
    2 1.73E-4,  1.98E-4,  2.23E-4, 2.47E-4, 2.71E-4, 2.93E-4, 3.14E-4,
    2 3.29E-4,  3.34E-4,  3.23E-4, 2.92E-4, 2.45E-4, 1.91E-4, 1.41E-4,
    2 9.94E-5,  6.87E-5,  4.72E-5, 3.29E-5, 2.39E-5, 1.85E-5, 1.85E-5/
C------------THERMAL CONDUCTIVITY
      DATA THKTAB
    3 /.14277,  .14277,  .3408,  .5378,   .7277,   .9366,    1.139,
    3 1.337,    1.530,   1.721,  1.910,  2.104,   2.321,    2.60,
    3 2.985,    3.459,   3.990,  4.611,  5.428,   6.556,    8.011,
    3 9.618,    10.98,   11.65,  11.36,  10.30,   8.982,    8.982/
C------------SPECIFIC HEAT
      DATA CPTAB
    4 /5193.,   5193.,   5193.,   5193.,   5193.,   5191.,   5191.,
    4 5195.,    5191.,   5195.,   5208.,   5265.,   5452.,   5923.,
    4 6952.,    8912.,   12320.,  17776.,  25879.,  37198.,  51820.,
    4 68788.,   84905.,  95249.,  94937.,  83825.,  67023.,  67023./
C------------RADIATION LOSS
      DATA RADTAB
    5 /7*0.0,
    5 0.0,      0.0,     0.0,     4.00E6,  3.53E7,  1.12E8, 3.31E8,
    5 7.86E8,   1.37E9,  1.92E9,  2.27E9,  2.26E9,  2.26E9, 2.63E9,
    5 3.11E9,   3.89E9,  4.74E9,  5.71E9,  6.32E9,  6.70E9, 6.70E9/
C------------ELECTRICAL CONDUCTIVITY
      DATA SIGTAB
    6 /6*0.0,    8.1,
    6 86.6,     377.,    1010.,   1920.,   2980.,   4150.,  5320.,
    6 6450.,    7580.,   8430.,   9290.,   9940.,  10600.,  11200.,
    6 11800.,  12300.,  12900.,  13500.,  14100.,  14700.,  14700./
C------------PRANDTL NUMBER
      DATA PRTAB
    7 /.682,   .682,    .672,    .672,    .672,     .672,   .672,
    7 .672,   .672,    .672,    .673,    .677,     .689,   .715,
```

```
     7 .766,    .861,     .997,     1.126,    1.169,     1.086,   .911,
     7 .711,    .532,     .386,     .275,    .194,      .138,     .138/
C
      ENTRY HELRHO(LOOK,TT,RHOONE,JTOP,JBOT)
      TTT=TT
      IF(LOOK.EQ.1)THEN
      CALL LOOKONE(TTT,RHOONE,RHOTAB,JTOP,JBOT)
      ELSE
      CALL INTONE(TTT,RHOONE,RHOTAB,JTOP,JBOT)
      ENDIF
      RETURN
C------------VISCOSITY
      ENTRY HELEMU(LOOK,TT,EMUONE,JTOP,JBOT)
      TTT=TT
      IF(LOOK.EQ.1)THEN
      CALL LOOKONE(TTT,EMUONE,EMUTAB,JTOP,JBOT)
      ELSE
      CALL INTONE(TTT,EMUONE,EMUTAB,JTOP,JBOT)
      ENDIF
      RETURN
C------------THERMAL CONDUCTIVITY
      ENTRY HELTHK(LOOK,TT,THKONE,JTOP,JBOT)
      TTT=TT
      IF(LOOK.EQ.1)THEN
      CALL LOOKONE(TTT,THKONE,THKTAB,JTOP,JBOT)
      ELSE
      CALL INTONE(TTT,THKONE,THKTAB,JTOP,JBOT)
      ENDIF
      RETURN
C------------SPECIFIC HEAT
      ENTRY HELCP(LOOK,TT,CPONE,JTOP,JBOT)
      TTT=TT
      IF(LOOK.EQ.1)THEN
      CALL LOOKONE(TTT,CPONE,CPTAB,JTOP,JBOT)
      ELSE
      CALL INTONE(TTT,CPONE,CPTAB,JTOP,JBOT)
      ENDIF
      RETURN
C------------RADIATION LOSS
      ENTRY HELRAD(LOOK,TT,RADONE,JTOP,JBOT)
      TTT=TT
      IF(LOOK.EQ.1)THEN
      CALL LOOKONE(TTT,RADONE,RADTAB,JTOP,JBOT)
      ELSE
      CALL INTONE(TTT,RADONE,RADTAB,JTOP,JBOT)
      ENDIF
      RETURN
C------------ELECTRICAL CONDUCTIVITY
      ENTRY HELSIG(LOOK,TT,SIGONE,JTOP,JBOT)
      TTT=TT
      IF(LOOK.EQ.1)THEN
      CALL LOOKONE(TTT,SIGONE,SIGTAB,JTOP,JBOT)
      ELSE
      CALL INTONE(TTT,SIGONE,SIGTAB,JTOP,JBOT)
      ENDIF
      RETURN
C------------PRANDTL NUMBER
      ENTRY HELPRH(LOOK,TT,PRONE,JTOP,JBOT)
```

```
      TTT=TT
      IF(LOOK.EQ.1)THEN
      CALL LOOKONE(TTT,PRONE,PRTAB,JTOP,JBOT)
      ELSE
      CALL INTONE(TTT,PRONE,PRTAB,JTOP,JBOT)
      ENDIF
      RETURN
      END
C
      SUBROUTINE LOOKONE(TTT,VALUE,YTAB,JTOP,JBOT)
      DIMENSION YTAB(28),TTAB(28)
C------------TEMPERATURE
      DATA TTAB
     T /1.E-20,  275.,    1000.,   2000.,   3000.,    4000.,  5000.,
     T 6000.,    7000.,   8000.,   9000.,  10000.,   11000., 12000.,
     T 13000.,  14000.,   15000., 16000.,  17000.,   18000., 19000.,
     T 20000.,  21000.,   22000., 23000.,  24000.,   25000., 1.E20/
C------------BEGIN SEARCH
      JTOP=28
      JBOT=1
C------------START AT MIDDLE
 10   J=(JTOP+JBOT)/2
      IF(TTT.LT.TTAB(J))THEN
      JTOP=J
      ELSE
      JBOT=J
      ENDIF
      IF(JTOP-JBOT .NE. 1)GO TO 10
C------------ENTRY POINT IF JTOP AND JBOT KNOWN
      ENTRY INTONE(TTT,VALUE,YTAB,JTOP,JBOT)
      VALUE=YTAB(JBOT)+(YTAB(JTOP)-YTAB(JBOT))*(TTT-TTAB(JBOT))/
     1 (TTAB(JTOP)-TTAB(JBOT))
      RETURN
C
      END


      SUBROUTINE TEMPHE(KTEMP,GVALUE,HVALUE,TVALUE)
      DIMENSION HONE(48),HTWO(48),TE(48)
C
C----- GASONE(ARGON) AND GASTWO(AIR) -----
C
C------------ENTHALPY ARGON
       DATA HONE
     H /1.E-20,  1.43E5,  2.6E5,   5.2E5,   7.8E5,   1.04E6,  1.3E6,
     H  1.56E6,  1.82E6,  2.08E6,  2.34E6,  2.6E6,   2.87E6,  3.13E6,
     H  3.4E6,   3.66E6,  3.96E6,  4.25E6,  4.63E6,  5.01E6,  5.62E6,
     H  6.23E6,  7.30E6,  8.36E6,  1.02E7,  1.21E7,  1.51E7,  1.80E7,
     H  2.2E7,   2.6E7,   3.07E7,  3.53E7,  3.96E7,  4.39E7,  4.68E7,
     H  4.97E7,  5.16E7,  5.36E7,  5.49E7,  5.62E7,  5.72E7,  5.81E7,
     H  6.29E7,  6.72E7,  7.4E7,   8.38E7,  9.59E7,  1.E20/
C------------ENTHALPY HELIUM
       DATA HTWO
     1/1.E-20,  1.43E6, 2.60E6, 5.19E6,  7.79E6,  1.04E7, 1.30E7,
     1 1.56E7,  1.82E7, 2.08E7, 2.34E7,  2.60E7,  2.86E7, 3.12E7,
     1 3.38E7,  3.63E7, 3.89E7, 4.15E7,  4.41E7,  4.67E7, 4.94E7,
     1 5.20E7,  5.46E7, 5.73E7, 6.01E7,  6.30E7,  6.61E7, 6.94E7,
     1 7.31E7,  7.72E7, 8.21E7, 8.78E7,  9.45E7,  1.03E8, 1.12E8,
```

```
     1 1.24E8,  1.39E8, 1.56E8, 1.76E8,  2.00E8,  2.28E8, 2.60E8,
     1 3.37E8,  4.28E8. 5.24E8, 6.14E8,  6.89E8,  1.E20/
C------------TEMPERATURE
      DATA TE
     7 /1.E-20,   275.,    500.,    1000.,   1500.,    2000.,  2500.,
     7 3000.,    3500.,   4000.,   4500.,   5000.,    5500.,  6000.,
     7 6500.,    7000.,   7500.,   8000.,   8500.,    9000.,  9500.,
     7 10000.,  10500.,   11000., 11500.,  12000.,   12500., 13000.,
     7 13500.,  14000.,   14500., 15000.,  15500.,   16000., 16500.,
     7 17000.,  17500.,   18000., 18500.,  19000.,   19500., 20000.,
     7 21000.,  22000.,   23000., 24000.,  25000.,   1.E10/
C-----------SET UP INITIAL VALUES
      JTOP=48
      JBOT=1
      GG=GVALUE
C------------FOR TEMPERATURE
      IF(KTEMP.EQ.1)THEN
       HMIXJT=1.E20
       HMIXJB=1.E-20
       TTT=HVALUE
 10    J=(JTOP+JBOT)/2
       HMIXJ=HONE(J)*GG+(1.-GG)*HTWO(J)
       IF(TTT.LT.HMIXJ)THEN
        JTOP=J
        HMIXJT=HMIXJ
       ELSE
        JBOT=J
        HMIXJB=HMIXJ
       ENDIF
       IF(JTOP-JBOT.NE.1)GO TO 10
        TVALUE=TE(JBOT)+(TE(JTOP)-TE(JBOT))*(TTT-HMIXJB)
     1  /(HMIXJT-HMIXJB)
        RETURN
      ENDIF
C-------------FOR ENTHALPY
      TTT=TVALUE
 20   J=(JTOP+JBOT)/2
      IF(TTT.LT.TE(J))THEN
        JTOP=J
      ELSE
        JBOT=J
      ENDIF
       IF(JTOP-JBOT.NE.1)GO TO 20
      H1=HONE(JBOT)+(HONE(JTOP)-HONE(JBOT))*(TTT-TE(JBOT))
     1/(TE(JTOP)-TE(JBOT))
      H2=HTWO(JBOT)+(HTWO(JTOP)-HTWO(JBOT))*(TTT-TE(JBOT))
     1/(TE(JTOP)-TE(JBOT))
      HVALUE=H1*GG+(1.-GG)*H2
      RETURN
      END
```

Biographical Note:

The author was born Richard Charles Westhoff in Boulder Colorado, on January 4, 1961 as the tenth of twelve children to Edwin and Frances Westhoff. He attended grade school at Bolitho Elementary, in Glenwood Springs Colorado where his greatest thrills were winning the "Word of the Day" competition in first grade, and the District Spelling Bee championships in fifth and sixth grade, though he does admit that Mike Dalrymple had to remind him what one of the words of the day was. His first positive influence in the area of science was probably through the "Rick Brant" series of books in which the scientists were portrayed as the "good guys" rather than as wide-eyed psychotics out to "rule the world!"

He later attended Junior High and High school in Nogales, Arizona. He completed high school in Tucson, Arizona at Canyon Del Oro high school. He is grateful to Mr. Capen, who didn't throw him out of class for sleeping, and helped him discover an aptitude for physics. Also, he is grateful to the guidance counselor who "woke him up" and told him to go to college. Maureen Oulette was another very positive influence through her Wednesday night Bible studies for high school students which opened up a whole new world of insight into life.

Graduation sent him off to Carroll College in Helena, Montana to catch up on his mathematics skills. Three years of Calculus and Differential equations from Mr. Al Murray and Dr. John Scharf brought him back to Arizona State University in Tempe to complete the engineering degree.

Some of the best memories of his life are in Tempe: "The Boys of 1630" living at "The Dump" in Tempe, meeting Cindy Porter and getting married. He received the B.S. in Mechanical Engineering from ASU in May of 1985, and the B.A. in Mathematics from Carroll College in September of 1985. While completing his last year as an undergraduate he began working for Epsilon Technology, a division of Advanced Semiconductor Materials America, where he stayed two and one-half years working in research and development on the design of a chemical vapor deposition (CVD) reactor for silicon epitaxy. He is very grateful to Dr. MacDonald Robinson for recommending that he go to MIT to pursue graduate studies.

He came to M.I.T. in 1987, received a Masters degree in Materials Engineering in 1989 and plans to get the Ph.D. in June of 1992. His research interests include Transport Phenomena in Plasma Processing, Arc Phenomena Applied to Welding Processes, Transport Phenomena in CVD reactors, and Mathematical Modeling of Materials Processing Systems in general.